1977

Soil - Pile Interaction Under Vibratory Loading

Toyoaki Nogami

NOTICE

The quality of this microfiche is heavily dependent upon the quality of the original thesis submitted for microfilming. Every effort has been made to ensure the highest quality of reproduction possible.

If pages are missing, contact the university which granted the degree.

Some pages may have indistinct print especially if the original pages were typed with a poor typewriter ribbon or if the university sent us a poor photocopy.

Previously copyrighted materials (journal articles, published tests, etc.) are not filmed.

Reproduction in full or in part of this film is governed by the Canadian Copyright Act, R.S.C. 1970, c. C-30. Please read the authorization forms which accompany this thesis.

THIS DISSERTATION
HAS BEEN MICROFILMED
EXACTLY AS RECEIVED

AVIS

La qualité de cette microfiche dépend grandement de la qualité de la thèse soumise au microfilmage. Nous avons tout fait pour assurer une qualité supérieure de reproduction.

S'il manque des pages, veuillez communiquer avec l'université qui a conféré le grade.

La qualité d'impression de certaines pages peut laisser à désirer, surtout si les pages originales ont été dactylographiées à l'aide d'un ruban usé ou si l'université nous a fait parvenir une photocopie de mauvaise qualité.

Les documents qui font déjà l'objet d'un droit d'auteur (articles de revue, examens publiés, etc.) ne sont pas microfilmés.

La reproduction, même partielle, de ce microfilm est soumise à la Loi canadienne sur le droit d'auteur, SRC 1970, c. C-30. Veuillez prendre connaissance des formules d'autorisation qui accompagnent cette thèse.

LA THÈSE A ÉTÉ
MICROFILMÉE TELLE QUE
NOUS L'AVONS REÇUE

SOIL - PILE INTERACTION
UNDER VIBRATORY LOADING

by

Toyoaki Nogami
Faculty of Engineering Science

Submitted in partial fulfillment
of the requirements for the degree of
Doctor of Philosophy

Faculty of Graduate Studies
The University of Western Ontario
London, Ontario
October, 1976

ABSTRACT

When dynamic loadings are applied to the structure supported by a pile foundation, the pile foundation resists the movement of the structure relative to that of the ground. Thus, the pile foundation provides the stiffness and damping to the structure. The characteristics of stiffness and damping result from the dynamic soil-pile interaction and are very little known.

As the first step of the research on the complicated dynamic soil-pile interaction, the general trends of this interaction were investigated theoretically for the simple, ideal conditions. The model of a soil-pile system was chosen so that it could clearly provide the basic trends of the soil-pile interaction; thus, the complicated behavior of soil and other complicated conditions of a soil-pile system were simplified.

The soil reaction to a pile subjected to dynamic loadings results from superimposing the soil reaction in each wave generated from the pile into the soil medium. The analytical solutions for the soil reactions in an individual wave were derived and the characteristics of this reaction were investigated. It was found that the soil reaction in the n-th mode wave approached quickly to that for the plane strain case as frequency increases above the n-th natural frequency of the stratum.

The stiffness and damping of a pile set in the ground were analytically obtained at the pile head, and this soil-pile interaction was investigated in terms of those stiffness and damping. Significantly different frequency-dependent behaviors of stiffness

and damping were observed between the weak and the strong soil effects. It was found that certain dimensionless parameters shown in this dissertation could indicate the intensity of the soil effect. In order to illustrate the observed characteristics of soil-pile interaction, the displacements of pile were shown at the pile head under harmonic excitation applied at the pile head.

Using the derived solution for the soil-pile system, the coefficient of soil reaction was further obtained along the length of pile. The results for the static case showed that the coefficient of soil reaction is not uniform along the length of pile even if the soil medium is uniform. It further showed that the coefficient for the dynamic case approached that for the plane strain case as the excitation frequency increased. Therefore, the dynamic condition provides a more favorable situation for modeling a soil medium as Winkler's model than the static condition does. The spring and damping constants in this model may be obtained from the plane strain condition.

Since the commonly used method to estimate the coefficients of soil reaction are based on crude assumptions, some of those methods were assessed by comparing theoretically the coefficients obtained by using them with those obtained by the derived solution in this dissertation. The application of the modified Baranov's formula to estimate the coefficient for the pile was also assessed. It was found that the plate loading test possibly overestimates the coefficient for a slender pile but Vesić's formula underestimates it for the weak soil effect. It was also found that the modified Baranov's formula could be applicable to estimate the coefficient

of soil reaction for high excitation frequencies and was more favourable to do so for more slender pile and weaker soil effect.

ACKNOWLEDGMENTS

The author wishes to express his profound gratitude to Professor M. Novak for his guidance, encouragement, and valuable assistance throughout the course of this study.

This study was supported by the National Research Council of Canada. The financial support is gratefully acknowledged. The teaching assistantship provided to the author during his graduate study is also acknowledged.

The author would also like to express his appreciation to Mr. Bill Harman for reviewing the manuscript, and to Mrs. Lois Sakamoto and Mrs. Lyn Parnell for their careful typing.

For the encouragement received from his wife, the author wishes to express his most sincere appreciation.

TABLE OF CONTENTS

LIST OF TABLES

LIST OF FIGURES

NOMENCLATURE

$\bar{A}_h$, $\bar{A}_v$	dimensionless amplitudes of displacements of pile in horizontal and vertical vibrations
a_0	frequency parameter; $a_0 = \frac{H}{v_s}\omega$
$\bar{a}_0$	frequency parameter normalized by the fundamental natural frequency of stratum in horizontal vibration
a_0'	frequency parameter; $a_0' = \frac{r_0}{v_s}\omega$
a_{j1}	elements of coefficient matrix concerned with soil effect in Eq. D-24
$\bar{a}_{j1}$	dimensionless form of a_{j1}
b_j	elements of coefficient matrix not concerned with soil effect in Eq. D-24
$\bar{b}$	normalized frequency parameter; $\bar{b} = \frac{\bar{\lambda}_{h,v}}{\bar{\lambda}_0}$
$\bar{b}_j$	dimensionless form of b_j
c	viscous constant in dashpot

D	displacements D_v and D_h
$\overline{D}$	dimensionless form of D
D, D'	damping factors for complex spring and Voigt model, respectively; $D = \frac{k'}{k}$ and $D' = \frac{c\omega}{k}$.
D_h, D_v	displacements of pile subjected to unit forces at its head in horizontal and vertical vibrations, respectively
$\overline{D}_h$, $\overline{D}_v$	dimensionless forms of D_h and D_v, respectively
D_l, D_s	damping factors of soil for the longitudinal and shear wave propagations, respectively; $D_l = \frac{\lambda' + 2\mu'}{\lambda + 2\mu}$ and $D_s = \frac{\mu'}{\mu}$
D_{nl}	n-th coefficient obtained by expanding the l-th mode shape of pile with sine Fourier series
E	Young's modulus of soil
E_p	Young's modulus of pile
E_s	constant used in the expression for soil reaction

F_{1n}, F_{2n}, F_{3n}, F_{4n}	n-th coefficients obtained by expanding the horizontal displacement of pile with sine Fourier series
f_{1n}, f_{2n}, f_{3n}, f_{4n}	$(f_{1n}, f_{2n}, f_{3n}, f_{4n})^T$ $= \frac{\alpha_{hn}}{E_p I h_n^4 - m\omega^2 + \alpha_{hn}} (F_{1n}, F_{2n}, F_{3n}, F_{4n})^T$
H	thickness of stratum and length of pile
$\bar{H}$	slenderness ratio of pile; $\bar{H} = H/r_0$
H_0^2	Hankel function of the second kind of the order zero
h_n	$h_n = \frac{\pi}{2H} (2n - 1)$
$\bar{h}_n$	dimensionless form of h_n; $\bar{h}_n = \frac{\pi}{2} (2n - 1)$
I	second moment of area of pile
i	$i = \sqrt{-1}$
I_0	modified Bessel function of the zero-th order of the first kind

I_1	modified Bessel function of the first order of the first kind
K	stiffnesses of soil-pile system at the pile head, K_h and K_v
$\bar{K}$	dimensionless form of K
$k(z)$	coefficients of soil reaction, $k_h(z)$ and $k_v(z)$
$\bar{k}(\bar{z})$	dimensionless form of k(z); $k(z) = \mu\bar{k}(\bar{z})$
k, k'	real and imaginary parts of the complex stiffness
k*	coefficient of subgrade reaction; $k(z) = 2r_0 k^*$
K_0	modified Bessel function of the zero-th order of the second kind
K_1	modified Bessel function of the first order of the second kind
K_h, K_v	stiffnesses of the installed pile at its head in horizontal and vertical vibrations, respectively

$\bar{K}_h$, $\bar{K}_v$	dimensionless forms of K_h and K_v, respectively
k_h, $k_h(z)$; k_v, $k_v(z)$	coefficients of horizontal and vertical soil reactions, respectively
$\bar{k}_h$, $\bar{k}_h(\bar{z})$; $\bar{k}_v$, $\bar{k}_v(\bar{z})$	dimensionless forms of $k_h(z)$ and $k_v(z)$, respectively
l', q', s'	parameters used in the plane strain case
$\bar{l}'$, $\bar{q}'$, $\bar{s}'$	dimensionless forms of l', q' and s', respectively
L_n, L_{rn}, L_s, L_{zn}	wave lengths
l_n, q_n, s_n	parameters in the n-th mode of wave
$\bar{l}_n$, $\bar{q}_n$, $\bar{s}_n$	dimensionless form of l_n, q_n and s_n, respectively
M	moment force
m	mass density of unit length of pile
N_j	j-th generalized force

P	shear force or normal force on the cross area of pile
p, p'	real and imaginary parts of force in the complex spring, respectively
$p(z)$	soil reactions $p_h(z)$ and $p_v(z)$
P_0, P_0'	amplitudes of forces p and p', respectively
p_h, $p_h(z)$; p_v, $p_v(z)$	horizontal and vertical soil reactions, respectively
$R(r)$, $Z(z)$, $\Theta(\theta)$	$w(r,z) = R(r) \cdot Z(z)$ or $\phi(r,z,\theta) = R(r)\, Z(z)\, \Theta(\theta)$
r, θ, z	coordinates
r_0	radius of pile
S	area of cross section of pile
T_n	parameter
$\overline{T}_n$	dimensionless form of T; $\overline{T}_n = \frac{T_n}{H}$
T'	parameter used in the plane strain case

$\bar{T}'$	dimensionless form of T'; $\bar{T}' = \frac{T'}{H}$
t	time
T_d, T_k, T_s	lost energy, strain energy, and kinetic energy, respectively
U(t,z), W(t,z), ζ(t,z)	horizontal, vertical and rotational displacements of pile, respectively
U(z), W(z), ζ(z)	$U(t,z) = U(z)e^{i\omega t}$, $W(t,z) = W(z)e^{i\omega t}$, and $\zeta(t,z) = \zeta(z)e^{i\omega t}$
U, W, ζ	U(z=H), W(z=H) and ζ(z=H)
u(t), v(t), w(t)	displacements of the stratum
u, v, w	$u(t) = u\,e^{i\omega t}$; $v(t) = v\,e^{i\omega t}$ and $w(t) = w\,e^{i\omega t}$
$U_h(z)$, $U_p(z)$	homogeneous and particular solutions for U(z), respectively; $U(z) = U_h(z) + U_p(z)$
U_n, W_n	n-th coefficients of sine series expressing U(z) and W(z), respectively
$\bar{v}$	wave velocity ratio; $\bar{v} = \frac{v_s}{v_p}$

v_l, v_s	longitudinal and shear wave velocities, respectively
v_p	$v_p = \sqrt{\frac{\bar{E}_p}{\rho_p}}$
x	deformation of complex spring
x_0	amplitude of deformation of complex spring
Y	parameters Y_h and Y_v
Y_h, Y_v	parameters determining soil effect in horizontal and vertical vibrations, respectively
$\bar{\alpha}$	dimensionless form of soil resistance factors for the plane strain case, $\bar{\alpha}_h$ and $\bar{\alpha}_v$
$\bar{\alpha}_h$, $\bar{\alpha}_v$	dimensionless forms of horizontal and vertical soil resistance factors for the plane strain case, respectively
α_n	soil resistance factors in the n-th mode wave, α_{hn} and α_{vn}
$\bar{\alpha}_n$	dimensionless form of α_n; $\bar{\alpha}_n = H\alpha_n$

α_{hn}, α_{vn}	horizontal and vertical soil resistance factors, respectively
$\bar{\alpha}_{hn}$, $\bar{\alpha}_{vn}$	dimensionless forms of α_{hn} and α_{vn}, respectively
$\bar{\alpha}'_{hn}$, $\bar{\alpha}'_{vn}$	$\bar{\alpha}'_{hn} = \frac{\mu}{\mu^*} \bar{\alpha}_{hn}$, $\bar{\alpha}'_{vn} = \frac{\mu}{\mu^*} \bar{\alpha}_{vn}$
β_n	direction of the n-th mode primary wave propagation
γ	phase shift between applied force and displacement of pile at the pile head
$\Delta(t)$	dilatational strain
Δ	$\Delta(t) = \Delta e^{i\omega t}$
δ	delta function
$\delta\eta_n$	vertical displacement in the n-th generalized coordinate
δW	virtual work done
η	$\eta = \frac{v_l}{v_s} = \sqrt{\frac{2 - 2\nu}{1 - 2\nu}}$

η_n	n-th generalized coordinate
λ, μ	real parts of complex Lame's constants (μ = shear modulus)
λ', μ'	imaginary parts of complex Lame's constants
$\bar{\lambda}_0$	reference dimensionless frequency parameter in terms of $\bar{\lambda}_h$ or $\bar{\lambda}_v$
λ_h, λ_v	frequency parameters in horizontal and vertical vibrations, respectively
$\bar{\lambda}_h$, $\bar{\lambda}_v$	dimensionless forms of λ_h and λ_v, respectively
μ^*	reference shear modulus
ν	Poisson's ratio
$\xi_n(z)$	n-th mode shape of pile free from soil effect
ρ	density of unit mass of soil
$\bar{\rho}$	mass ratio; $\bar{\rho} = \frac{\rho}{\rho_p}$
ρ_p	density of unit mass of pile

σ_r, σ_z, $\tau_{r\theta}$, τ_{rz}, $\tau_{\theta z}$	stresses in the stratum
ϕ, ψ	potential functions related to longitudinal and shear waves, respectively
ω	frequency (rad/sec)
ω_z	rotational strain about z axis
∇^2	Laplacian operator in cylindrical coordinates

CHAPTER 1. INTRODUCTION

Dynamic loadings applied to structure built on ground may be classified into two types. One is the direct loading which may be induced by wind and operation of big machines. The other is the inertia loading of every mass of the structure induced by ground shaking. The ground shaking may be a dynamic disturbance transmitted through the ground - an earthquake, for example.

Since ground has some flexibility, the base of a structure tends to move due to those dynamic loadings. The forces at the base of a structure are determined by the force-displacement relationship of the ground at the contact. Therefore, this relationship affects the behavior of structures built on ground.

Significant amounts of research have been conducted to clarify this force-displacement relationship for a structure placed directly on the ground (Arnold, 1955; Awojobi and Groatenhuis, 1965; Awojobi, 1972; Bycroft, 1956; Elorduy, 1967; Kobori, etc., 1967, 1968, 1971; Luco and Westman, 1971; 1972; Luco, 1976; Novak, 1971; Reissner, 1936). As a result of such efforts, it is possible to estimate this relationship reasonably well for a structure resting directly on the ground.

When a structure is supported by a pile foundation, the force-displacement relationship of the soil-pile system at the pile head must be included in the above mentioned force-displacement relationship. This relationship results from soil-pile interaction and is not well understood yet because of its extreme complexity.

Static behavior of a pile foundation is governed by soil characteristics, contact conditions between soil and pile, confining pressure,

boundary conditions of ground and pile, magnitude of applied force, etc. In addition, damping and inertia forces of the soil-pile system affect the dynamic behavior of the soil-pile system. In the past, very few studies have been made on the dynamic behavior of soil-pile system. However, in most of those studies, the effect of inertia and damping in a soil medium are not properly taken into account. Instead of those important factors in dynamics, much effort has been placed on accounting for other governing factors as much as possible. Because of ignorance of important factors in dynamics and so many parameters considered in a complicated manner, it has been hardly possible to draw a clear picture of dynamic characteristics of soil-pile interaction.

There are basically two kinds of treatment for soil medium when a soil-pile system is modeled. In one of them, the soil reaction to a pile at a certain location is assumed to be related to the pile displacement only at the location where the reaction is considered. Thus the soil medium is treated as locally independent springs and dashpots distributed along the pile length. This model is called Winkler's model. Since the displacement at one location in a soil medium influences mechanical behavior of the medium at other locations, it is difficult to estimate the constants of equivalent locally independent springs and dashpots distributed along the pile length. In Penzien's work on seismic response of a pile (Penzien, 1970), however, the spring constant is estimated from the static force-displacement relationship which is obtained by applying a uniform ring load at the location of the spring in an elastic half-space. This estimated spring constant does not include the effects of damping and inertia forces of the soil

medium. On the other hand, Baranov's formula for estimating the constant of soil springs (Baranov, 1967) includes those effects to some extent. In this formula, the constant is obtained by applying a harmonic excitation uniformly distributed along the circular, rigid, massless cylinder which extends infinitely in an infinite elastic medium. Novak recently applied this formula to a dynamic soil-pile interaction problem in estimating the locally independent spring and dashpot constants of a soil medium (Novak, 1974).

In the second kind of treatment, a soil medium is modeled as a three dimensional continuum medium. In this model the displacement at any location of soil medium affects the soil reaction at all depths of a pile. However, considerable difficulty is usually encountered in deriving a formula for soil reaction. For a visco-elastic stratum overlying a rigid base, Tajimi derived the solution for seismic response of a soil-pile system neglecting vertical displacement of the stratum (Tajimi, 1969). However, his solution is not for general boundary conditions at both ends of a pile but only for the rotationally fixed head and pinned tip.

In this dissertation, dynamic characteristics of soil-pile interaction are mainly investigated under harmonic excitations. Main emphasis is placed on drawing the physical insight of the dynamic behavior so that general trends can be seen clearly. Dynamic behavior of a soil medium is associated with waves generated in this medium, and therefore, can be interpreted by the nature of those waves. Since a continuum model is the only model which can simulate the wave motions in the medium, this model is chosen from the above mentioned

two kinds of models. The assumed conditions of soil medium are simplified as much as possible in order to avoid extreme complexity and attain a clear picture of physical insight of dynamic soil-pile interaction. In deriving the solution for horizontal vibration, the vertical displacement of a soil medium is neglected following the Tajimi's solution. However, the solution is obtained in a different manner so as to be applicable to general boundary conditions at both ends of the pile. Although Tajimi did not consider the solution for vertical vibration of soil-pile system, the solution for this mode of vibration is also obtained.

Scope of the Dissertation

Deformation of a pile accompanies the reaction from a soil medium. The reaction forces for vertical and horizontal vibrations are derived and their characteristics are discussed (Chapter 2).

Utilizing those obtained formulas for soil reactions, the equations for motions of a pile surrounded by a soil medium are set up for vertical and horizontal vibrations and solved for the stiffnesses of a soil-pile system at the pile head (Chapter 3). Then, the characteristics of dynamic soil-pile interaction are investigated in terms of those stiffnesses (Chapter 3).

In order to further illustrate those characteristics, the displacements of an installed pile are obtained at the pile head for harmonic excitation forces applied at the pile head (Chapter 4).

The solutions obtained in Chapters 2 and 3 can also provide the pile displacement and soil reaction to a pile at any depth. Thus, the locally independent soil springs or the coefficients of soil reactions

are obtained from them and their characteristics are discussed together with some of the commonly used methods to estimate those spring constants (Chapter 5).

CHAPTER 2. SOIL REACTIONS TO HARMONIC MOTIONS OF A PILE

2.1 Introduction

When a pile is subjected to dynamic loadings, the energy applied to the pile is transmitted to the surrounding soil. Some of the transmitted energy is temporarily stored in the soil and returned to the pile during a cyclic loading and unloading process. The remainder of the energy is dissipated in the soil through conversion into heat and radiation to infinity. The energy loss is called damping, and classified into material and radiation dampings which result from the energy conversion and radiation, respectively. Soil acts as a spring through the former energy transition and as a damper through the latter energy transition. Soil reaction is governed by these "spring" and "damping" functions of soil. In this study, the soil reaction is expressed analytically and then its characteristics are investigated.

The soil medium is modeled as a single stratum overlying bedrock (see Fig. 2.1-1). Other assumptions made in this study are:

1. The soil stratum is homogeneous, isotropic, and linearly visco-elastic.
2. The top surface of the soil stratum is free from stresses.
3. The soil stratum is fixed at the bedrock; i.e., no displacements are allowed at the bedrock surface.
4. The soil stratum is horizontal and extends to infinity with a constant thickness.
5. Vertical and horizontal displacements are small enough to be negligible in horizontal and vertical vibrations, respectively.

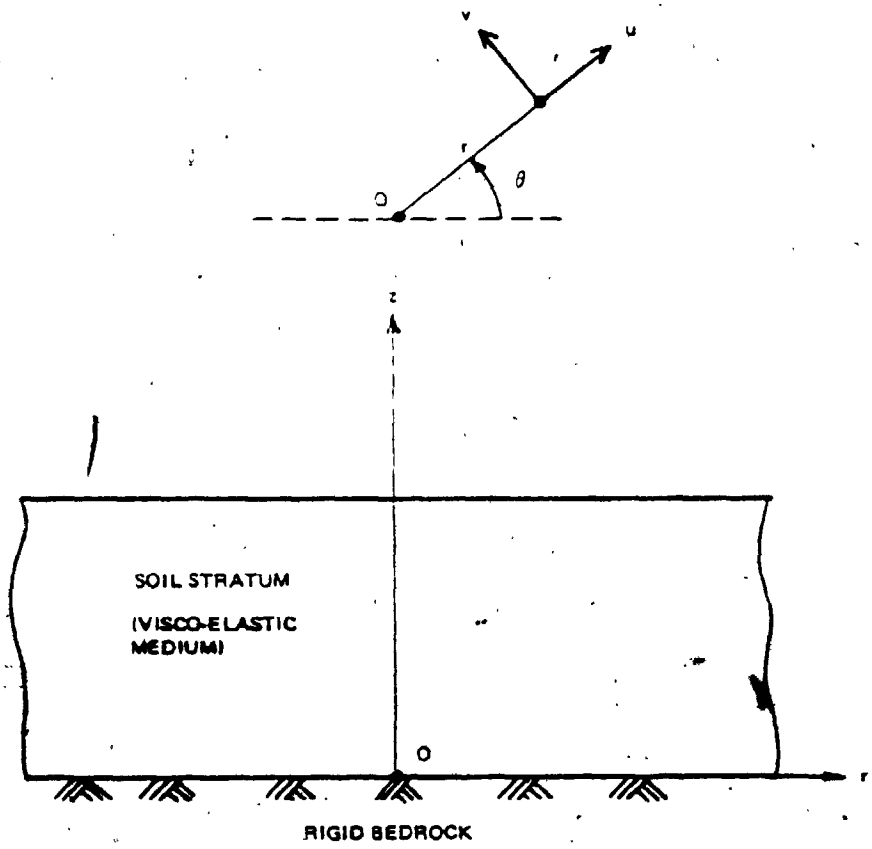

Fig. 2.1-1. Model of Soil Stratum Overlying Rigid Bedrock and Coordinate System

6. The load is applied to the soil through the circumference of the circular pile.

7. The pile is vertical and driven to the bedrock.

These conditions are rather ideal; first, soil is never uniform nor isotropic because of the increasing pressure with depth and the complicated formation process of soils. Second, the structure supported by the pile foundation may contact the soil directly, thus producing stresses in the soil which the above made assumption does not account for. Third, it is difficult to encounter rigid bedrock underneath soil; flexible bedrock transmits energy and provides flexibility to the stratum.

Most analytical solutions in soil dynamics adopted the Voigt-type visco-elastic model. This model yields linearly frequency-dependent damping. Contrary to this, experimental results on soils show that the material damping is rather frequency independent (Richart, Hall, and Woods, 1970; Dobry, 1970; Krizek and Franklin, 1967; Seed and Idriss, 1970; Hardin and Drnevich, 1972). Therefore, the complex elastic constants are used here in order to simulate a frequency-independent material damping of soil. The real and imaginary parts of the complex elastic constants can be determined from the elastic and damping nature of soil as described in Appendix A.

2.2 Analytical Solutions for Soil Reactions

The analytical solutions for the soil reactions to a vertically and horizontally vibrating pile are derived individually in this section. The assumptions used in these derivations are given in

Section 2.1. The soil stratum overlying bedrock is shown in Fig. 2.1-1 along with the coordinate system.

2.2.A Soil Reaction to Vertical Motion of A Pile

Neglecting a horizontal displacement, the equation for vertical motion of the soil stratum is given by

$$\left\{(\lambda + 2\mu) + i(\lambda' + 2\mu')\right\} \frac{\partial^2}{\partial z^2} w(t)$$

$$+ (\mu + i\mu')\left(\frac{1}{r}\frac{\partial}{\partial r} + \frac{\partial^2}{\partial r^2}\right) w(t) = \rho \frac{\partial^2}{\partial t^2} w(t) \qquad (2.2\text{-}1)$$

where

$w(t)$ = vertical displacement of soil mass at time t,

λ, μ = real part of Lame's constants associated with strain energy,

λ', μ' = imaginary parts of Lame's constants associated with energy dissipation due to material damping,

ρ = mass density of soil,

t = time, and

i = $\sqrt{-1}$.

Under steady-state motion with frequency ω, the amplitude of the displacement, w, can be separated as

$$w(t) = w\, e^{i\omega t} \qquad (2.2\text{-}2)$$

in which w is the amplitude of the vertical displacement depending on r and z. When Eq. 2.2-2 is substituted into Eq. 2.2-1, the above equation of motion can be rewritten as

$$\eta^2(1 + iD_1)\frac{\partial^2 w}{\partial z^2} + (1 + iD_s)\left(\frac{1}{r}\frac{\partial w}{\partial r} + \frac{\partial^2 w}{\partial r^2}\right) = -\left(\frac{\omega}{V_s}\right)^2 w \qquad (2.2\text{-}3)$$

where

$$\eta = \frac{V_1}{V_s} = \sqrt{\frac{2 - 2\nu}{1 - 2\nu}}$$

$D_1 = \frac{\lambda' + 2\mu'}{\lambda + 2\mu}$ = damping factor associated with the longitudinal wave,

$D_s = \frac{\mu'}{\mu}$ = Damping factor associated with the shear wave,

$V_1 = \sqrt{\frac{\lambda + 2\mu}{\rho}}$ = longitudinal wave velocity,

$V_s = \sqrt{\frac{\mu}{\rho}}$ = shear wave velocity, and

ν = Poisson's ratio.

It should be noted that the above defined damping D_1 and D_s are different from the commonly used definitions in which the damping factors are half of the above defined factors.

Separating the variables in w further, the vertical displacement w can be expressed by

$$w = R(r)\,Z(z) \qquad (2.2\text{-}4)$$

After substituting Eq. 2.2-4 into Eq. 2.2-3, the equation of motion can be written as

$$\eta^2(1 + iD_1)\frac{1}{Z}\frac{\partial^2 Z}{\partial z^2} + (1 + iD_s)\left(\frac{\partial^2 R}{\partial r^2} + \frac{1}{r}\frac{\partial R}{\partial r}\right)\frac{1}{R} = -\left(\frac{\omega}{V_s}\right)^2 \qquad (2.2\text{-}5)$$

This equation can be split into two ordinary differential equations:

$$\frac{d^2 Z}{dz^2} + h^2 Z = 0 \qquad (2.2\text{-}6a)$$

$$\frac{d^2 R}{dr^2} + \frac{1}{r}\frac{dR}{dr} - l^2 R = 0 \qquad (2.2\text{-}6b)$$

where h and l must satisfy the following relationship:

$$l^2 = \frac{\eta^2(1 + iD_1)h^2 - (\omega/V_s)^2}{1 + iD_s} \qquad (2.2\text{-}7)$$

The solutions of Eqs. 2.2-6 are

$$R(r) = A\,K_0(lr) + B\,I_0(lr) \qquad (2.2\text{-}8a)$$

$$Z(z) = C\sin(hz) + D\cos(hz) \qquad (2.2\text{-}8b)$$

where $I_0(lr)$ and $K_0(lr)$ are the modified Bessel functions of the zero-th order of the first and second kinds, respectively, and A, B, C, and D are the constants determined by the boundary conditions. Therefore, the complete solution for w is

$$w = \left[A\, K_0(lr) + B\, I_0(lr)\right]\left[C \sin(hz) + D \cos(hz)\right] \qquad (2.2\text{-}9)$$

The constant B must be zero in order to satisfy the condition that w decays with distance r. Since no horizontal displacement is assumed, zero stress on the top surface of the stratum can never be achieved. The approximate solution can be obtained by selecting D = 0 and $h_n = \frac{\pi}{2H}(2n-1)$ where n is an integer from one to infinity. This approximate solution always yields the shear stress on the top surface of the stratum. However, as shown in Appendix B, the displacement of the pile as obtained by using the approximate solution agrees very well with that obtained by Poulos and Mattes (1969) although they adopted different assumptions and methods of analysis. The displacement amplitude w of the stratum can finally be expressed as

$$w = \sum_{n=1}^{\infty} C_n\, K_0(l_n r)\, \sin(h_n z) \qquad (2.2\text{-}10)$$

where

$$h_n = \frac{\pi}{2H}(2n - 1) \qquad (2.2\text{-}11a)$$

$$l_n = \sqrt{\frac{\eta^2(1 + iD_l)h_n^2 - (\omega/V_s)^2}{1 + iD_s}} \qquad (2.2\text{-}11b)$$

Then the shear stress amplitude τ_{rz} is

$$\tau_{rz} = (\mu + i\mu')\frac{\partial w}{\partial r} = -\mu(1 + iD_s)\sum_{n=1}^{\infty} C_n\, l_n\, K_1(l_n r)\, \sin(h_n z) \qquad (2.2\text{-}12)$$

where $K_1(l_n r)$ is the modified Bessel function of the first order of the second kind.

The displacement amplitude of the stratum at the radius of the pile, W(z), may be expressed from Eq. 2.2-10 as

$$W(z) = w(r=r_0, z) = \sum_{n=1}^{\infty} W_n \sin(h_n z) \tag{2.2-13}$$

where r_0 is the radius of pile and

$$W_n = C_n K_0(l_n r_0) \tag{2.2-14}$$

The soil reaction induced by the displacement W(z) can be obtained by integrating the shear stresses τ_{rz} around the circumference of the pile. Thus, substituting Eq. 2.2-10 into Eq. 2.2-12, and using the relationship in Eq. 2.2-14, the soil reaction $p_v(z)$ is obtained as follows:

$$p_v(z) = -\int_0^{2\pi} \tau_{rz}(r=r_0) r_0 \, d\theta = 2\pi \mu(1 + iD_s) r_0 \sum_{n=1}^{\infty} l_n \frac{K_1(l_n r_0)}{K_0(l_n r_0)} W_n \sin(h_n z) \tag{2.2-15}$$

This expression can be simplified by introducing the parameter α_{vn}, so that

$$p_v(z) = \sum_{n=1}^{\infty} \alpha_{vn} W_n \sin(h_n z) \tag{2.2-16}$$

where

$$\alpha_{vn} = 2\pi\mu r_0(1 + iD_s)l_n \frac{K_1(l_n r_0)}{K_0(l_n r_0)} \tag{2.2-17}$$

Using the dimensionless parameters, the soil reaction $p_v(z)$ in Eqs. 2.2-16 and 2.2-17 can be rewritten as

$$p_v(z) = \pi\mu \sum_{n=1}^{\infty} \bar{\alpha}_{vn} W_n \sin(\bar{h}_n \bar{z}) \tag{2.2-18}$$

where

$$\bar{\alpha}_{vn} = 2\,\bar{l}_n(1 + iD_s) \frac{K_1(\bar{l}_n/\bar{H})}{\bar{H}\,K_0(\bar{l}_n/\bar{H})} \tag{2.2-19}$$

$$\bar{l}_n = Hl_n = \sqrt{\frac{\eta^2(1 + iD_1)\bar{h}_n^2 - a_0^2}{1 + iD_s}} \tag{2.2-20}$$

$$\begin{aligned} \bar{h}_n &= H h_n = \frac{\pi}{2}(2n - 1) \\ a_0 &= \frac{H}{v_s}\omega \\ \bar{H} &= \frac{H}{r_0} \\ \bar{z} &= \frac{z}{H} \end{aligned} \tag{2.2-21}$$

2.2.B Soil Reaction for Horizontal Motion of a Pile

Neglecting a vertical displacement, the equations of horizontal motions of the soil stratum are given by

$$\left\{(\lambda + 2\mu) + i(\lambda' + 2\mu')\right\}\frac{\partial}{\partial r}\Delta(t) - 2(\mu + i\mu')\frac{1}{r}\frac{\partial}{\partial \theta}\omega_z(t)$$

$$= \rho\frac{\partial^2}{\partial t^2}u(t) - (\mu + i\mu')\frac{\partial^2}{\partial z^2}u(t) \qquad (2.2\text{-}22a)$$

$$\left\{(\lambda + 2\mu) + i(\lambda' + 2\mu')\right\}\frac{1}{r}\frac{\partial}{\partial \theta}\Delta(t) + 2(\mu + i\mu')\frac{\partial}{\partial r}\omega_z(t)$$

$$= \rho\frac{\partial^2}{\partial t^2}v(t) - (\mu + i\mu')\frac{\partial^2}{\partial z^2}v(t) \qquad (2.2\text{-}22b)$$

where

$$\Delta(t) = \frac{1}{r}\frac{\partial}{\partial r}\{ru(t)\} + \frac{1}{r}\frac{\partial}{\partial \theta}v(t)$$

$$\omega_z(t) = \frac{1}{2r}\left[\frac{\partial}{\partial r}\{rv(t)\} - \frac{\partial}{\partial \theta}u(t)\right] \qquad (2.2\text{-}23)$$

$u(t)$ = displacement in r coordinate

$v(t)$ = displacement in θ coordinate

Under steady-state motion with frequency ω, the amplitude of the displacements u and v can be separated as

$$u(t) = u\, e^{i\omega t}$$

$$v(t) = v\, e^{i\omega t} \qquad (2.2\text{-}24)$$

in which u and v are the amplitudes of the displacements u(t) and v(t), respectively, and depend on r, z and θ. Substituting Eqs. 2.2-24 into Eqs. 2.2-22, the equations of motion can be rewritten as

$$(\lambda + 2\mu)(1 + iD_1)\frac{\partial \Delta}{\partial r} - 2\mu(1 + iD_s)\frac{1}{r}\frac{\partial \omega_z}{\partial \theta} = -\rho\omega^2 u - \mu(1 + iD_s)\frac{\partial^2 u}{\partial z^2} \tag{2.2-25}$$

$$(\lambda + 2\mu)(1 + iD_1)\frac{1}{r}\frac{\partial \Delta}{\partial \theta} + 2\mu(1 + iD_s)\frac{\partial \omega_z}{\partial r} = -\rho\omega^2 v - \mu(1 + 2D_s)\frac{\partial^2 v}{\partial z^2}$$

Let the potential functions ϕ and ψ be defined as

$$u = \frac{\partial \phi}{\partial r} + \frac{1}{r}\frac{\partial \psi}{\partial \theta} \tag{2.2-26}$$

$$v = \frac{1}{r}\frac{\partial \phi}{\partial \theta} - \frac{\partial \psi}{\partial r}$$

where ϕ and ψ are related to the longitudinal and shear waves, respectively. Expressing Eqs. 2.2-22 with the above defined potential functions, the following decoupled equations are derived:

$$\eta^2(1 + iD_1)\nabla^2\phi + \left\{(1 + iD_s)\frac{\partial^2}{\partial z^2} + \left(\frac{\omega}{v_s}\right)^2\right\}\phi = 0 \tag{2.2-27a}$$

$$\nabla^2\psi + \left\{(1 + iD_s)\frac{\partial^2}{\partial z^2} + \left(\frac{\omega}{v_s}\right)^2\right\}\psi = 0 \tag{2.2-27b}$$

where

$$\nabla^2 = \frac{\partial^2}{\partial r^2} + \frac{1}{r}\frac{\partial}{\partial r} + \frac{1}{r^2}\frac{\partial^2}{\partial \theta^2} \tag{2.2-28}$$

Separating the variables, the potential function ϕ can be rewritten as

$$\phi = R(r)\,\Theta(\theta)\,Z(z) \tag{2.2-29}$$

Substituting ϕ in Eq. 2.2-29 into Eq. 2.2-27a and dividing by $R\cdot\Theta\cdot Z$ leads to

$$\eta^2(1 + iD_1)\left(\frac{1}{R}\frac{\partial^2 R}{\partial r^2} + \frac{1}{r}\frac{1}{R}\frac{\partial R}{\partial r} + \frac{1}{r^2}\frac{1}{\Theta}\frac{\partial^2\Theta}{\partial\theta^2}\right) + (1 + iD_s)\frac{1}{Z}\frac{\partial^2 Z}{\partial z^2} + \left(\frac{\omega}{v_s}\right)^2 = 0 \qquad (2.2\text{-}30)$$

Eq. 2.2-30 can be split into the following three ordinary differential equations:

$$\frac{1}{R}\frac{d^2R}{dr^2} + \frac{1}{r}\frac{1}{R}\frac{dR}{dr} - \frac{m^2}{r^2} = q^2 \qquad (2.2\text{-}31a)$$

$$\frac{1}{Z}\frac{d^2Z}{dz^2} = -h^2 \qquad (2.2\text{-}31b)$$

$$\frac{1}{\Theta}\frac{d^2\Theta}{d\theta^2} = -m^2 \qquad (2.2\text{-}31c)$$

where h and q must satisfy the relationship

$$q = \sqrt{\frac{(1 + iD_s)h^2 - \left(\frac{\omega}{v_s}\right)^2}{\eta^2(1 + iD_1)}} \qquad (2.2\text{-}32)$$

The solutions for Eqs. 2.2-31 are

$$R = A_1 K_m(qr) + B_1 I_m(qr) \qquad (2.2\text{-}33a)$$

$$Z = A_2 \sin(hz) + B_2 \cos(hz) \qquad (2.2\text{-}33b)$$

$$\Theta = A_3 \sin(m\theta) + B_3 \cos(m\theta) \tag{2.2-33c}$$

where $I_m(qr)$ and $K_m(qr)$ are the modified Bessel functions of the m-th order of the first and second kinds, respectively, and A and B are constants determined by the boundary conditions. Therefore, the complete solution for ϕ is

$$\phi = \left\{A_1 K_m(qr) + B_1 I_m(qr)\right\}\left\{A_2 \sin(hz) + B_2 \cos(hz)\right\} \times \left\{A_3 \sin(m\theta) + B_3 \cos(m\theta)\right\} \tag{2.2-34}$$

Following a process similar to that used for ϕ, the solution of Eq. 2.2-27b for ψ can be derived and is

$$\psi = \left\{A_4 K_m(sr) + B_4 I_m(sr)\right\}\left\{A_5 \sin(hz) + B_5 \cos(hz)\right\} \times \left\{A_6 \sin(m\theta) + B_6 \cos(m\theta)\right\} \tag{2.2-35}$$

where A and B are the constants determined by the boundary conditions and s is

$$s = \sqrt{\frac{(1 + iD_s)h^2 - \left(\frac{\omega}{v_s}\right)^2}{1 + iD_s}} \tag{2.2-36}$$

Then the displacements and stresses in the stratum can be obtained by using the following relationships:

$$u = \frac{\partial \phi}{\partial r} + \frac{1}{r}\frac{\partial \psi}{\partial \theta}$$

$$v = \frac{1}{r}\frac{\partial \phi}{\partial \theta} - \frac{\partial \psi}{\partial r}$$

$$\sigma_r = \left\{(\lambda + 2\mu) + i(\lambda' + 2\mu')\right\}\nabla^2\phi - 2(\mu + i\mu')\left(\frac{1}{r}\frac{\partial \phi}{\partial r} + \frac{1}{r^2}\frac{\partial^2 \phi}{\partial \theta^2} - \frac{1}{r}\frac{\partial^2 \psi}{\partial r \partial \theta} + \frac{1}{r^2}\frac{\partial \psi}{\partial \theta}\right)$$

$$\sigma_z = (\lambda + i\lambda')\nabla^2\phi + 2(\mu + i\mu')\frac{\partial^2 \phi}{\partial z^2} \qquad (2.2\text{-}37)$$

$$\tau_{r\theta} = (\mu + i\mu')\left(-\frac{1}{r^2}\frac{\partial \phi}{\partial \theta} + \frac{2}{r}\frac{\partial^2 \phi}{\partial r \partial \theta} + \frac{\partial^2 \phi}{\partial r^2} + \frac{1}{r}\frac{\partial \psi}{\partial r}\right) + \frac{1}{r^2}\frac{\partial^2 \psi}{\partial \theta^2}$$

$$\tau_{rz} = (\mu + i\mu')\left\{2\frac{\partial^2 \phi}{\partial r \partial z} + \frac{\partial^2 \psi}{\partial \theta \partial z}\right\}$$

$$\tau_{\theta z} = (\mu + i\mu')\left(\frac{2}{r}\frac{\partial^2 \phi}{\partial \theta \partial z} - \frac{\partial^2 \psi}{\partial r \partial z}\right)$$

The constants B_1 and B_4 must be zero in order to satisfy the condition that the stresses and displacements decay with r. Since no vertical displacement is allowed, zero stresses on the top surface of the stratum can never be achieved. The approximate solution can be obtained by selecting $B_2 = B_5 = 0$ and $h = \frac{\pi}{2H}(2n - 1)$ where n is an integer from one to infinity. This approximate solution always yields the normal stress σ_z on the top surface of the stratum. However, as shown in Appendix B, such an approximate solution gives satisfactory

results. The loading condition in which a horizontal displacement $U(z)\, e^{i\omega t}$ is applied around the circumference of the pile ($r = r_0$), further calls for $m = 1$, $A_3 = B_6 = 0$ and

$$u(r = r_0,\ \theta = 0,\ z) = U(z)$$

$$v(r = r_0,\ \theta = \frac{\pi}{2},\ z) = -U(z) \qquad (2.2\text{-}38)$$

Therefore, the potential functions ϕ and ψ can be finally written as

$$\phi = \cos\theta \sum_{n=1}^{\infty} A_n\, K_1(q_n r)\, \sin(h_n z) \qquad (2.2\text{-}39a)$$

$$\psi = \sin\theta \sum_{n=1}^{\infty} B_n\, K_1(s_n r)\, \sin(h_n z) \qquad (2.2\text{-}39b)$$

where the constants A_n and B_n must further satisfy the conditions in Eqs. 2.2-38, and

$$h_n = \frac{\pi}{2H}(2n-1)$$

$$q_n = \sqrt{\frac{(1 + iD_s)h_n^2 - \left(\frac{\omega}{v_s}\right)^2}{\eta^2(1 + iD_1)}} \qquad (2.2\text{-}40)$$

$$s_n = \sqrt{\frac{(1 + iD_s)h_n^2 - \left(\frac{\omega}{v_s}\right)^2}{1 + iD_s}}$$

Substituting the above obtained potential functions into Eqs. 2.2-37, the displacements u and v and the stresses σ_r and $\tau_{r\theta}$ can be expressed with the constants A_n and B_n as

$$u = \cos\theta \sum_{n=1}^{\infty} \sin(h_n z) \left[- A_n \left\{ \frac{1}{r} K_1(q_n r) + q_n K_0(q_n r) \right\} + B_n \frac{1}{r} K_1(s_n r) \right] \tag{2.2-41a}$$

$$v = \sin\theta \sum_{n=1}^{\infty} \sin(h_n z) \left[- A_n \frac{1}{r} K_1(q_n r) + B_n \left\{ \frac{1}{r} K_1(s_n r) + s_n K_0(s_n r) \right\} \right] \tag{2.2-41b}$$

$$\sigma_r = \cos\theta \sum_{n=1}^{\infty} \sin(h_n z) \left[A_n (\lambda + 2\mu)(1 + iD_1) q_n^2 K_1(q_n r) + 2 A_n \mu (1 + iD_s) \left\{ 2 \frac{q_n}{r} K_0(q_n r) + \frac{1}{r^2} K_1(q_n r) \right\} - 2 B_n \mu (1 + iD_s) \left\{ 2 \frac{s_n}{r} K_0(s_n r) + \frac{1}{r^2} K_1(s_n r) \right\} \right] \tag{2.2-41c}$$

$$\tau_{r\theta} = \sin\theta \sum_{n=1}^{\infty} \sin(h_n z) \mu (1 + iD_s) \left[A_n 4 \left\{ \frac{q_n}{r} K_0(q_n r) + \frac{2}{r^2} K_1(q_n r) \right\} + B_n \left\{ s_n^2 K_1(s_n r) + 4 \frac{s_n}{r} K_0(s_n r) + \frac{2}{r^2} K_1(s_n r) \right\} \right] \tag{2.2-41d}$$

Substituting u and v in Eqs. 2.2-41 into Eqs. 2.2-38, the condition expressed by Eqs. 2.2-38 can be rewritten as

$$\sum_{n=1}^{\infty}\left[-A_n\left\{\frac{1}{r_0}K_1(q_n r_0) + q_n K_0(q_n r_0)\right\} + B_n\frac{1}{r_0}K_1(s_n r_0)\right]\sin(h_n z) \qquad (2.2\text{-}42a)$$

$$= U(z)$$

$$\sum_{n=1}^{\infty}\left[-A_n\left\{\frac{1}{r_0}K_1(q_n r_0)\right\} + B_n\left\{\frac{1}{r_0}K_1(s_n r_0) + s_n K_0(s_n r_0)\right\}\right]\sin(h_n z) \qquad (2.2\text{-}42b)$$

$$= -U(z)$$

In the above, U(z) can also be written from the expressions in Eqs. 2.2-41a and 2.2-41b as

$$U(z) = \sum_{n=1}^{\infty} U_n \sin(h_n z) \qquad (2.2\text{-}43)$$

Substituting Eq. 2.2-43 into Eqs. 2.2-42 and solving for A_n and B_n, the constants A_n and B_n are obtained as

$$A_n = -\frac{2K_1(s_n r_0) + s_n r_0 K_0(s_n r_0)}{q_n K_0(q_n r_0)K_1(s_n r_0) + s_n K_1(q_n r_0)K_0(s_n r_0) + q_n s_n r_0 K_0(q_n r_0)K_0(s_n r_0)}\,U_n \qquad (2.2\text{-}44a)$$

$$B_n = -\frac{2K_1(q_n r_0) + q_n r_0 K_0(q_n r_0)}{q_n K_0(q_n r_0)K_1(s_n r_0) + s_n K_1(q_n r_0)K_0(s_n r_0) + q_n s_n r_0 K_0(q_n r_0)K_0(s_n r_0)}\,U_n \qquad (2.2\text{-}44b)$$

Horizontal reaction of the stratum $p_h(z)e^{i\omega t}$ resulting from the displacement $U(z)e^{i\omega t}$ is

$$p_h(z) = -\int_0^{2\pi} \left\{\sigma_r(r=r_0)\cos\theta - \tau_{r\theta}(r=r_0)\sin\theta\right\} r_0 d\theta \qquad (2.2\text{-}45)$$

Substituting σ_r and $\tau_{r\theta}$ in Eqs. 2.2-41 into Eq. 2.2-45 together with the above obtained constants A_n and B_n, the horizontal soil reaction $p_h(z)$ is obtained as

$$p_h(z) = \pi\mu r_0 \sum_{n=1}^{\infty} \left\{(1 + iD_s)h_n^2 - \left(\frac{\omega}{v_s}\right)^2\right\} T_n U_n \sin(h_n z) \qquad (2.2\text{-}46a)$$

where

$$T_n = \frac{4K_1(q_n r_0)K_1(s_n r_0) + s_n r_0 K_1(q_n r_0)K_0(s_n r_0) + q_n r_0 K_0(q_n r_0)K_1(s_n r_0)}{q_n K_0(q_n r_0)K_1(s_n r_0) + s_n K_1(q_n r_0)K_0(s_n r_0) + q_n s_n r_0 K_0(q_n r_0)K_0(s_n r_0)} \qquad (2.2\text{-}46b)$$

Eq. 2.2-46a can be simplified by introducing the parameter α_{hn} as

$$p_h(z) = \sum_{n=1}^{\infty} \alpha_{hn} U_n \sin h_n z \qquad (2.2\text{-}47)$$

$$\alpha_{hn} = \pi\mu r_0 \left\{(1 + iD_s)h_n^2 - \left(\frac{\omega}{v_s}\right)^2\right\} T_n \qquad (2.2\text{-}48)$$

Using the dimensionless parameters, the soil reaction $p_h(z)$ can be rewritten as

$$p_h(\bar{z}) = \pi\mu \sum_{n=1}^{\infty} \bar{\alpha}_{hn} \bar{U}_n \sin(\bar{h}_n \bar{z}) \qquad (2.2\text{-}49)$$

where

$$\bar{\alpha}_{hn} = \left\{ \bar{T}_n (1 + iD_s)\bar{h}_n^2 - a_0^2/\bar{H} \right\} \qquad (2.2\text{-}50a)$$

$$\bar{T}_n = \frac{T_n}{H}$$

$$= \frac{4\bar{H}K_1(\bar{q}_n/\bar{H})K_1(\bar{s}_n/\bar{H}) + \bar{s}_n K_1(\bar{q}_n/\bar{H})K_0(\bar{s}_n/\bar{H}) + \bar{q}_n K_0(\bar{q}_n/\bar{H})K_1(\bar{s}_n/\bar{H})}{\bar{H}\bar{q}_n K_0(\bar{q}_n/\bar{H})K_1(\bar{s}_n/\bar{H}) + \bar{H}\bar{s}_n K_1(\bar{q}_n/\bar{H})K_0(\bar{s}_n/\bar{H}) + \bar{q}_n\bar{s}_n K_0(\bar{q}_n/\bar{H})K_0(\bar{s}_n/\bar{H})} \qquad (2.2\text{-}50b)$$

$$\bar{q}_n = Hq_n = \sqrt{\frac{(1 + iD_s)\bar{h}_n^2 - a_0^2}{\eta^2(1 + iD_1)}} \qquad (2.2\text{-}50c)$$

$$\bar{s}_n = Hs_n = \sqrt{(1 + iD_s)\bar{h}_n^2 - a_0^2} \qquad (2.2\text{-}50d)$$

In addition to the frequency parameter a_0, another frequency parameter a_0' is defined as

$$a_0' = \frac{r_0}{v_s}\omega \qquad (2.2\text{-}51a)$$

which has the following relationship with a_0:

$$a_0' = \frac{a_0}{\bar{H}} \qquad (2.2\text{-}51b)$$

2.3 Characteristics of Soil Reactions to Harmonic Motions of a Pile

The dynamic response of a pile forms waves in the stratum. The displacements and stresses in the stratum result from those induced by each wave. The wave pattern of each wave along the depth forms the mode shape of the stratum which satisfies the boundary condition at the top and bottom of the stratum. The parameter α_n is interpreted as a modal force amplitude to yield a unit displacement amplitude of the n-th mode at the circumference of the pile. Therefore, this parameter is viewed as stiffness of the stratum associated with the n-th mode wave and is called "resistance factor."

The resistance factor is generally written in terms of a complex number; the real part expresses the stiffness for the spring function of the stratum and the imaginary part does the intensity of damping for the damping function of the stratum. The spring and damping functions of the stratum are governed by the nature of the wave propagation in the stratum.

2.3.A Nature of Wave Propagation in Stratum

In this paragraph, the stratum is further simplified and assumed to have no material damping. Then 1_n in Eq. 2.2-11b for this case is

$$1_n = \sqrt{n^2 h_n^2 - \left(\frac{\omega}{v_s}\right)^2} \qquad (2.3\text{-}1)$$

When the excitation frequency ω is larger than $v_1 h_n$, the inside of the square root is negative. Then, the displacement w for n=n in Eq. 2.2-10, w_n, is rewritten as

$$w_n = C_n \sin(h_n z) H_0^2(l_n r)$$

where $H_0^2(l_n r)$ is the Hankel function of the second kind of the order zero and l_n is

$$l_n = \sqrt{\left(\frac{\omega}{v_s}\right)^2 - n^2 h_n^2} \qquad (2.3\text{-}2)$$

The displacement $w_n(t)$ is expressed from the above expression for w_n as

$$w_n(t) = w_n \sin(\omega t)$$

$$= \frac{C_n}{2} \cos\left(\omega t - \frac{2\pi}{L_{zn}} z\right) H_0^2\left(\frac{2\pi}{L_{rn}} r\right) - \frac{C_n}{2} \cos\left(\omega t + \frac{2\pi}{L_{zn}} z\right) H_0^2\left(\frac{2\pi}{L_{rz}} r\right) \qquad (2.3\text{-}3)$$

where

$$L_{zn} = \frac{2\pi}{h_n} \qquad (2.3\text{-}4a)$$

$$L_{rn} = \frac{2\pi}{l_n} \qquad (2.3\text{-}4b)$$

Eq. 2.3-3 shows that the n-th mode wave progresses in the radial direction reflecting successively at the top and bottom of the stratum. Such n-th mode wave propagation forms the wave patterns in vertical and horizontal directions. Those wave patterns are called the secondary waves, which consist of the progressive waves for the horizontal wave pattern and the standing waves for the vertical wave pattern. The wave lengths of the standing and progressive waves are given by L_{zn} and L_{rn}, respectively, and are shown in Fig. 2.3-1.

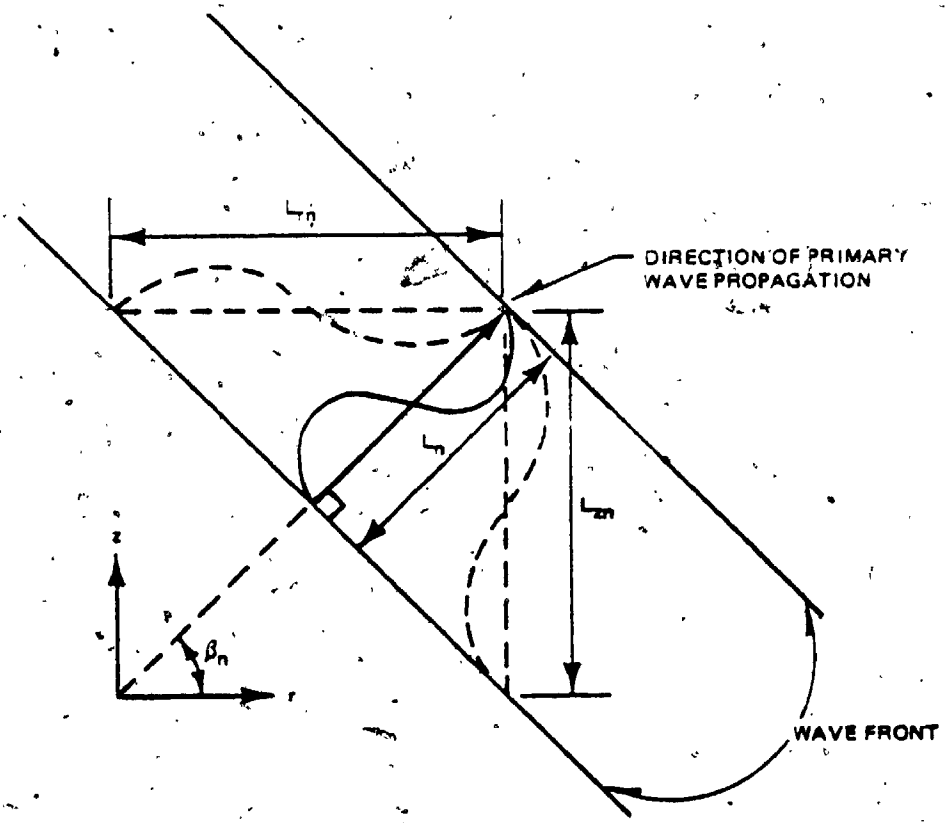

Fig. 2.3-1. Primary Wave and Secondary Waves

The wave length of the n-th mode primary wave, L_n, can be obtained from the geometry shown in Fig. 2.3-1, and is

$$L_n = \frac{2\pi}{\sqrt{\left(\frac{\omega}{v_s}\right)^2 + h_n^2(1-\eta^2)}} \qquad (2.3\text{-}5a)$$

Using previously defined dimensionless parameters, Eq. 2.3-5a can be rewritten as

$$L_n = \frac{2\pi H}{\sqrt{a_0^2 + \bar{h}_n^2(1-\eta^2)}} \qquad (2.3\text{-}5b)$$

Then the direction of the ray path of the n-th mode wave, $\pm\beta_n$, is obtained from the equation

$$\cos\beta_n = \frac{L_n}{L_{rn}} = \frac{\sqrt{\left(\frac{\omega}{v_s}\right)^2 - \eta^2 h_n^2}}{\sqrt{\left(\frac{\omega}{v_s}\right)^2 + h_n^2(1-\eta^2)}} = \frac{\sqrt{a_0^2 - \eta^2 \bar{h}_n^2}}{\sqrt{a_0^2 + \bar{h}_n^2(1-\eta^2)}} \qquad (2.3\text{-}6)$$

When the frequency a_0 is equal to $\eta\bar{h}_n$, the n-th mode primary wave propagates in the vertical direction. Then the n-th primary wave is identical to the n-th standing wave and its wave length is

$$L_n = \frac{4H}{2n-1} \qquad (2.3\text{-}7)$$

Under this situation, the energy in the stratum is built up to infinity by successive reflections at the top and bottom of the stratum. This

condition is called resonance and the frequencies at which this condition occurs are called the natural frequencies for undamped system. Therefore, the natural frequencies for the vertical vibration of the stratum are

$$a_0 = n\bar{h}_n \qquad n = 1, 2, \ldots, \infty$$

As the excitation frequency increases from the n-th natural frequency, the n-th primary wave propagates more horizontally. When the frequency is well higher than this natural frequency, the progressive wave is nearly identical to the primary wave. Under this high frequency, the wave length of the primary wave is nearly equal to $2\pi v_s/\omega$ which is the wave length of the shear wave.

When the excitation frequency is lower than the n-th natural frequency, Eq. 2.3-3 can be rewritten as

$$w_n(t) = \frac{C_n}{2}\cos\left(\omega t - \frac{2\pi}{L_{zn}}z\right)K_0(l_n r) - \frac{C_n}{2}\cos\left(\omega t + \frac{2\pi}{L_{zn}}z\right)K_0(l_n r) \tag{2.3-8}$$

Eq. 2.3-8 shows that the n-th mode wave does not radiate horizontally and the displacement w_n is in phase along the horizontal plane. In this case, the progressive wave does not appear but the standing wave does. However, when the stratum has material damping, the progressive wave appears slightly even in this frequency range (Kobori, Minai and Suzuki, 1971).

In horizontal vibration, mutually independent solutions for the potential functions ϕ and ψ are derived. The waves associated with those potential functions ϕ and ψ are respectively called ϕ and ψ waves here: The ψ wave is identical to the shear wave. The expressions

for ϕ and ψ in Eqs. 2.2-39 can be rewritten in a similar form as that for w in Eq. 2.3-3, and the same arguments as those given for the vertical vibration are still valid for the ϕ and ψ waves.

Following a procedure similar to that used for vertical vibration, the wave lengths and the directions of the ray path of the n-th mode primary waves are found.

ϕ wave

$$L_n = \frac{2\pi}{\sqrt{\left(\frac{\omega}{v_1}\right)^2 + h_n^2\left(1 - \frac{1}{\eta^2}\right)}} = \frac{2\pi\eta H}{\sqrt{a_0^2 + \bar{h}_n^2(\eta^2 - 1)}} \qquad (2.3\text{-}9a)$$

$$\cos\beta_n = \frac{\sqrt{\left(\frac{\omega}{v_1}\right)^2 - h_n^2\frac{1}{\eta^2}}}{\sqrt{\left(\frac{\omega}{v_1}\right)^2 + h_n^2\left(1 - \frac{1}{\eta^2}\right)}} = \frac{\sqrt{a_0^2 - \bar{h}_n^2}}{\sqrt{a_0^2 + \bar{h}_n^2(\eta^2 - 1)}} \qquad (2.3\text{-}9b)$$

ψ wave

$$L_n = \frac{2\pi}{\frac{\omega}{v_s}} = \frac{2\pi H}{a_0} \qquad (2.3\text{-}10a)$$

$$\cos\beta_n = \frac{\sqrt{\left(\frac{\omega}{v_s}\right)^2 - h_n^2}}{\frac{\omega}{v_s}} = \frac{\sqrt{a_0^2 - \bar{h}_n^2}}{a_0} \qquad (2.3\text{-}10b)$$

From those expressions, the natural frequencies are obtained

$$a_0 = \bar{h}_n \qquad , n = 1, 2, \ldots, \infty$$

At the high frequencies ($a_0 >> \bar{h}_n^2(n^2-1)$), the ϕ wave is nearly identical to the longitudinal wave. Under this situation, its wave length is nearly the same as that of the longitudinal wave.

The frequency parameters a_0 and a_0' can be rewritten as

$$a_0 = \frac{1}{2\pi}\frac{H}{L_s} \tag{2.3-11a}$$

$$a_0' = \frac{1}{2\pi}\frac{r_0}{L_s} \tag{2.3-11b}$$

where L_s is the wave length of the shear wave and is

$$L_s = \frac{2\pi v_s}{\omega} \tag{2.3-12}$$

Therefore, the frequency parameters a_0 and a_0' are concerned with the shear wave length relative to the thickness of the stratum and the radius of the pile, respectively.

2.3.B Characteristics of Soil Reactions

The explicit solutions for the soil resistance factors in Eqs. 2.2-19 and 2.2-50 show that the spring and damping functions of the stratum affecting the dynamic behavior of the pile depend on the relative thickness ($\bar{H}$), material damping (D_1, D_s), shear modulus (μ), Poisson's ratio (ν), wave mode number (n) and excitation frequency (a_0).

In the following paragraphs, the effect of those parameters on the spring and damping functions of the stratum will be examined in

terms of the resistance factor. The material damping parameters are assumed to be $D_l = D_s$; the following definitions of frequency are used.

1. Natural frequency is the natural frequency which is associated with the specific mode under discussion.
2. Low frequency range is the frequency range lower than the above defined natural frequency.
3. High frequency range is the frequency range higher than the above defined natural frequency.

(i) Frequency and Wave Mode Number

Figs. 2.3-2 show the variation of the resistance factors $\bar{\alpha}_v$ and $\bar{\alpha}_h$ with frequency. In these figures, the characteristics of the relationship between soil reaction and frequency may be classified into those in the low, resonant, and high frequency ranges.

In the low frequency range, very little of the progressive wave is generated in the stratum. Therefore the damping is mostly caused by the material damping and is nearly frequency independent. In this frequency range, the characteristics of the standing wave appear strongly. The characteristics of this wave are governed by the wave length of the standing wave relative to the thickness of the stratum, which is governed by the wave mode number under a given frequency. Therefore the stiffness in the low frequency range is significantly affected by the mode number. Figs. 2.3-2 indicate that the stiffness increases with mode number. As shown in Fig. 2.3-3, such an increase is more rapid for a thinner stratum (relative to the radius of the pile) and for vertical vibration than horizontal vibration.

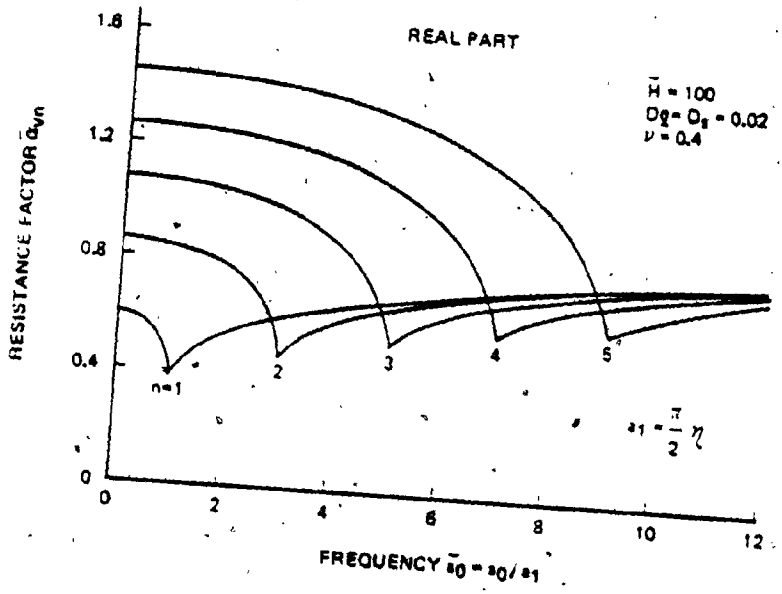

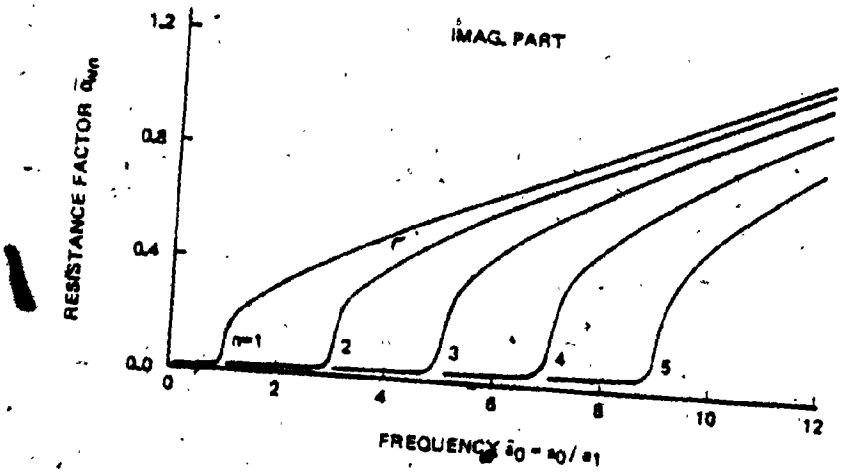

Fig. 2.3-2a. Resistance Factor $\bar{\alpha}_{yn}$ for Various Modes (Vertical Vibration)

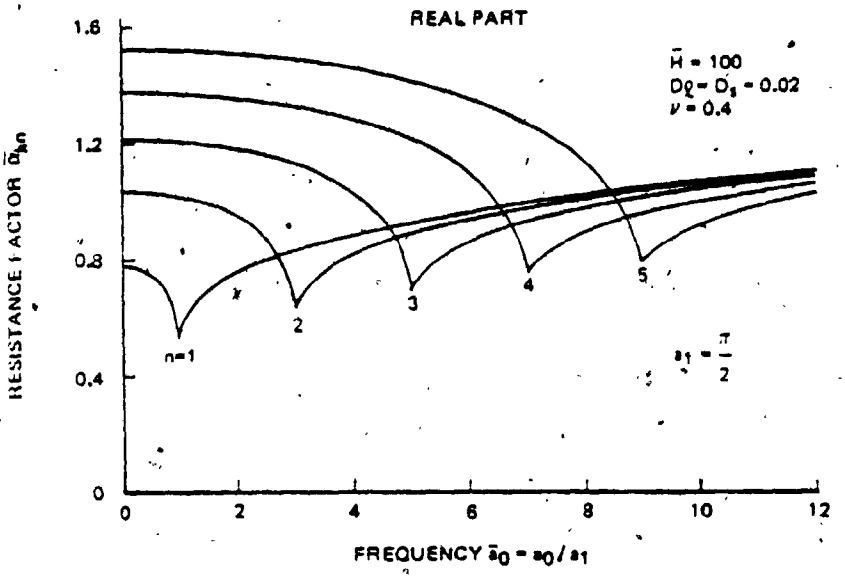

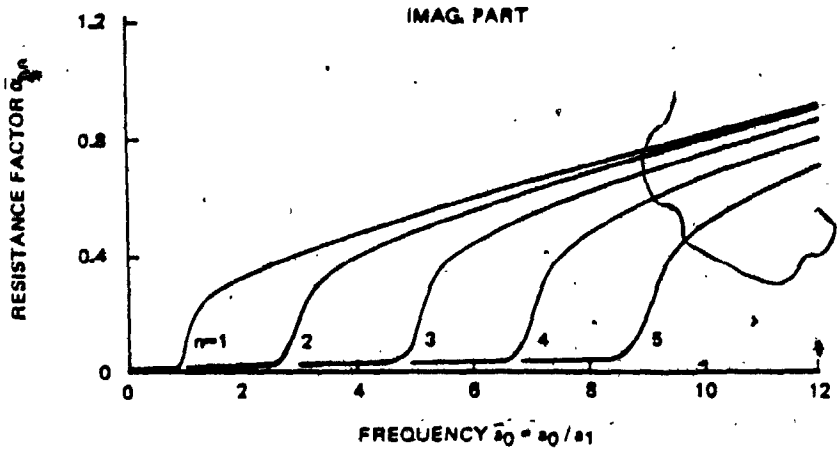

Fig. 2.3-2b. Resistance Factor $\bar{\alpha}_{hn}$ for Various Modes (Horizontal Vibration)

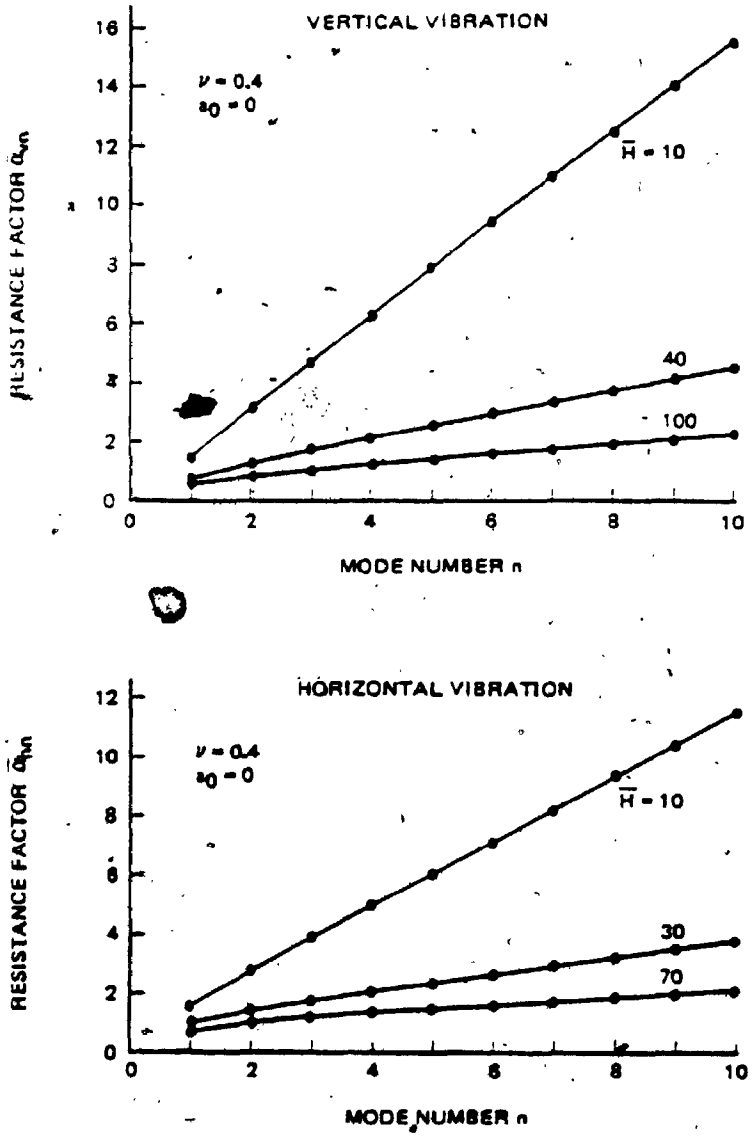

Fig. 2.3-3. Variation of Static Resistance Factor $\bar{\alpha}_n$ with Mode Number n

When excitation frequency is around the resonant frequency of the stratum, the intensity of the progressive wave suddenly increases. This accompanies a sharp increase of the damping and drop of the stiffness as shown in Figs. 2.3-2.

As the excitation frequency increases further, the primary wave propagates more horizontally and the effect of the standing wave tends to diminish. Thus the wave length of the progressive wave approaches that of the primary wave which is nearly or completely independent of the mode number in this frequency range. This situation results in reducing the dependence of the soil resistance on the mode number as shown in Figs. 2.3-2. Since the wave length of the primary wave relative to the radius of the pile affects the behavior of the horizontally propagating primary wave, it may be more convenient to use the frequency parameter a_0' in this high frequency range.

(ii) Relative Thickness of Stratum

Frequency-dependent spring and damping functions of the stratum are shown in Figs. 2.3-4 and 2.3-5 for various thicknesses $\bar{H}$. As can be seen in those figures, the spring function of the stratum is significantly affected by the thickness $\bar{H}$ in the low frequency range; the static case is further shown in Fig. 2.3-6. Fig. 2.3-6 indicates that the stiffness in the higher mode wave is more affected by the thickness $\bar{H}$.

The comparison of the previously obtained soil resistance factors $\bar{\alpha}_{vn}$ and $\bar{\alpha}_{hn}$ with those for the plane strain case indicates that, as the frequency increases above the resonant frequency of the stratum, the primary waves become closer to those for the plane strain case and also

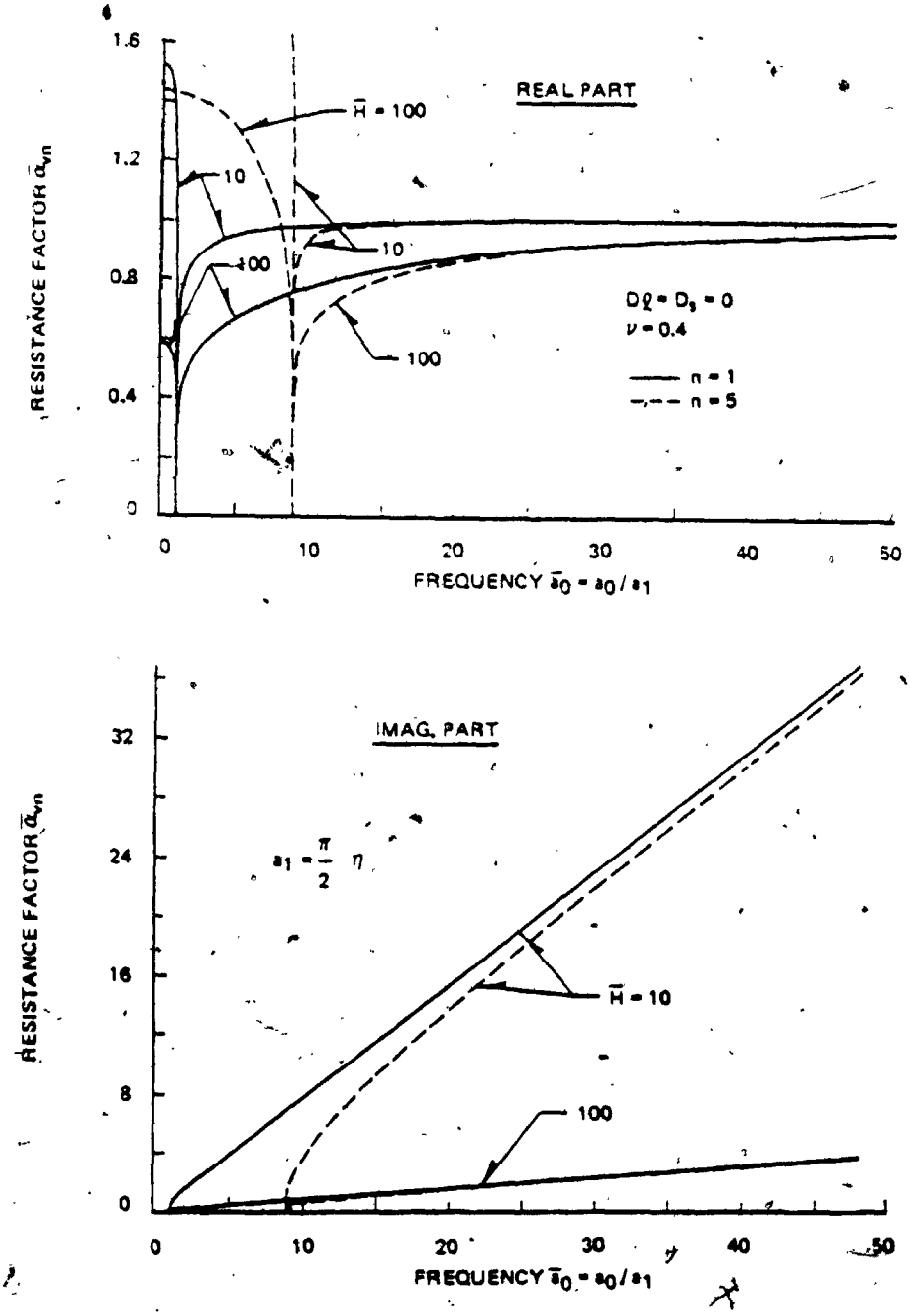

Fig. 2.3-4a. Variation of Resistance Factor $\bar{\alpha}_{vn}$ with Frequency a_0 for Various Relative Thickness Ratios of Stratum (Vertical Vibration)

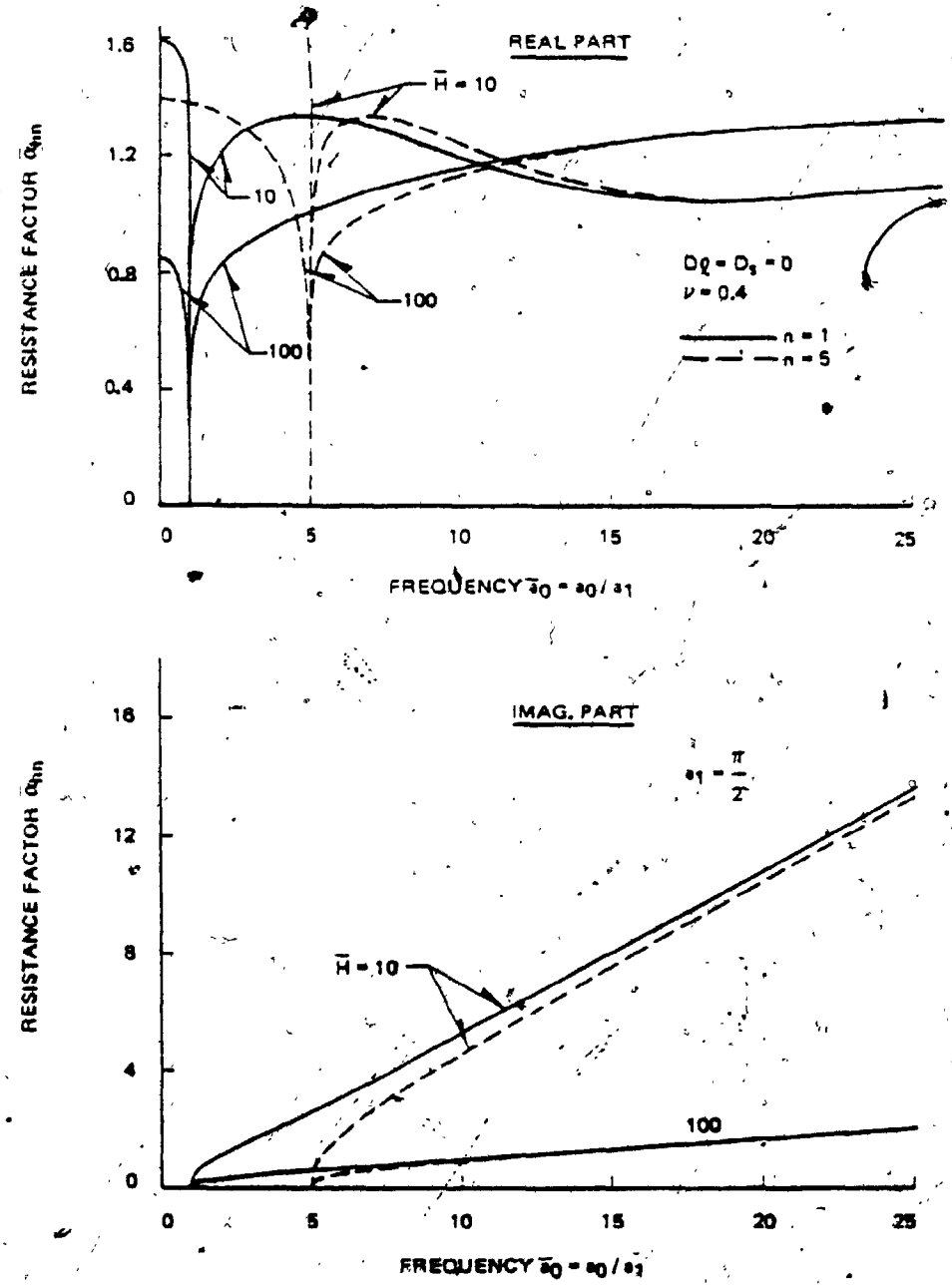

Fig. 2.3-4b. Variation of Resistance Factor $\bar{\alpha}_{hn}$ with Frequency a_0 for Various Relative Thickness Ratios of Stratum (Horizontal Vibration)

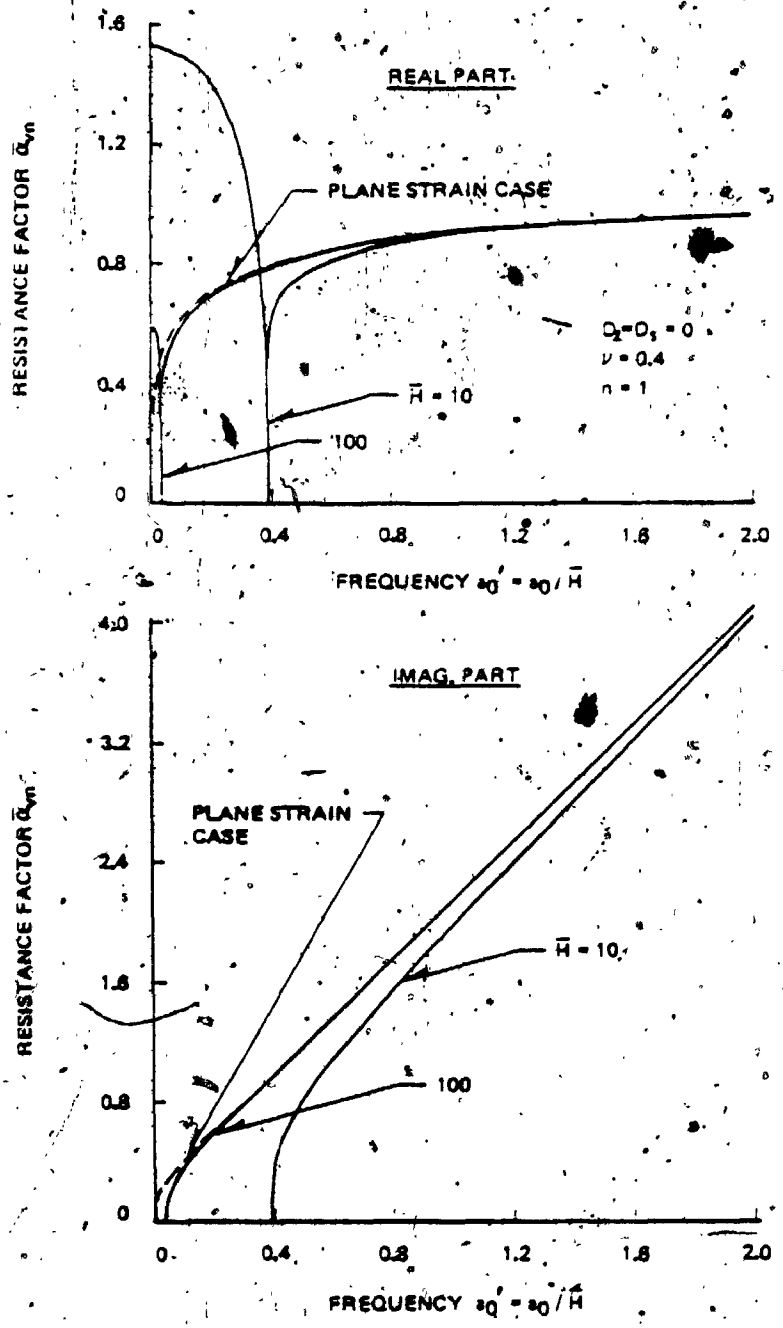

Fig. 2.3-5a. Variation of Resistance Factor $\bar{\alpha}_{vn}$ with Frequency a_0' for Various Relative Thickness Ratios of Stratum (Vertical Vibration)

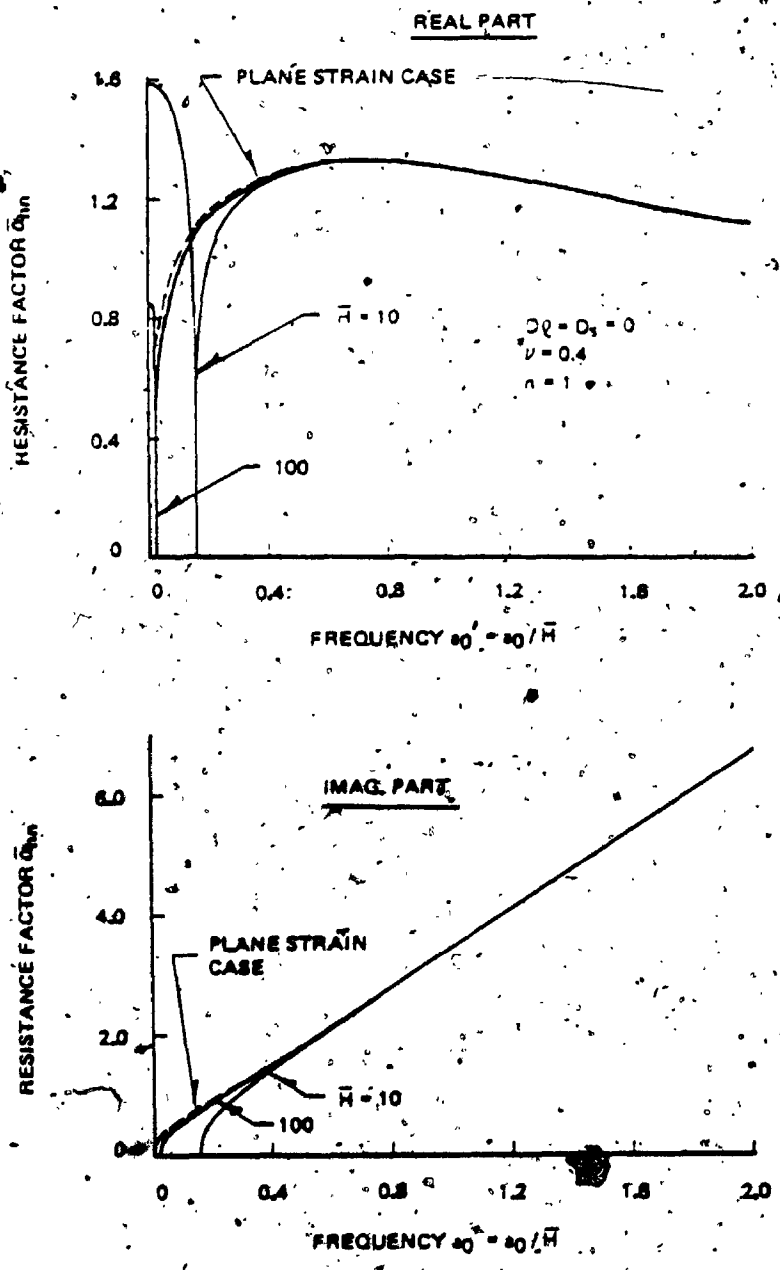

Fig. 2.3-5b. Variation of Resistance Factor $\bar{\alpha}_{hn}$ with Frequency a_0' for Various Relative Thickness Ratios of Stratum (Horizontal Vibration)

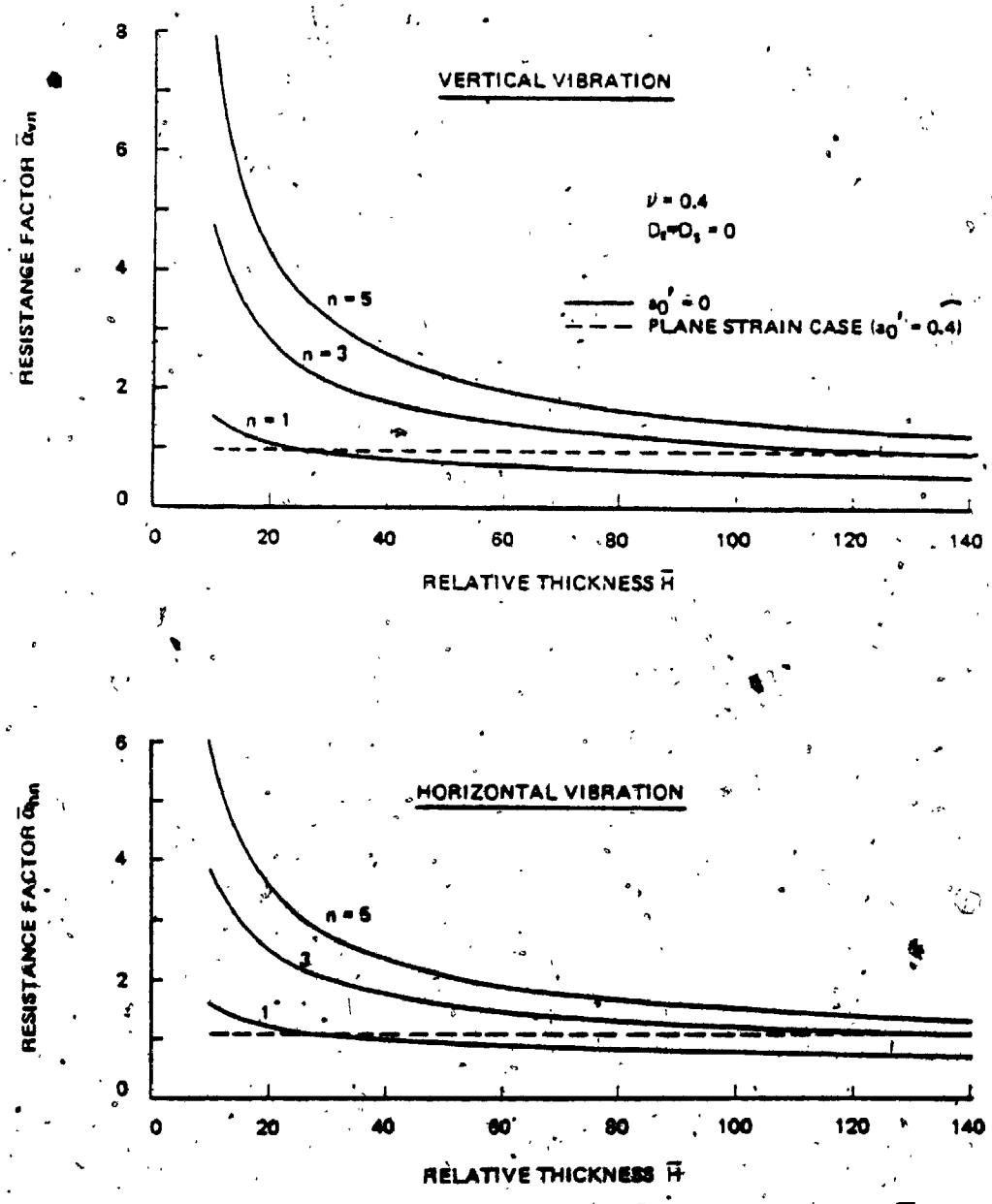

Fig. 2.3-6. Variation of Real Part of Resistance Factor $\bar{\alpha}_n$ with Relative Thickness of Stratum

propagate more horizontally. The plane strain case referred to here is defined in Appendix C and yields the wave propagation in only the horizontal direction no matter what the excitation frequency is. As the primary waves propagate more horizontally, the behavior of the stratum is governed more by the wave length of the primary wave relative to the radius r_0 but less by the wave length relative to the thickness of the stratum. Thus, as the excitation frequency increases in the high frequency range, the stiffness and damping become less dependent on the thickness $\bar{H}$ and rapidly converge to those for the plane strain case as shown in Figs. 2.3-5.

At the resonant frequency of the undamped stratum, the primary wave propagates in a vertical direction and the wave length relative to the thickness of the stratum determines the resonance. Therefore, as shown in Figs. 2.3-4, the n-th undamped resonance appears at the constant ratio between the thickness of the stratum and the wave length of the primary wave: $n\bar{h}_n/(2\pi)$ for vertical vibration and $\bar{h}_n/(2\pi)$ for horizontal vibration.

(iii) Material Damping

Figs. 2.3-7 and 2.3-8 show the variation of the soil reaction with frequency for both presence and absence of the material damping in the stratum. In the low frequency range, it can be seen in those figures that the material damping affects the damping function of the stratum but little does the spring function. The material damping generates the damping although no damping appears in the elastic stratum. This generated damping results mostly from the material damping and varies very little with frequency.

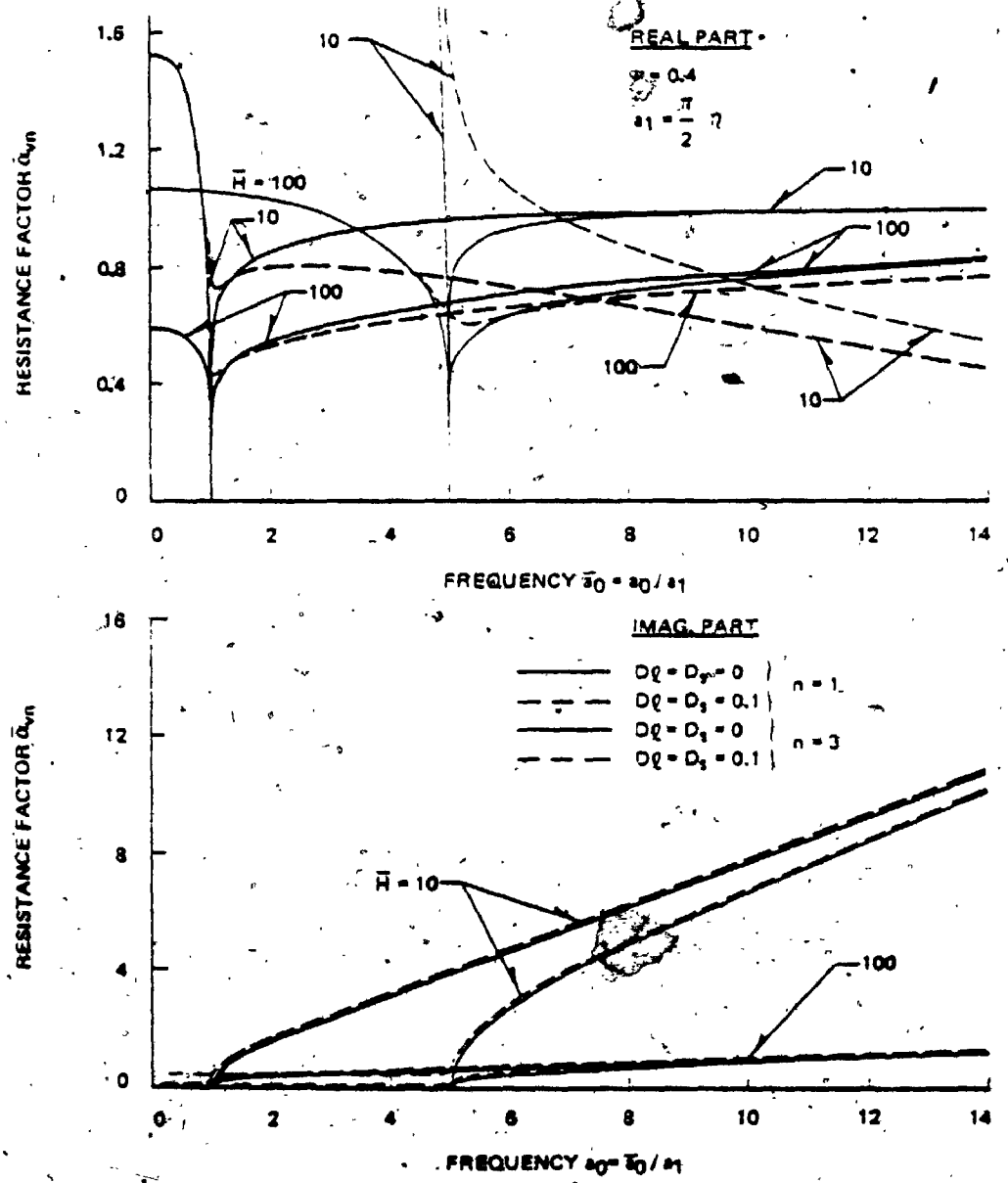

Fig. 2.3-7a. Variation of Resistance Factor $\bar{\alpha}_{vn}$ with Frequency $\bar{a}_0$ for Various Damping Factors (Vertical Vibration)

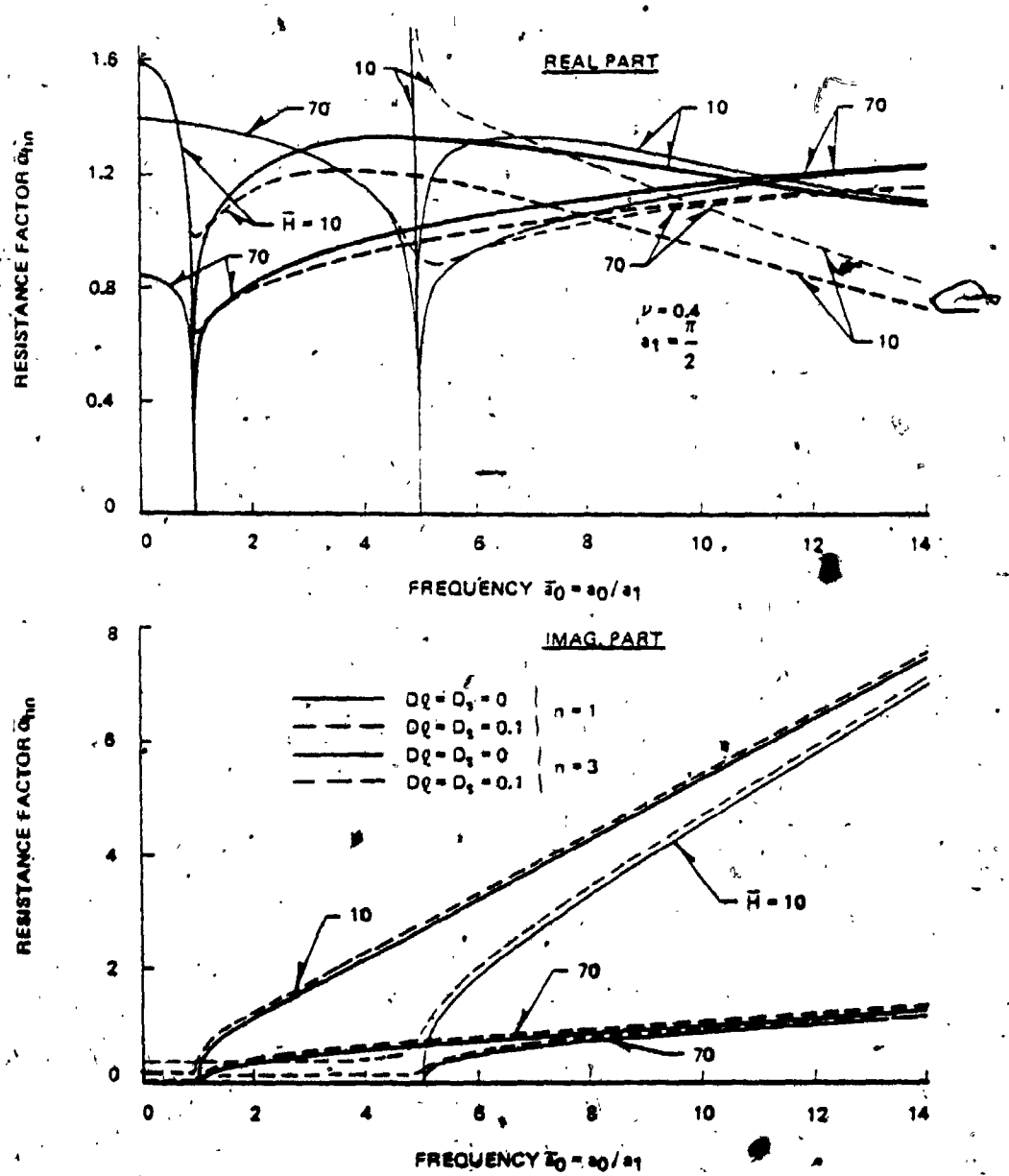

Fig. 2.3-7b. Variation of Resistance Factor $\bar{\alpha}_{hn}$ with Frequency $\bar{a}_0$ for Various Damping Factors (Horizontal Vibration)

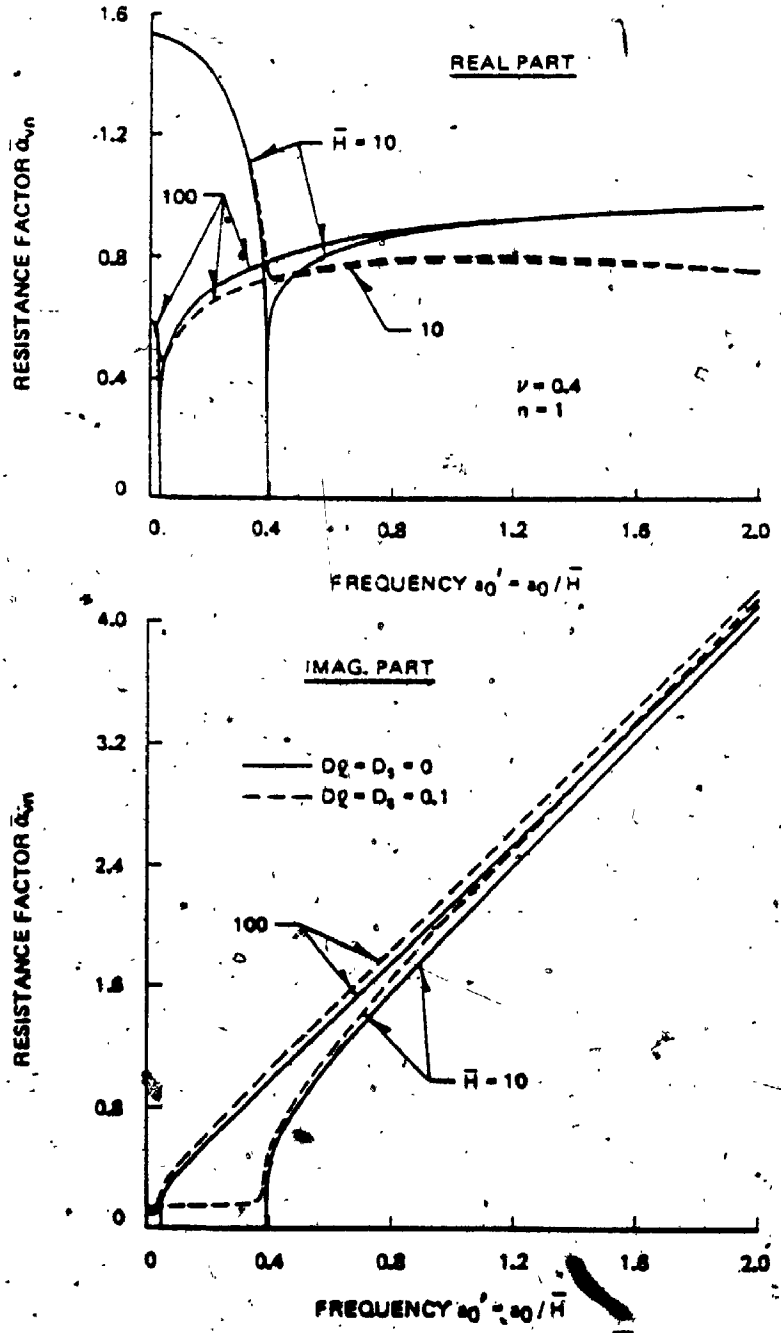

Fig. 2.3-8a. Variation of Resistance Factor $\bar{\alpha}_{vn}$ with Frequency $\bar{a}_0$ for Various Damping Factors (Vertical Vibration)

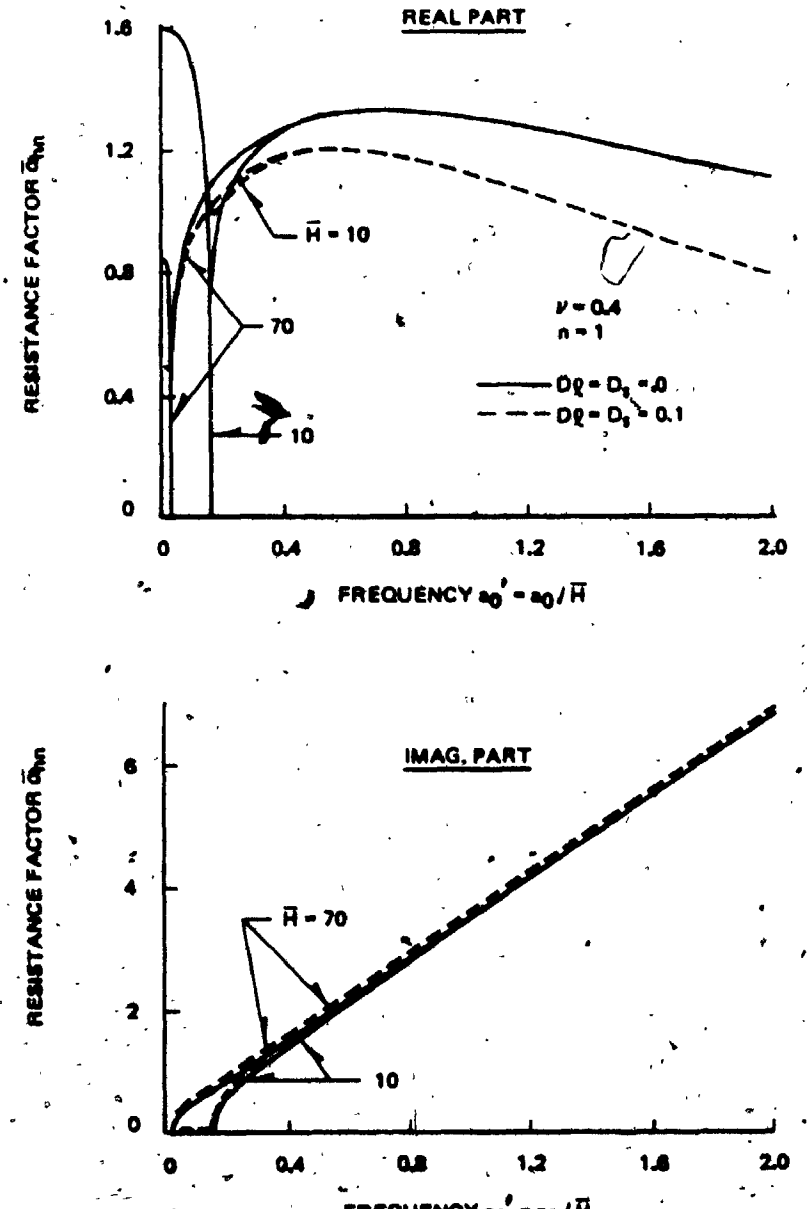

Fig. 2.3-8b. Variation of Resistance Factor $\bar{\alpha}_{hn}$ with Frequency $\bar{a}_0$ for Various Damping Factors (Horizontal Vibration)

The dramatic effect of the material damping can be seen at the natural frequency of the stratum. At this frequency, the elastic stratum does not have any stiffness but the material damping yields a certain value of stiffness which is higher for higher material damping (Fig. 2.3-9). The stiffness at the natural frequency depends on the thickness $\bar{H}$ as shown in Fig. 2.3-9.

In the high frequency range, the material damping tends to reduce the stiffness with increasing frequency and creates the damping in addition to the radiational damping (Figs. 2.3-7 and 2.3-8). This additional damping seems to be nearly constant through the high frequency range although the radiational damping grows linearly with frequency. Thus, the material damping affects the damping function of the stratum less as the frequency increases.

(iv) Poisson's Ratio

Figs. 2.3-10 and 2.3-11 show how the variation of the soil reaction with frequency depends on Poisson's ratio.

The natural frequency in the vertical vibration is higher for higher Poisson's ratios since it is $a_0 = \eta\bar{h}$, and η is larger for higher Poisson's ratios. Contrary to this, the natural frequency a_0 in horizontal vibration is independent of Poisson's ratio.

In the low frequency range, high Poisson's ratios yield higher stiffness for both vertical and horizontal vibrations. In the high frequency range, however, the variation of Poisson's ratio affects the spring function differently for vertical and horizontal vibrations. The stiffness in vertical vibration tends to asymptotically approach a unique value regardless of any Poisson's ratio as the frequency a_0

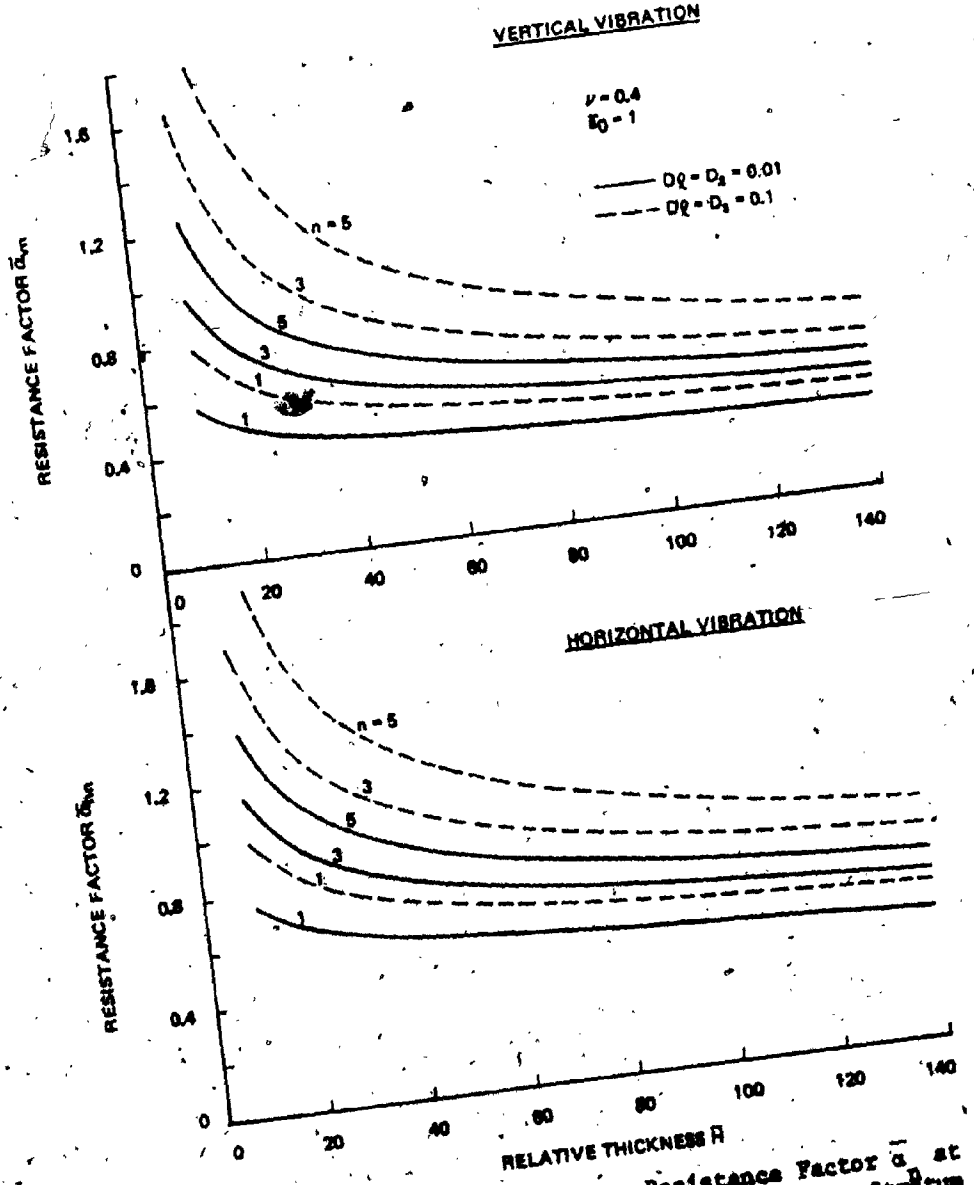

Fig. 2.3-9. Effect of Damping on Resistance Factor $\bar{\alpha}_n$ at the Fundamental Natural Frequency of the Stratum

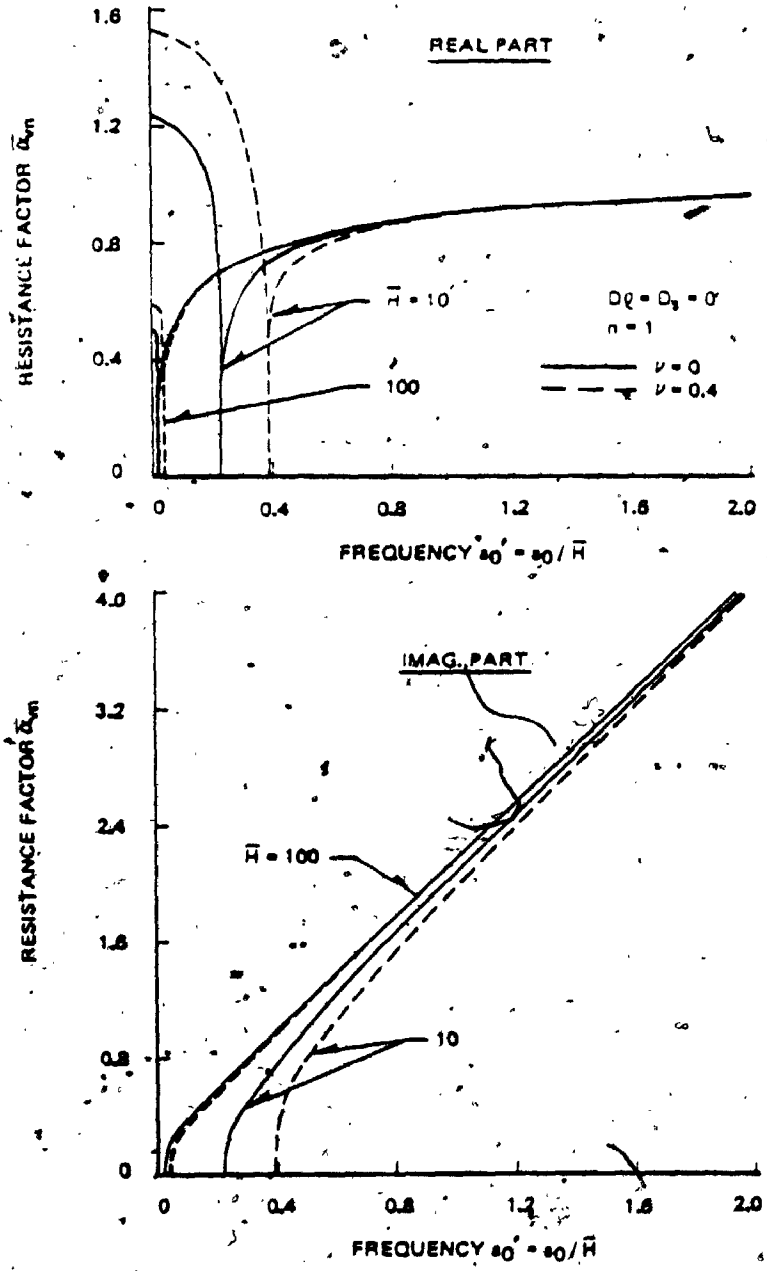

Fig. 2.3-10a. - Variation of Resistance Factor $\bar{\alpha}_{vn}$ with Frequency a_0' for Various Poisson's Ratios (Vertical Vibration)

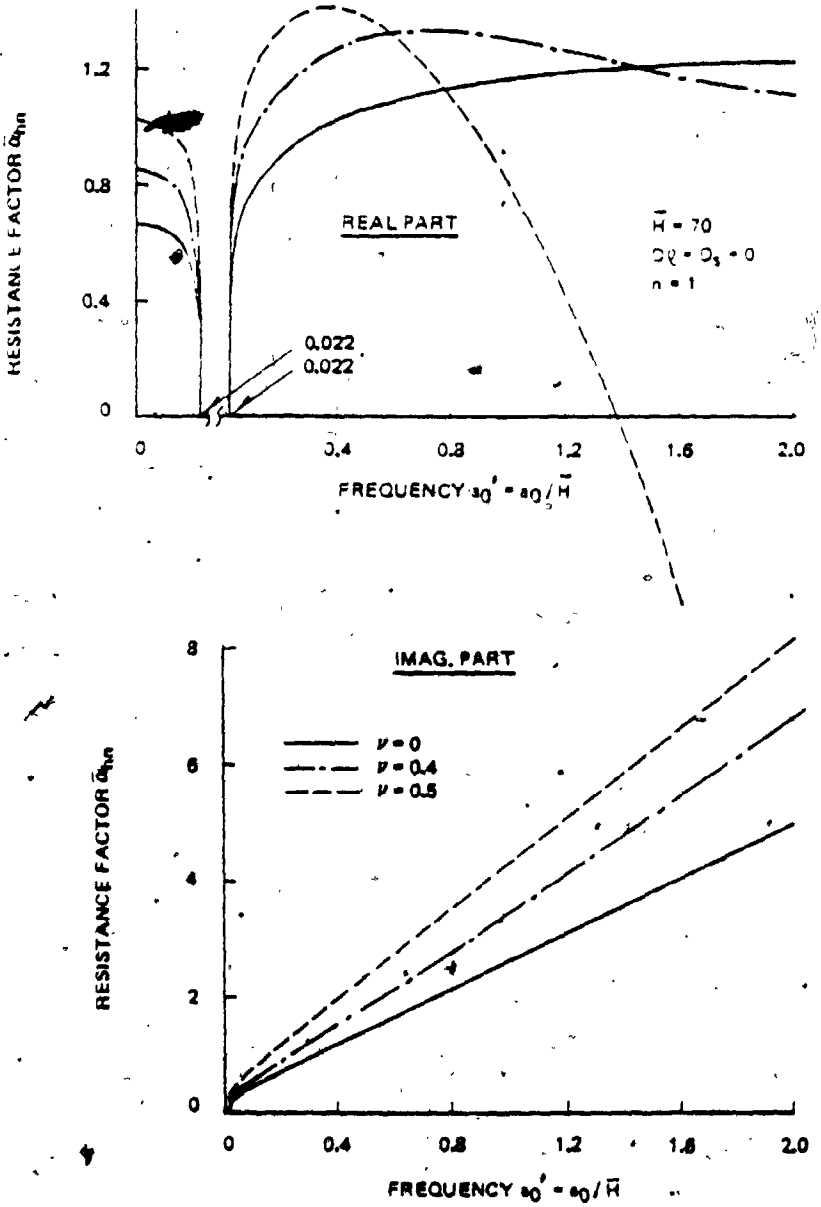

Fig. 2.3-10b. Variation of Resistance Factor $\bar{\alpha}_{hn}$ with Frequency a_0' for Various Poisson's Ratios (Horizontal Vibration)

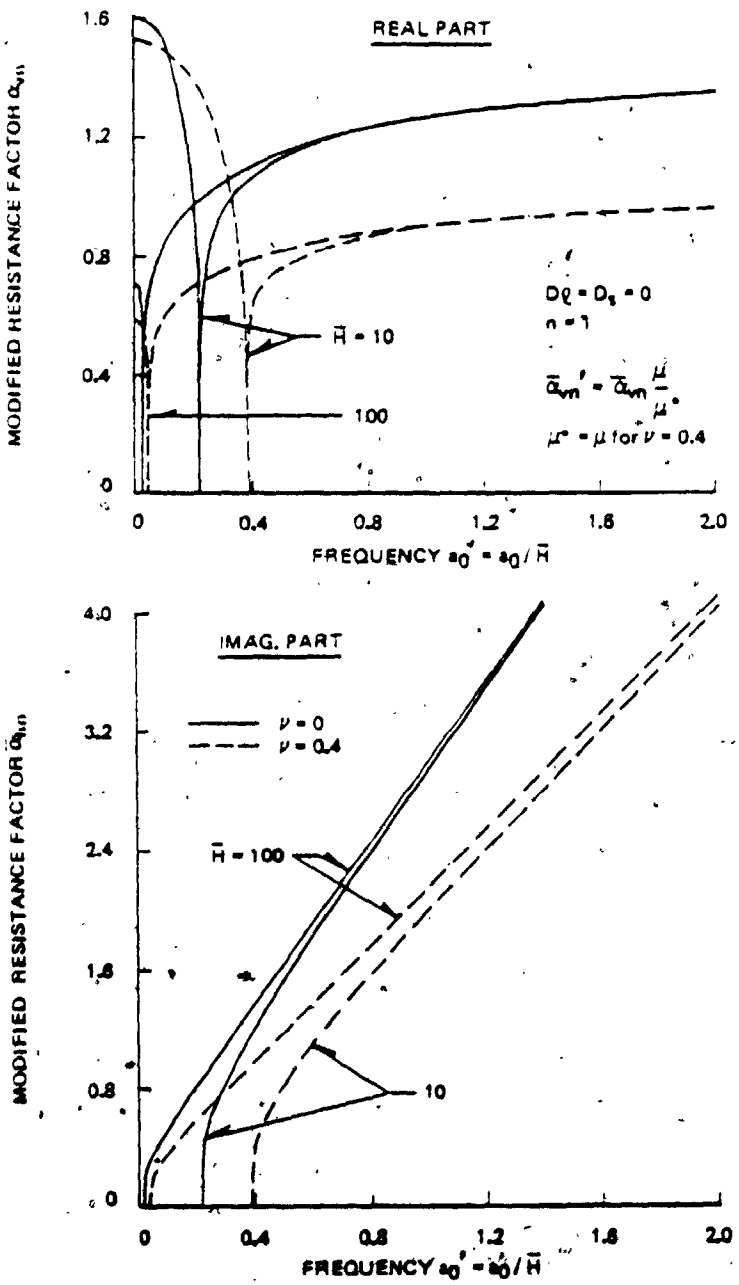

Fig. 2.3-11a. Variation of Modified Resistance Factor $\bar{\alpha}_{vn}'$ with Frequency a_0' for Various Poisson's Ratios (Vertical Vibration)

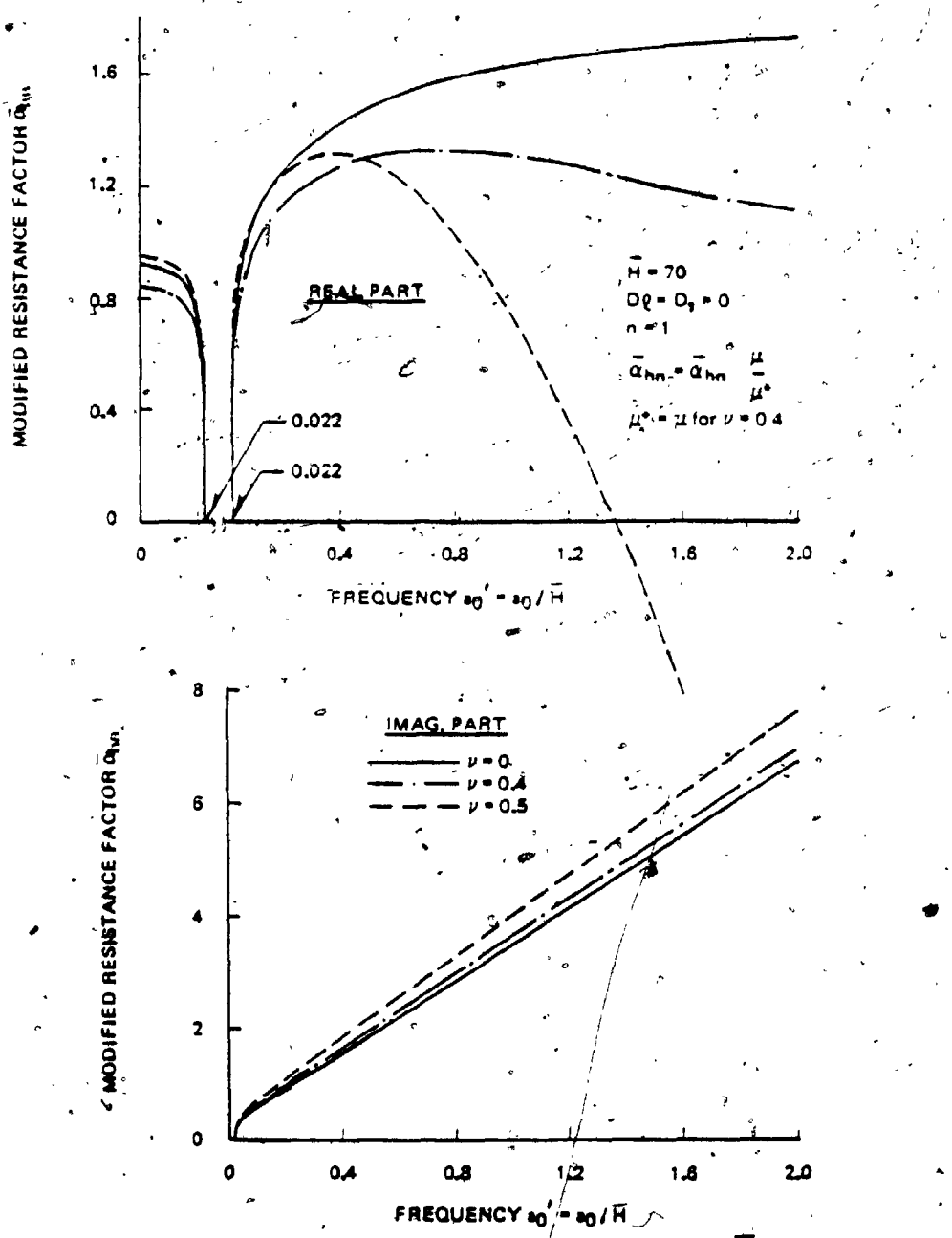

Fig. 2.3-11b. Variation of Modified Resistance Factor $\bar{\alpha}'_{hn}$ with Frequency a_0' for Various Poisson's Ratios (Horizontal Vibration)

increases. On the other hand, that in horizontal vibration tends to drop when Poisson's ratio is extremely high. Only when Poisson's ratio is extremely low, does it follow a trend similar to that observed in vertical vibration.

In the high frequency range, the variation of Poisson's ratio affects the damping function differently for vertical and horizontal vibrations. It does not affect the damping in vertical vibration whereas the damping in horizontal vibration grows more rapidly with frequency for higher Poisson's ratios.

Since the variation of Poisson's ratio affects the shear modulus as well as the resistance factor $\bar{\alpha}_n$, the previous result does not show the full effect of the variation of Poisson's ratio on the soil reaction. Thus the following new parameters, modified resistance factors $\bar{\alpha}'$, are defined in order to account fully for this variation:

$$\begin{Bmatrix} \bar{\alpha}'_{vn} \\ \bar{\alpha}'_{hn} \end{Bmatrix} = \frac{\mu}{\mu^*} \begin{Bmatrix} \bar{\alpha}_{vn} \\ \bar{\alpha}_{hn} \end{Bmatrix} \qquad (2.3\text{-}13)$$

where μ^* is the reference shear modulus. The variation of the modified resistance factor with frequency is shown in Figs. 2.3-11 where the shear modulus for $\nu = 0.4$ is taken as the reference shear modulus.

2 4

OF/DE

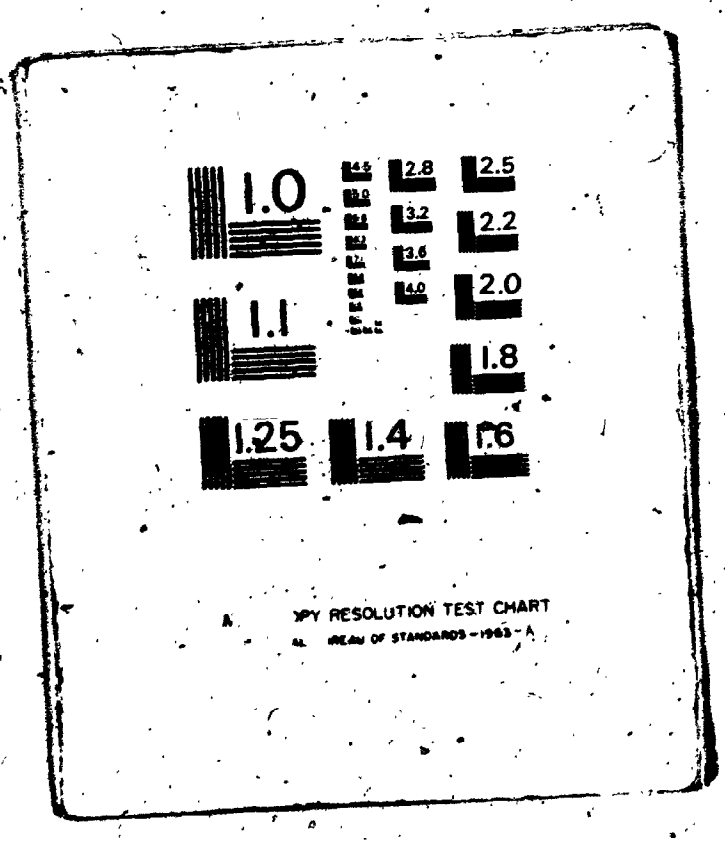
1.0
1.1
1.25
1.4
1.6
2.8
3.2
3.6
4.0
2.5
2.2
2.0
1.8
XPY RESOLUTION TEST CHART
NATIONAL BUREAU OF STANDARDS-1963-A

CHAPTER 3. STIFFNESSES AND DAMPINGS OF SOIL-PILE SYSTEM AT THE PILE HEAD FOR HARMONIC MOTIONS OF A PILE

3.1 Introduction

A pile exposed to dynamic loadings interacts with surrounding soil. The result of this interaction is the modification of pile stiffness, and generation of damping through the energy radiation and dissipation. The energy radiation and dissipation result from the progressive waves and material damping of soil, respectively.

In this chapter, the equations for the pile vibrations are solved using the resistance factors obtained in the previous chapter, and the effect of soil on the stiffness and damping of the pile is studied. The adopted assumptions other than those for the stratum are as follows:

1. The pile stands vertically.
2. The pile is composed of a linear elastic and uniform material.
3. The pile has a uniform circular cross section.
4. No separation between pile and soil is allowed.
5. The pile tip is either pinned or clamped at the bedrock.

3.2 Stiffness and Damping in Vertical Vibration

3.2.A Derivation of Solution

A pile driven into the ground is subjected to an excitation force, $P e^{i\omega t}$, at its head and a soil reaction, $p_v(z)e^{i\omega t}$, along its entire length as shown in Fig. 3.2-1. The solution for a free vibration of this pile is obtained by solving the following homogeneous equation:

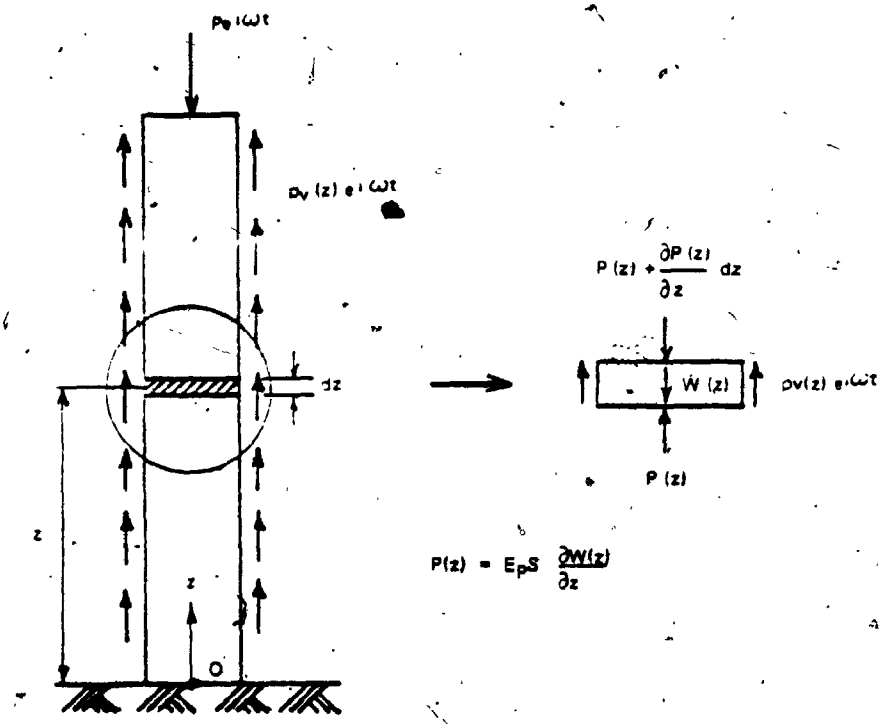

Fig. 3.2-1. External Forces Acting on Pile and Forces Acting on Segment dz of Pile

$$-E_p S \frac{\partial^2}{\partial z^2}\left\{W(z)e^{i\omega t}\right\} + m\frac{\partial^2}{\partial z^2}\left\{W(z)e^{i\omega t}\right\} = 0 \qquad (3.2\text{-}1)$$

where

E_p = Young's modulus of the pile,

S = area of cross section of the pile,

m = mass of unit length of the pile,

$W(z)$ = amplitude of vertical displacement of the pile, and

ω = frequency.

The solution for this equation is

$$W(z) = A\sin(\lambda_v z) + B\cos(\lambda_v z) \qquad (3.2\text{-}2)$$

where

$$\lambda_v = \sqrt{\frac{m}{E_p S}\omega^2} \qquad (3.2\text{-}3)$$

The boundary conditions of the pile for free vibration are fixed tip and free head. Those conditions called for $B = 0$ and $\lambda_v = \frac{\pi}{2H}(2n-1)$ in which n is an integer from one to infinity.

Therefore, the mode shape of this pile in the n-th mode, $\xi_n(z)$, is

$$\xi_n(z) = \sin(\lambda_{vn} z) \qquad (3.2\text{-}4)$$

where

$$\lambda_{vn} = \frac{\pi}{2H}(2n-1) \qquad (3.2\text{-}5)$$

Using the above obtained mode shape, the amplitude of the pile deformation, W(z), can be described by

$$W(z) = \sum_{n=1}^{\infty} C_n \sin(\lambda_{vn} z) \tag{3.2-6}$$

where C_n is the n-th generalized coordinate.

The external forces acting on the pile are the excitation force, $P\, e^{i\omega t}$, at the head and soil reaction, $p_v(z)e^{i\omega t}$, along the length. Therefore the equilibrium condition of the forces acting on infinitesimally thin slice of the pile, dz, leads to

$$-E_p S \frac{\partial^2}{\partial z^2}\left\{W(z)e^{i\omega t}\right\} + m \frac{\partial^2}{\partial z^2}\left\{W(z)e^{i\omega t}\right\} = P\delta(H)e^{i\omega t} - p_v(z)e^{i\omega t} \tag{3.2-7}$$

where

P = amplitude of the vertical excitation force,

$p_v(z)$ = amplitude of the vertical soil reaction, and

$\delta(H)$ = 1 at $z=H$
0 at $z\neq H$

Since no separation between pile and soil is assumed and λ_{vn} is identical to h_n, W_n in Eq. 2.2-13 is equal to C_n in Eq. 3.2-6 and the soil reaction, $p_v(z)$, is expressed by Eq. 2.2-16. Hence, multiplying Eq. 3.2-7 by the above obtained n-th mode shape and integrating over the length of the pile leads to

$$W_n E_p S\left(h_n^2 - \lambda_v^2\right)\int_0^H \sin^2(h_n z)dz = P\int_0^H \delta(H)\sin(h_n z)dz - W_n \alpha_{vn}\int_0^H \sin^2(h_n z)dz \tag{3.2-8}$$

The solution of Eq. 3.2-8 for W_n is

$$W_n = \frac{2P}{H}\frac{(-1)^{n-1}}{E_p S\left(h_n^2 - \lambda_v^2\right) + \alpha_{vn}} \tag{3.2-9}$$

Therefore, after substituting the above obtained W_n into Eq. 3.2-6 ($W_n = C_n$), the stiffness of the soil-pile system at the pile head is

$$K_v = \frac{P}{W(z=H)} = \frac{H}{2}\left\{\sum_{n=1}^{\infty}\frac{(-1)^{n-1}}{E_p S\left(h_n^2 - \lambda_v^2\right) + \alpha_{vn}}\right\}^{-1} \tag{3.2-10}$$

K_v in Eq. 3.2-10 can be rewritten with the dimensionless parameters as

$$K_v = \frac{E_p S}{H}\,\bar{K}_v \tag{3.2-11a}$$

or

$$K_v = \frac{E_p S}{r_0}\,\frac{\bar{K}_v}{\bar{H}} \tag{3.2-11b}$$

where

$$\left.\begin{aligned}
\bar{K}_v &= \frac{1}{2}\left\{\sum_{n=1}^{\infty}\frac{(-1)^{n-1}}{\bar{h}_n^2 - \bar{\lambda}_v^2 + Y_v\,\bar{\alpha}_{vn}}\right\}^{-1} \\
Y_v &= \pi\mu\, H^2/(E_p S) = \bar{v}^2\,\bar{\rho}\,\bar{H}^2 \\
\bar{v} &= v_s/v_p \text{ (wave velocity ratio)} \\
\rho &= \rho/\rho_p \text{ (mass ratio)} \\
\bar{\lambda}_v &= \lambda_v H = H\sqrt{\frac{m}{E_p S}\,\omega^2} = a_0\sqrt{Y_v/(\bar{\rho}\,\bar{H}^2)} \\
\bar{\rho}_p &= m/\pi r_0^2 \\
v_p &= \sqrt{E_p/\rho_p}
\end{aligned}\right\} \qquad (3.2\text{-}12)$$

In Eqs. 3.2-11, $\bar{K}_v$ accounts for the variation of pile radius whereas $\bar{K}_v/\bar{H}$ accounts for the variation of pile length.

3.2.B Effect of Soil on Stiffness and Damping

The stiffness K_v of the soil-pile system is a complex number and is called "complex stiffness" here. The real and imaginary parts of the complex stiffness represent, respectively, the stiffness and damping of the soil-pile system at the pile head. In this study, they are simply called "stiffness" and "damping," respectively. The vector sum of the real and imaginary parts of the complex stiffness expresses the

amplitude and phase shift of the force required to yield a unit amplitude of the vertical displacement at the pile head.

The effect of the surrounding soil on the stiffness and damping of the pile appears through the parameters Y_v and $\bar{\alpha}_{vn}$ in the explicit solution. Thus soil modifies the stiffness of the pile and generates the damping. This situation is called soil-pile interaction. The above defined complex stiffness $\bar{K}_v$ indicates that the interaction is governed by the parameters: slenderness ratio ($\bar{H}$); soil resistance factor ($\bar{\alpha}_{vn}$) which is further governed by $\bar{H}$, a_0, ν, D_1 and D_s; frequency ($\bar{\lambda}_v$ and a_0); and parameter Y_v. In this paragraph the effects of soil on the stiffness of pile are studied for vertical vibration.

(i) General Features for the Static Case

In the static case, no damping is generated and the complex stiffness is composed of the real part only. The variation of this stiffness with the parameter Y_v is shown in Fig. 3.2-2 for the various slenderness ratios. In this figure the stiffness parameter $\bar{K}_v$ stays at $\bar{K}_v \approx 1$ under the negligible soil effect, and becomes larger as this effect increases. When the soil effect is very strong, the stiffness of the soil-pile system is completely controlled by soil and the value of log $\bar{K}_v$ grows nearly proportionally with log Y_v. The figure indicates that the relationship between soil effect and Y_v is rather unique regardless of any slenderness of the pile: the transition from very weak to intermediate soil effect lies around $Y_v = 0.3$, and that from intermediate to very strong soil effect lies around $Y_v = 10$. This nature of parameter Y_v and the expression of Y_v in Eqs. 3.2-12 indicates that;

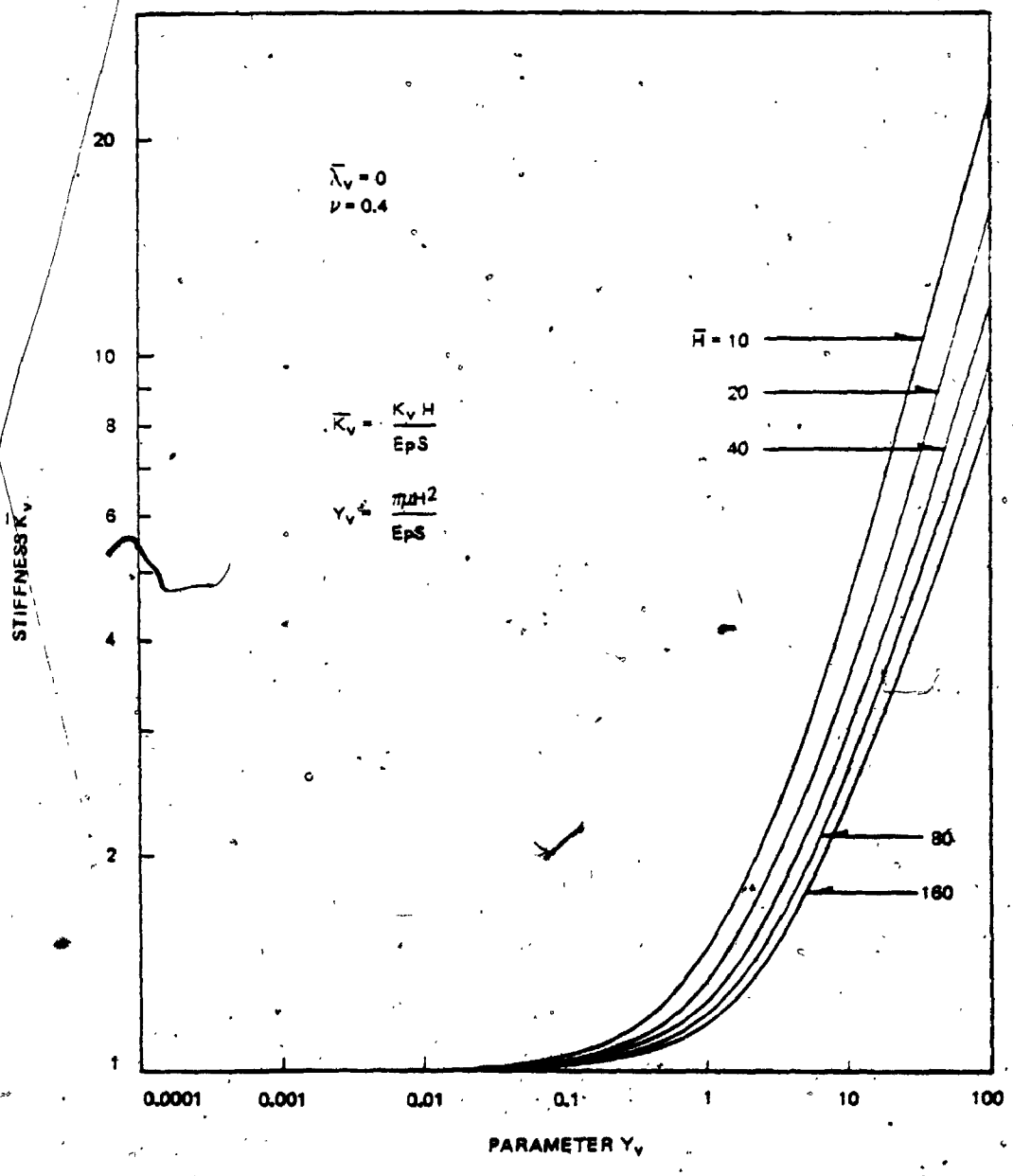

Fig. 3.2-2. Variation of Static Stiffness $\bar{K}_v$ with Parameter Y_v

1. the stiffness of a more slender pile in harder soil is more modified by the surrounding soil;
2. the modification of the pile stiffness is more sensitive to the hardness of soil when the pile is more slender, and to the slenderness of pile when the soil is harder;
3. the variations of pile slenderness and of shear wave velocity of soil (in terms of $\bar{v}$) affect the pile stiffness in about the same order of magnitude.

The effect of the variation of pile length and soil hardness on the pile stiffness can be seen directly in Fig. 3.2-3, in which the parameter $\bar{K}_v/\bar{H}$ is used in order to account fully for the variation of pile length. As soil effect increases, the parameter $\bar{K}_v/\bar{H}$ of the soil-pile system becomes independent of the pile length. This is because the surrounding soil tends to restrict the movement of the pile at the lower portion and the portion in which the pile mostly deforms becomes independent of its total length. The previously drawn conclusions concerning the nature of Y_v and its mathematical expression can be visually observed in Fig. 3.2-3.

(ii) General Features for the Dynamic Case

When the soil effect is absent, the stiffness $\bar{K}_v$ decreases from $\bar{K}_{v_0} = 1$ with frequency $\bar{b}$ ($\bar{b} \leq 1.5$) as shown in Fig. 3.2-4. In this figure the new parameter $\bar{b}$ is defined by

$$\bar{b} = \bar{\lambda}_v/\bar{\lambda}_0 \qquad \left(\bar{\lambda}_0 = \frac{\pi}{2}\right) \tag{3.2-13}$$

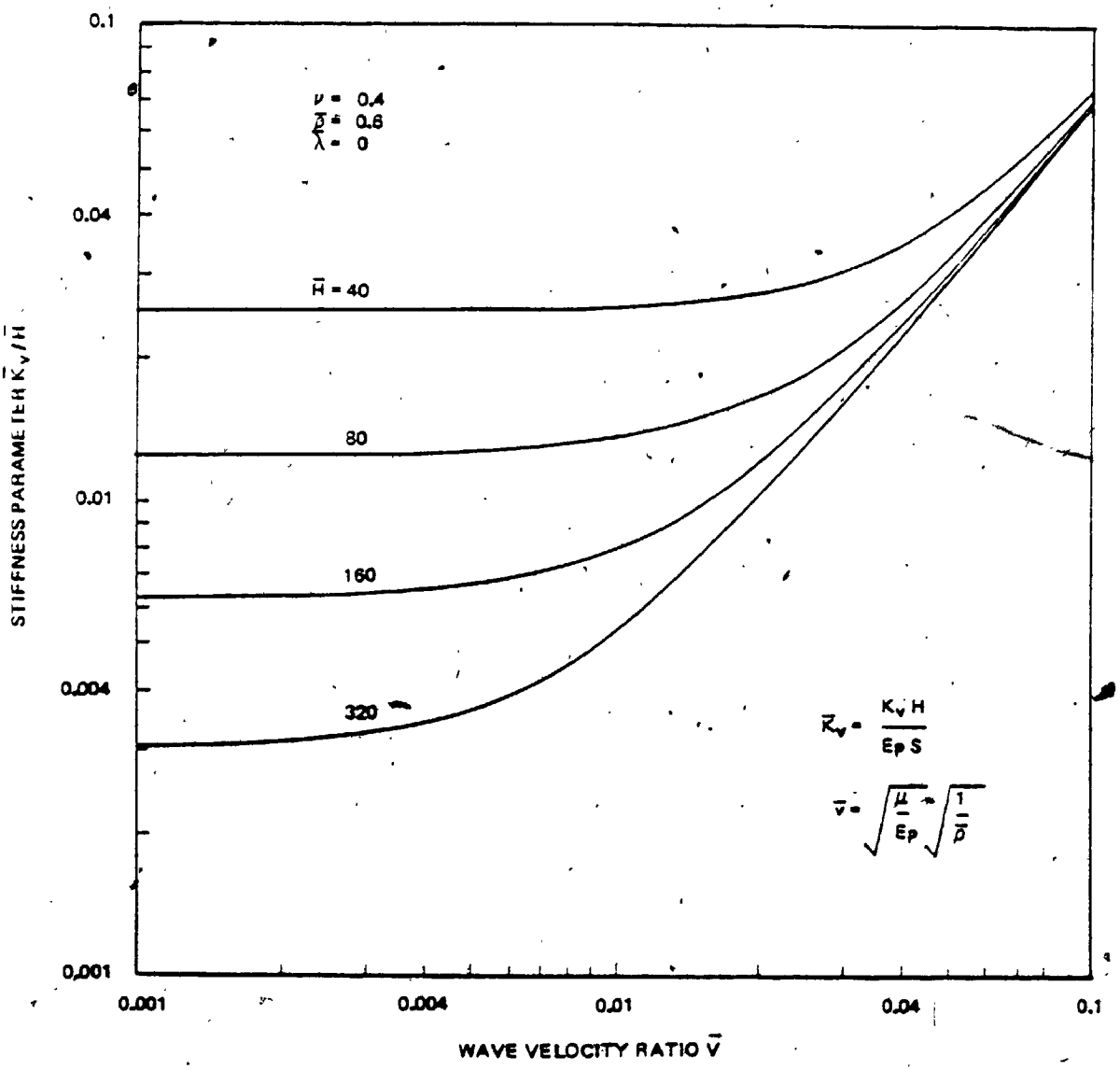

Fig. 3.2-3. Variation of Stiffness Parameter $\bar{K}_v/\bar{H}$ with Wave Velocity Ratio

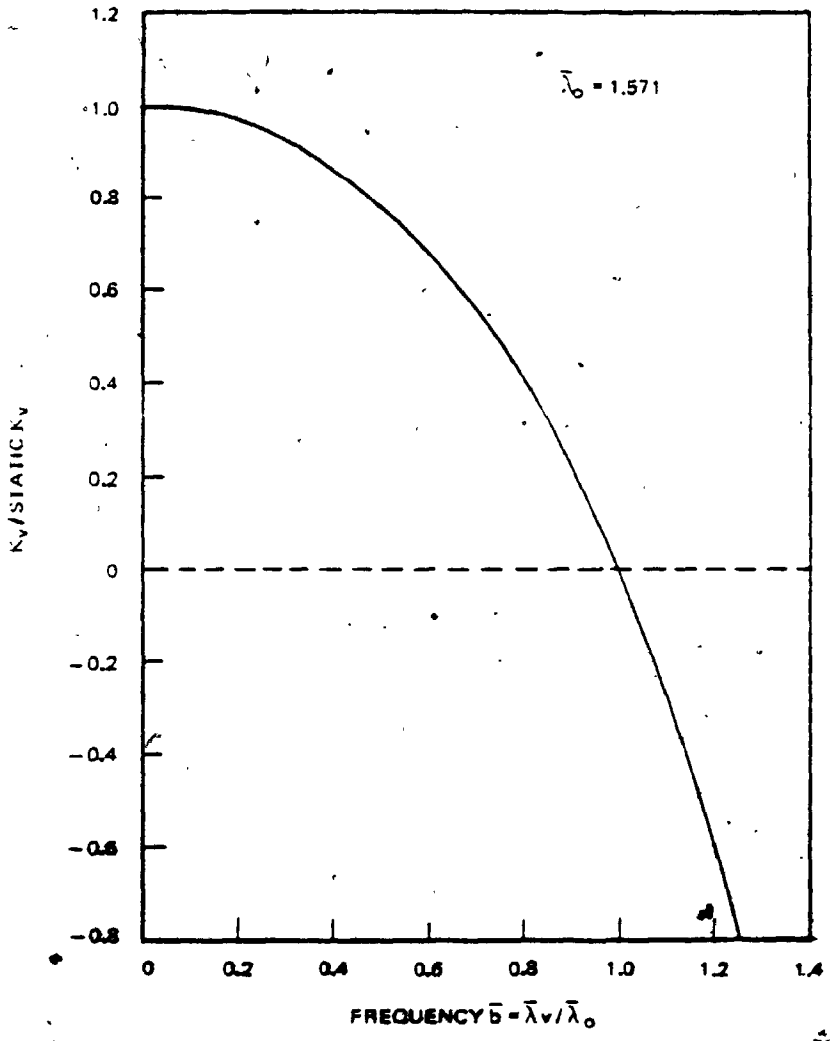

Fig. 3.2-4. Variation of Stiffness K_v with Frequency $\bar{b}$ for Pile Isolated from Soil

Since material damping in the pile is not considered, no damping appears in this situation.

When this pile is surrounded by soil, the surrounding soil modifies the pile stiffness and generates the damping as shown in Figs. 3.2-5. In these figures, zero stiffness appears at frequencies higher than $\bar{b} = 1$ or even does not appear under the strong soil effect. The frequency at which the stiffness is zero is approximately equal to the undamped natural frequency of the soil-pile system. The first natural frequencies of the soil-pile system can be obtained by solving the following equation for the frequency,

$$\bar{h}_n^2 - \bar{\lambda}_v^2 + \text{Real}\,(Y_v \bar{\alpha}_{vn}) = 0 \qquad \text{with } n = 1 \tag{3.2-14}$$

and are shown for various Y_v in Fig. 3.2-6. It should be noted in Fig. 3.2-6 that the undamped first natural frequency of the soil-pile system is independent of pile slenderness when the parameter Y_v is kept constant. This is because the first natural frequency of the soil-pile system is located at the higher frequency than that of the stratum and, therefore, the resistance factor $\bar{\alpha}_{vn}$ for $n = 1$ in this frequency range is independent of the pile slenderness. The similarity of Figs. 3.2-6 and 3.2-2 indicates that, under the given conditions of the soil-pile system, the dynamic pile stiffness is modified by the surrounding soil nearly as much as the static one is. Therefore, the degree of soil effect for the dynamic case does not differ much from that for the static case and is known from the parameter Y_v.

The stiffness tends to be reduced at the resonance of the stratum as shown in Figs. 3.2-5. Such reduction is not significant until $Y_v \approx 0.3$ and increases with soil effect or Y_v until $Y_v \approx 10$ (Fig. 3.2-7).

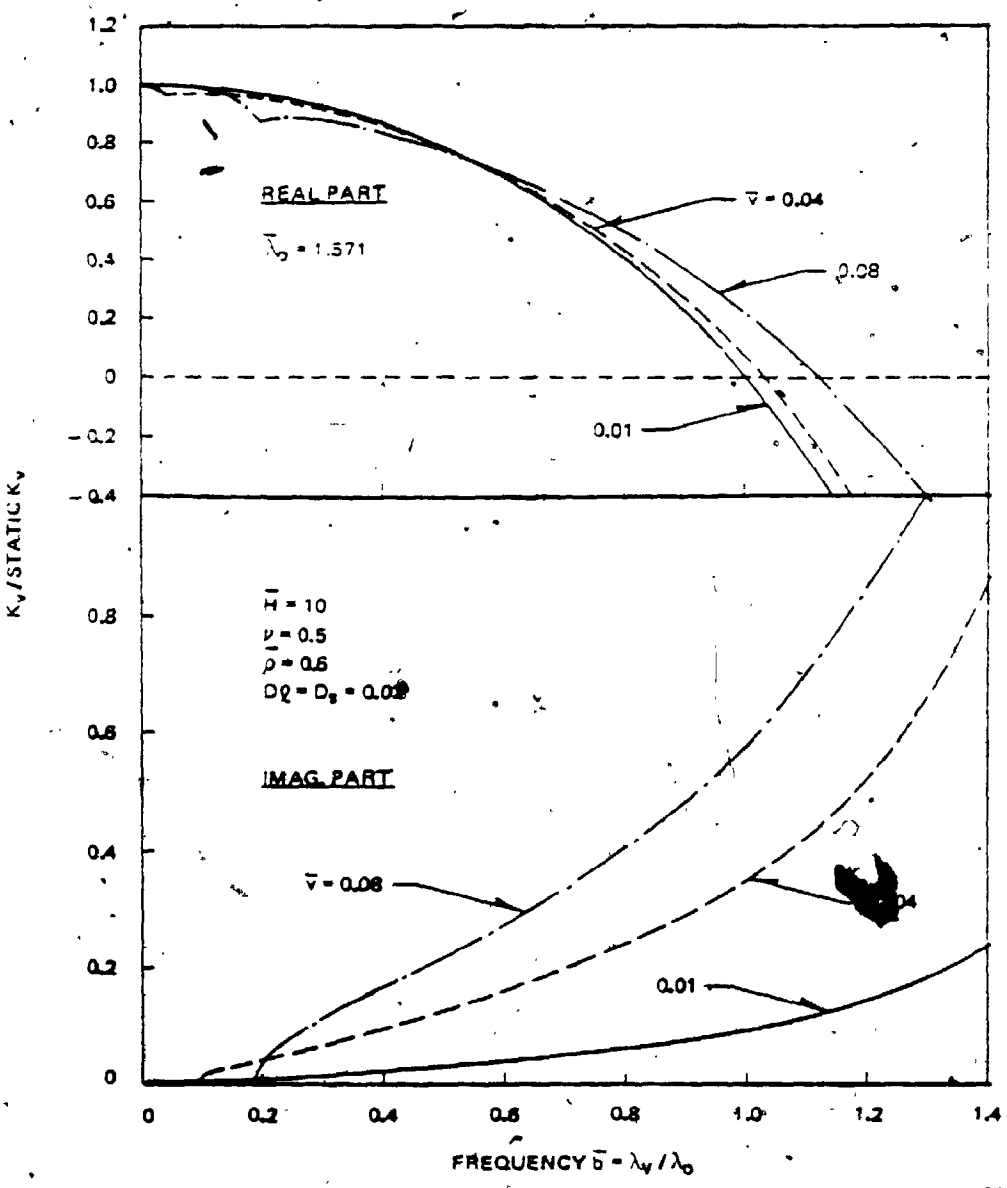

Fig. 3.2-5a. Variation of Complex Stiffness with Frequency $\bar{b}$ for Various Wave Velocity Ratios ($\bar{H}$ = 10)

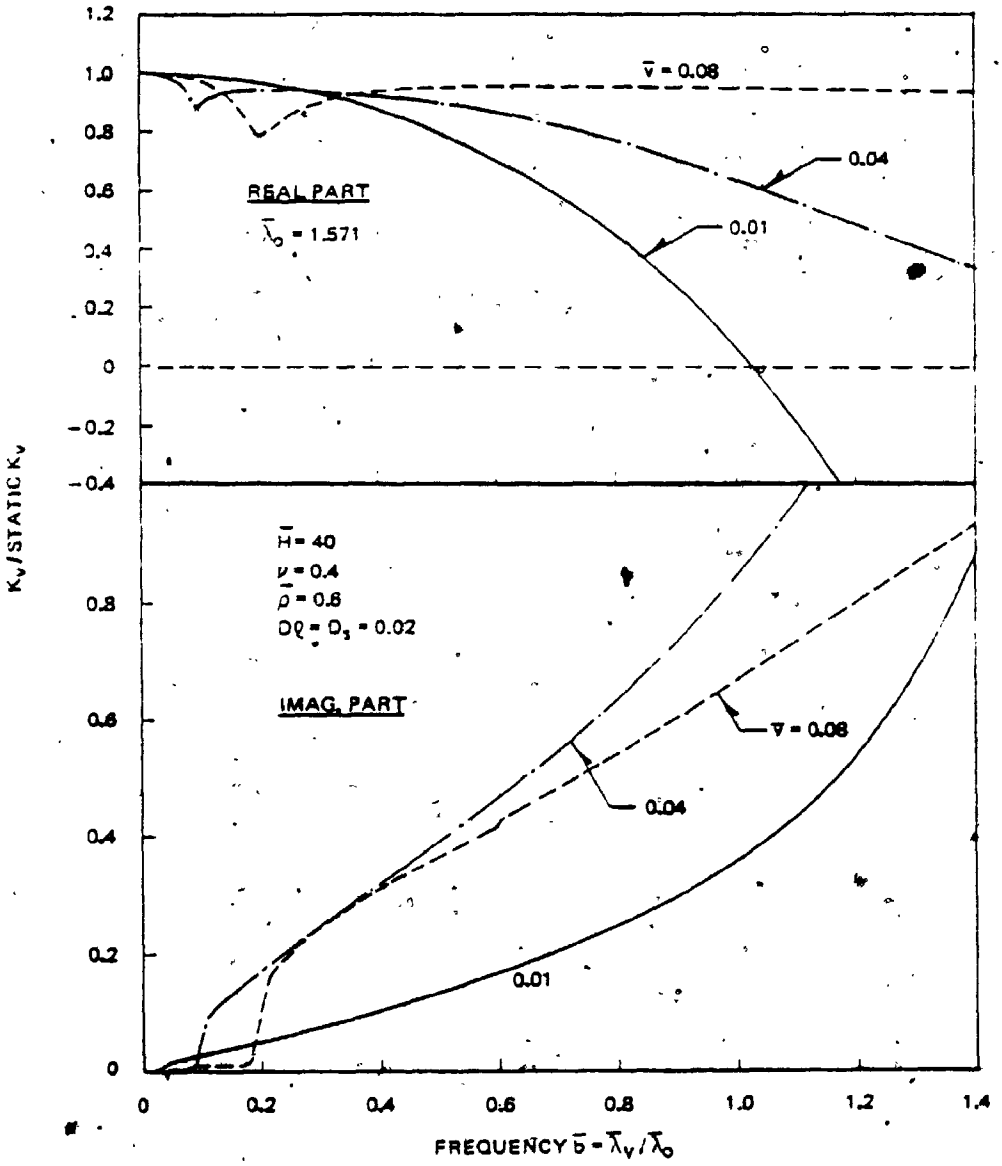

Fig. 3.2-5b. Variation of Complex Stiffness with Frequency $\bar{b}$ for Various Wave Velocity Ratios ($\bar{H}$ = 40)

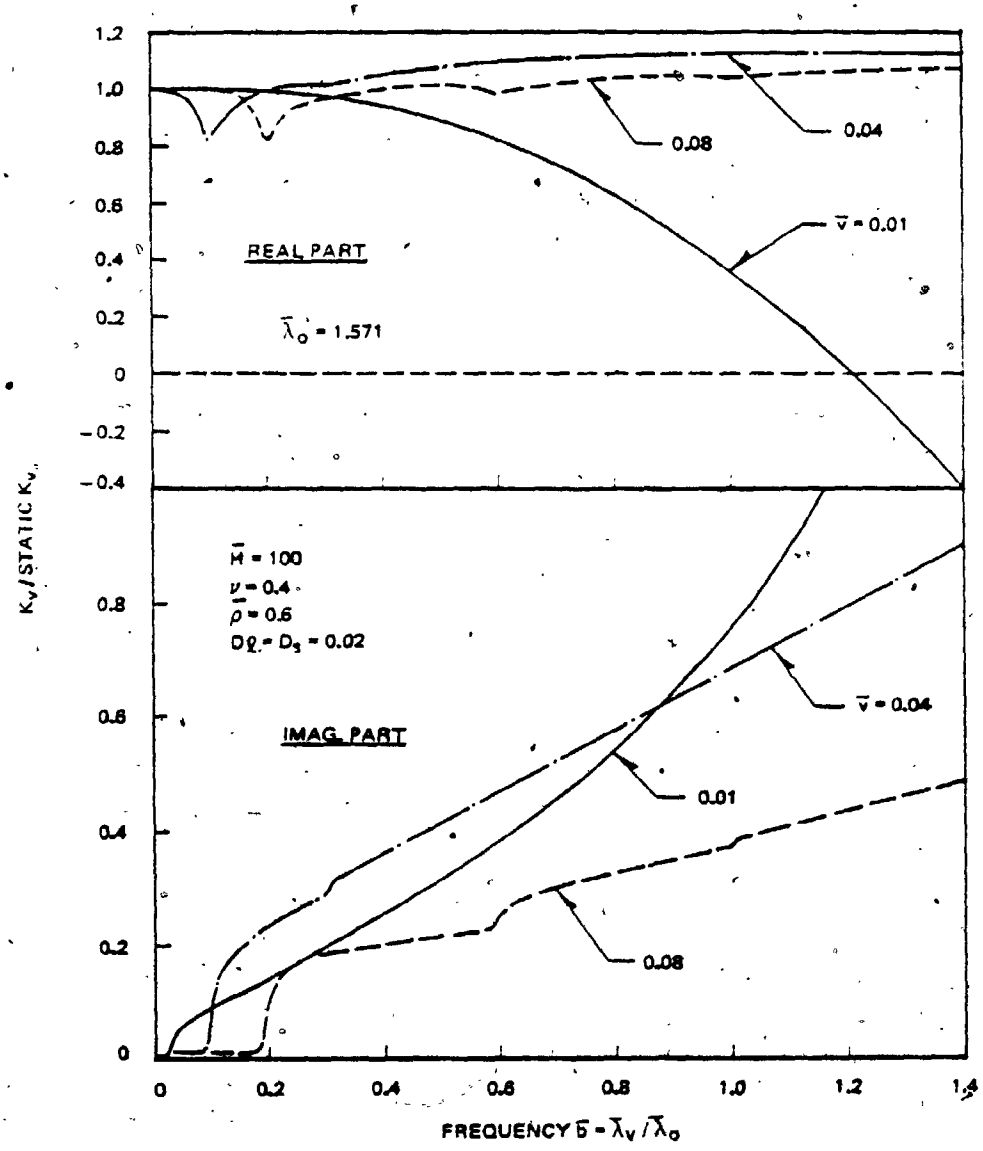

Fig. 3.2-5c. Variation of Complex Stiffness with Frequency $\bar{b}$ for Various Wave Velocity Ratios ($\bar{H}$ = 100)

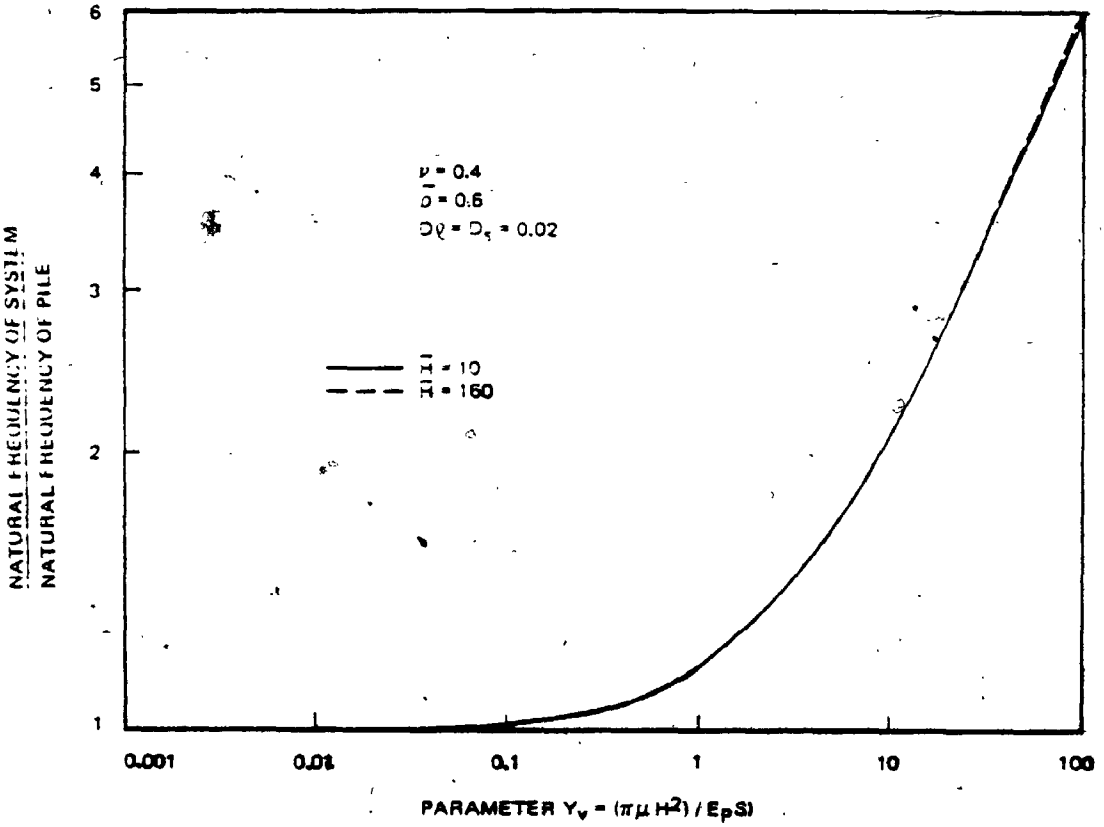

Fig. 3.2-6. Variation of the First Natural Frequency of Soil-Pile System with Parameter Y_v

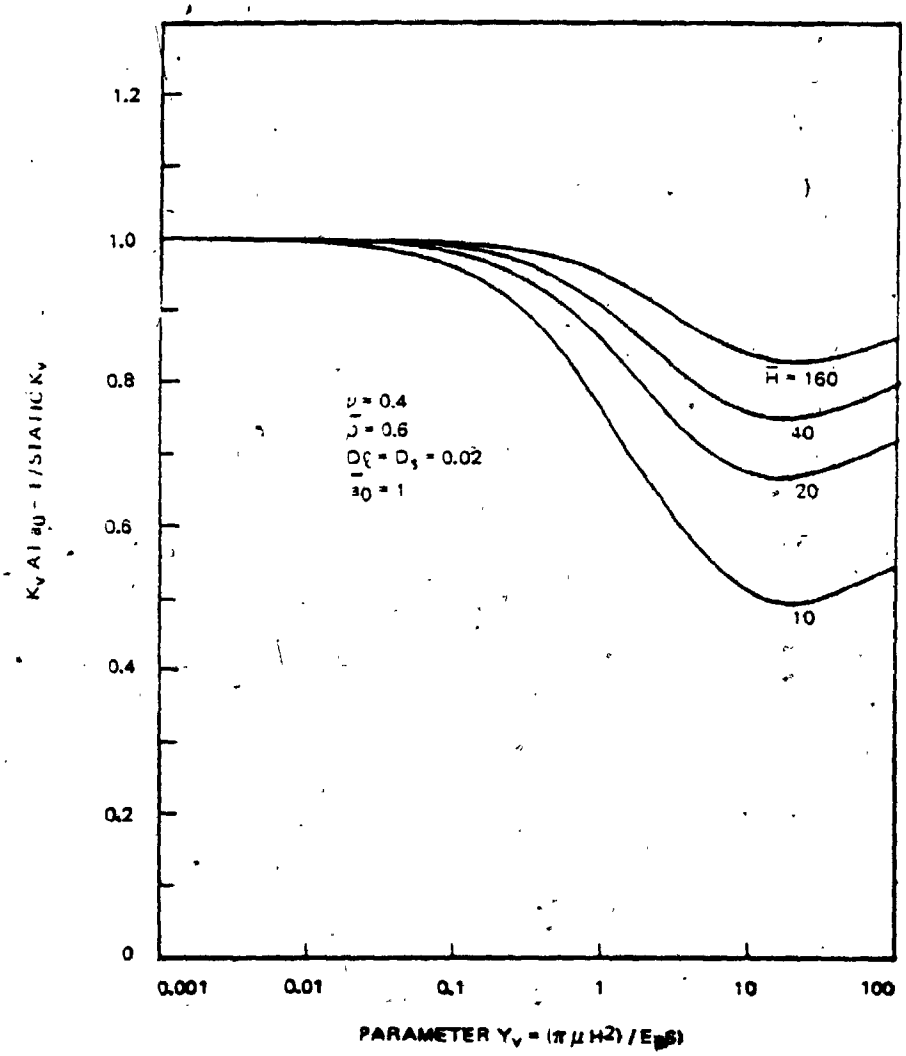

Fig. 3.2-7. Reduction of Real Part of Stiffness $\bar{K}_v$ at the First Natural Frequency of Stratum

Those values of the parameter Y_v correspond to the transitions from the very weak to intermediate soil effect and from the intermediate to very strong soil effect, respectively. The values Y_v at those transitions coincide with those for the static case. This trend further supports the above mentioned identity of the soil effect for the dynamic and static cases. Fig. 3.2-7 indicates also that the stiffness at the resonance of the stratum decreases less for a more slender pile.

The variation of the damping with frequency can be seen in Figs. 3.2-5 for various soil effects. Below the fundamental resonant frequency of the stratum, the damping of the pile results mostly from the material damping in the soil, and therefore, varies very little with frequency. However, around the fundamental resonant frequency of the stratum, a significant amount of the progressive wave appears suddenly and brings an abrupt increase of the damping due to the energy radiation. Thereafter the damping grows linearly with frequency until the next higher mode progressive wave becomes significant. This behavior of damping can be seen more clearly under the stronger soil effect. On the other hand, under the weak soil effect the above mentioned abrupt increase of the damping cannot be seen clearly but another type sharp increase of damping can be seen around the frequency where the stiffness of the soil-pile system is zero. This sharp increase of the damping is due to the resonance of the soil-pile system.

Fig. 3.2-8 shows the variation of the stiffness $\bar{K}_v$ with frequency a_0' under the strong soil effect for $\bar{H} = 40$ and 160. Above the fundamental resonant frequency of the stratum, the stiffness $\bar{K}_v$ tends to be independent of slenderness as frequency increases. This is because the stiffness of the soil-pile system is governed by the surrounding soil

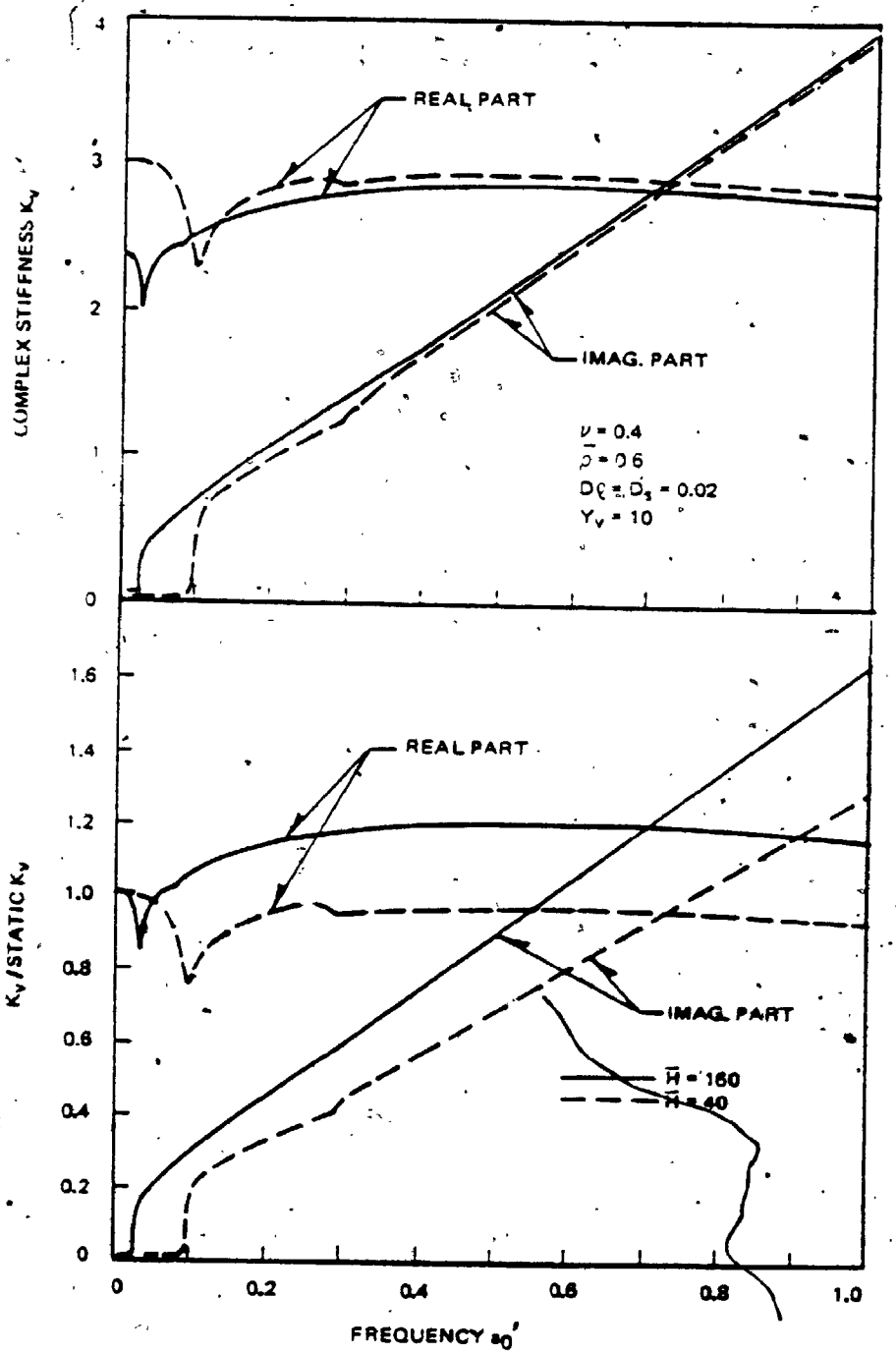

Fig. 3.2-8. Variation of Complex Stiffness $\bar{K}_v$ with Frequency a_0' for Various Slendernesses

and the soil resistance factor becomes independent of slenderness as the frequency a_0' increases. However, even if the effect of soil is weak, the variation of the damping $\bar{K}_v$ with frequency a_0' is quite independent of slenderness as shown in Fig. 3.2-9. Thus, regardless of any soil effect, the damping $\bar{K}_v$ does not depend much on slenderness. Fig. 3.2-10 also shows this trend and further indicates that the damping $\bar{K}_v$ increases with the parameter Y_v.

Under the strong soil effect, the static stiffness $\bar{K}_v$ decreases with slenderness whereas the dynamic stiffness $\bar{K}_v$ is fairly independent of slenderness in the high frequency range. Therefore, the ratio between the dynamic and static stiffnesses in the high frequency range is larger for a more slender pile. This trend can be seen in Fig. 3.2-11 where the ratio is shown only for the strong soil effect and the stiffness at $a_0' = 0.4$ is selected as the dynamic stiffness. Regardless of any slenderness, the maximum value of this ratio appears around $Y_v = 10$ which corresponds to the transition from the intermediate to very strong soil effect. The figure further indicates that the dynamic stiffness can be larger than the static one and this trend is more significant for a more slender pile.

(iii) Effect of the Variation of Poisson's Ratio

The variation of Poisson's ratio affects the statical stiffness of the soil-pile system, $\bar{K}_v$, as shown in Fig. 3.2-12. In this figure, higher Poisson's ratio leads to the higher stiffness of the soil-pile system. This is simply because the real part of the soil resistance factor $\bar{\alpha}_{vn}$ is larger for higher Poisson's ratio in the low frequency range. The more slender a pile is, the less it is affected by the

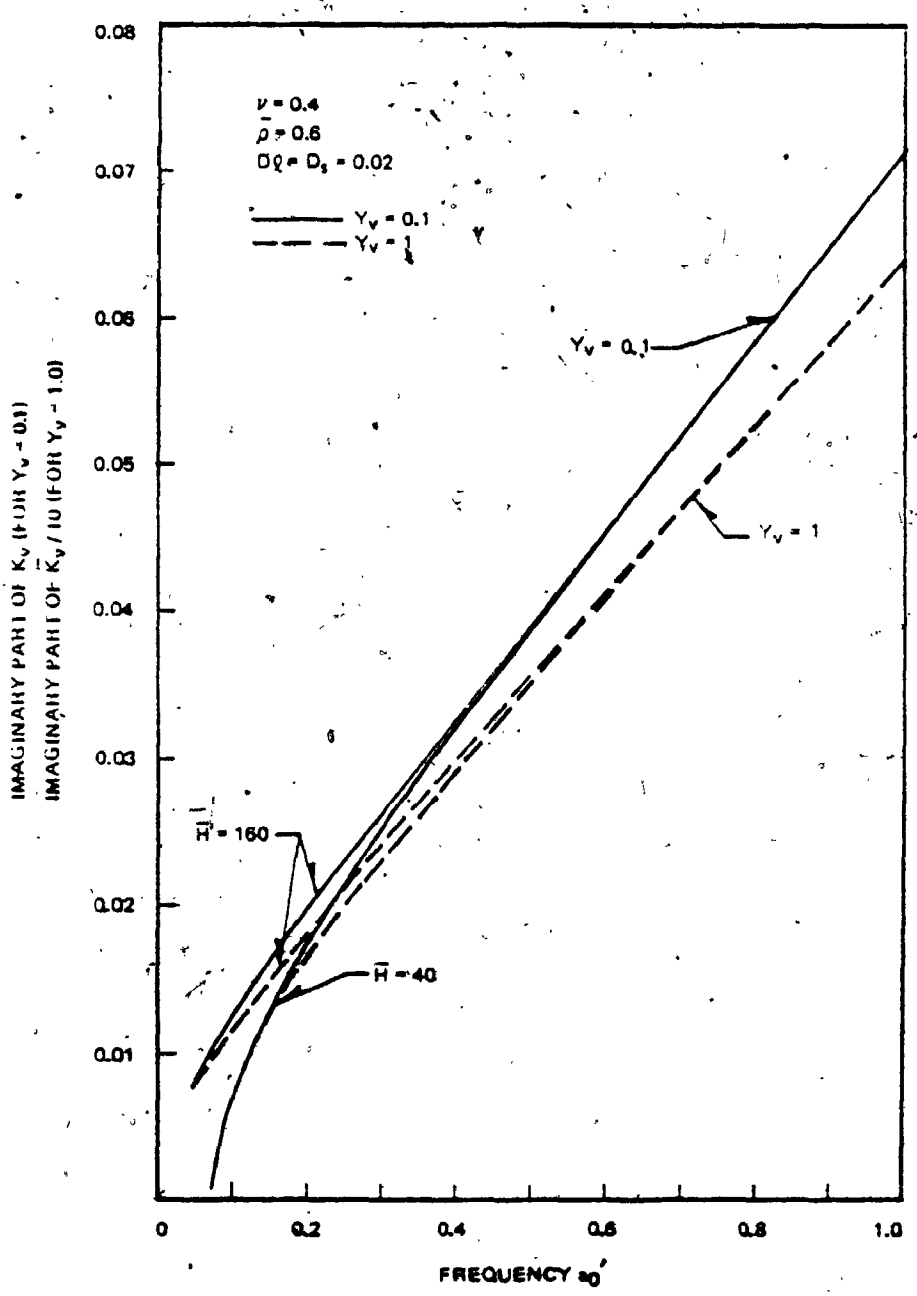

Fig. 3.2-9. Variation of Imaginary Part of Complex Stiffness $\bar{K}_v$ with Frequency a_0' Under Weak Soil Effect

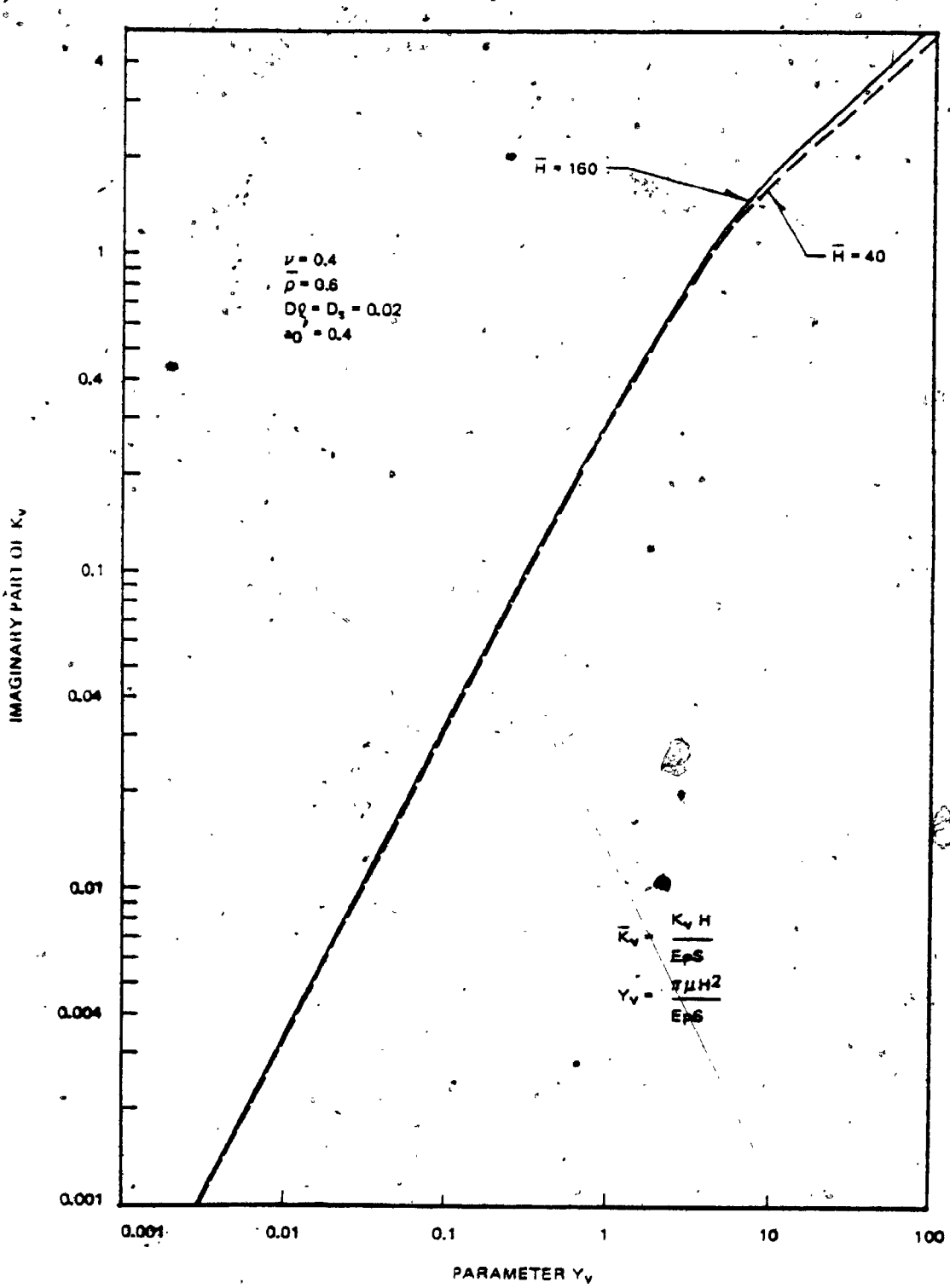

Fig. 3.2-10. Variation of Imaginary Part of Complex Stiffness $\bar{K}_v$ with Parameter Y_v

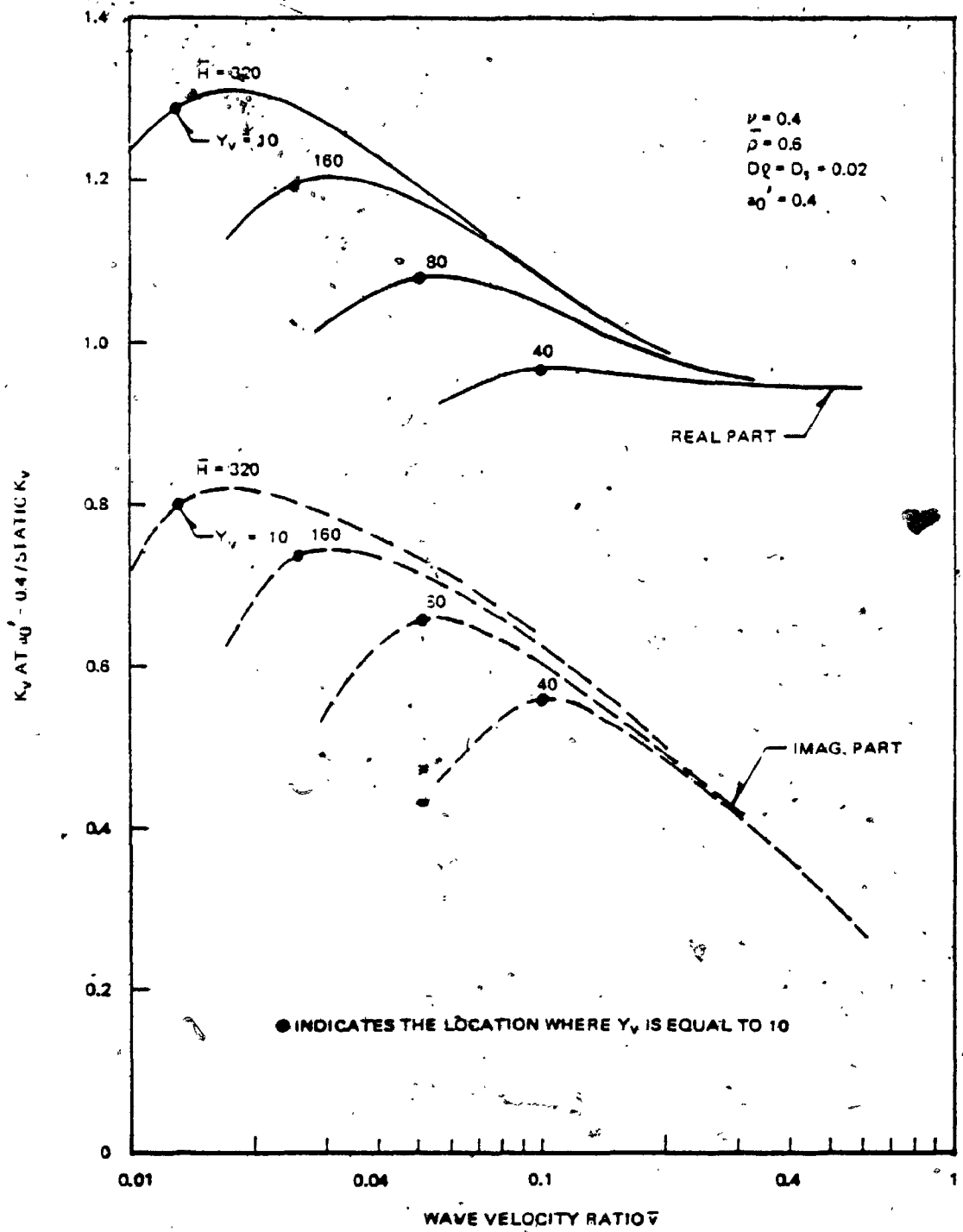

Fig. 3.2-11. Variation of the Ratio, $K_v(a_0' = 0.4)/K_v(a_0' = 0)$, with Wave Velocity Ratio

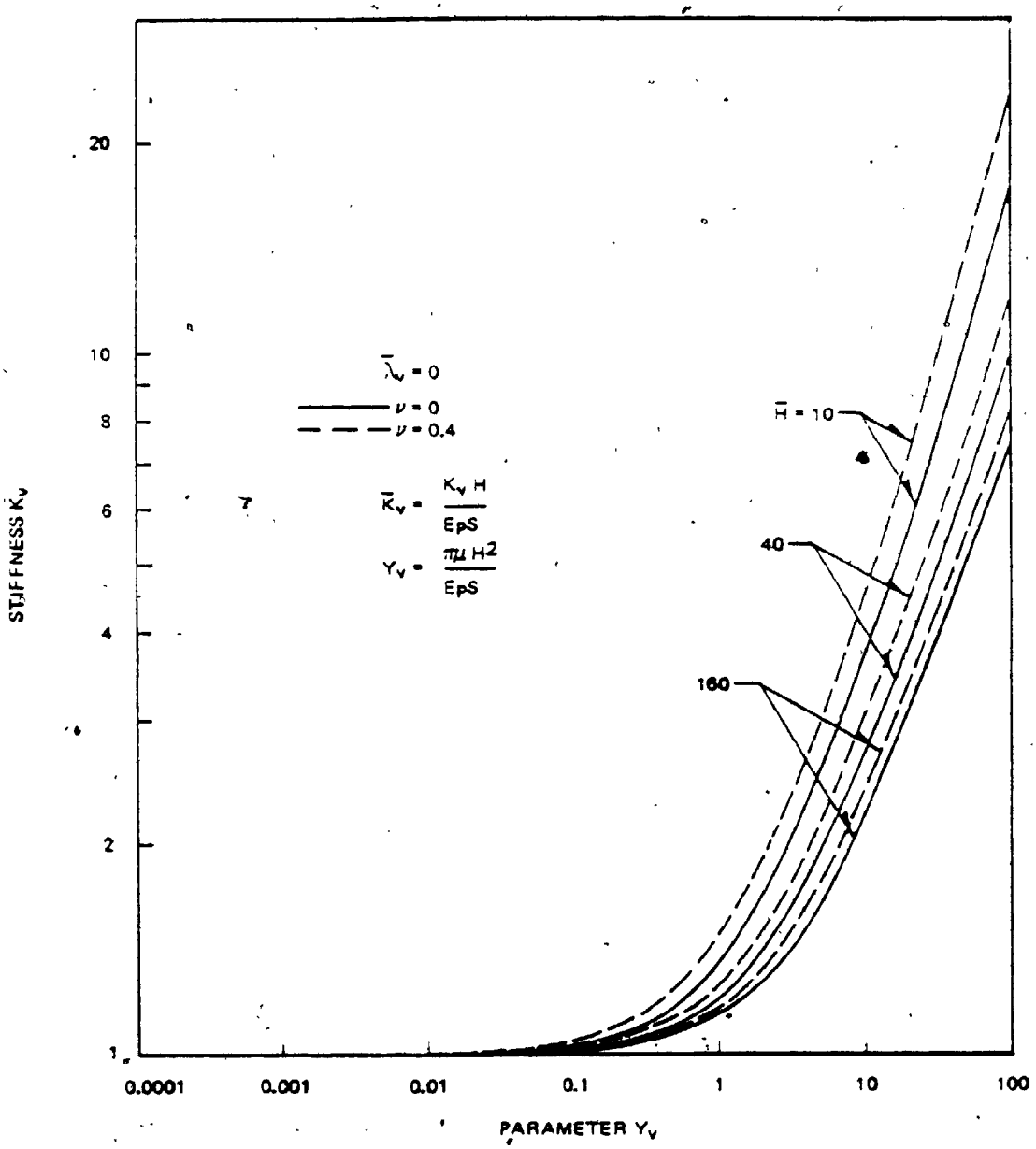

Fig. 3.2-12. Variation of Static Stiffness $\bar{K}_v$ with Parameter Y_v for Various Poisson's Ratios

variation of Poisson's ratio. Fig. 3.2-12 shows also that the previously mentioned transitions in the soil effect appear at the more or less unique values of Y_v regardless of any Poisson's ratio; however, the values of Y_v at those transitions are slightly larger for a lower Poisson's ratio.

It was found previously that the soil resistance factor is nearly independent of Poisson's ratio in the high frequency range, and that a higher Poisson's ratio yields a higher resonant frequency of the stratum. Those trends are reflected in the complex stiffness of the soil-pile system as shown in Fig. 3.2-13. The reduction of the stiffness at the fundamental resonant frequency of the stratum is further shown in Fig. 3.2-14. In this figure, the reduction is smaller for a lower Poisson's ratio and a more slender pile. The figure also indicates that the variation of the soil effect with the parameter Y_v is fairly independent of Poisson's ratio for the dynamic case.

(iv) Effect of the Variation of Mass Ratio

When the mass ratio is varied while Y_v is held constant, the relationship between the complex stiffness and the frequency a_0' is affected only through the parameter $\bar{\lambda}_v$ (see the expressions for $\bar{K}_v$ and $\bar{\lambda}_v$ in Eqs. 3.2-12). Therefore the variation of the mass ratio does not affect the complex stiffness in the static case, but does affect in the dynamic case more as frequency increases. This trend can be seen in Fig. 3.2-15 where the lower mass ratio yields lower stiffness and higher damping in the dynamic case. Fig. 3.2-16 indicates that those trends appear to be more significant in the stronger soil effect and a less slender pile. This is because the difference in the mass ratio

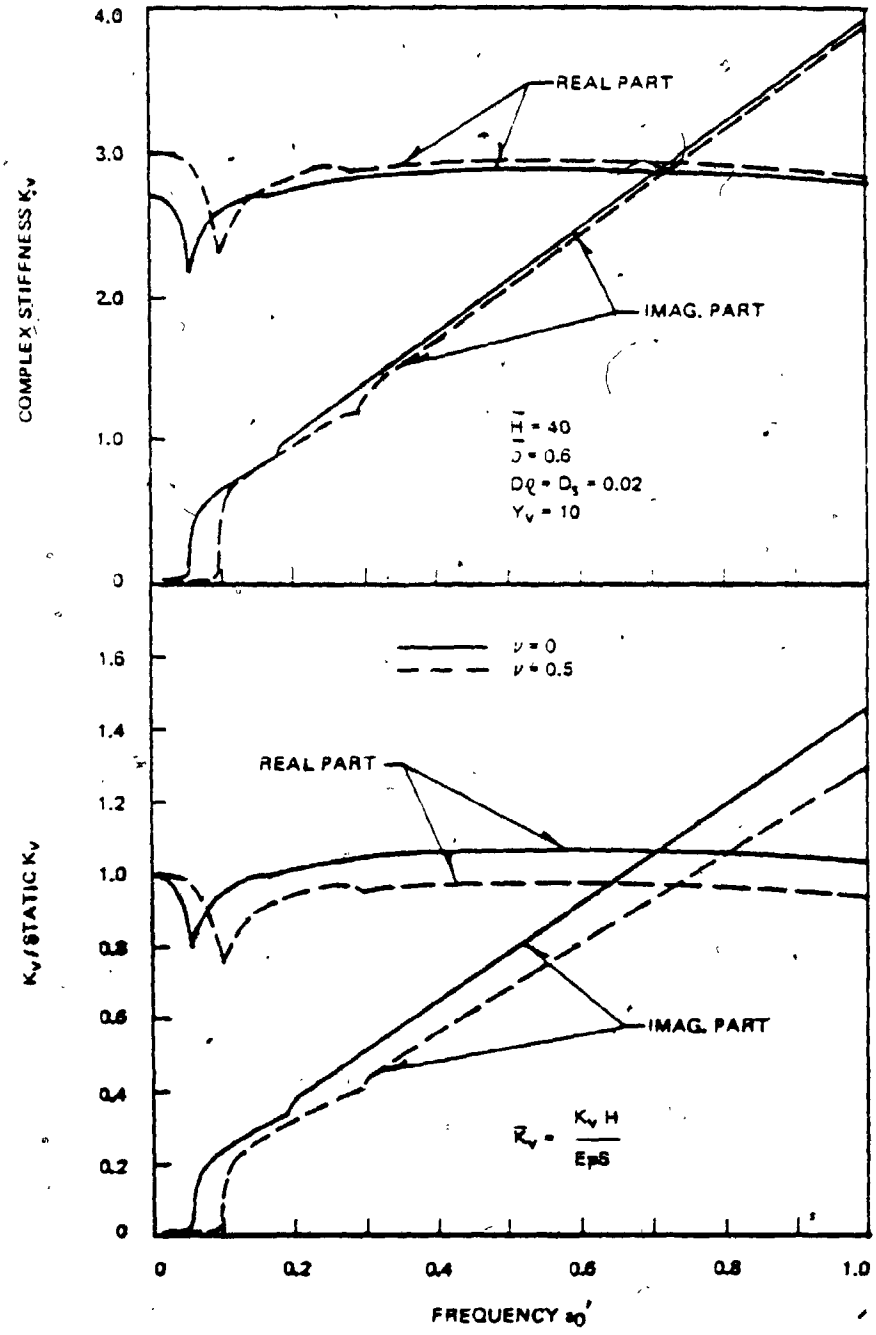

Fig. 3.2-13. Variation of Complex Stiffness $\bar{K}_v$ with Frequency a_0' for Various Poisson's Ratios

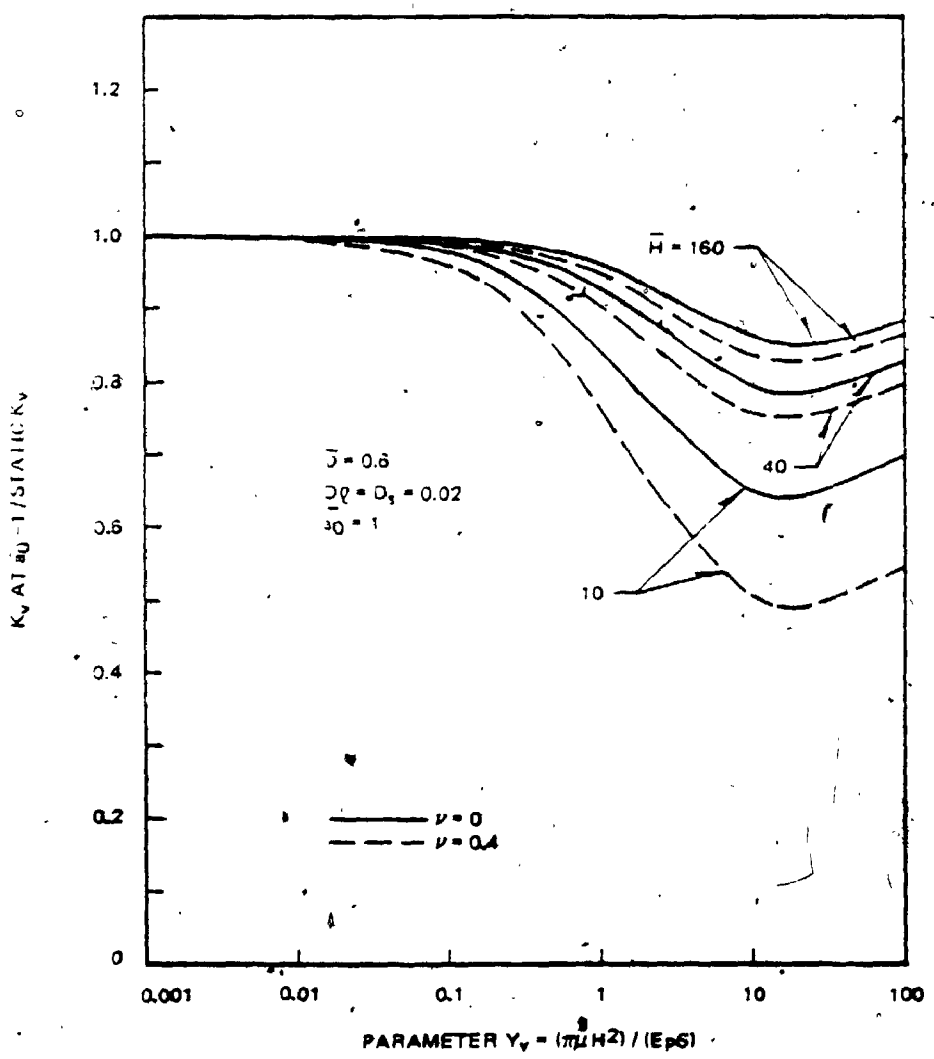

Fig. 3.2-14. Reduction of Real Part of Stiffness K_v at the First Natural Frequency of Stratum for Various Poisson's Ratios

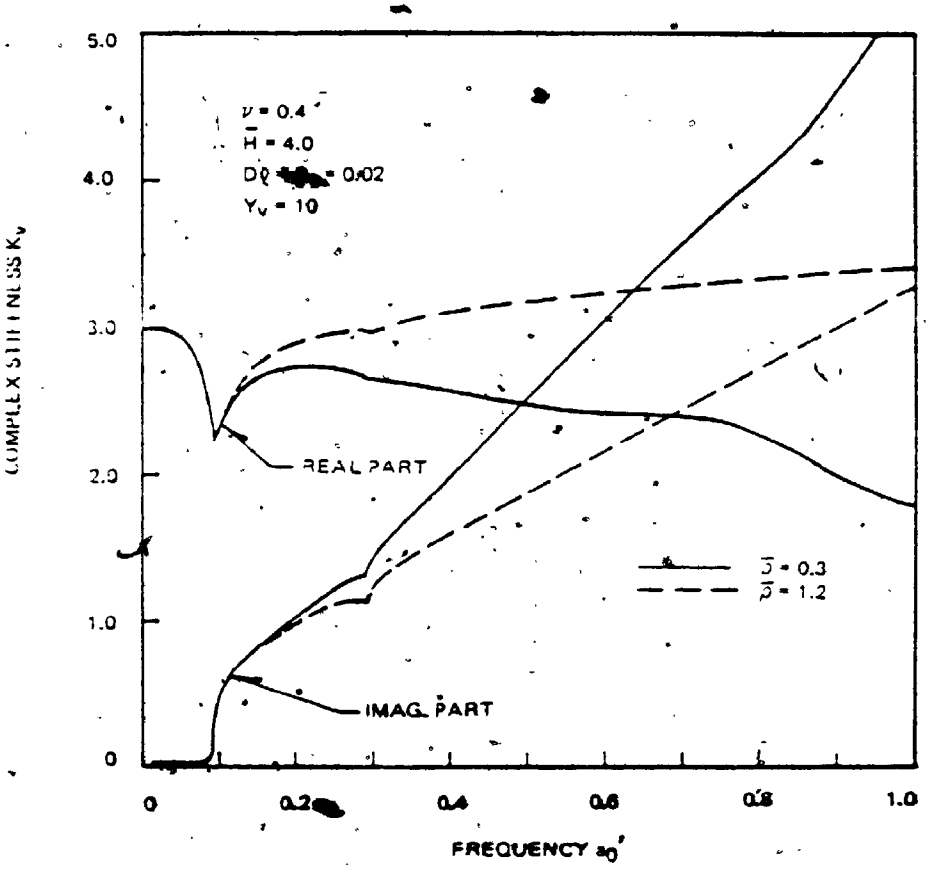

Fig. 3.2-15. Variation of Complex Stiffness $\bar{K}_v$ with Frequency a_0' for Various Mass Ratios

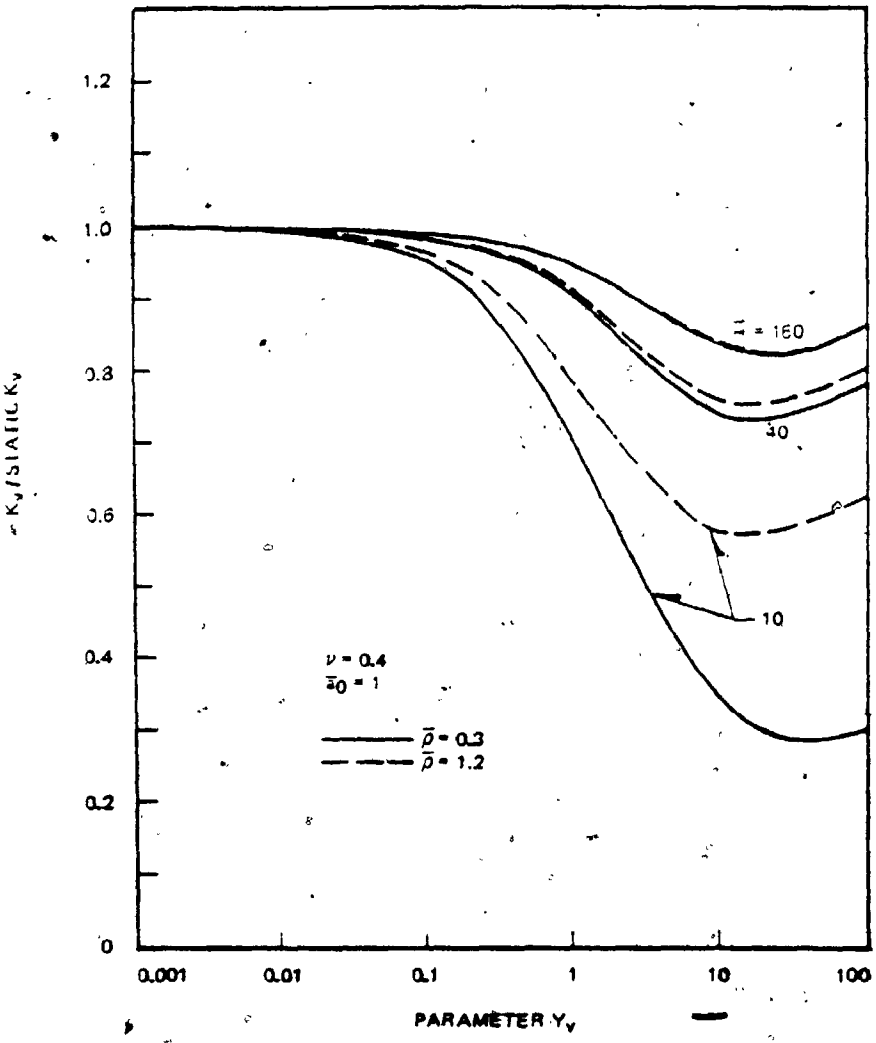

Fig. 3.2-16. Reduction of Real Part of Stiffness K_v at the First Natural Frequency of Stratum for Various Mass Ratios

leads to a larger difference in $\bar{\lambda}_v$ for larger Y_v and smaller $\bar{H}$ (see Y_v and $\bar{\lambda}_v$ in Eqs. 3.2-12).

The variation of the complex stiffness with frequency $\bar{b}$ is shown in Fig. 3.2-17 for the various mass ratios. The damping for the lower mass ratio is smaller in this figure, although it is larger in Fig. 3.2-15. This is because the frequency $\bar{b}$ is larger for the smaller mass ratio under the specified a_0' (see $\bar{\lambda}_v$ in Eqs. 3.2-12).

3.3 Stiffnesses and Dampings in Horizontal Vibration

When a pile is subjected to a horizontal or rotational excitation at the pile head, the pile deforms both laterally and rotationally along its length. This situation is called here a horizontal vibration. Thus, in horizontal vibration, the horizontal and rotational displacements of the pile are coupled to each other.

In vertical vibration, the mode shape of the pile coincides with that of stratum. However, it is not necessarily so in horizontal vibration. If the mode shape of the pile is not identical to that of the stratum, the application of the modal analysis in horizontal vibration leads to simultaneous linear equations - as many as the number of modes of pile required to describe the displacement. The currently available explicit solution (Tajimi, 1969) is based on modal analysis and only for the pile with "rotationally fixed head - pinned tip" in which the mode shape of pile coincides with that of the stratum. The modal analysis, however, can also handle other end conditions as shown in Appendix D where the solution is derived using modal analysis.

When the soil effect on the pile is strong, many modes of the pile are required to describe the pile deformation modified by soil. Since

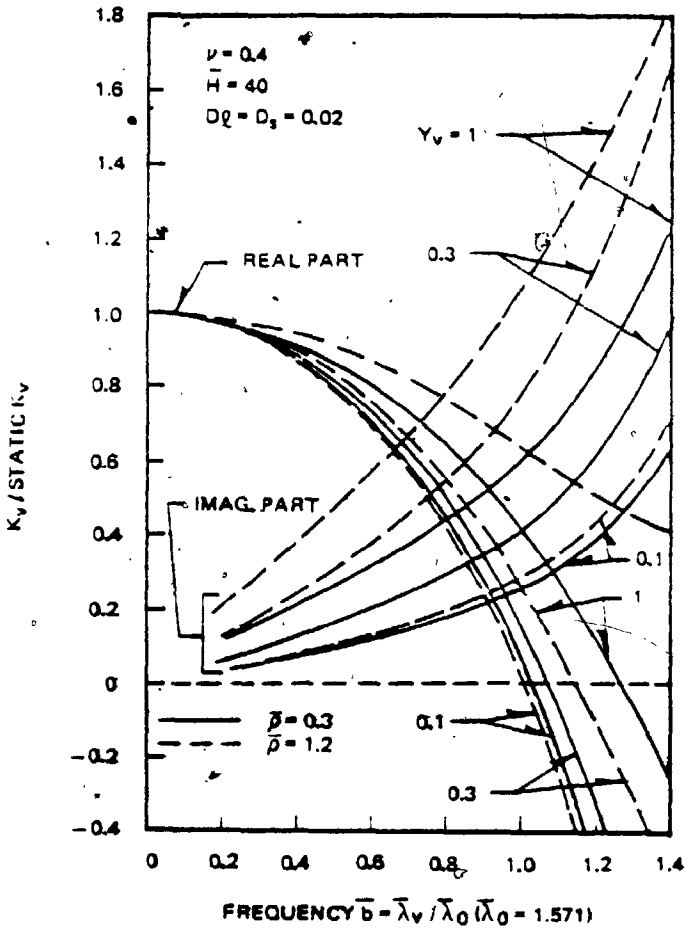

Fig. 3.2-17. Variation of Stiffness K_v with Frequency $\bar{b}$ for Various Poisson's Ratios

the soil effect in horizontal vibration of the pile is usually very strong, modal analysis results in considerable effort in solving a large number of simultaneous linear equations. In order to avoid such difficulty, a new solution called "direct solution" without using modal analysis is developed here. The direct solution leads to only four simultaneous linear equations and is far more efficient than the other solution.

3.3.A Derivation of Solution

The surrounding soil affects the behavior of a pile through the resistance force $p_h(z)e^{i\omega t}$ acting around the circumference of the pile. Then the equilibrium condition of the forces, acting on the infinitesimally thin slice of the pile as shown in Fig. 3.3-1, leads to the following equation.

$$E_pI \frac{\partial^4}{\partial z^4}\left\{U(z)e^{i\omega t}\right\} + m\frac{\partial^2}{\partial t^2}\left\{U(z)e^{i\omega t}\right\} = -p_h(z)e^{i\omega t} \qquad (3.3\text{-}1)$$

where

E_pI = bending stiffness of the pile, and

$U(z)$ = amplitude of horizontal displacement of the pile.

Since separation between soil and pile is not allowed, the soil resistance $p_h(z)$ is expressed by Eq. 2.2-47. Substitution of $p_h(z)$ in Eq. 2.2-47 into Eq. 3.3-1 yields the following equation.

$$E_pI \frac{d^4U(z)}{dz^4} - m\omega^2U(z) = -\sum_{n=1}^{\infty} \alpha_{hn}U_n \sin(h_n z) \qquad (3.3\text{-}2)$$

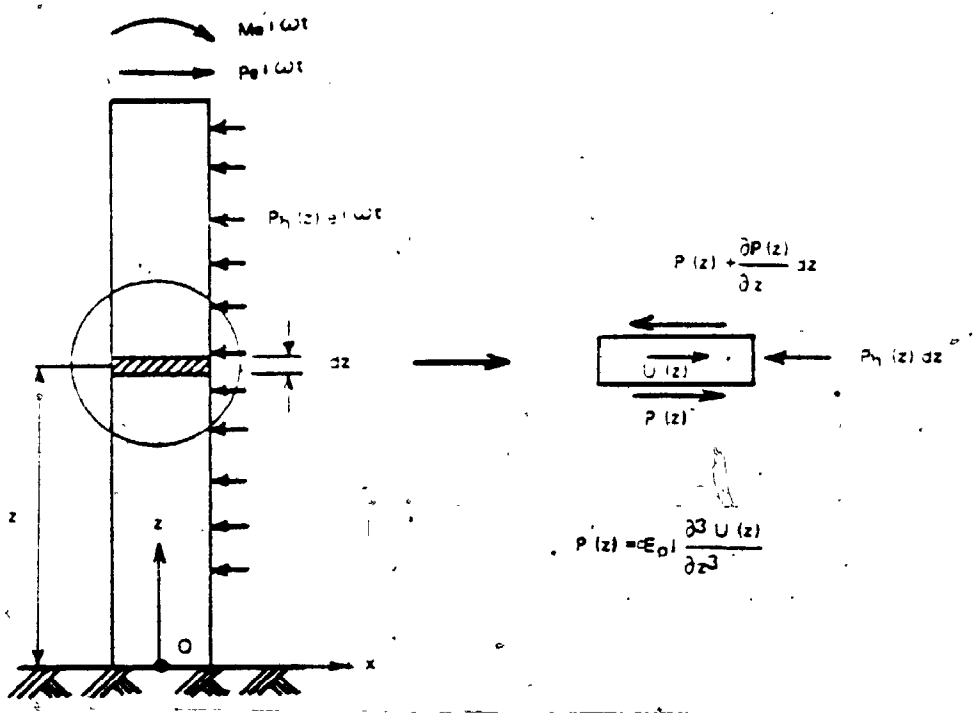

Fig. 3.3-1. External Forces Acting on Pile and Forces Acting on Segment dz of Pile

The solution of Eq. 3.3-2 for U(z) can be obtained by superimposing the homogeneous and particular solutions of Eq. 3.3-2, and hence is

$$U(z) = U_h(z) + U_p(z) \tag{3.3-3}$$

where $U_h(z)$ and $U_p(z)$ are homogeneous and particular solutions of Eq. 3.3-2, respectively.

The particular solution, $U_p(z)$, can be written as

$$U_p(z) = \sum_{n=1}^{\infty} a_n \sin(h_n z) \tag{3.3-4}$$

where a_n is the constant determined by substituting $U_p(z)$ in Eq. 3.3-4 into Eq. 3.3-2 and is

$$a_n = \frac{-\alpha_{hn} U_n}{E_p I h_n^4 - m\omega^2} \tag{3.3-5}$$

The homogeneous solution $U_h(z)$ can be written as

$$U_h(z) = A \sin(\lambda_h z) + B \cos(\lambda_h z) + C \, sh(\lambda_h z) + D \, ch(\lambda_h z) \tag{3.3-6}$$

where A, B, C, and D are the constants determined by the boundary conditions at the head and tip of the pile, and

$$\lambda_h = \sqrt[4]{\frac{m\omega^2}{E_p I}} \tag{3.3-7}$$

Since a perfect connection between pile and soil is assumed, the horizontal displacement of the surrounding soil in Eq. 2.2-43 must be

equal to that of the pile expressed in Eq. 3.3-3. Substituting the above solutions for $U_h(z)$ and $U_p(z)$ into Eq. 3.3-3, this condition leads to

$$A \sin(\lambda_h z) + B \cos(\lambda_h z) + C \, sh(\lambda_h z) + D \, ch(\lambda_h z)$$

$$- \sum_{n=1}^{\infty} \frac{\alpha_{hn} U_n}{EI \, h_n^4 - m\omega^2} \sin(h_n z) = \sum_{n=1}^{\infty} U_n \sin(h_n z) \tag{3.3-8}$$

By expanding $\sin(\lambda_h z)$, $\cos(\lambda_h z)$, $sh(\lambda_h z)$, and $ch(\lambda_h z)$ into a sine Fourier series of argument $h_n z$, Eq. 3.3-8 can be rewritten as

$$\sum_{n=1}^{\infty} \left(AF_{1n} + BF_{2n} + CF_{3n} + DF_{4n} - \frac{\alpha_{hn} U_n}{E_p I \, h_n^4 - m\omega^2} \right) \sin(h_n z)$$

$$= \sum_{n=1}^{\infty} U_n \sin(h_n z) \tag{3.3-9}$$

where

$$\begin{Bmatrix} F_{1n} \\ F_{2n} \\ F_{3n} \\ F_{4n} \end{Bmatrix} = \frac{2}{H} \int_0^H \sin(h_n z) \begin{Bmatrix} \sin(\lambda_h z) \\ \cos(\lambda_h z) \\ sh(\lambda_h z) \\ ch(\lambda_h z) \end{Bmatrix} dz \tag{3.3-10}$$

Solution of Eq. 3.3-9 for U_n is

$$U_n = \frac{\left(AF_{1n} + BF_{2n} + CF_{3n} + DF_{4n} \right) \left(E_p I \, h_n^4 - m\omega^2 \right)}{E_p I \, h_n^2 - m\omega^2 + \alpha_{hn}} \tag{3.3-11}$$

From Eqs. 3.3-4, 3.3-5, and 3.3-11, $U_p(z)$ can be expressed with the unknown constants A, B, C, and D. After substituting such $U_p(z)$ and $U_h(z)$ in Eq. 3.3-6 into Eq. 3.3-3, $U(z)$ is now written as

$$U(z) = \begin{Bmatrix} \sin(\lambda_h z) \\ \cos(\lambda_h z) \\ \mathrm{sh}(\lambda_h z) \\ \mathrm{ch}(\lambda_h z) \end{Bmatrix} - \sum_{n=1}^{\infty} \sin(h_n z) \begin{Bmatrix} f_{1n} \\ f_{2n} \\ f_{3n} \\ f_{4n} \end{Bmatrix}^T \begin{Bmatrix} A \\ B \\ C \\ D \end{Bmatrix} \qquad (3.3\text{-}12)$$

where

$$\begin{Bmatrix} f_{1n} \\ f_{2n} \\ f_{3n} \\ f_{4n} \end{Bmatrix} = \frac{\alpha_{hn}}{E_p I\, h_n^4 - m\omega^2 + \alpha_{hn}} \begin{Bmatrix} F_{1n} \\ F_{2n} \\ F_{3n} \\ F_{4n} \end{Bmatrix} \qquad (3.3\text{-}13)$$

Using the dimensionless parameters, U(z) in Eq. 3.3-12 can be rewritten as

$$U(z) = \begin{Bmatrix} \sin(\bar{\lambda}_h \bar{z}) \\ \cos(\bar{\lambda}_h \bar{z}) \\ \mathrm{sh}(\bar{\lambda}_h \bar{z}) \\ \mathrm{ch}(\bar{\lambda}_h \bar{z}) \end{Bmatrix} - Y_h \sum_{n=1}^{\infty} \sin(\bar{h}_n \bar{z}) \begin{Bmatrix} \bar{f}_{1n} \\ \bar{f}_{2n} \\ \bar{f}_{3n} \\ \bar{f}_{4n} \end{Bmatrix}^T \begin{Bmatrix} A \\ B \\ C \\ D \end{Bmatrix} \qquad (3.3\text{-}14)$$

where

$$Y_h = \pi \mu H^4/(E_p I) = 4\, \bar{\nu}^2\, \bar{\rho}\, \bar{H}^4$$

$$\begin{Bmatrix} \bar{f}_{1n} \\ \bar{f}_{2n} \\ \bar{f}_{3n} \\ \bar{f}_{4n} \end{Bmatrix} = \frac{\bar{\alpha}_{hn}}{\bar{h}_n^4 - \bar{\lambda}_h^4 + Y_h\, \bar{\alpha}_{hn}} \begin{Bmatrix} F_{1n} \\ F_{2n} \\ F_{3n} \\ F_{4n} \end{Bmatrix} \qquad (3.3\text{-}15)$$

$$\bar{\lambda}_h = \lambda_h H = H \sqrt[4]{\frac{m\omega^2}{E_p I}}$$

After evaluating the integration in Eq. 3.3-10, $\{F_n\}$ in Eqs. 3.3-15 can be expressed as

$$\begin{Bmatrix} F_{1n} \\ F_{2n} \\ F_{3n} \\ F_{4n} \end{Bmatrix} = 2 \begin{Bmatrix} \bar{\lambda}_h \cos \bar{\lambda}_h \sin \bar{h}_n / \left(\bar{h}_n^2 - \bar{\lambda}_h^2\right) \\ -\left(\bar{\lambda}_h \sin \bar{h}_n \sin \bar{\lambda}_h - \bar{h}_n\right) / \left(\bar{h}_n^2 - \bar{\lambda}_h^2\right) \\ \bar{\lambda}_h \operatorname{ch} \bar{\lambda}_h \sin \bar{h}_n / \left(\bar{h}_n^2 + \bar{\lambda}_h^2\right) \\ \left(\bar{\lambda}_h \sin \bar{h}_n \operatorname{sh} \bar{\lambda}_h + \bar{h}_n\right) / \left(\bar{h}_n^2 + \bar{\lambda}_h^2\right) \end{Bmatrix} \cdots \bar{\lambda}_h \neq \bar{h}_n \tag{3.3-16}$$

$$\begin{Bmatrix} F_{1n} \\ F_{2n} \\ F_{3n} \\ F_{4n} \end{Bmatrix} = 2 \begin{Bmatrix} \bar{h}_n/2 \\ 0 \\ \bar{\lambda}_h \operatorname{ch} \bar{\lambda}_h \sin \bar{h}_n / \left(\bar{h}_n^2 + \bar{\lambda}_h^2\right) \\ \left(\bar{\lambda}_h \sin \bar{h}_n \operatorname{sh} \bar{\lambda}_h + \bar{h}_n\right) / \left(\bar{h}_n^2 + \bar{\lambda}_h^2\right) \end{Bmatrix} \cdots \bar{\lambda}_h = \bar{h}_n$$

The displacements for the static case can be obtained from the above equations as a limit case for $\bar{\lambda}_h \to 0$, after the constants A, B, C, and D are evaluated. However, no simple explicit formulas can be obtained for $\omega = 0$ from the dynamic solution. Therefore, it appears more suitable to derive a special solution for the static case.

In the static case, Eq. 3.3-2 becomes

$$E_P I \frac{d^4 U(z)}{dz^4} = -\sum_{n=1}^{\infty} \alpha_{hn} U_n \sin(h_n z) \tag{3.3-17}$$

The particular and homogeneous solutions of Eq. 3.3-17 are, respectively,

$$U_p(z) = -\sum_{n=1}^{\infty} \frac{\alpha_{hn} U_n}{E_p I h_n^4} \sin(h_n z) \qquad (3.3\text{-}18a)$$

$$U_h(z) = AZ^3 + BZ^2 + CZ + D \qquad (3.3\text{-}18b)$$

The complete solution for $U(z)$ can be obtained by superimposing the above two solutions and are

$$U(z) = U_h(z) + U_p(z)$$

$$= AZ^3 + BZ^2 + CZ + D - \sum_{n=1}^{\infty} \frac{\alpha_{hn} U_n}{E_p I h_n^4} \sin(h_n Z) \qquad (3.3\text{-}19)$$

Following the same procedure as that in the dynamic case, U_n for the static case can be obtained as

$$U_n = \frac{(AF_{1n} + BF_{2n} + CF_{3n} + DF_{4n}) E_p I h_n^4}{E_p I h_n^4 + \alpha_{hn}} \qquad (3.3\text{-}20)$$

where

$$\begin{Bmatrix} F_{1n} \\ F_{2n} \\ F_{3n} \\ F_{4n} \end{Bmatrix} = \frac{2}{H} \int_0^H \sin(h_n z) \begin{Bmatrix} Z^3 \\ Z^2 \\ Z \\ 1 \end{Bmatrix} dz \qquad (3.3\text{-}21)$$

Substituting U_n in Eq. 3.3-20 into Eq. 3.3-19 and introducing the dimensionless parameters lead finally to

$$U(z) = \left\{ \begin{matrix} \bar{z}^3 \\ \bar{z}^2 \\ \bar{z} \\ 1 \end{matrix} \right\} - Y_h \sum_{n=1}^{\infty} \sin(\bar{h}_n z) \left\{ \begin{matrix} \bar{f}_{1n} \\ \bar{f}_{2n} \\ \bar{f}_{3n} \\ \bar{f}_{4n} \end{matrix} \right\}^T \left\{ \begin{matrix} A \\ B \\ C \\ D \end{matrix} \right\} \qquad (3.3\text{-}22)$$

where

$$\left\{ \begin{matrix} \bar{f}_{1n} \\ \bar{f}_{2n} \\ \bar{f}_{3n} \\ \bar{f}_{4n} \end{matrix} \right\} = \frac{\bar{\alpha}_{hn}}{\bar{h}_n^4 + Y_h \bar{\alpha}_{hn}} \left\{ \begin{matrix} F_{1n}/H^3 \\ F_{2n}/H^2 \\ F_{3n}/H \\ F_{4n} \end{matrix} \right\} \qquad (3.3\text{-}23)$$

and evaluation of the integration in Eq. 3.3-21 leads to

$$\left\{ \begin{matrix} F_{1n}/H^3 \\ F_{2n}/H^2 \\ F_{3n}/H \\ F_{4n} \end{matrix} \right\} = \frac{2}{\bar{h}_n^4} \sin(\bar{h}_n) \left\{ \begin{matrix} 3\,\bar{h}_n^2 - 6 \\ 2\,\bar{h}_n^2 \\ \bar{h}_n^2 \\ 0 \end{matrix} \right\} + \frac{2}{\bar{h}_n^3} \left\{ \begin{matrix} 0 \\ -1 \\ 0 \\ \bar{h}_n^2 \end{matrix} \right\} \qquad (3.3\text{-}24)$$

With the displacement of the pile expressed in Eqs. 3.3-14 and 3.3-22 the amplitude of the angle of rotation ζ, the bending moment M, and shear force P are obtained from the standard relationships:

$$\zeta(z) = \frac{dU(z)}{dz} \tag{3.3-25a}$$

$$M(z) = E_p I \frac{d^2U(z)}{dz^2} \tag{3.3-25b}$$

$$P(z) = E_p I \frac{d^3U(z)}{dz^3} \tag{3.3-25c}$$

All these quantities are listed in matrix form in Table 3.3-1.

The displacements and forces at the pile head are related through the stiffness K_h at the pile head as

$$\begin{Bmatrix} P \\ M \end{Bmatrix} = \begin{bmatrix} K_h(P,U) & -K_h(P,\zeta) \\ -K_h(M,U) & K_h(M,\zeta) \end{bmatrix} \begin{Bmatrix} U \\ \zeta \end{Bmatrix} \tag{3.3-26}$$

where $K_h(P,\zeta)$ is equal to $K_h(M,U)$, since a linear soil-pile system is assumed; and U and ζ are $U(\bar{z}=1)$ and $\zeta(\bar{z}=1)$, respectively.

The stiffnesses K_h are defined by the forces applied at the pile head which yield appropriate unit displacements at the pile head as shown in Fig. 3.3-2. This leads to the following boundary conditions at the pile head.

$$\begin{aligned} &K_h(P,U) \text{ and } K_h(M,U) \quad \ldots \quad U(\bar{z}=1) = 1,\ \zeta(\bar{z}=1) = 0 \\ &K_h(P,\zeta) \text{ and } K_h(M,\zeta) \quad \ldots \quad U(\bar{z}=1) = 0,\ \zeta(\bar{z}=1) = 1 \end{aligned} \tag{3.3-27}$$

The boundary conditions at the pile tip are

Pinned tip $\quad U(\bar{z}=0) = 0,\ M(\bar{z}=0) = 0$ (3.3-28a)

Clamped tip $\quad U(\bar{z}=0) = 0,\ \zeta(\bar{z}=0) = 0$ (3.3-28b)

Table 3.3-1

General Expressions for Displacements and Forces of Pile

Static Case ($\omega = 0$)

$$\begin{Bmatrix} U(\bar{z}) \\ \zeta(\bar{z}) \cdot H \\ M(\bar{z}) \cdot \frac{H^2}{E_p I} \\ P(\bar{z}) \cdot \frac{H^3}{E_p I} \end{Bmatrix} = \begin{bmatrix} \bar{z}^3 & \bar{z}^2 & \bar{z} & 1 \\ 3\bar{z}^2 & 2\bar{z} & 1 & 0 \\ 6\bar{z} & 2 & 0 & 0 \\ 6 & 0 & 0 & 0 \end{bmatrix} - Y_h \sum_{n=1}^{\infty} \begin{bmatrix} \bar{f}_{1n} \sin \bar{h}_n \bar{z} & \bar{f}_{2n} \sin \bar{h}_n \bar{z} & \bar{f}_{3n} \sin \bar{h}_n \bar{z} & \bar{f}_{4n} \sin \bar{h}_n \bar{z} \\ \bar{f}_{1n} \bar{h}_n \cos \bar{h}_n \bar{z} & \bar{f}_{2n} \bar{h}_n \cos \bar{h}_n \bar{z} & \bar{f}_{3n} \bar{h}_n \cos \bar{h}_n \bar{z} & \bar{f}_{4n} \bar{h}_n \cos \bar{h}_n \bar{z} \\ -\bar{f}_{1n} \bar{h}_n^2 \sin \bar{h}_n \bar{z} & -\bar{f}_{2n} \bar{h}_n^2 \sin \bar{h}_n \bar{z} & -\bar{f}_{3n} \bar{h}_n^2 \sin \bar{h}_n \bar{z} & -\bar{f}_{4n} \bar{h}_n^2 \sin \bar{h}_n \bar{z} \\ -\bar{f}_{1n} \bar{h}_n^3 \cos \bar{h}_n \bar{z} & -\bar{f}_{2n} \bar{h}_n^3 \cos \bar{h}_n \bar{z} & -\bar{f}_{3n} \bar{h}_n^3 \cos \bar{h}_n \bar{z} & -\bar{f}_{4n} \bar{h}_n^3 \cos \bar{h}_n \bar{z} \end{bmatrix} \begin{Bmatrix} A \\ B \\ C \\ D \end{Bmatrix}$$

Dynamic Case ($\omega \neq 0$)

$$\begin{Bmatrix} U(\bar{z}) \\ \zeta(\bar{z}) \cdot H \\ M(\bar{z}) \frac{H^2}{E_p I} \\ P(\bar{z}) \frac{H^3}{E_p I} \end{Bmatrix} = \begin{bmatrix} \sin\bar{\lambda}\bar{z} & \cos\bar{\lambda}\bar{z} & \sh\bar{\lambda}\bar{z} & \ch\bar{\lambda}\bar{z} \\ \bar{\lambda}\cos\bar{\lambda}\bar{z} & -\bar{\lambda}\sin\bar{\lambda}\bar{z} & \bar{\lambda}\ch\bar{\lambda}\bar{z} & \bar{\lambda}\sh\bar{\lambda}\bar{z} \\ -\bar{\lambda}^2\sin\bar{\lambda}\bar{z} & -\bar{\lambda}^2\cos\bar{\lambda}\bar{z} & \bar{\lambda}^2\sh\bar{\lambda}\bar{z} & \bar{\lambda}^2\ch\bar{\lambda}\bar{z} \\ -\bar{\lambda}^3\cos\bar{\lambda}\bar{z} & \bar{\lambda}^3\sin\bar{\lambda}\bar{z} & \bar{\lambda}^3\ch\bar{\lambda}\bar{z} & \bar{\lambda}^3\sh\bar{\lambda}\bar{z} \end{bmatrix} - Y_h \sum_{n=1}^{\infty} \begin{bmatrix} \bar{f}_{1n} \sin \bar{h}_n \bar{z} & \bar{f}_{2n} \sin \bar{h}_n \bar{z} & \bar{f}_{3n} \sin \bar{h}_n \bar{z} & \bar{f}_{4n} \sin \bar{h}_n \bar{z} \\ \bar{f}_{1n} \bar{h}_n \cos \bar{h}_n \bar{z} & \bar{f}_{2n} \bar{h}_n \cos \bar{h}_n \bar{z} & \bar{f}_{3n} \bar{h}_n \cos \bar{h}_n \bar{z} & \bar{f}_{4n} \bar{h}_n \cos \bar{h}_n \bar{z} \\ -\bar{f}_{1n} \bar{h}_n^2 \sin \bar{h}_n \bar{z} & -\bar{f}_{2n} \bar{h}_n^2 \sin \bar{h}_n \bar{z} & -\bar{f}_{3n} \bar{h}_n^2 \sin \bar{h}_n \bar{z} & -\bar{f}_{4n} \bar{h}_n^2 \sin \bar{h}_n \bar{z} \\ -\bar{f}_{1n} \bar{h}_n^3 \cos \bar{h}_n \bar{z} & -\bar{f}_{2n} \bar{h}_n^3 \cos \bar{h}_n \bar{z} & -\bar{f}_{3n} \bar{h}_n^3 \cos \bar{h}_n \bar{z} & -\bar{f}_{4n} \bar{h}_n^3 \cos \bar{h}_n \bar{z} \end{bmatrix} \begin{Bmatrix} A \\ B \\ C \\ D \end{Bmatrix}$$

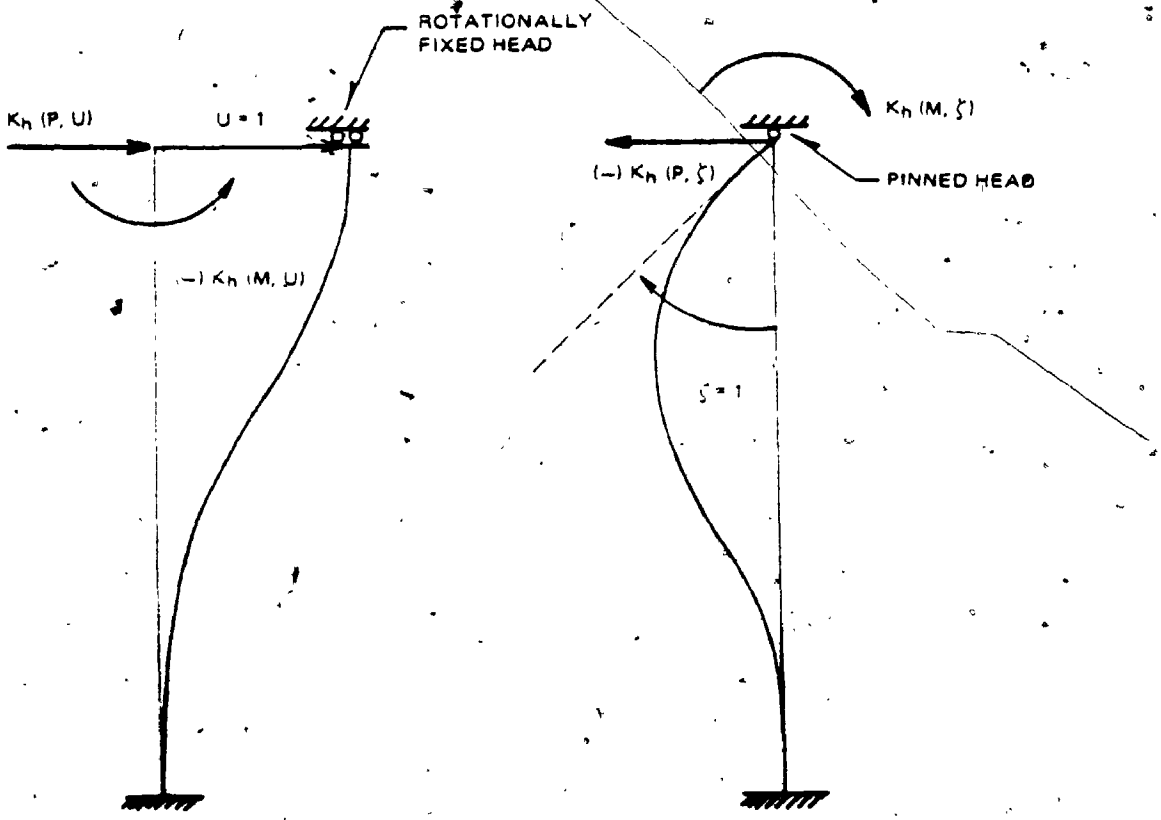

Fig. 3.3-2. Boundary Conditions at Pile Head in Deriving Stiffness K_h

Thus, four simultaneous linear equations are established for the given boundary conditions and are listed in Table 3.3-2. After solving these equations for the constants A, B, C and D, the stiffness or the corresponding forces at the pile head are obtained from the equations listed in Table 3.3-3.

The following dimensionless parameters for the stiffnesses $\bar{K}_h$ are defined for convenience.

$$\begin{bmatrix} \bar{K}_h(P,U) & -\bar{K}_h(P,\zeta) \\ -\bar{K}_h(M,U) & \bar{K}_h(M,\zeta) \end{bmatrix} = \frac{1}{E_P I} \begin{bmatrix} H^3 K_h(P,U) & -H^2 K_h(P,\zeta) \\ -H^2 K_h(M,U) & H K_h(M,\zeta) \end{bmatrix} \tag{3.3-29a}$$

or

$$\begin{bmatrix} \bar{K}_h(P,U)/\bar{H}^3 & -\bar{K}_h(P,\zeta)/\bar{H}^2 \\ -\bar{K}_h(M,U)/\bar{H}^2 & \bar{K}_h(M,\zeta)/\bar{H} \end{bmatrix} = \frac{1}{E_P I} \begin{bmatrix} r_0^3 K_h(P,U) & -r_0^2 K_h(P,\zeta) \\ -r_0^2 K_h(M,U) & r_0 K_h(M,\zeta) \end{bmatrix} \tag{3.3-29b}$$

Dimensionless parameters on the left hand side of Eq. 3.3-29a can show fully the effect of the variation of pile radius, whereas those in Eq. 3.3-29b are more suitable for showing the effect of pile length.

3.3.B Effect of Soil on Stiffnesses and Dampings

The derived explicit solution shows that the complex stiffness $\bar{K}_h$ is governed by the slenderness ratio ($\bar{H}$); soil resistance factor ($\bar{\alpha}_{hn}$) which is further governed by $\bar{H}$, a_0, ν, D_1, Y and D_s; frequency ($\bar{\lambda}_h$ and a_0); and parameter Y_h. These parameters determine the effect of the surrounding soil on the stiffness of the pile. In this section the above mentioned effect of the surrounding soil is studied.

Table 3.3-2a

Simultaneous Linear Equations for Various Boundary Conditions (Pinned Tip)

Static Case ($\omega = 0$)

$$\left.\begin{matrix} K_h(P,U) \text{ and } K_h(M,U) \ldots \\ K_h(P,\zeta) \text{ and } K_h(M,\zeta) \ldots \end{matrix}\right\} = \left[\begin{matrix} 1 & 1 & 1 & 1 \\ 3 & 2 & 1 & 0 \\ 0 & 0 & 0 & 1 \\ 0 & 2 & 0 & 0 \end{matrix}\right] - Y_h \sum_{n=1}^{\infty} \left[\begin{matrix} \bar{f}_{1n}\sin\bar{h}_n & \bar{f}_{2n}\sin\bar{h}_n & \bar{f}_{3n}\sin\bar{h}_n & \bar{f}_{4n}\sin\bar{h}_n \\ \bar{f}_{1n}\bar{h}_n\cos\bar{h}_n & \bar{f}_{2n}\bar{h}_n\cos\bar{h}_n & \bar{f}_{3n}\bar{h}_n\cos\bar{h}_n & \bar{f}_{4n}\bar{h}_n\cos\bar{h}_n \\ 0 & 0 & 0 & 0 \\ 0 & 0 & 0 & 0 \end{matrix}\right] \left\{\begin{matrix} A \\ B \\ C \\ D \end{matrix}\right\}$$

Dynamic Case ($\delta \neq 0$)

$$\left.\begin{matrix} K_h(P,U) \text{ and } K_h(M,U) \ldots \\ K_h(P,\zeta) \text{ and } K_h(M,\zeta) \ldots \end{matrix}\right\} = \left[\begin{matrix} \sin\bar{\lambda} & \cos\bar{\lambda} & \sinh\bar{\lambda} & \cosh\bar{\lambda} \\ \bar{\lambda}\cos\bar{\lambda} & -\bar{\lambda}\sin\bar{\lambda} & \bar{\lambda}\cosh\bar{\lambda} & \bar{\lambda}\sinh\bar{\lambda} \\ 0 & 1 & 0 & 1 \\ 0 & -\bar{\lambda}^2 & 0 & \bar{\lambda}^2 \end{matrix}\right] - K_h \sum_{n=1}^{\infty} \left[\begin{matrix} \bar{f}_{1n}\sin\bar{h}_n & \bar{f}_{2n}\sin\bar{h}_n & \bar{f}_{3n}\sin\bar{h}_n & \bar{f}_{4n}\sin\bar{h}_n \\ \bar{f}_{1n}\bar{h}_n\cos\bar{h}_n & \bar{f}_{2n}\bar{h}_n\cos\bar{h}_n & \bar{f}_{3n}\bar{h}_n\cos\bar{h}_n & \bar{f}_{4n}\bar{h}_n\cos\bar{h}_n \\ 0 & 0 & 0 & 0 \\ 0 & 0 & 0 & 0 \end{matrix}\right] \left\{\begin{matrix} A \\ B \\ C \\ D \end{matrix}\right\}$$

Table 3.3-2b

Simultaneous Linear Equations for Various Boundary Conditions (Clamped Tip)

Static Case ($\omega = 0$)

$$K_h(P,U) \text{ and } K_h(M,U) \ldots \begin{Bmatrix} 1 \\ 0 \\ 0 \\ 0 \end{Bmatrix}$$

$$K_h(P,\zeta) \text{ and } K_h(M,\zeta) \ldots \begin{Bmatrix} 0 \\ M \\ 0 \\ 0 \end{Bmatrix} =$$

$$\begin{bmatrix} 1 & 1 & 1 & 1 \\ 3 & 2 & 1 & 0 \\ 0 & 0 & 0 & 1 \\ 0 & 0 & 1 & 0 \end{bmatrix} - \gamma_h \sum_{n=1}^{\infty} \begin{bmatrix} \bar{f}_{1n} \sin \bar{h}_n & \bar{f}_{2n} \sin \bar{h}_n & \bar{f}_{3n} \sin \bar{h}_n & \bar{f}_{4n} \sin \bar{h}_n \\ \bar{f}_{1n} \bar{h}_n \cos \bar{h}_n & \bar{f}_{2n} \bar{h}_n \cos \bar{h}_n & \bar{f}_{3n} \bar{h}_n \cos \bar{h}_n & \bar{f}_{4n} \bar{h}_n \cos \bar{h}_n \\ 0 & 0 & 0 & 0 \\ \bar{f}_{1n} \bar{h}_n & \bar{f}_{2n} \bar{h}_n & \bar{f}_{3n} \bar{h}_n & \bar{f}_{4n} \bar{h}_n \end{bmatrix} \begin{Bmatrix} A \\ B \\ C \\ D \end{Bmatrix}$$

Dynamic Case ($\omega \neq 0$)

$$K_h(P,U) \text{ and } K_h(M,U) \ldots \begin{Bmatrix} 1 \\ 0 \\ 0 \\ 0 \end{Bmatrix}$$

$$K_h(P,\zeta) \text{ and } K_h(M,\zeta) \ldots \begin{Bmatrix} 0 \\ M \\ 0 \\ 0 \end{Bmatrix} =$$

$$\begin{bmatrix} \sin\bar{\lambda} & \cos\bar{\lambda} & \sinh\bar{\lambda} & \cosh\bar{\lambda} \\ \bar{\lambda}\cos\bar{\lambda} & -\bar{\lambda}\sin\bar{\lambda} & \bar{\lambda}\cosh\bar{\lambda} & \bar{\lambda}\sinh\bar{\lambda} \\ 0 & 1 & 0 & 1 \\ \bar{\lambda} & 0 & \bar{\lambda} & 0 \end{bmatrix} - \gamma_h \sum_{n=1}^{\infty} \begin{bmatrix} \bar{f}_{1n} \sin \bar{h}_n & \bar{f}_{2n} \sin \bar{h}_n & \bar{f}_{3n} \sin \bar{h}_n & \bar{f}_{4n} \sin \bar{h}_n \\ \bar{f}_{1n} \bar{h}_n \cos \bar{h}_n & \bar{f}_{2n} \bar{h}_n \cos \bar{h}_n & \bar{f}_{3n} \bar{h}_n \cos \bar{h}_n & \bar{f}_{4n} \bar{h}_n \cos \bar{h}_n \\ 0 & 0 & 0 & 0 \\ \bar{f}_{1n} \bar{h}_n & \bar{f}_{2n} \bar{h}_n & \bar{f}_{3n} \bar{h}_n & \bar{f}_{4n} \bar{h}_n \end{bmatrix} \begin{Bmatrix} A \\ B \\ C \\ D \end{Bmatrix}$$

Table 3.3-3

Stiffnesses Derived from the Obtained Constants

Static Case

$$\begin{Bmatrix} ① \\ ② \end{Bmatrix} = -\left[\begin{bmatrix} 6 & 0 & 0 & 0 \\ 6 & 2 & 0 & 0 \end{bmatrix} + Y_h \sum_{n=1}^{\infty} \begin{bmatrix} \bar{f}_{1n}\bar{h}_n^3\cos\bar{h}_n & \bar{f}_{2n}\bar{h}_n^3\cos\bar{h}_n & \bar{f}_{3n}\bar{h}_n^3\cos\bar{h}_n & \bar{f}_{4n}\bar{h}_n^3\cos\bar{h}_n \\ \bar{f}_{1n}\bar{h}_n^2\sin\bar{h}_n & \bar{f}_{2n}\bar{h}_n^2\sin\bar{h}_n & \bar{f}_{3n}\bar{h}_n^2\sin\bar{h}_n & \bar{f}_{4n}\bar{h}_n^2\sin\bar{h}_n \end{bmatrix}\right] \begin{Bmatrix} A \\ B \\ C \\ D \end{Bmatrix}$$

Dynamic Case

$$\begin{Bmatrix} ① \\ ② \end{Bmatrix} = -\left[\begin{bmatrix} -\bar{\lambda}^3\cos\bar{\lambda} & \bar{\lambda}^3\sin\bar{\lambda} & \bar{\lambda}^3\mathrm{ch}\bar{\lambda} & \bar{\lambda}^3\mathrm{sh}\bar{\lambda} \\ -\bar{\lambda}^2\sin\bar{\lambda} & -\bar{\lambda}^2\cos\bar{\lambda} & \bar{\lambda}^2\mathrm{sh}\bar{\lambda} & \bar{\lambda}^2\mathrm{ch}\bar{\lambda} \end{bmatrix} + Y_h \sum_{n=1}^{\infty} \begin{bmatrix} \bar{f}_{1n}\bar{h}_n^3\cos\bar{h}_n & \bar{f}_{2n}\bar{h}_n^3\cos\bar{h}_n & \bar{f}_{3n}\bar{h}_n^3\cos\bar{h}_n & \bar{f}_{4n}\bar{h}_n^3\cos\bar{h}_n \\ \bar{f}_{1n}\bar{h}_n^2\sin\bar{h}_n & \bar{f}_{2n}\bar{h}_n^2\sin\bar{h}_n & \bar{f}_{3n}\bar{h}_n^2\sin\bar{h}_n & \bar{f}_{4n}\bar{h}_n^2\sin\bar{h}_n \end{bmatrix}\right] \begin{Bmatrix} A \\ B \\ C \\ D \end{Bmatrix}$$

where $\bar{K}_h(P,U) = ①$; $-\bar{K}_h(P,\zeta) = ①$; $\bar{K}_h(M,\zeta) = ②$; $-\bar{K}_h(M,U) = ②$

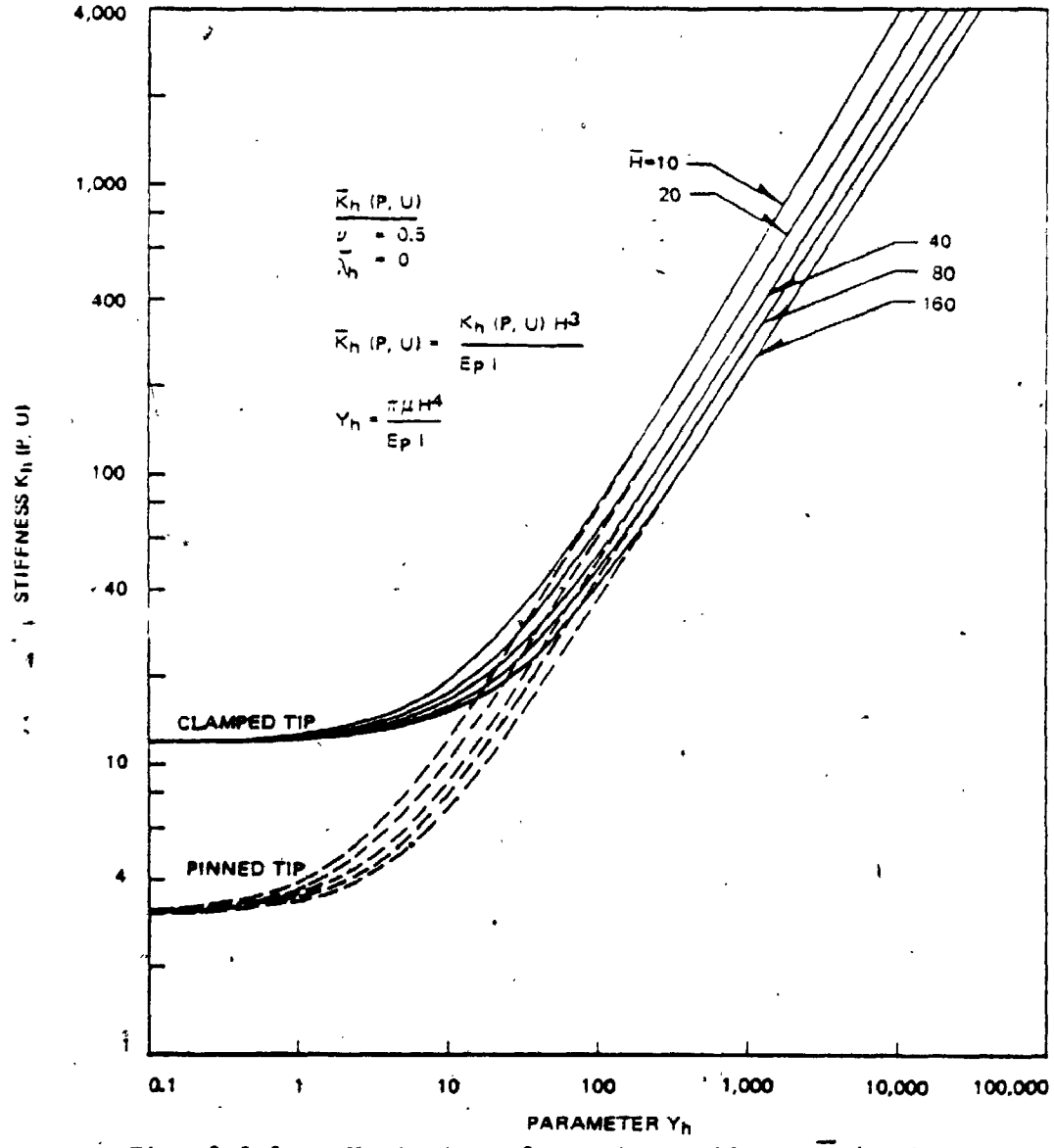

Fig. 3.3-3a. Variation of Static Stiffness $\bar{K}_h(P,U)$ with Parameter Y_h

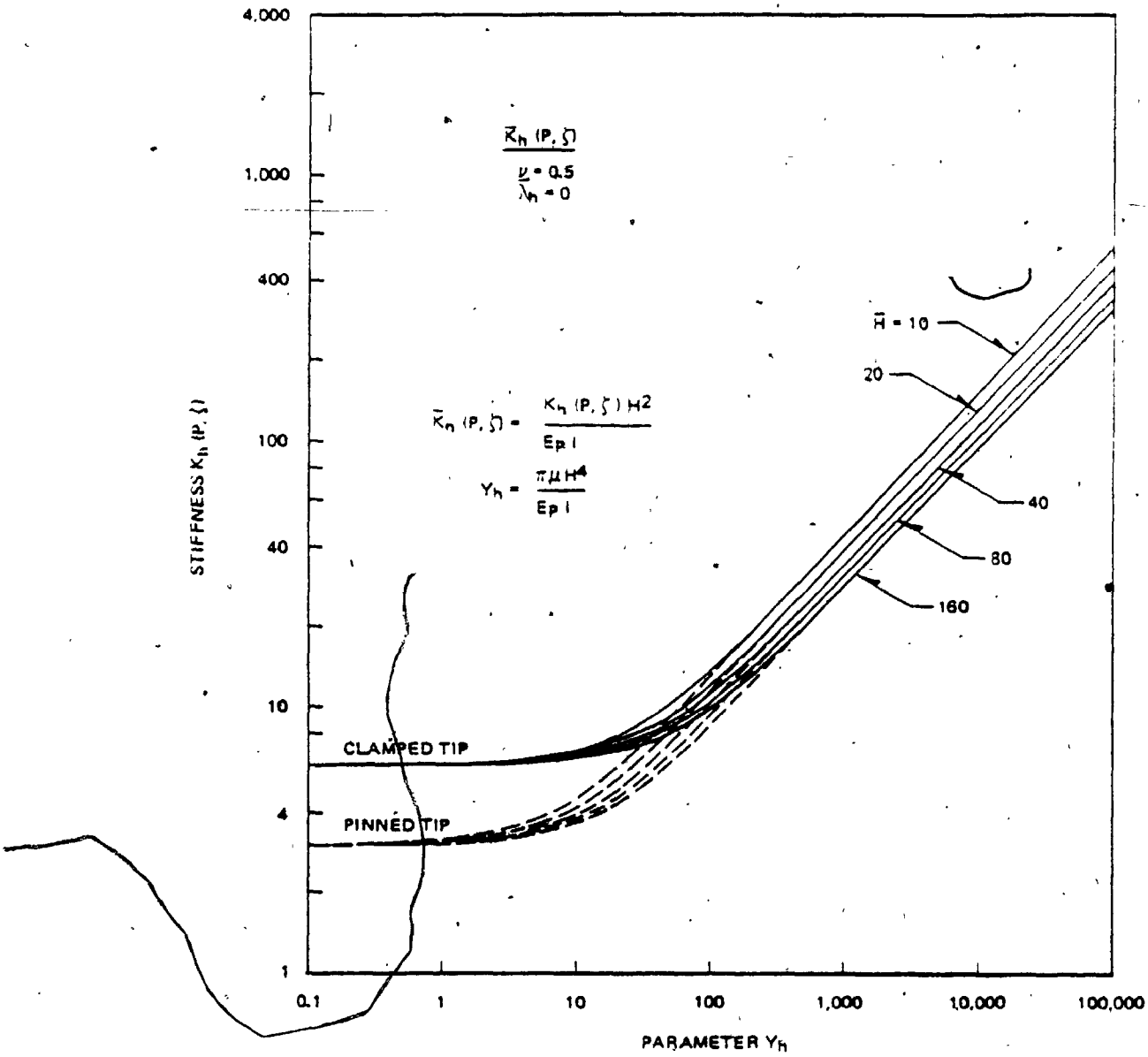

Fig. 3.3-3b. Variation of Static Stiffness $\bar{K}_h(P,\zeta)$ with Parameter Y_h

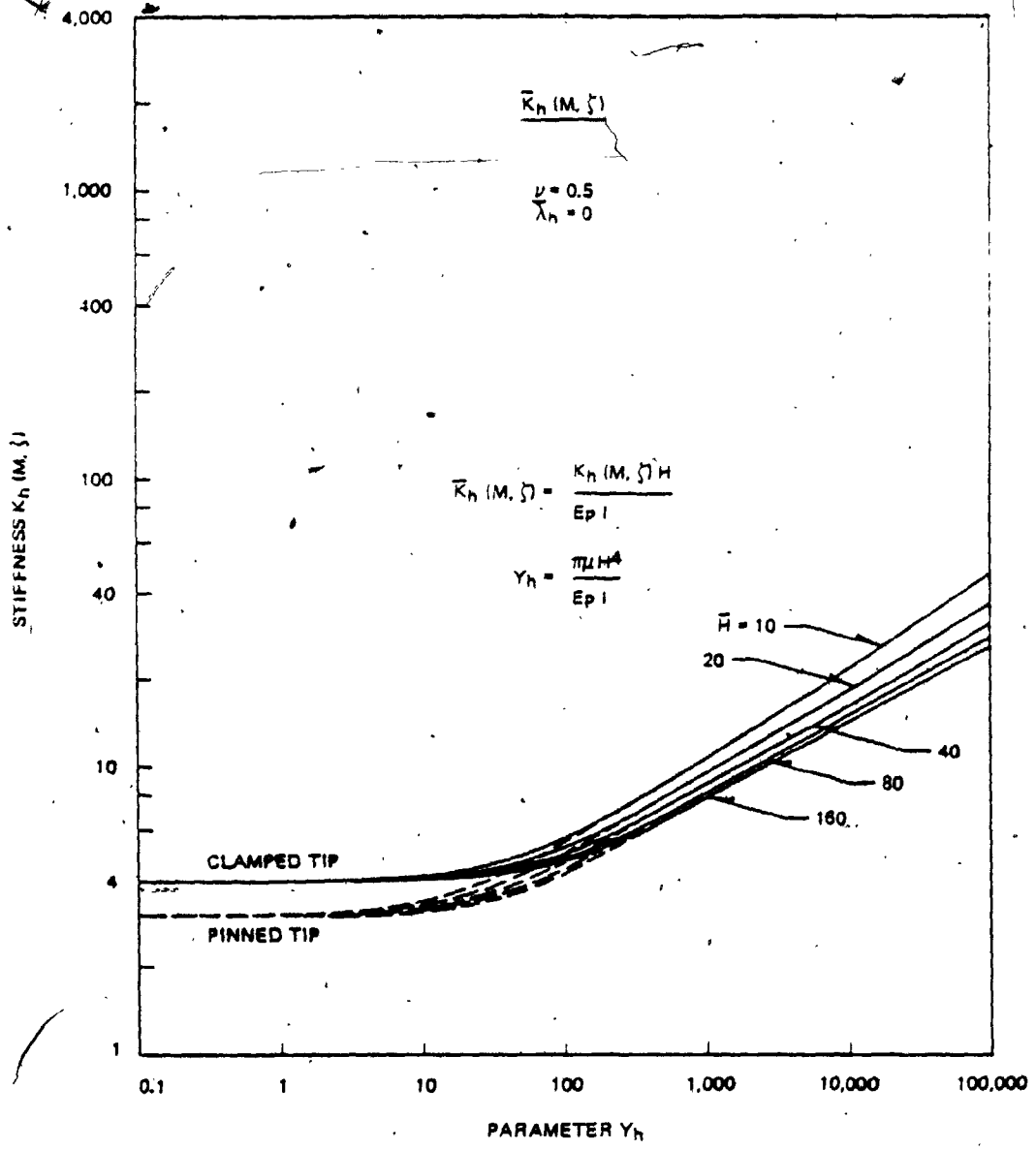

Fig. 3.3-3c. Variation of Static Stiffness $\bar{K}_h(M,\zeta)$ with Parameter Y_h

(i) General Features for the Static Case

When the effect of soil is absent, the parameters Y_h and $\bar{\alpha}_{hn}$ are zero. This situation leads to the following values of the stiffnesses $\bar{K}_h$.

$$\begin{Bmatrix} \bar{K}_h(P,U) \\ \bar{K}_h(P,\zeta) \\ \bar{K}_h(M,\zeta) \end{Bmatrix} = \begin{Bmatrix} 3 \\ 3 \\ 3 \end{Bmatrix} \qquad \text{(pinned tip)}$$

$$= \begin{Bmatrix} 12 \\ 6 \\ 4 \end{Bmatrix} \qquad \text{(clamped tip)}$$

When the surrounding soil affects the behavior of the pile, those stiffnesses become larger than the above values as shown in Figs. 3.3-3. In these figures, the growth of soil effect with parameter Y_h is slower for $K_h(M,\zeta)$ than $K_h(P,U)$. This is because the boundary conditions for $K_h(M,\zeta)$ provide the stiffer condition to the pile. The growth rate of soil effect in $K_h(P,\zeta)$ seems to be somewhere between those in $K_h(M,\zeta)$ and $K_h(P,U)$. The clamped tip also provides the stiffer condition to the pile than the pinned tip does. Thus, as can be seen in Figs. 3.3-3, the effect of soil on the stiffness grows more rapidly with Y_v for the pinned tip pile than for the clamped tip pile. However, when the surrounding soil effect is strong enough to fix the lower portion of pile, the difference in stiffness between pinned tip and clamped tip piles diminishes.

Figs. 3.3-3 further indicate a rather unique relationship between soil effect and Y_h regardless of any slenderness of pile. The transition from the very weak to intermediate soil effect lies at $Y_h \approx 0.6$ to 10 for the pinned tip and $Y_h \approx 5$ to 30 for the clamped tip. The transition from the intermediate to very strong soil effect lies at $Y_h \approx 60$ to 350 for the pinned tip and $Y_h \approx 350$ to 1000 for the clamped tip. The lower and upper bounds of the above ranges of Y_h are governed by the values Y_h for $K_h(P,U)$ and $K_h(M,\zeta)$, respectively. The unique relationship between soil effect and Y_h, and the expression of Y_h in Eqs. 3.3-16 lead to the same conclusions as those in vertical vibration (see (i) in paragraph 3.2.B) except the third conclusion. The third conclusion for horizontal vibration is that the stiffness $\bar{K}_h$ of the pile is more affected by the variation of the slenderness of the pile than by the variation of the shear wave velocity of the soil.

The stiffness parameter $\bar{K}_h$ does not show the full effect of the length of the pile. The full effect of the variation of the pile length is obtained by dividing the stiffness by the slenderness ratio as expressed in Eq. 3.3-29b and is shown in Figs. 3.3-4. These figures show that the stiffnesses of the soil-pile system for soft soil are strongly affected by the slenderness in $K_h(P,U)$, $K_h(P,\zeta)$, and $K_h(M,\zeta)$ in decreasing order. As soil gets harder, however, they become independent of the pile length. The reason for this has already been given in paragraph 3.2.B for vertical vibration.

(ii) General Features for the Dynamic Case

When soil does not affect the behavior of a pile, the damping does not appear and the stiffnesses decrease monotonically with frequency

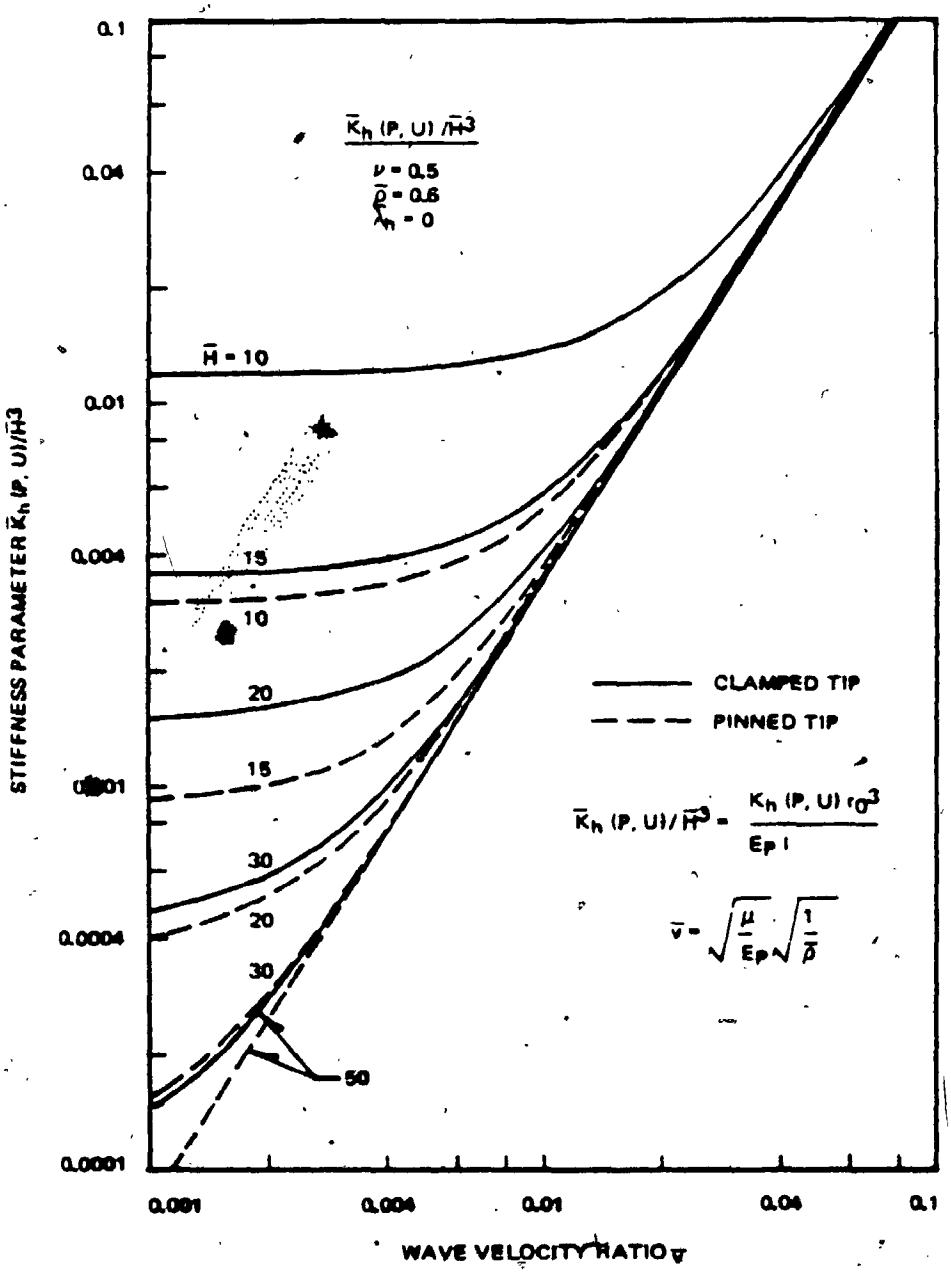

Fig. 3.3-4a. Variation of Static Stiffness Parameter $\bar{K}_h(P,U)/\bar{H}^3$ with Wave Velocity Ratio

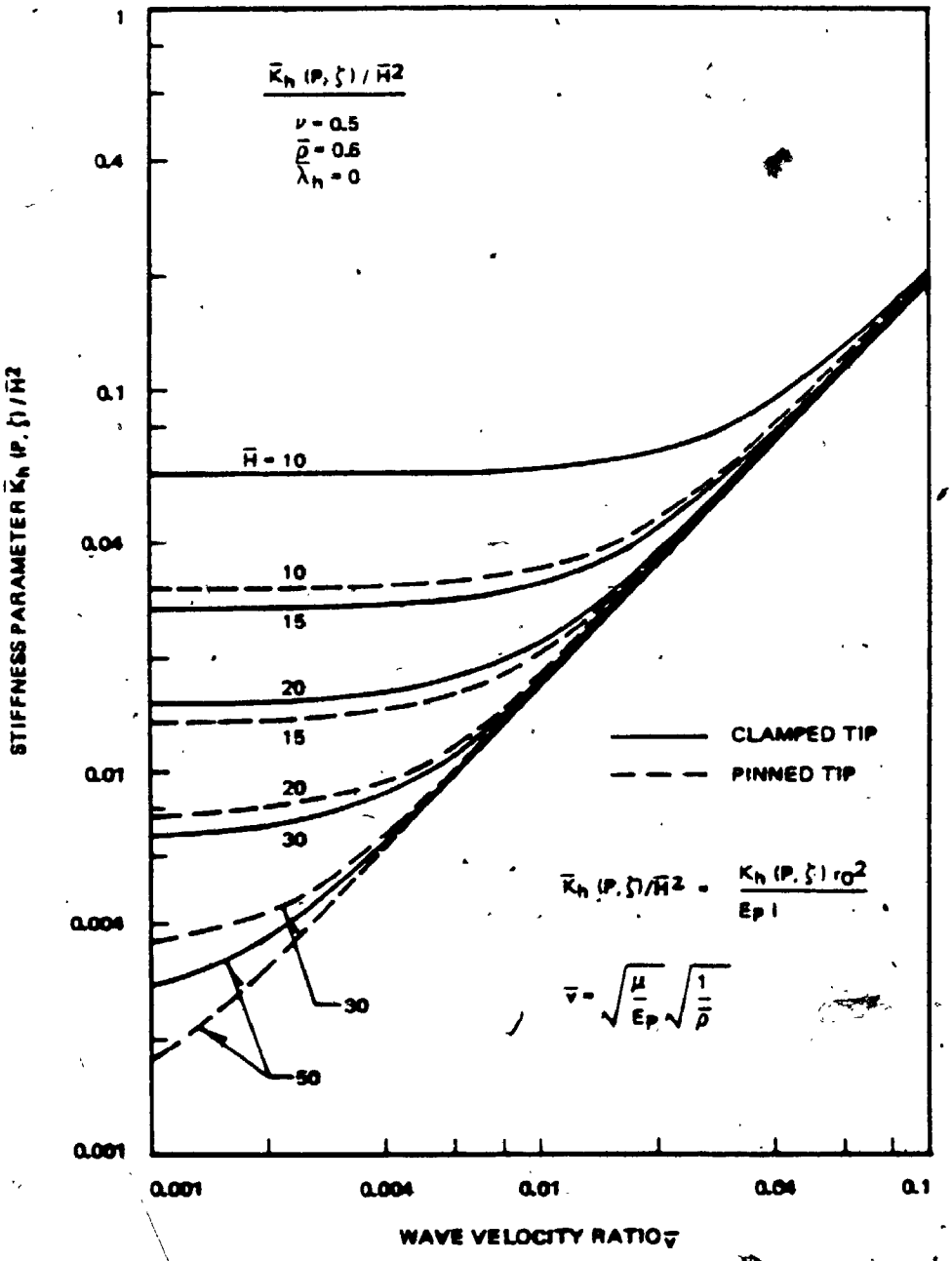

Fig. 3.3-4b. Variation of Static Stiffness Parameter $\bar{K}_h(\bar{P},\bar{\zeta})/\bar{H}^2$ with Wave Velocity Ratio

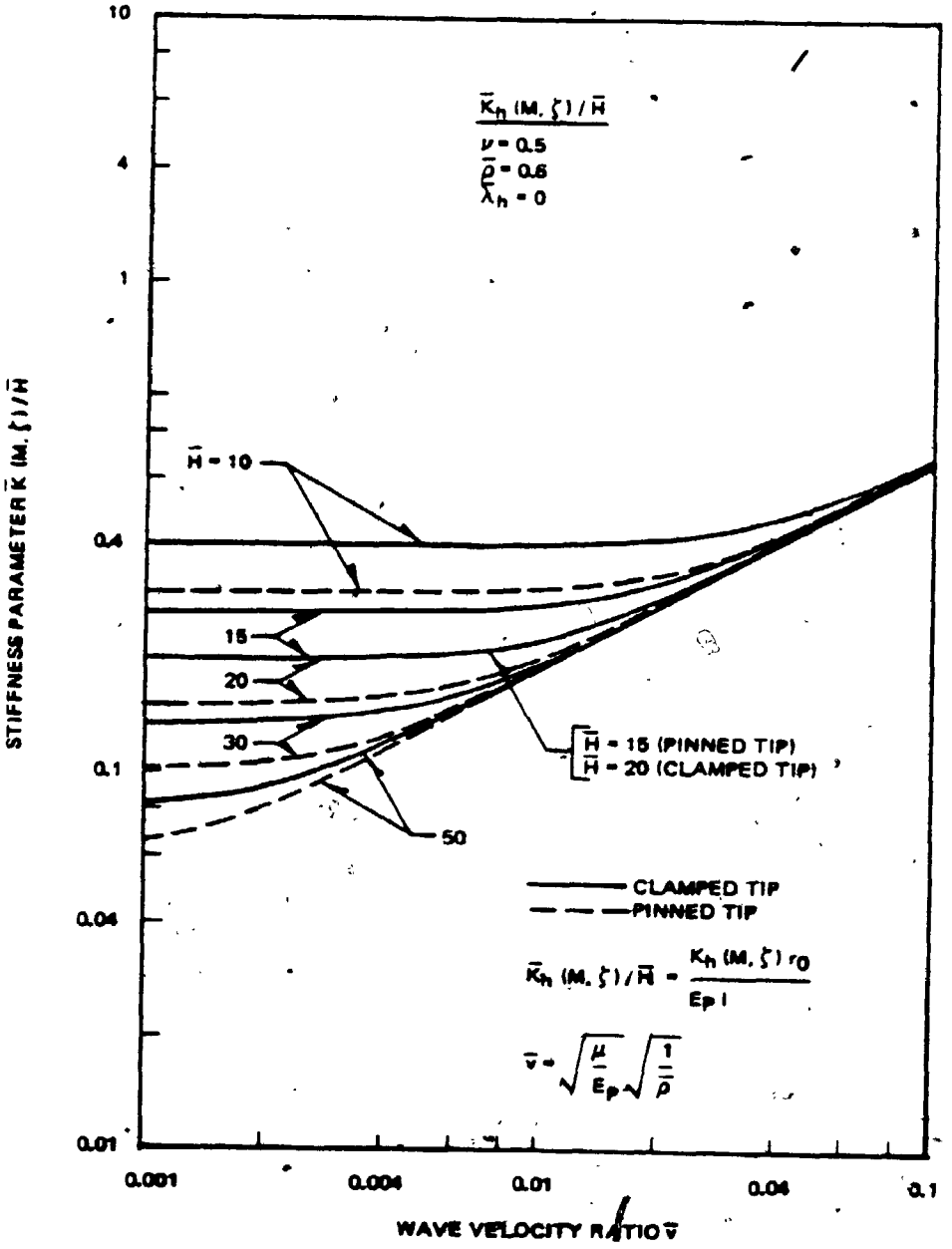

Fig. 3.3-4c. Variation of Static Stiffness Parameter $\bar{K}_h(M,\zeta)/\bar{H}$ with Wave Velocity Ratio

($\bar{b} \leq 1.5$) as shown in Fig. 3.3-5. In this case, the stiffnesses are zero at the following frequencies.

$$\bar{\lambda}_h \text{ for } \begin{Bmatrix} K_h(P,U) \\ K_h(P,\zeta) \\ K_h(M,\zeta) \end{Bmatrix} = \begin{Bmatrix} 1.571 \\ 2.365 \\ 3.142 \end{Bmatrix} \quad \ldots \quad \text{(pinned tip)}$$

$$= \begin{Bmatrix} 2.365 \\ 3.142 \\ 3.927 \end{Bmatrix} \quad \ldots \quad \text{(clamped tip)}$$

Those frequencies for $K_h(P,U)$ and $K_h(M,\zeta)$ are the natural frequencies of the pile under the boundary conditions with which those stiffnesses are obtained.

The soil surrounding the pile modifies the pile stiffness and generates the damping as shown in Figs. 3.3-6. Trends similar to those in vertical vibration can be seen in these figures. However, under "very weak soil effect," the noticeable difference between those two modes of vibration appears at the frequencies where the stiffnesses are zero; those frequencies in horizontal vibration, $\bar{b}$, can be below $\bar{b} = 1$ whereas those in vertical vibration cannot be. This is because, for small Y_h, the first natural frequency of the soil-pile system corresponds to the frequency a_0' large enough to yield a large negative soil reaction for $\nu = 0.5$.

The stiffness of the soil-pile system tends to drop at the resonance of the stratum as shown in Figs. 3.3-6. The variation of this reduction with the parameter Y_h is further shown in Fig. 3.3-7.

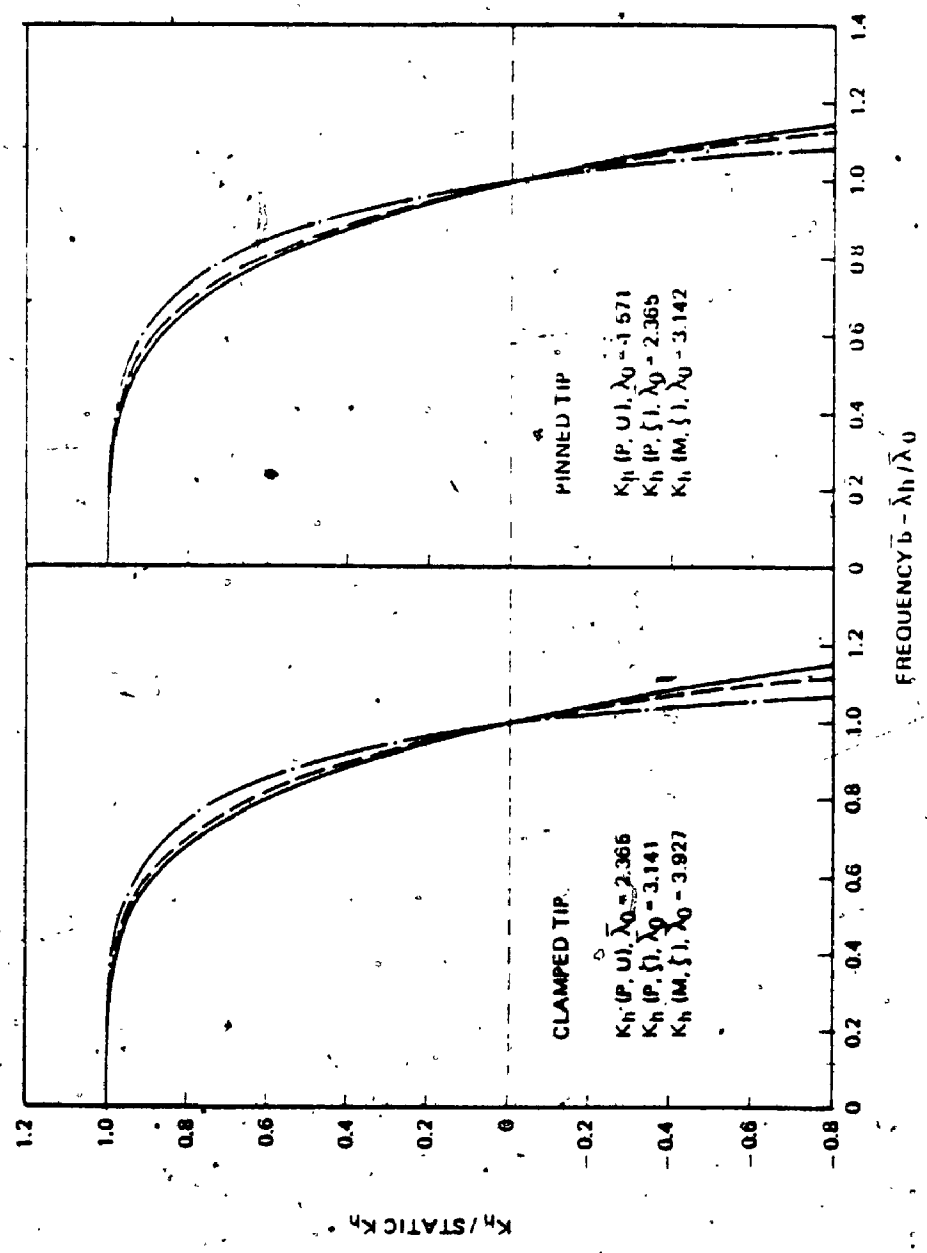

Fig. 3.3-5. Variation of Stiffness K_h with Frequency $\bar{b}$ for Pile Isolated from Soil

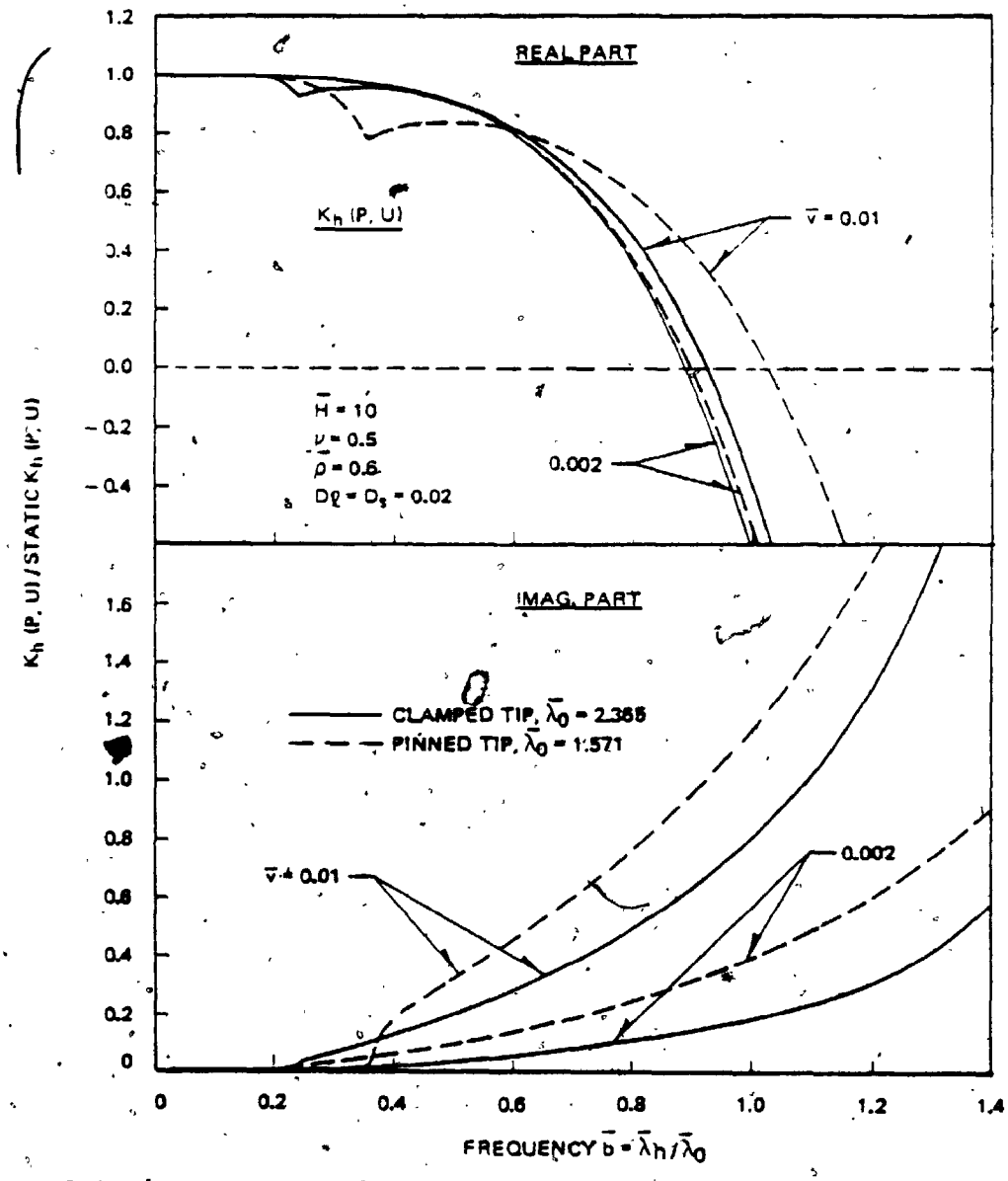

Fig. 3.3-6a. Variation of Complex Stiffness K_h (P,U) with Frequency b for Various Wave Velocity Ratios ($\bar{H}$ = 10)

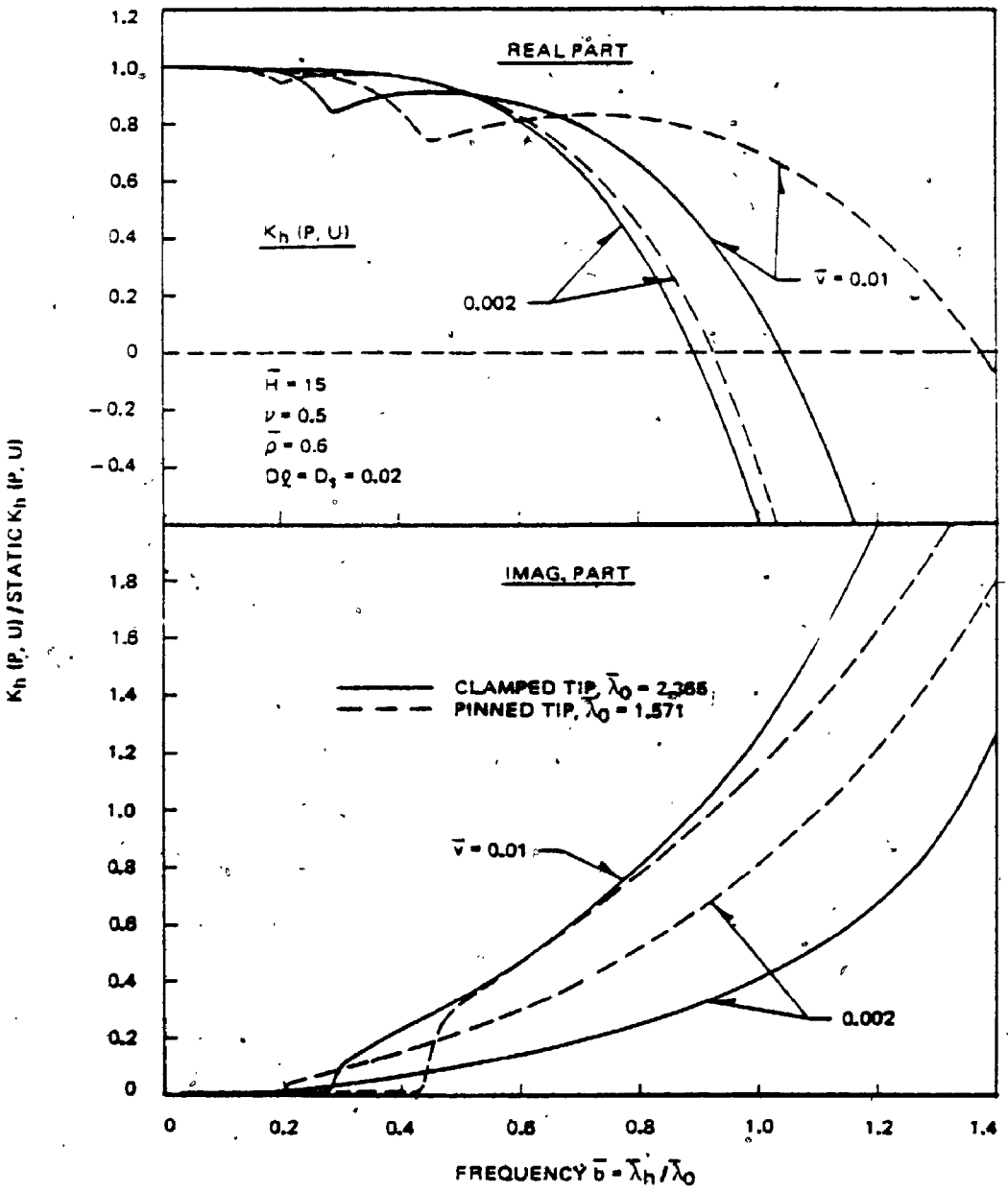

Fig. 3.3-6b. Variation of Complex Stiffness $K_h(P,\underline{U})$ with Frequency $\bar{b}$ for Various Wave Velocity Ratios ($\bar{H}$ = 15)

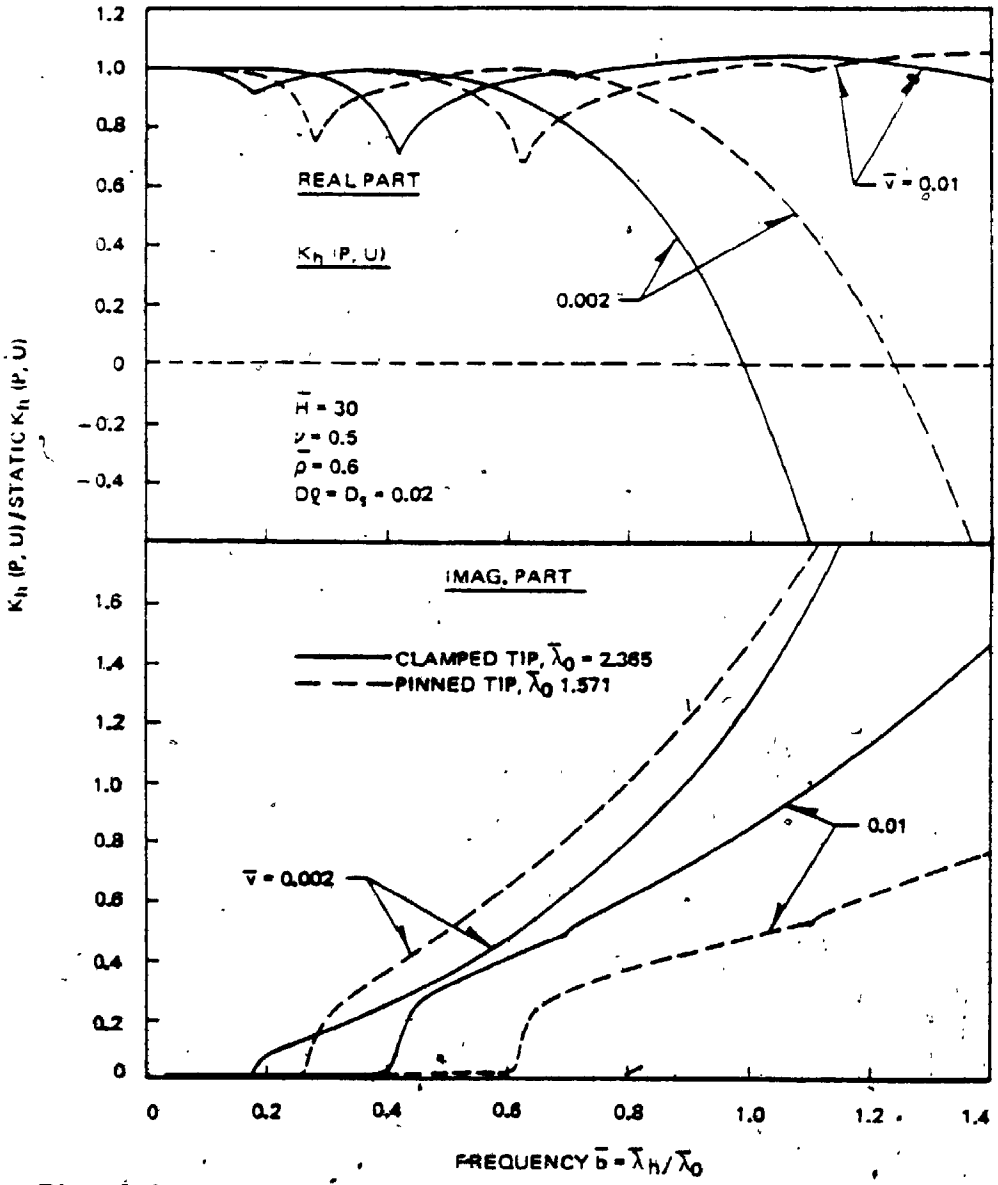

Fig. 3.3-6c. Variation of Complex Stiffness K_h (P,U) with Frequency b for Various Wave Velocity Ratios ($\bar{H}$ = 30)

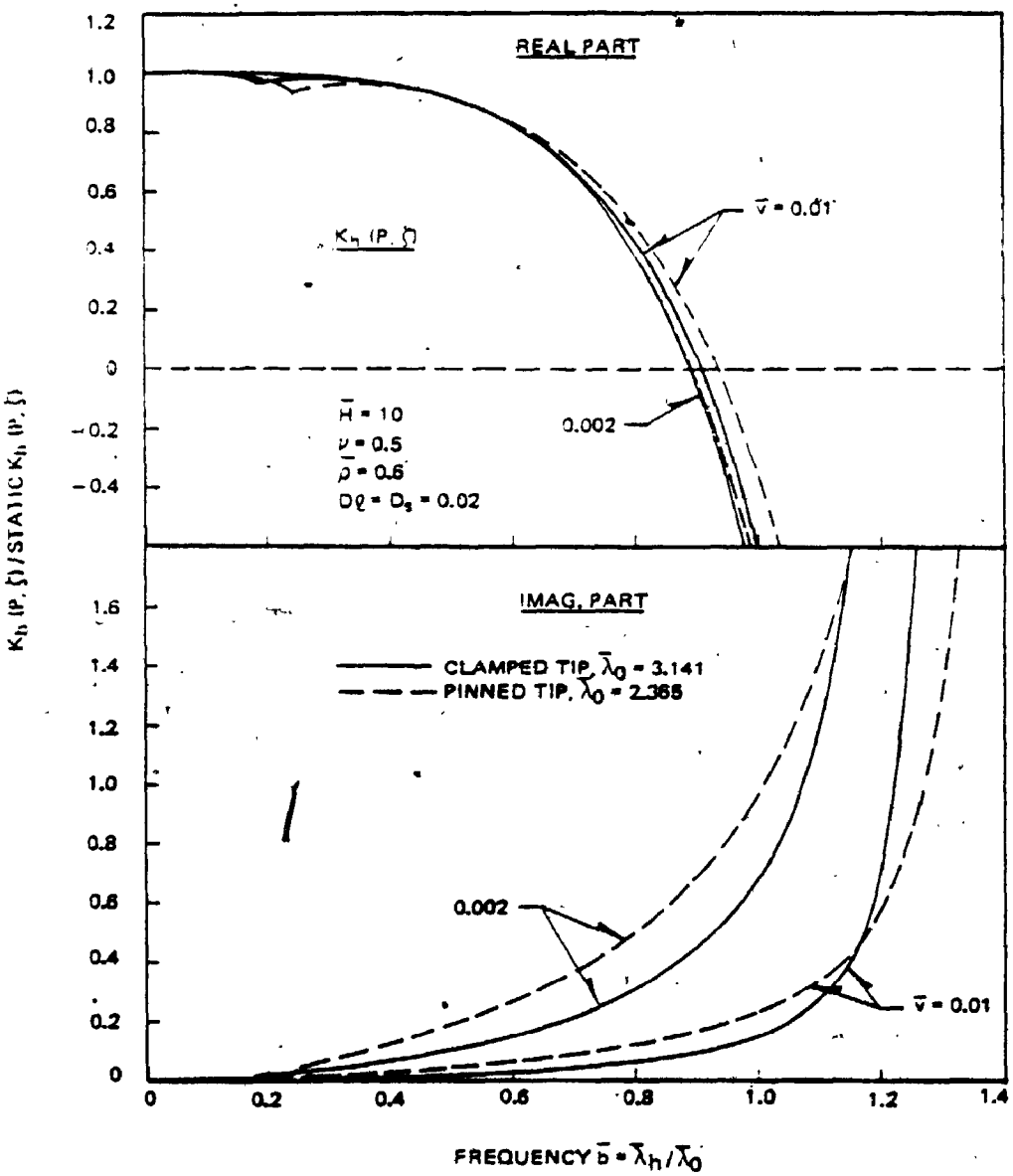

Fig. 3.3-6d. Variation of Complex Stiffness $K_h(P,\zeta)$ with Frequency $\bar{b}$ for Various Wave Velocity Ratios ($\bar{H} = 10$)

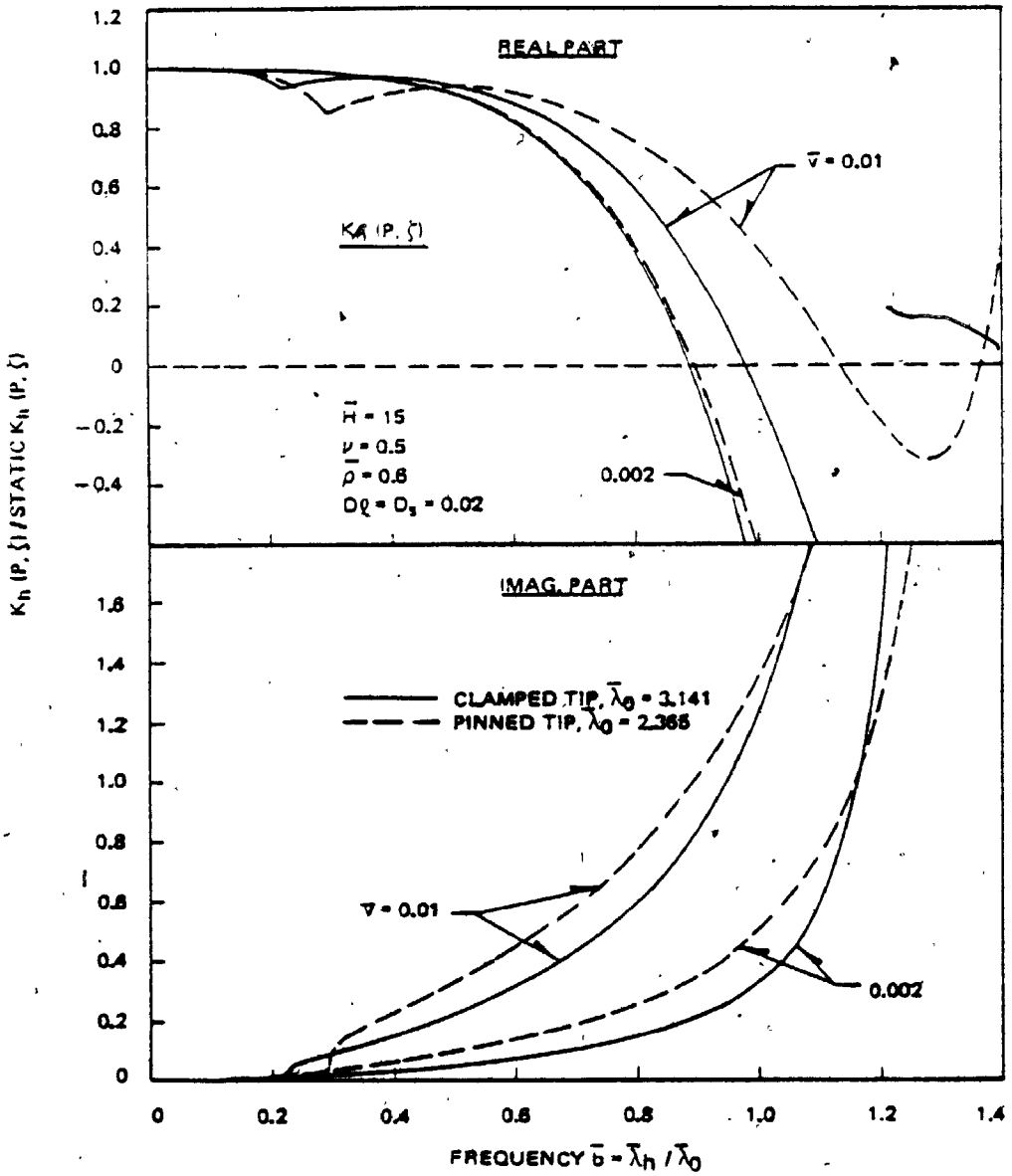

Fig. 3.3-6e. Variation of Complex Stiffness $K_h(P,\zeta)$ with Frequency $\bar{b}$ for Various Wave Velocity Ratios ($\bar{H} = 15$)

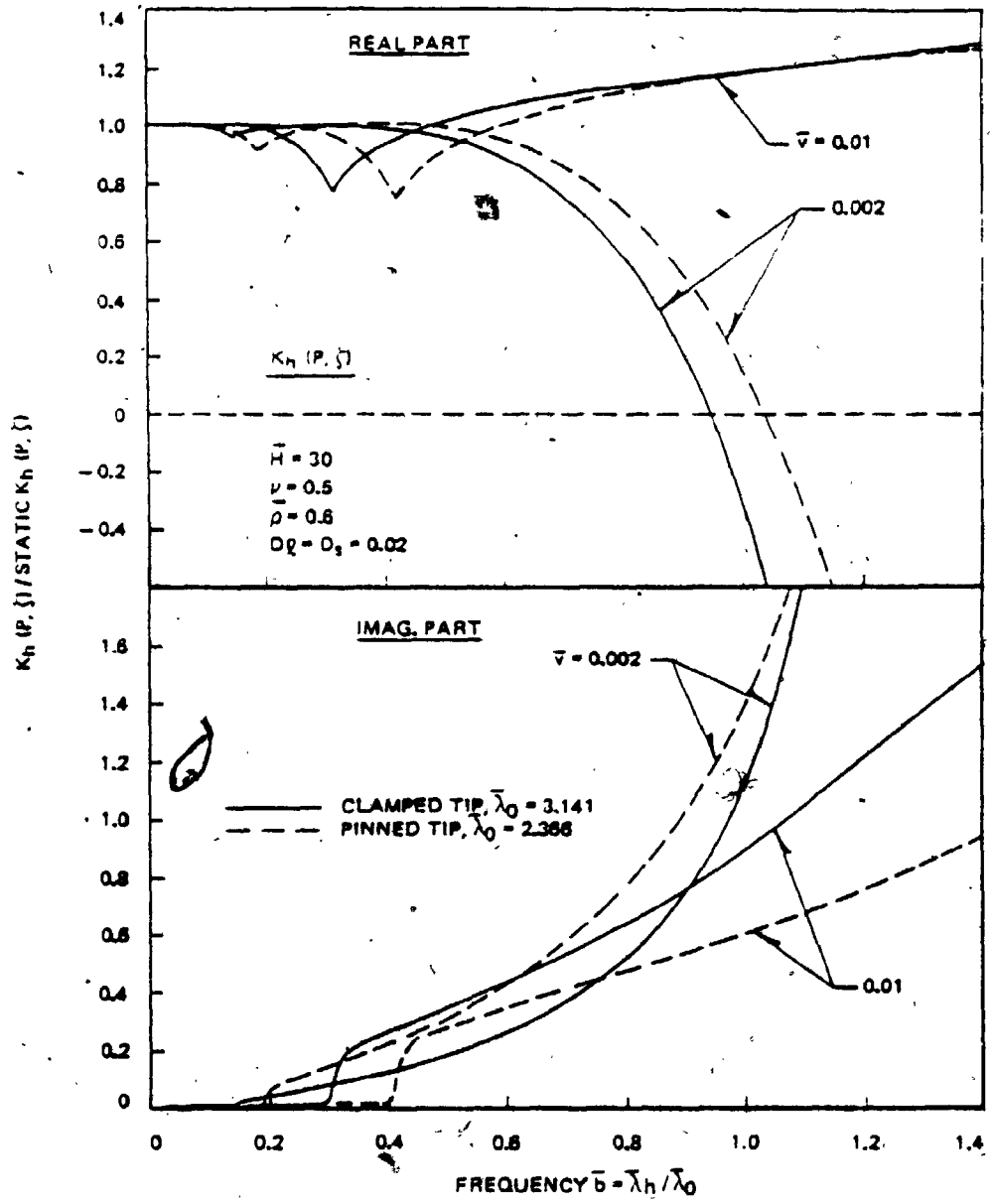

Fig. 3.3-6f. Variation of Complex Stiffness $K_h(P,\zeta)$ with Frequency $\bar{b}$ for Various Wave Velocity Ratios ($\bar{H}$ = 30)

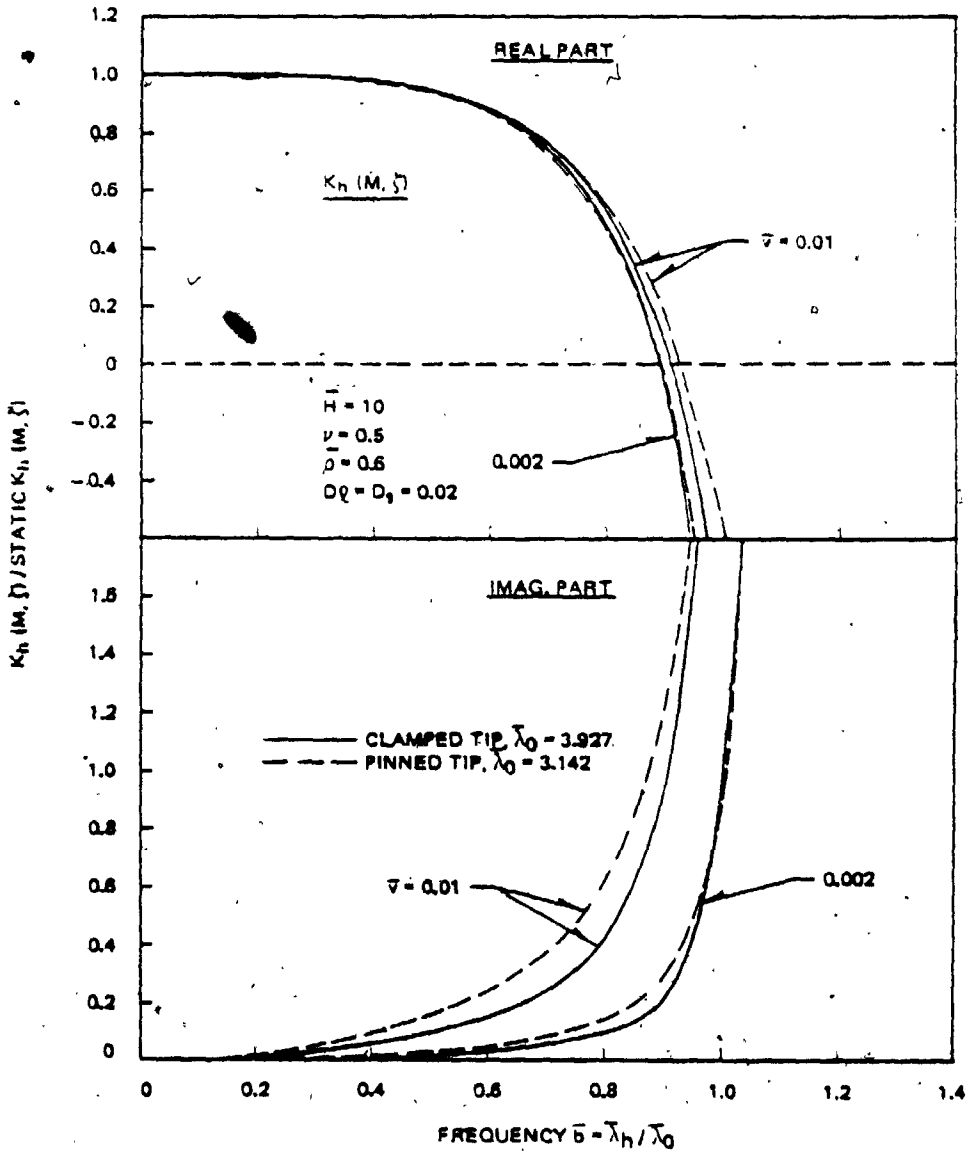

Fig. 3.3-6g. Variation of Complex Stiffness $K_h(\bar{M}, \zeta)$ with Frequency $\bar{b}$ for Various Wave Velocity Ratios ($\bar{H} = .10$)

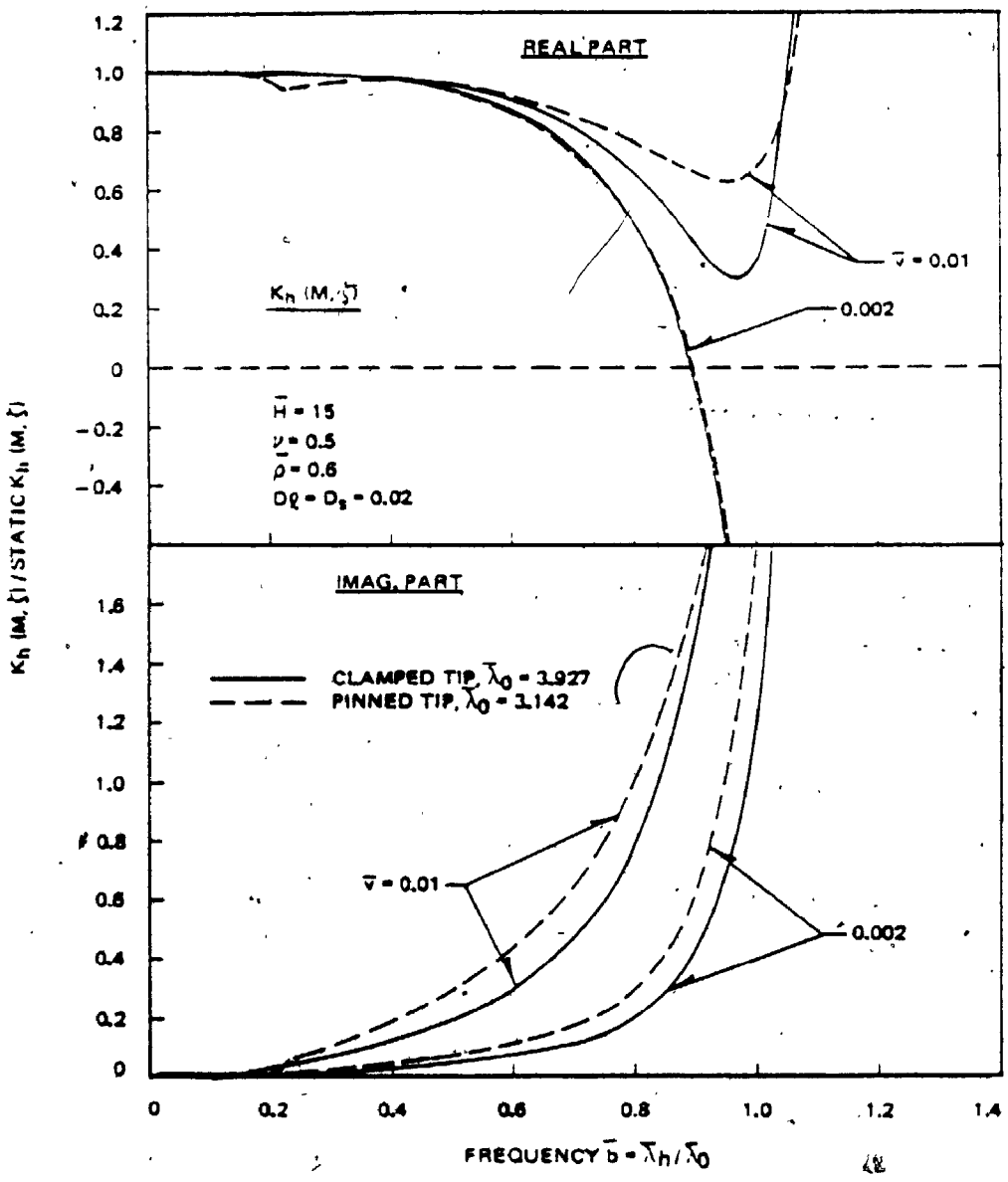

Fig. 3.3-6h. Variation of Complex Stiffness $K_h(M,\zeta)$ with Frequency b for Various Wave Velocity Ratios (H = 15)

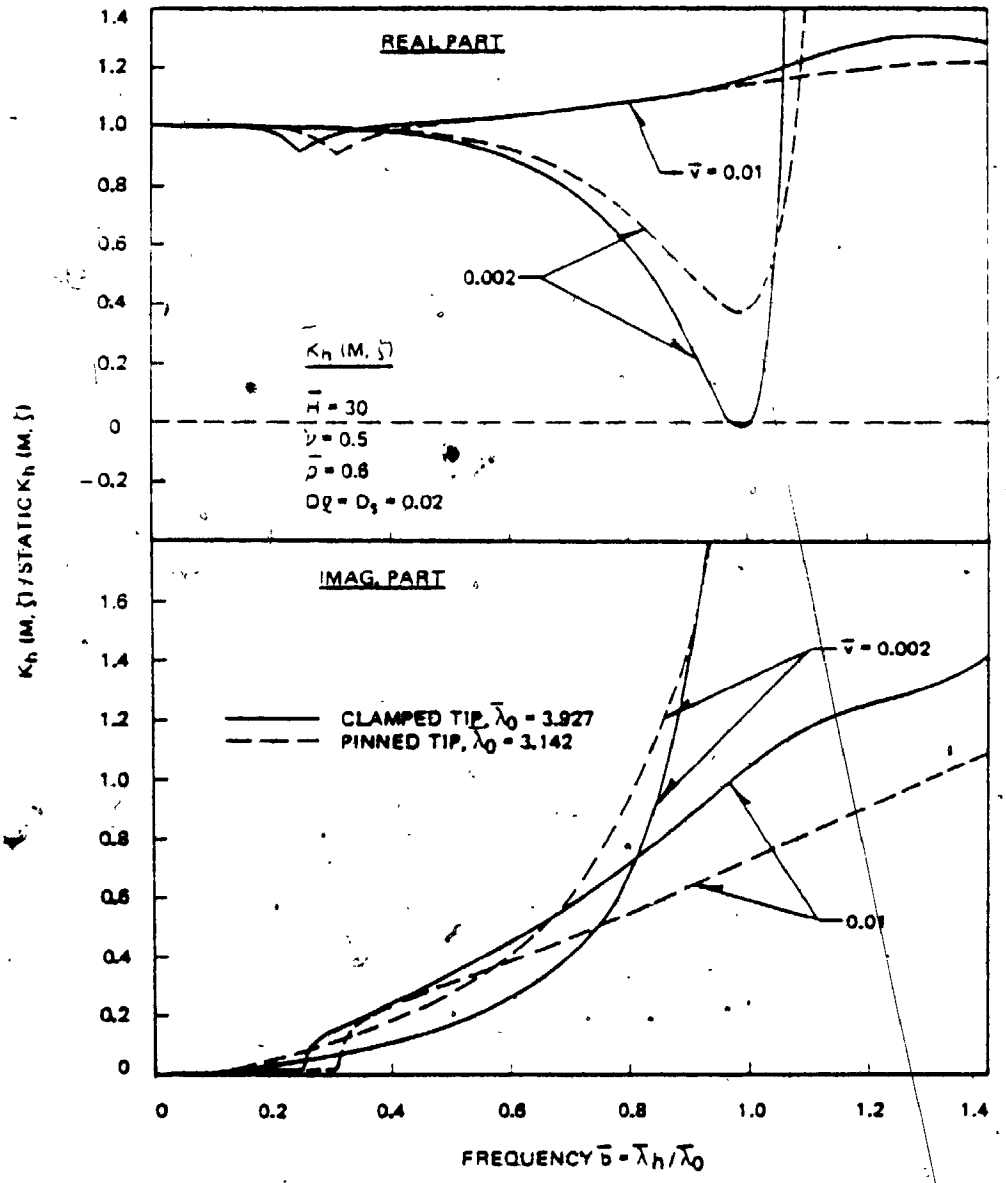

Fig. 3.3-61. Variation of Complex Stiffness $\bar{K}_h(M,\bar{\zeta})$ with Frequency $\bar{b}$ for Various Wave Velocity Ratios ($\bar{H}$ = 30)

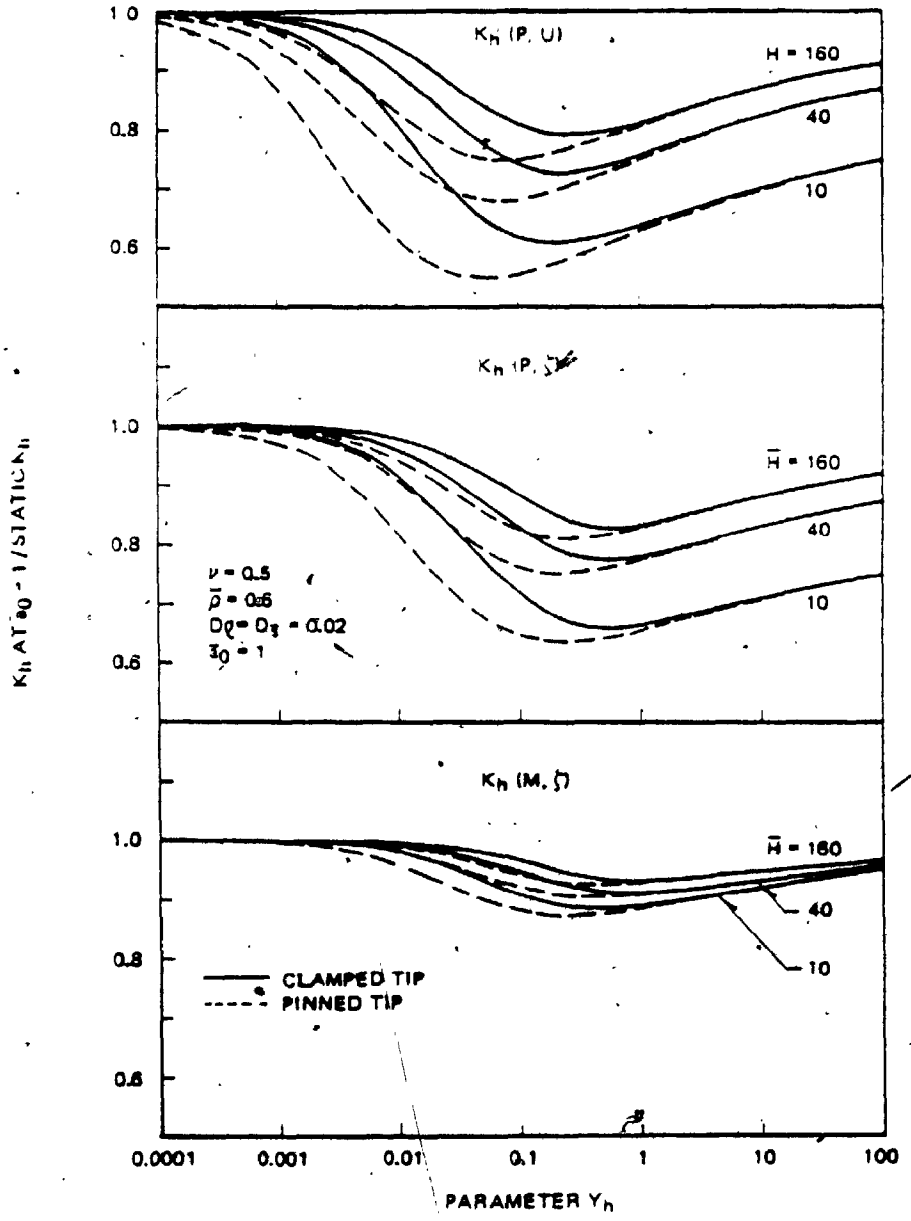

Fig. 3.3-7. Reduction of Real Part of Stiffness K_h at the First Natural Frequency of Stratum

It can be seen in this figure that the transitions, from the very weak to intermediate and from the intermediate to very strong soil effect, appear nearly at the same values of the parameter Y_h as those for the static case. Therefore, the degree of the soil effect can be known from the parameter Y_h in the dynamic case as well as in the static case. The relationship between the soil effect and the parameter Y_h is not much different between static and dynamic loadings. Fig. 3.3-7 further shows that the reduction of the stiffness at the resonance of the stratum is smaller for a more slender pile, and is large in $K(P,U)$, $K(P,\zeta)$, and $K(M,\zeta)$ in decreasing order.

The variation of the complex stiffness $\bar{K}_h$ with frequency a_0' is shown in Figs. 3.3-8 for the strong soil effect. Under this soil effect, the stiffness $K_h(P,U)$ tends to decrease with frequency whereas the stiffness $K_h(M,\zeta)$ tends to increase. The most important feature in this figure is that, as observed and explained in vertical vibration, the complex stiffness $\bar{K}_h$ tends to become independent of slenderness as frequency increases above the first resonant frequency of the stratum. On the other hand, the stiffness $\bar{K}_h$ in the static case is smaller for a more slender pile. Therefore, under the strong soil effect, the ratio between the dynamic and static stiffnesses increases with slenderness when the parameter Y_h is kept constant.

The ratio between the dynamic and static stiffnesses becomes maximum around a certain value of Y_h as shown in Fig. 3.3-9. Such a value of Y_h corresponds to the transition from the intermediate to very strong soil effect. As soil hardness increases beyond this condition, the ratio decreases. Those trends observed in Fig. 3.3-9 are most pronounced in $K_h(P,U)$ but least in $K_h(M,\zeta)$. Fig. 3.3-9 further

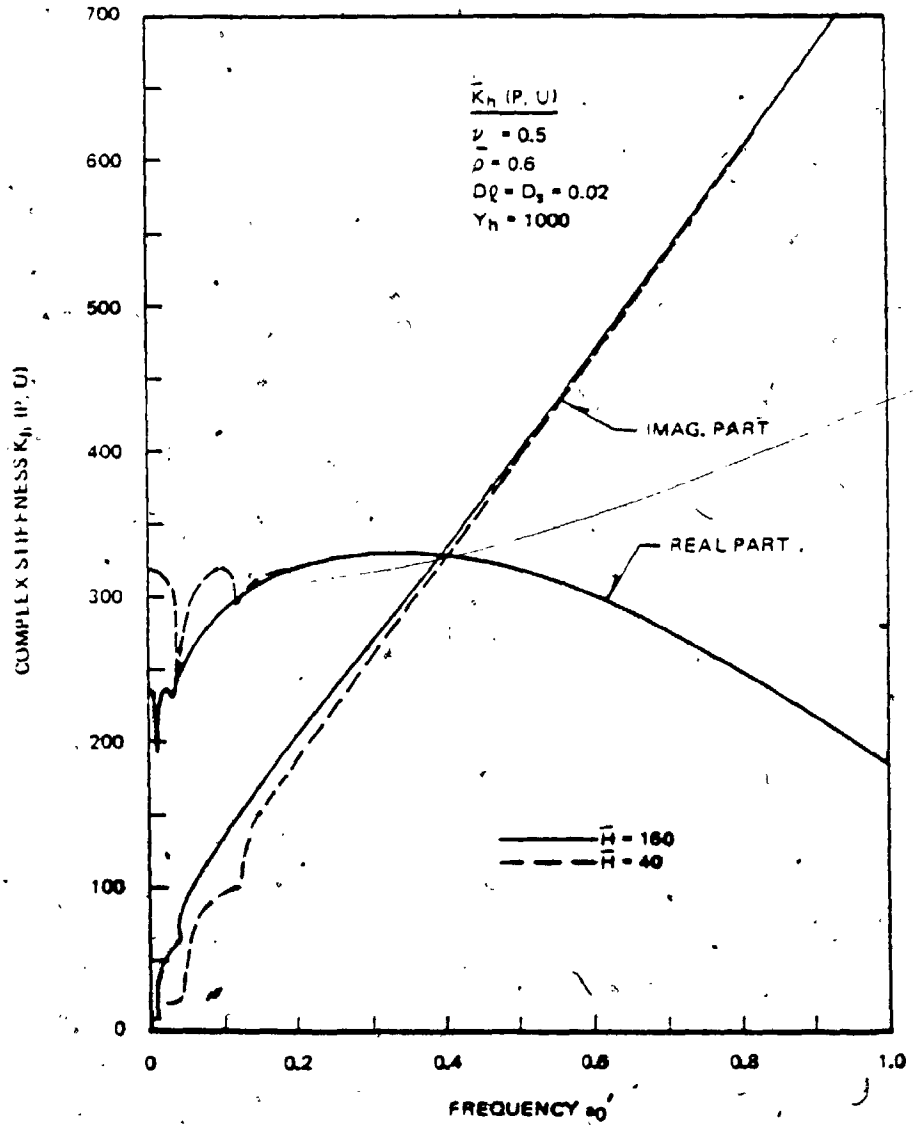

Fig. 3.3-8a. Variation of Complex Stiffness $\bar{K}_h$ (P,U) with Frequency a_0' for Various Slendernesses

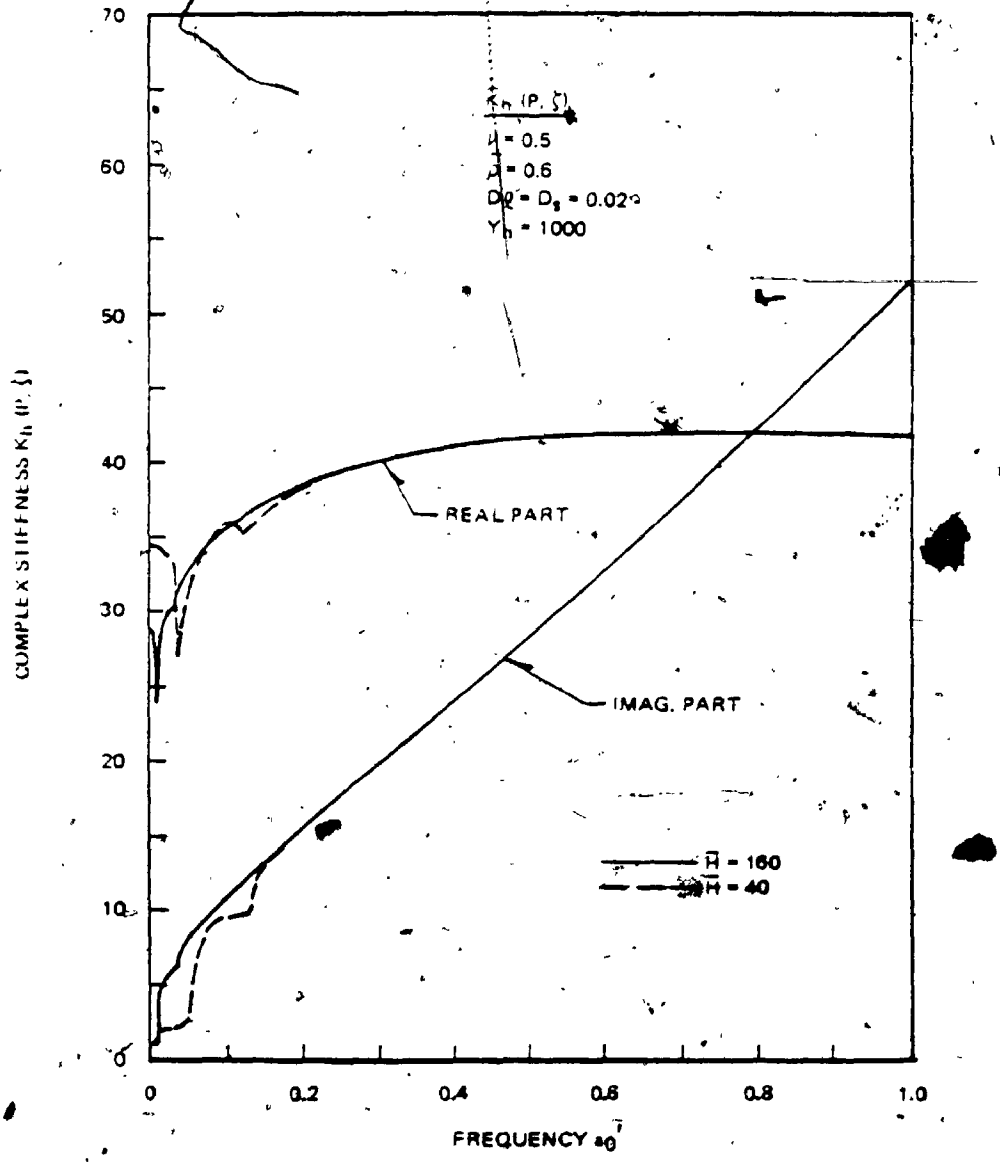

Fig. 3.3-8b. Variation of Complex Stiffness $\bar{K}_n(P,\zeta)$ with Frequency a_0' for Various Slendernesses

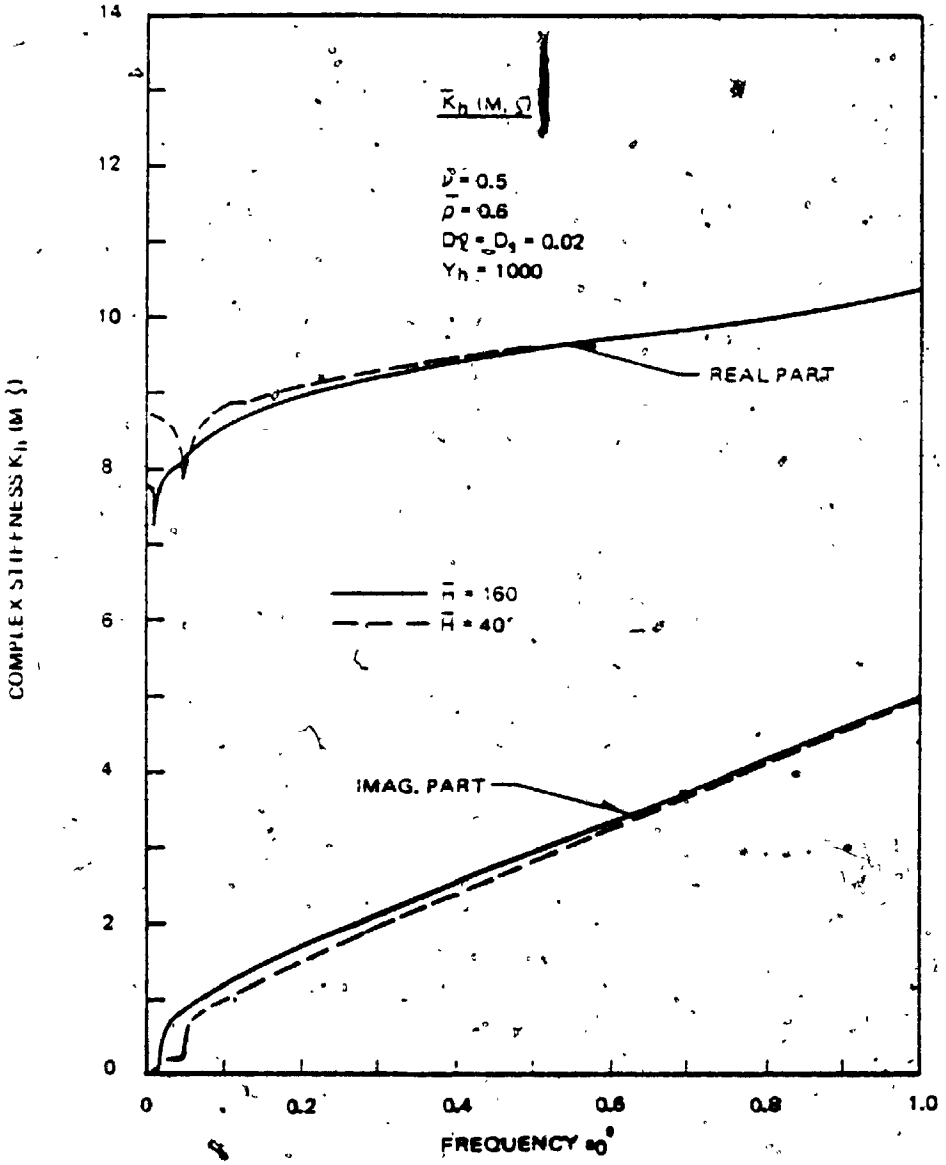

Fig. 3.3-8c. Variation of Complex Stiffness $\bar{K}_h(M,\zeta)$ with Frequency a_0' for Various Slendernesses

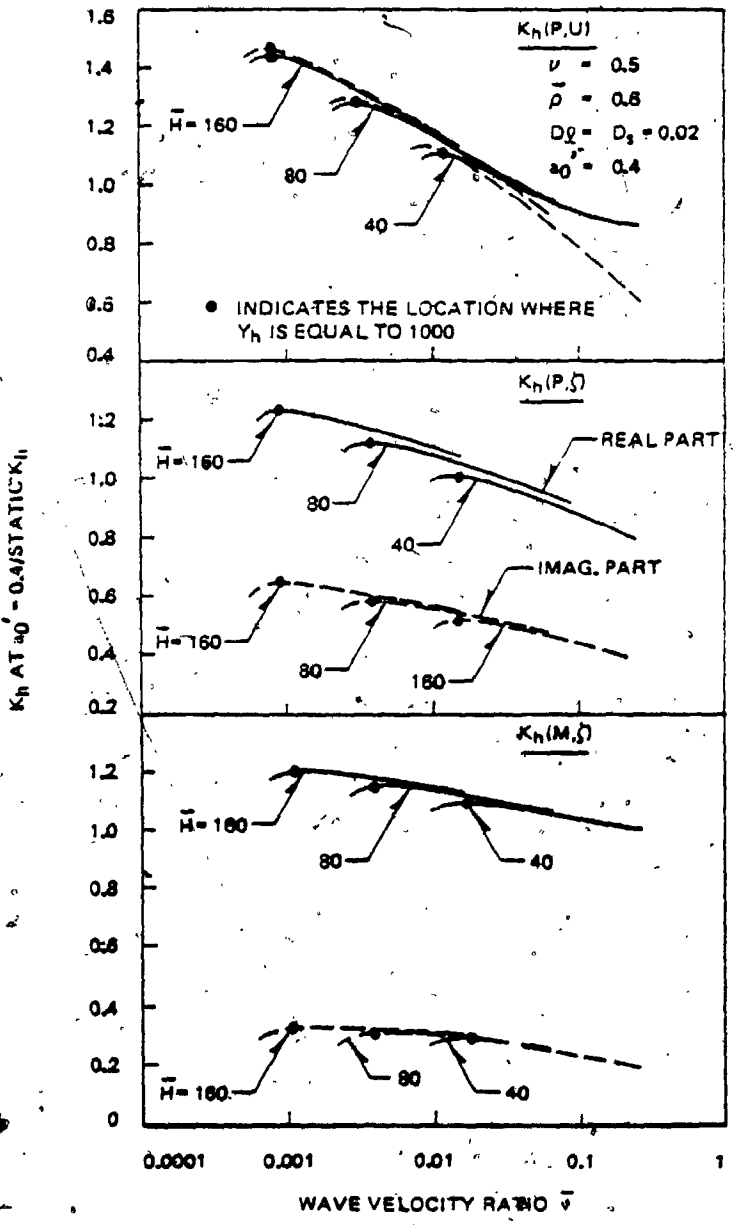

Fig. 3.3-9. Variation of Ratio $K_h(a_0' = 0.4)/K_h(a_0' = 0)$ with Wave Velocity Ratio

indicates that the dynamic stiffness of the soil-pile system can be larger than the static one.

The damping relative to the stiffness is large for $K_h(P,U)$, $K_h(P,\zeta)$, and $K_h(M,\zeta)$ in decreasing order as can be seen in Fig. 3.3-9. The variation of the damping $\bar{K}_h$ with Y_h is shown for $a_0' = 0.4$ and $\bar{H} = 160$ in Fig. 3.3-10 where the damping $\bar{K}_h$ is nearly identical to those for $\bar{H} \geq 10$. The figure indicates that the damping $\bar{K}_h$ grows with Y_h following the relationship, $I_m(\bar{K}_h) = C\, Y_h$, where C are

$$C \text{ for } \begin{Bmatrix} K_h(P,U) \\ K_h(P,\zeta) \\ K_h(M,\zeta) \end{Bmatrix} \approx \begin{Bmatrix} 0.97 \\ 0.16 \\ 0.036 \end{Bmatrix} \quad \text{(pinned tip)}$$

$$\approx \begin{Bmatrix} 0.74 \\ 0.1 \\ 0.019 \end{Bmatrix} \quad \text{(clamped tip)}$$

However, when the effect of soil is very strong the above constants tend to be reduced.

(iii) Effect of Variation of Poisson's Ratio

The effect of the variation of Poisson's ratio on the complex stiffness can be seen in Figs. 3.3-11 for the static case and in Figs. 3.3-12 and 3.3-13 for the dynamic case.

Under the weak soil effect, the static stiffness is very little affected by this variation although a higher Poisson's ratio generally tends to yield higher stiffness. However, the dynamic stiffness

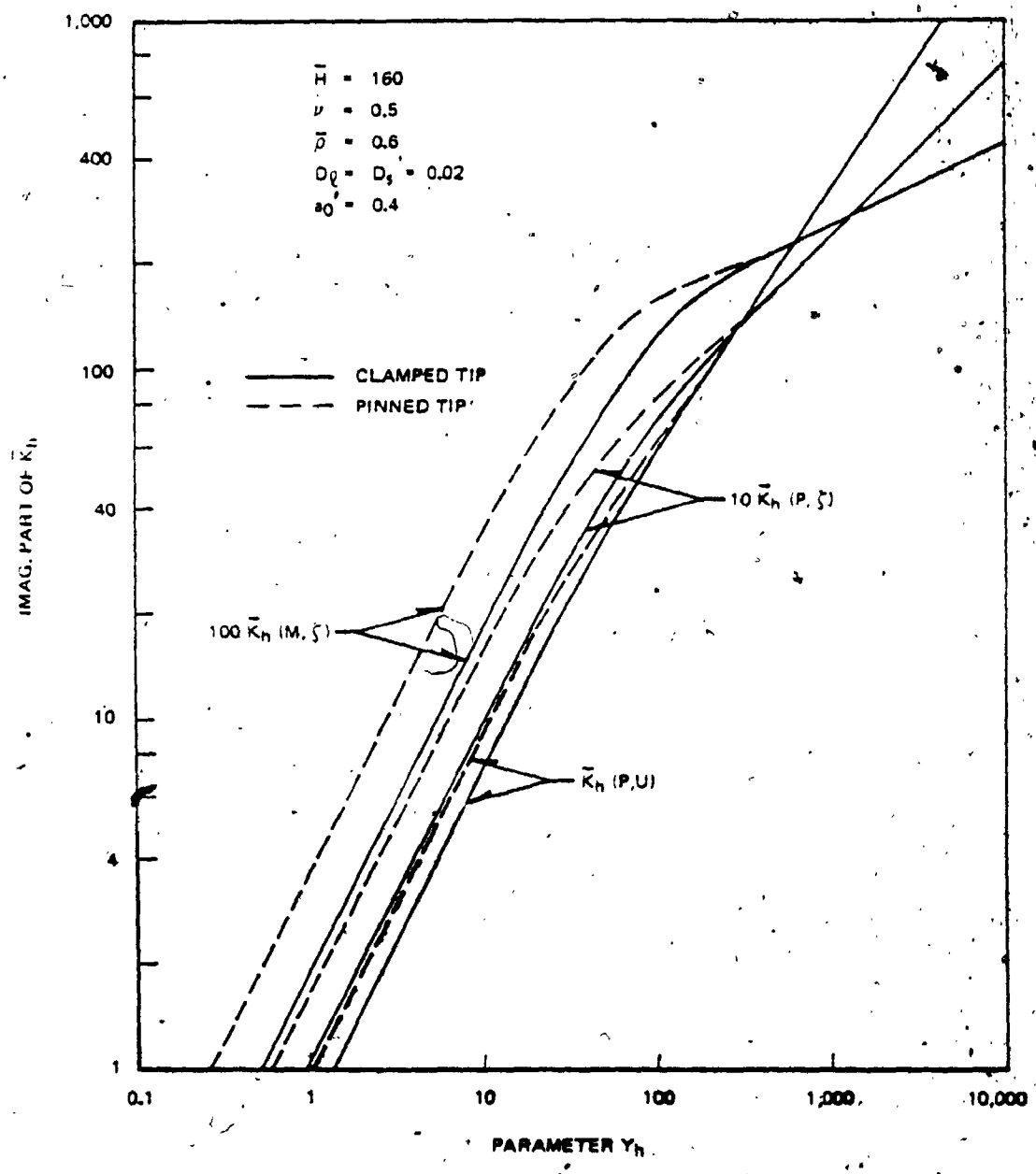

Fig. 3.3-10. Variation of Imaginary Part of Complex Stiffness $\bar{K}_h$ with Parameter Y_h.

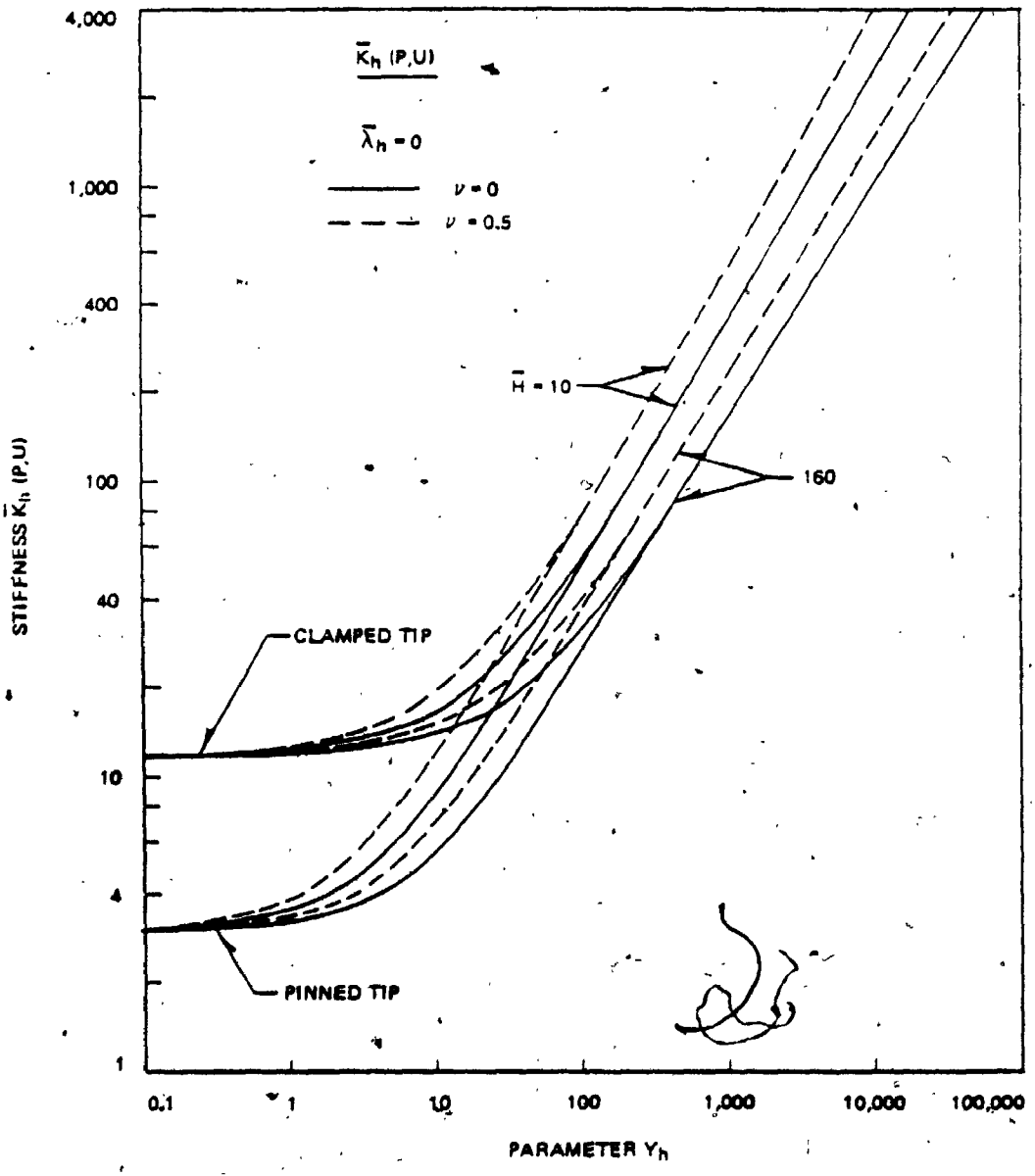

Fig. 3.3-11a. Variation of Static Stiffness $\bar{K}_h$(P,U) with Parameter Y_h for Various Poisson's Ratios

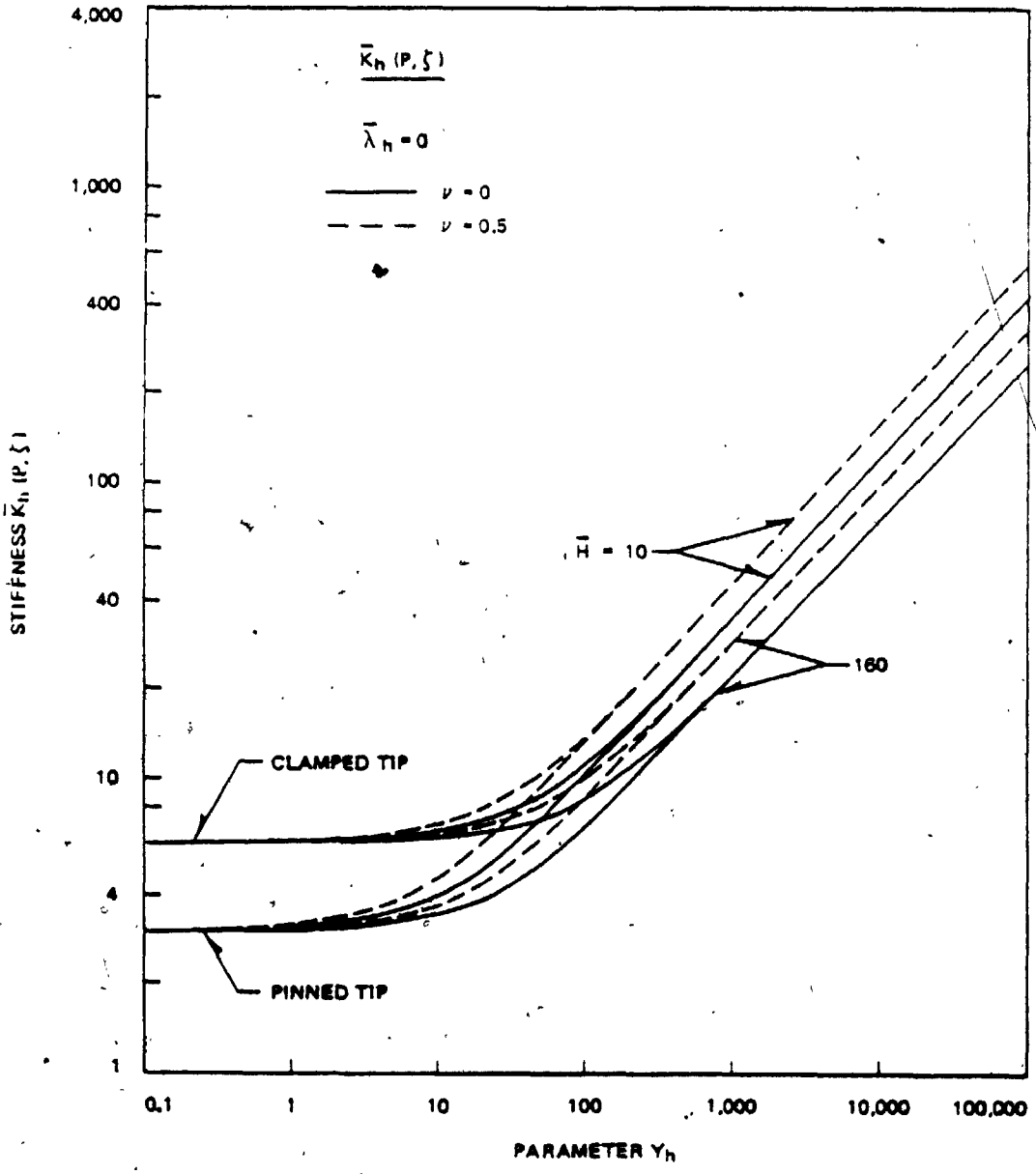

Fig. 3.3-11b. Variation of Static Stiffness $\bar{K}_h(P,\zeta)$ with Parameter Y_h for Various Poisson's Ratios

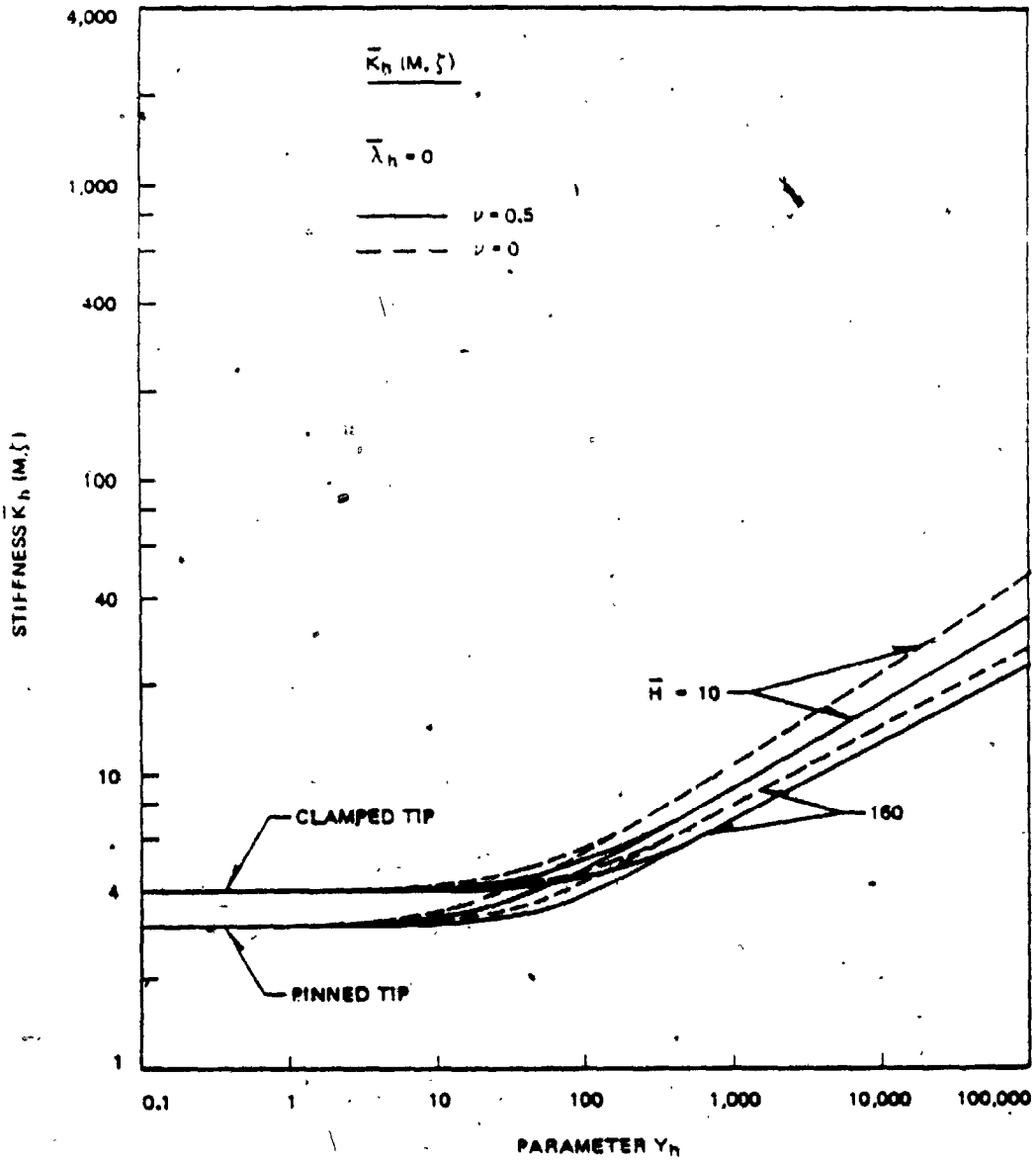

Fig. 3.3-11c. Variation of Static Stiffness $\bar{K}_h(M,\zeta)$ with Parameter Y_h for Various Poisson's Ratios

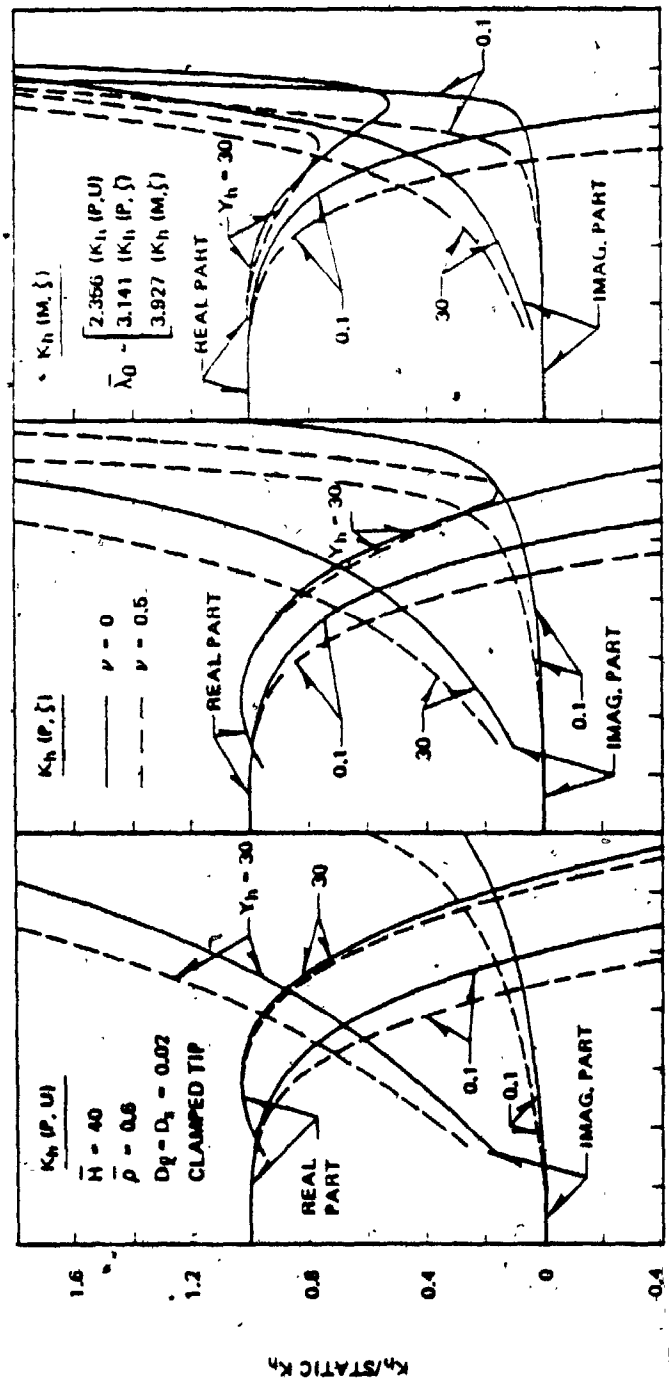

Fig. 3.3-12. Variation of Complex Stiffness K_h with Frequency $\bar{b}$ for Various Poisson's Ratios

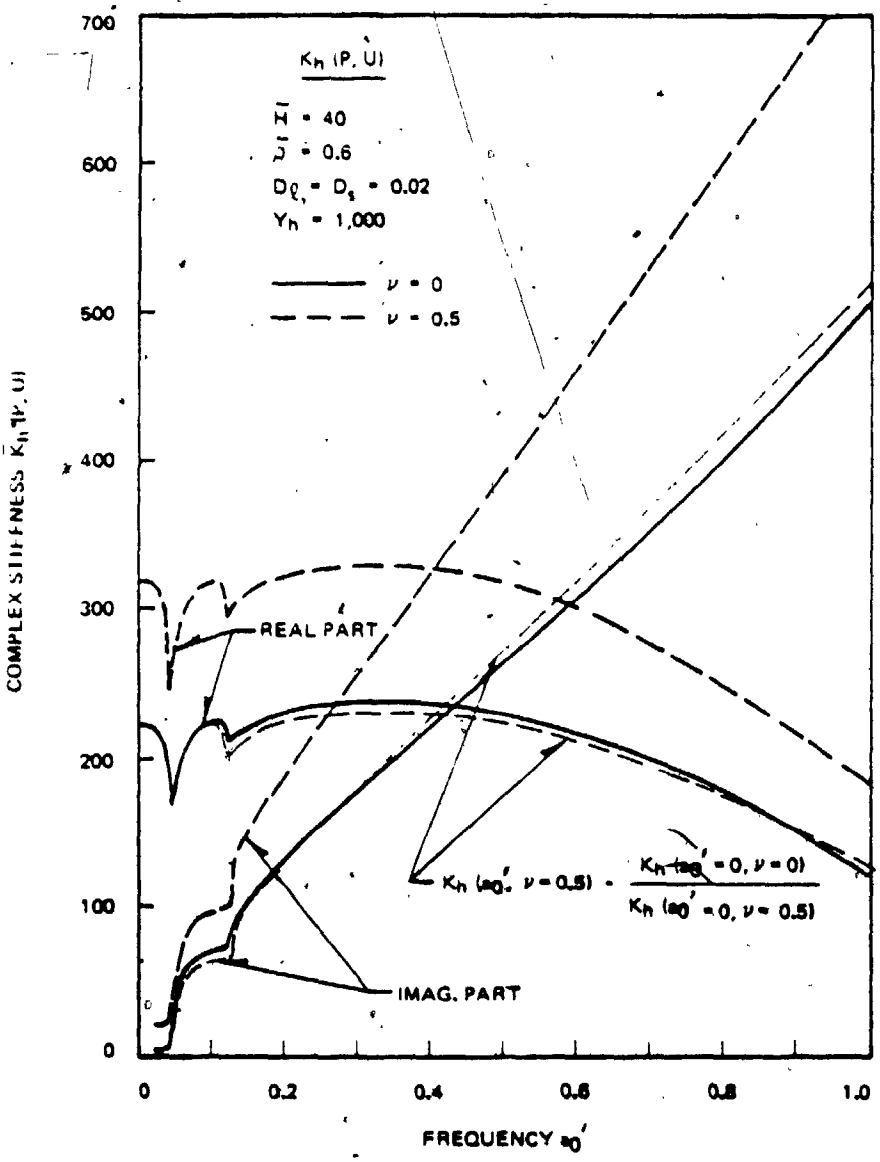

Fig. 3.3-13a. Variation of Complex Stiffness $\bar{K}_h(P,U)$ with Frequency a_0' for Various Poisson's Ratios

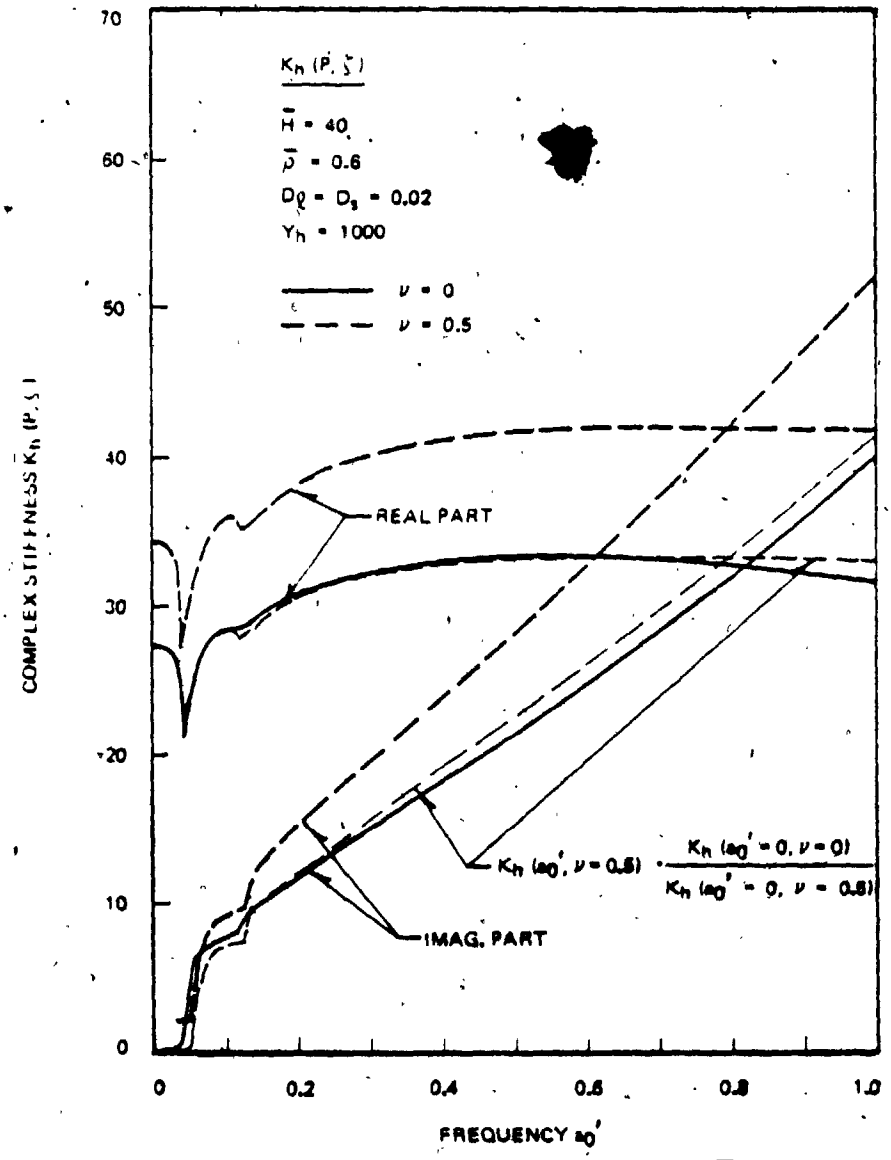

Fig. 3.3-13b. Variation of Complex Stiffness $\bar{K}_h(P,\zeta)$ with Frequency a_0' for Various Poisson's Ratios

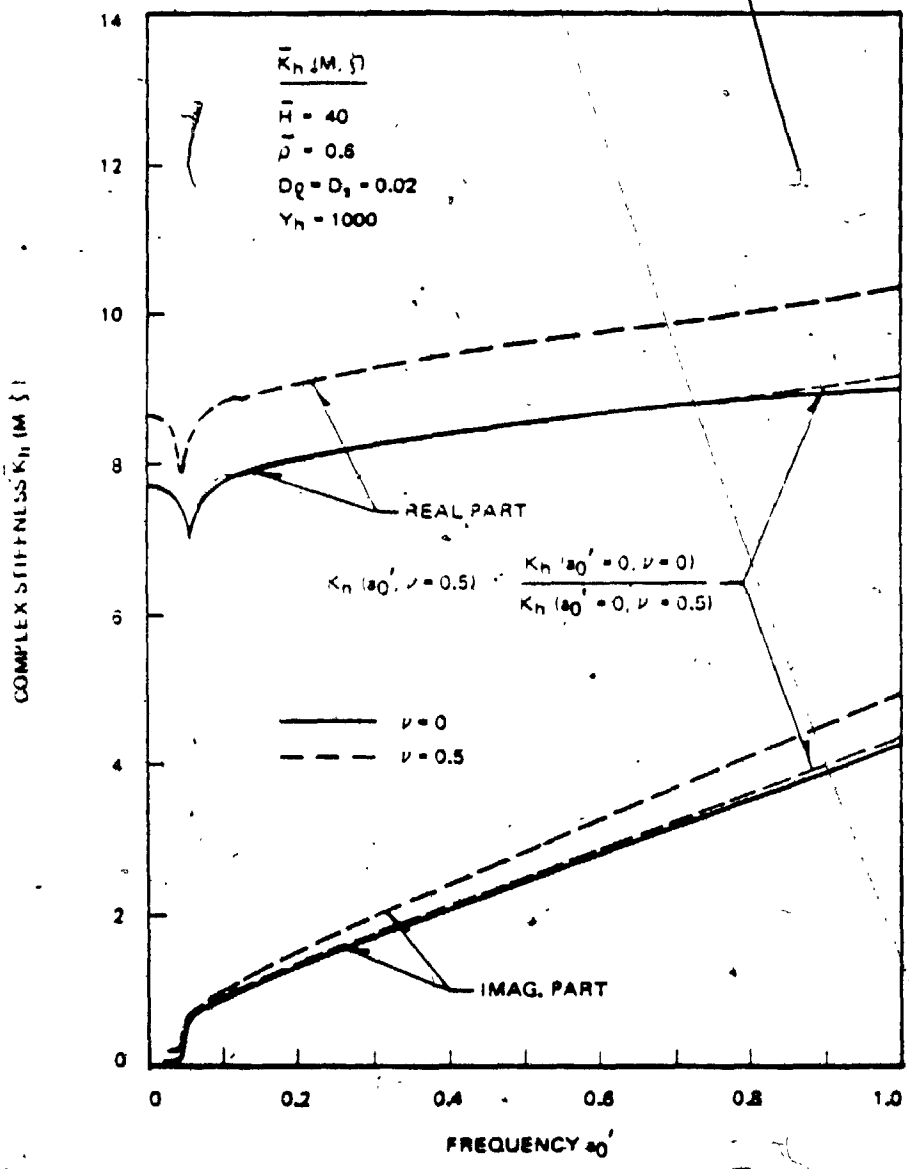

Fig. 3.3-13c. Variation of Complex Stiffness $\bar{K}_h(M,\zeta)$ with Frequency a_0' for Various Poisson's Ratios

decreases more rapidly with frequency for $\nu = 0.5$ than for $\nu = 0$ as shown in Fig. 3.3-12. This trend can also be seen in Fig. 3.3-14 where the natural frequency of the soil-pile system shows approximately the frequency at which the stiffness $K_h(P,U)$ is zero.

When the soil effect is very strong, the complex stiffness $\bar{K}_h$ reflects more sensitively the variation of Poisson's ratio and is clearly larger for a higher Poisson's ratio as shown in Figs. 3.3-13. When normalized by the statical stiffness, however, the normalized complex stiffness varies with frequency a_0' nearly independently of Poisson's ratio (Figs. 3.3-13). This trend is different from that in vertical vibration in which the unnormalized complex stiffness $\bar{K}_v$ little depends on Poisson's ratio at frequencies above the first resonant frequency of the stratum.

The variation of Poisson's ratio does not change much the relationship between soil effect and the parameter Y_h for the static case (Figs. 3.3-11). However, for the dynamic case, the previously mentioned transitions of soil effect appear at slightly larger values of Y_h for $\nu = 0$ than for $\nu = 0.5$ as shown in Fig. 3.3-15. This figure further indicates that the amount of the reduction of the stiffness at the resonance of the stratum is little affected by the variation of Poisson's ratio.

(iv) Effect of Variation of Mass Ratio

As explained in vertical vibration, the variation of mass ratio affects the complex stiffness of the soil-pile system through the parameter $\bar{\lambda}_h$. Thus, as shown in Figs. 3.3-16, the relationship between $\bar{K}_h$ and a_0' is affected by the variation of mass ratio in a

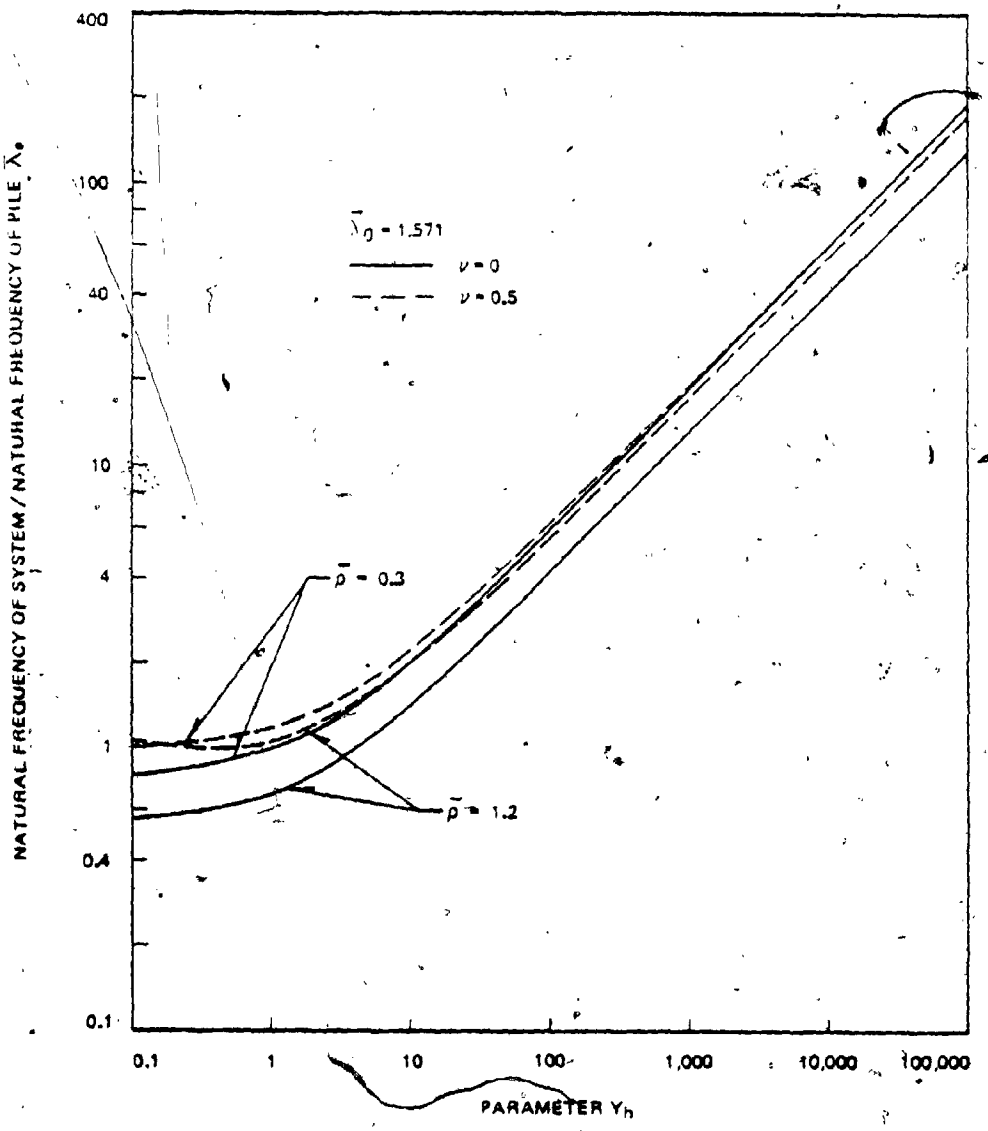

Fig. 3.3-14. Variation of the First Natural Frequency of Soil-Pile System with Parameter Y_h for various Poisson's and Mass Ratios (Fixed-Pinned)

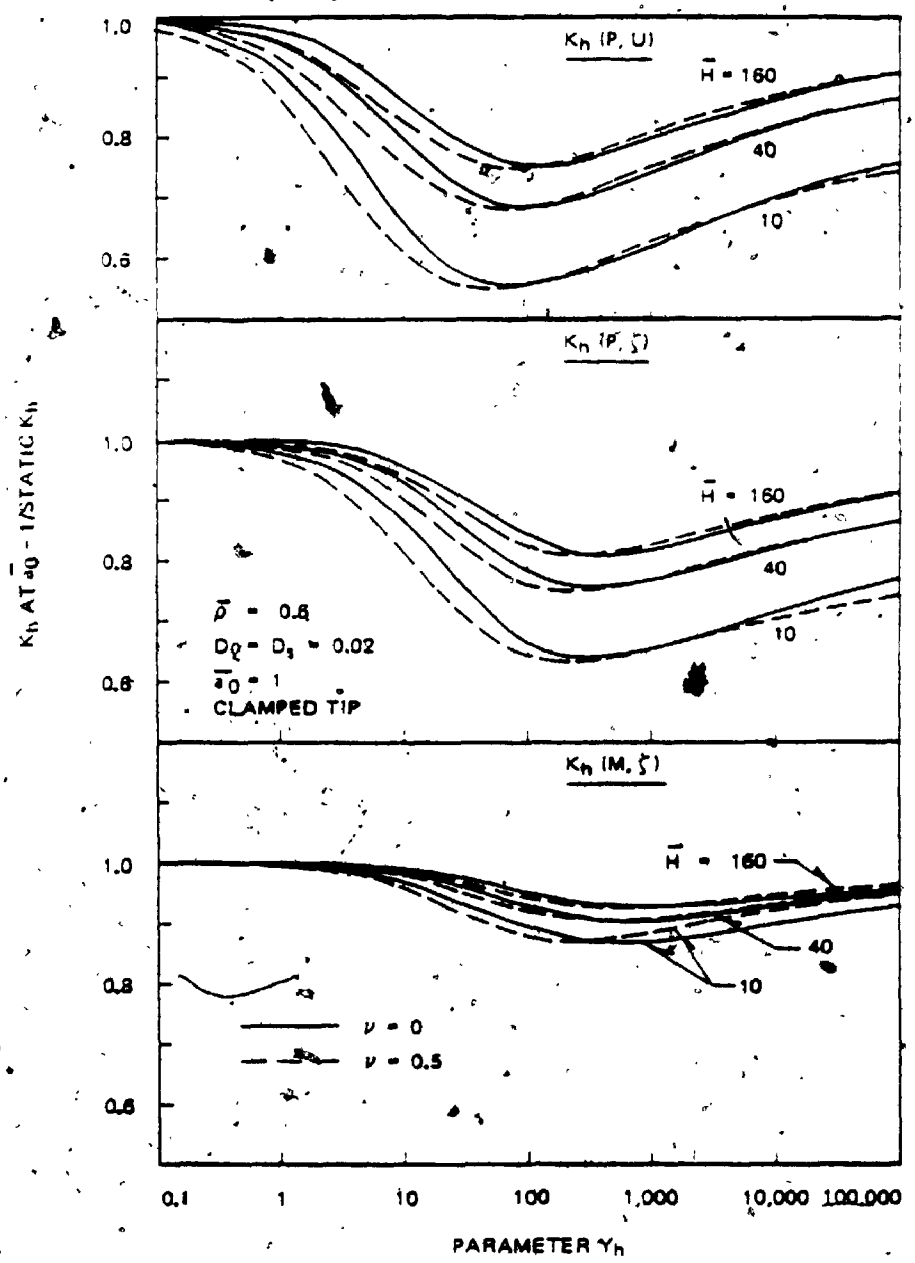

Fig. 3.3-15. Reduction of Real Part of Stiffness K_h at the First Natural Frequency of Stratum for Various Poisson's Ratios

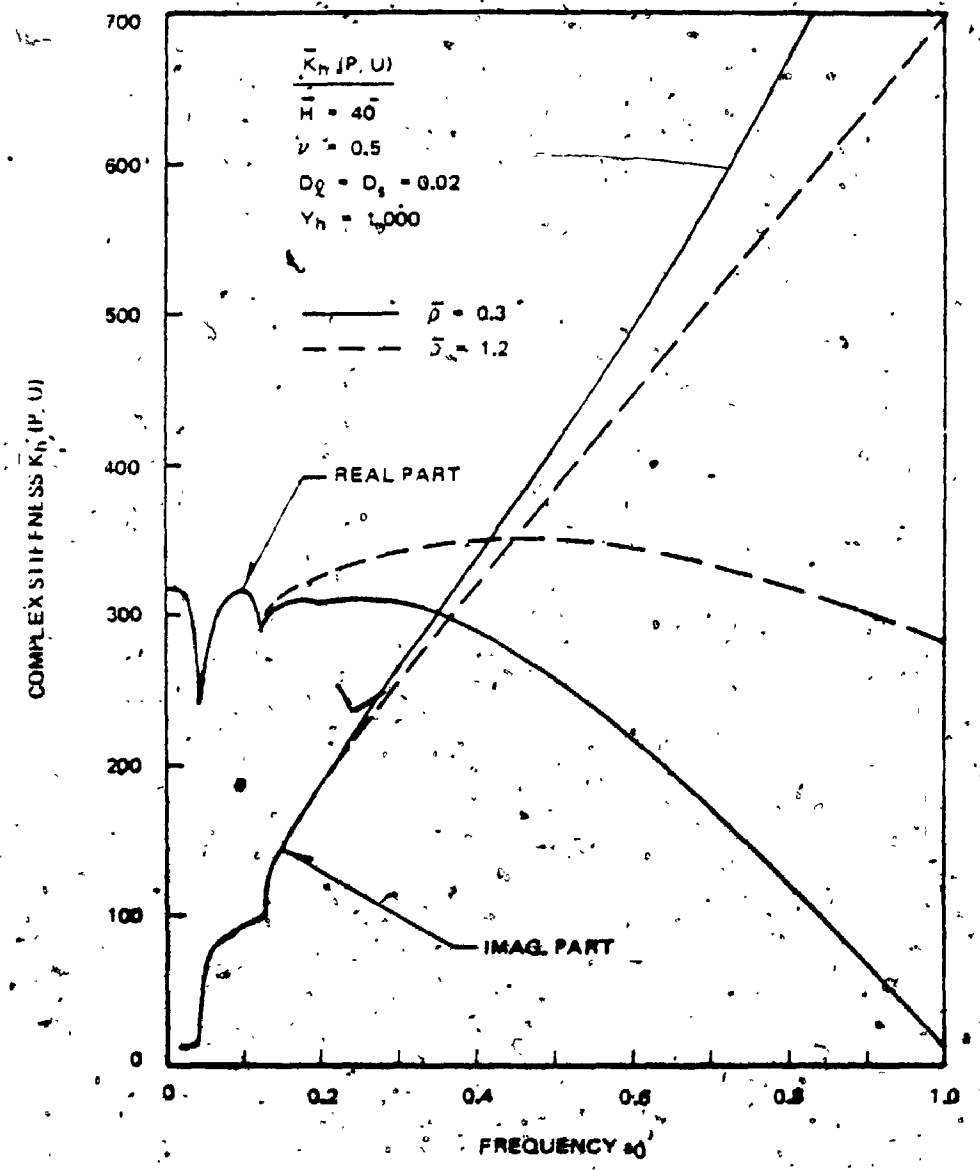

Fig. 3.3-16a. Variation of Complex Stiffness $\bar{K}_h(P,U)$ with Frequency a_0' for Various Mass Ratios

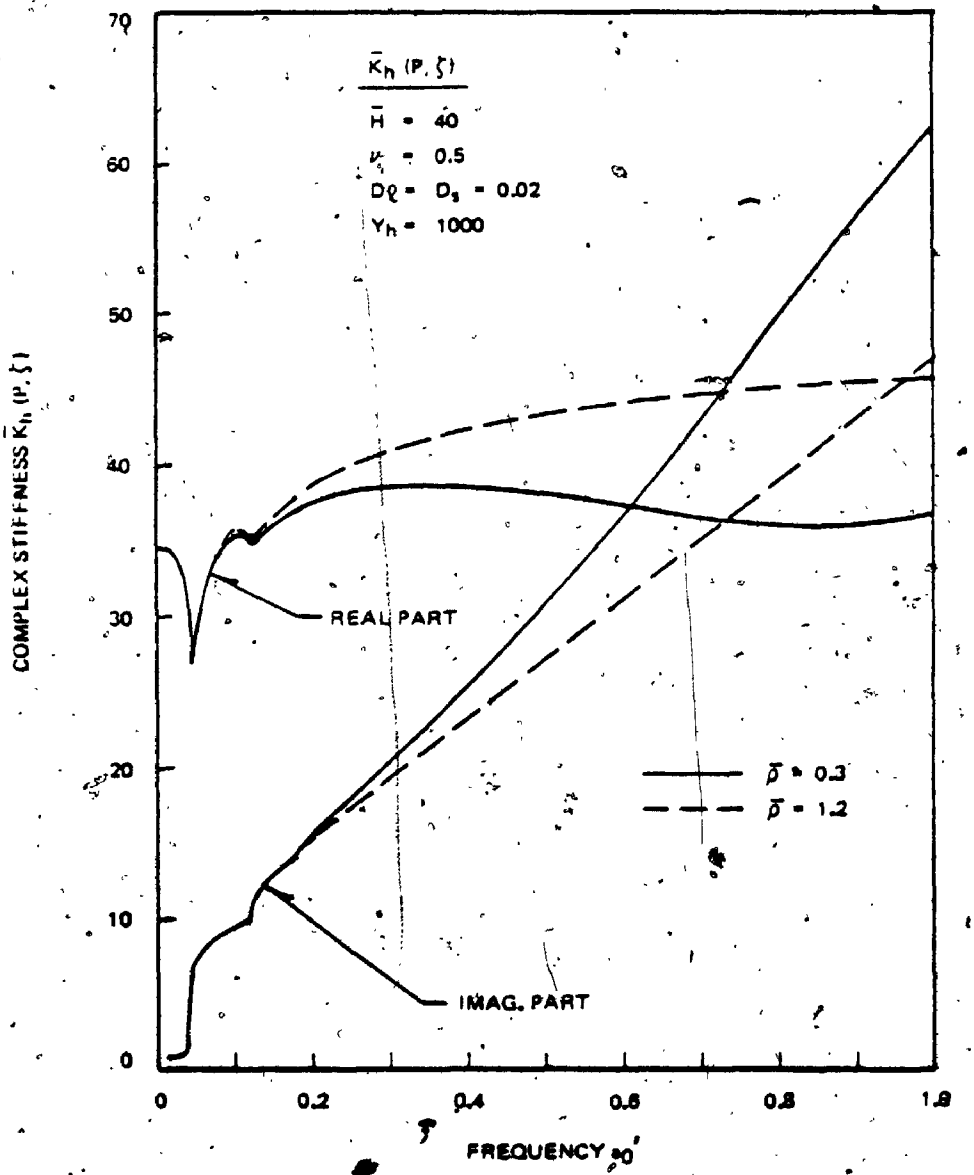

Fig. 3.3-16b. Variation of Complex Stiffness $\bar{K}_h(P,\zeta)$ with Frequency a_0' for Various Mass Ratios

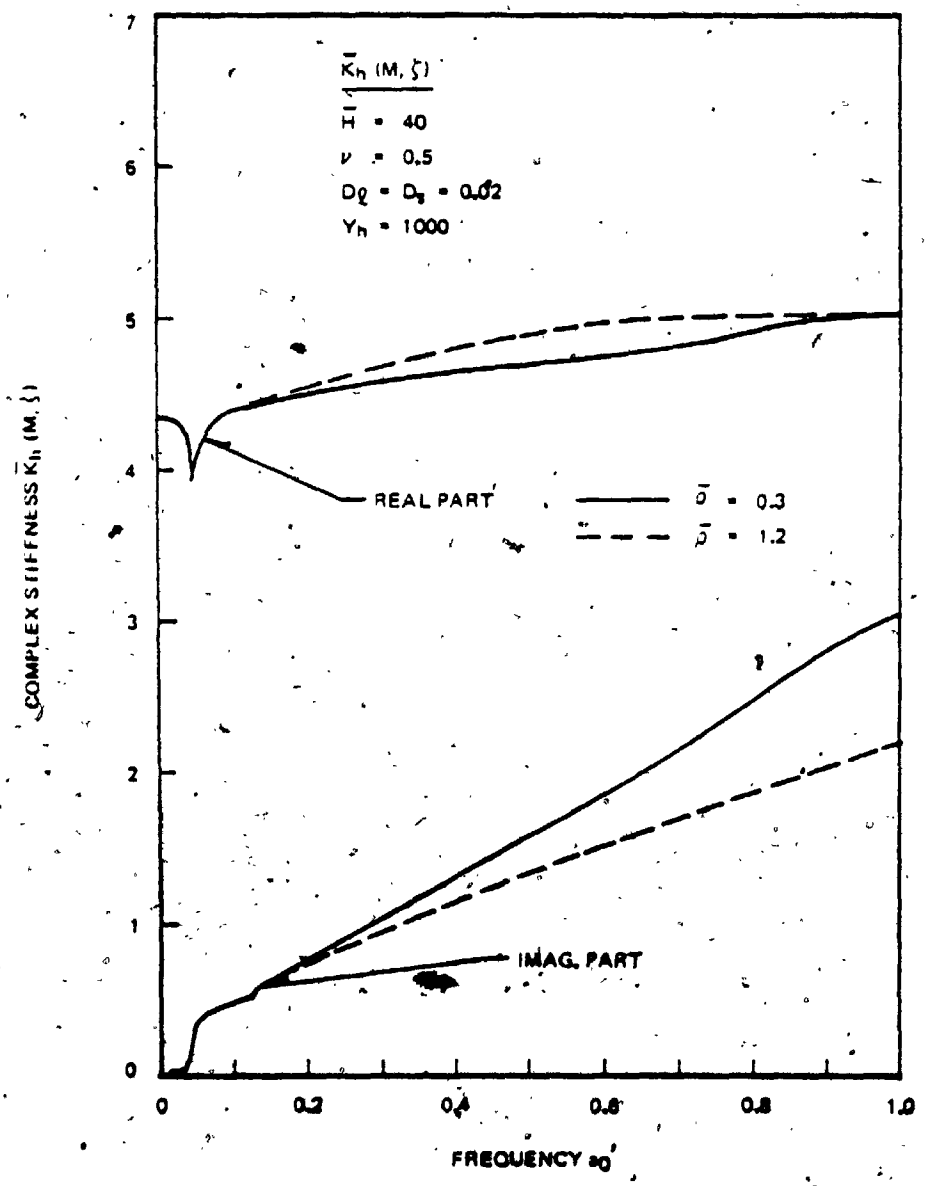

Fig. 3.3-16c. Variation of Complex Stiffness $\bar{K}_h(M,\zeta)$ with Frequency a_0' for Various Mass Ratios

manner similar to that in vertical vibration. However, the reduction of the stiffness at the resonance of the stratum is not so much affected in horizontal vibration as in vertical vibration (Fig. 3.3-17). Figs. 3.3-16 further show that the variation of mass ratio affects the stiffness $K_h(P,U)$ most and the stiffness $K_h(M,\zeta)$ least, whereas it affects the damping $K_h(M,\zeta)$ most but the damping $K_h(P,U)$ least.

3.4 Equivalent Springs and Dashpots with Frequency-Independent Constants for Soil-Pile System

When the dynamic response of the structure supported by the pile foundation is analyzed, the pile foundation is often replaced at the pile head by the equivalent spring and dashpot with frequency independent constants (Voigt model). The real and imaginary parts of the complex stiffness provide the information of the spring and viscous constants of this model.

The previously obtained results on the real part of the complex stiffness reveal that the equivalent spring stiffness depends highly on the frequency under the weak soil effect and large mass ratio but little depends on it under the strong soil effect and small mass ratio. Therefore when the effect of soil is strong and the mass ratio is small, the spring function of the pile foundation can be reasonably replaced by the frequency independent spring.

The viscous constant of the equivalent dashpot can be obtained by dividing the imaginary part of the complex stiffness by frequency. Such viscous constants are shown in Figs. 3.4-1 and 3.4-2 for vertical vibration and Figs. 3.4-3 and 3.4-4 for horizontal vibration. In those figures, the viscous constants under the weak soil effect tend to

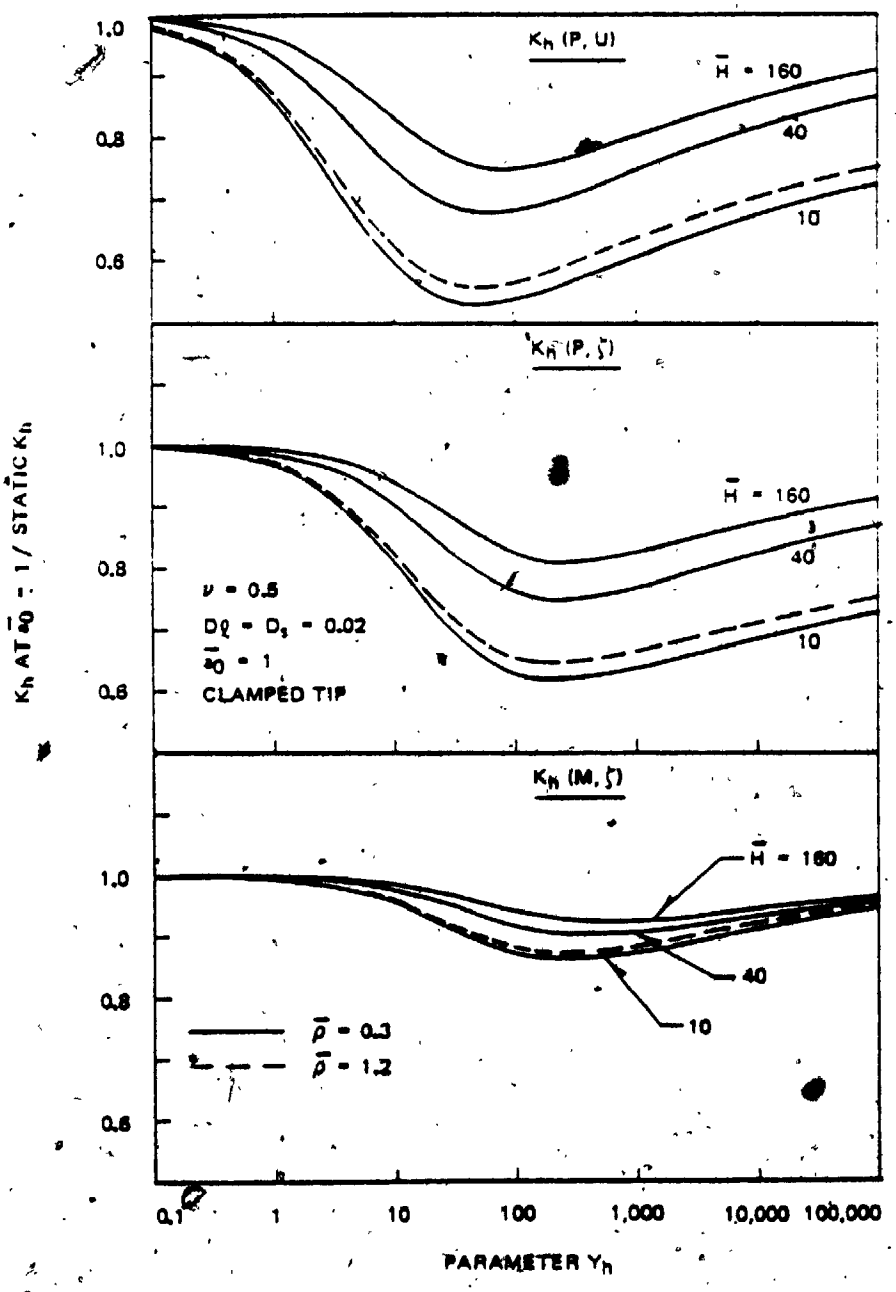

Fig. 3.3-17. Reduction of Real Part of Stiffness K_h at the First Natural Frequency of Stratum for Various Mass Ratios

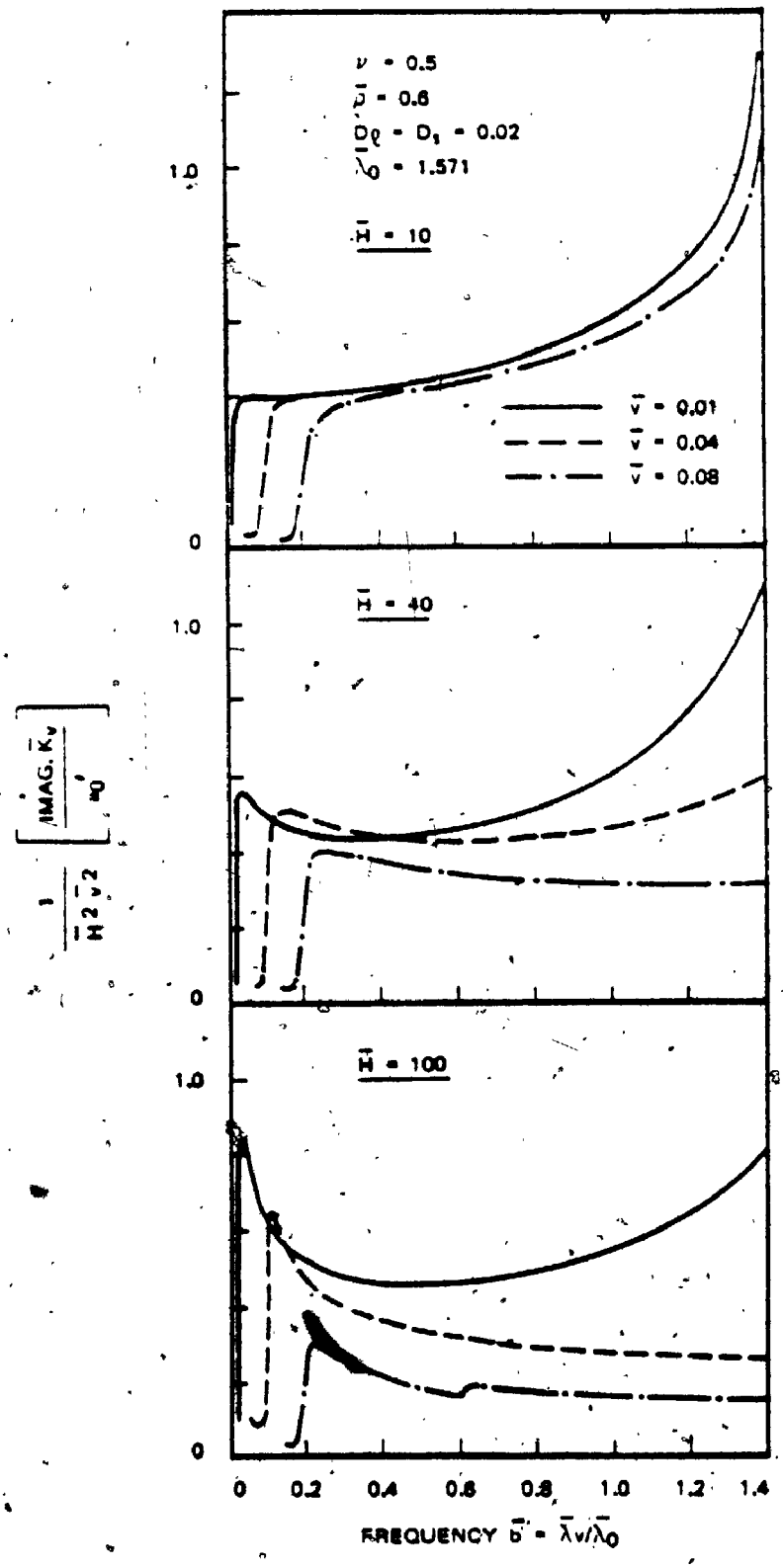

Fig. 3.4-1. Variation of Equivalent Viscous Constant with Frequency b̄ in Vertical Vibration

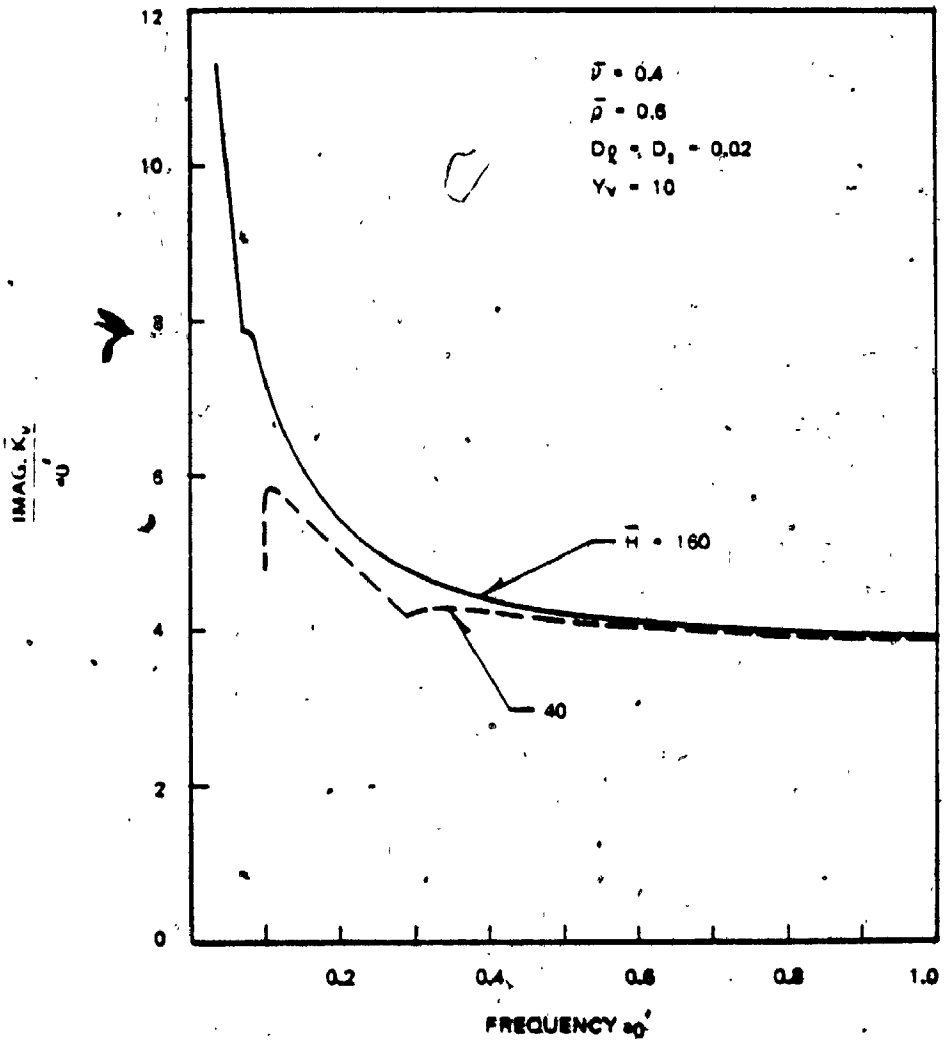

Fig. 3.4-2. Variation of Equivalent Viscous Constant with Frequency $\bar{a}_0'$ Under Strong Soil Effect in Vertical Vibration

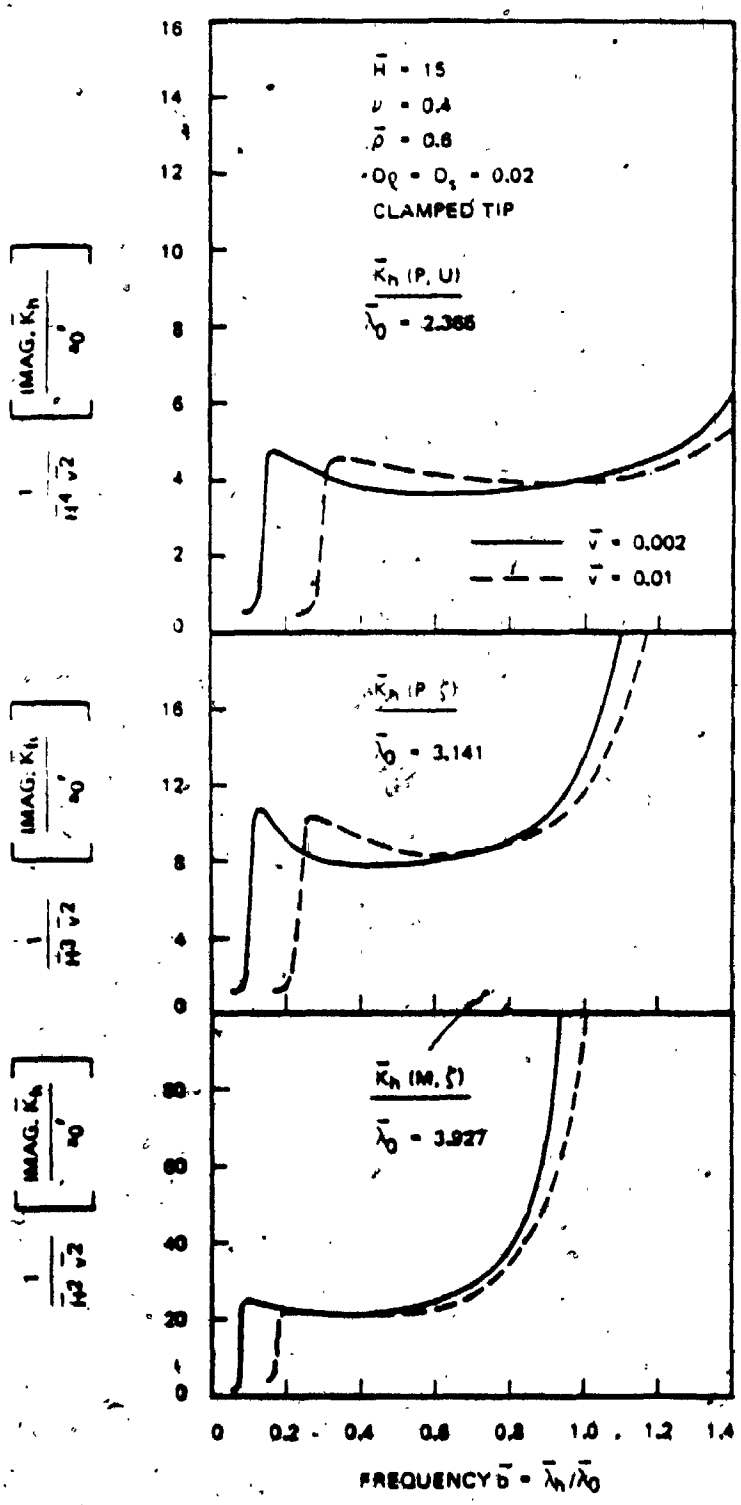

Fig. 3.4-3a. Variation of Equivalent Viscous Constant with Frequency b in Horizontal Vibration ($\bar{H}$ = 15)

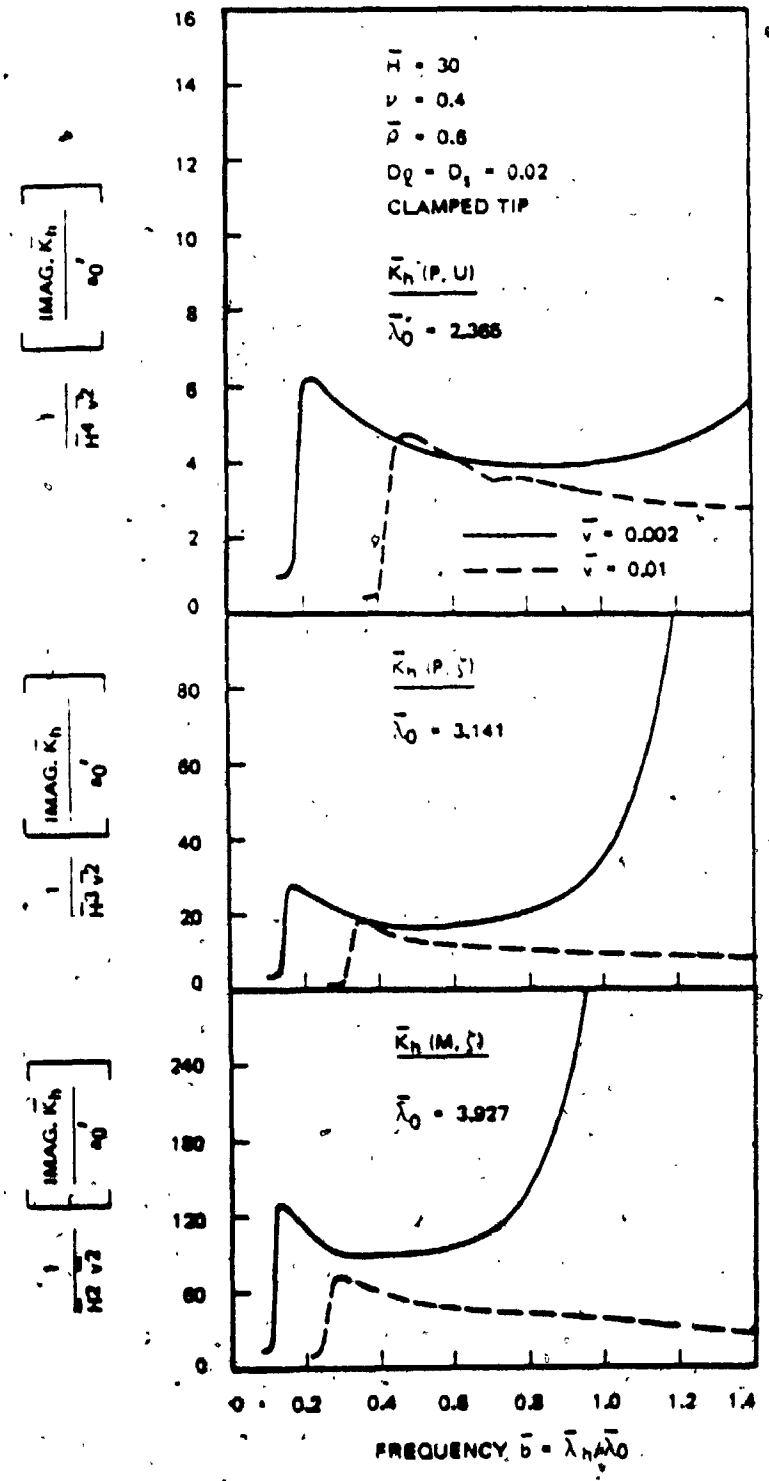

Fig. 3.4-3b. Variation of Equivalent Viscous Constant with Frequency $\bar{b}$ in Horizontal Vibration ($\bar{H}$ = 30)

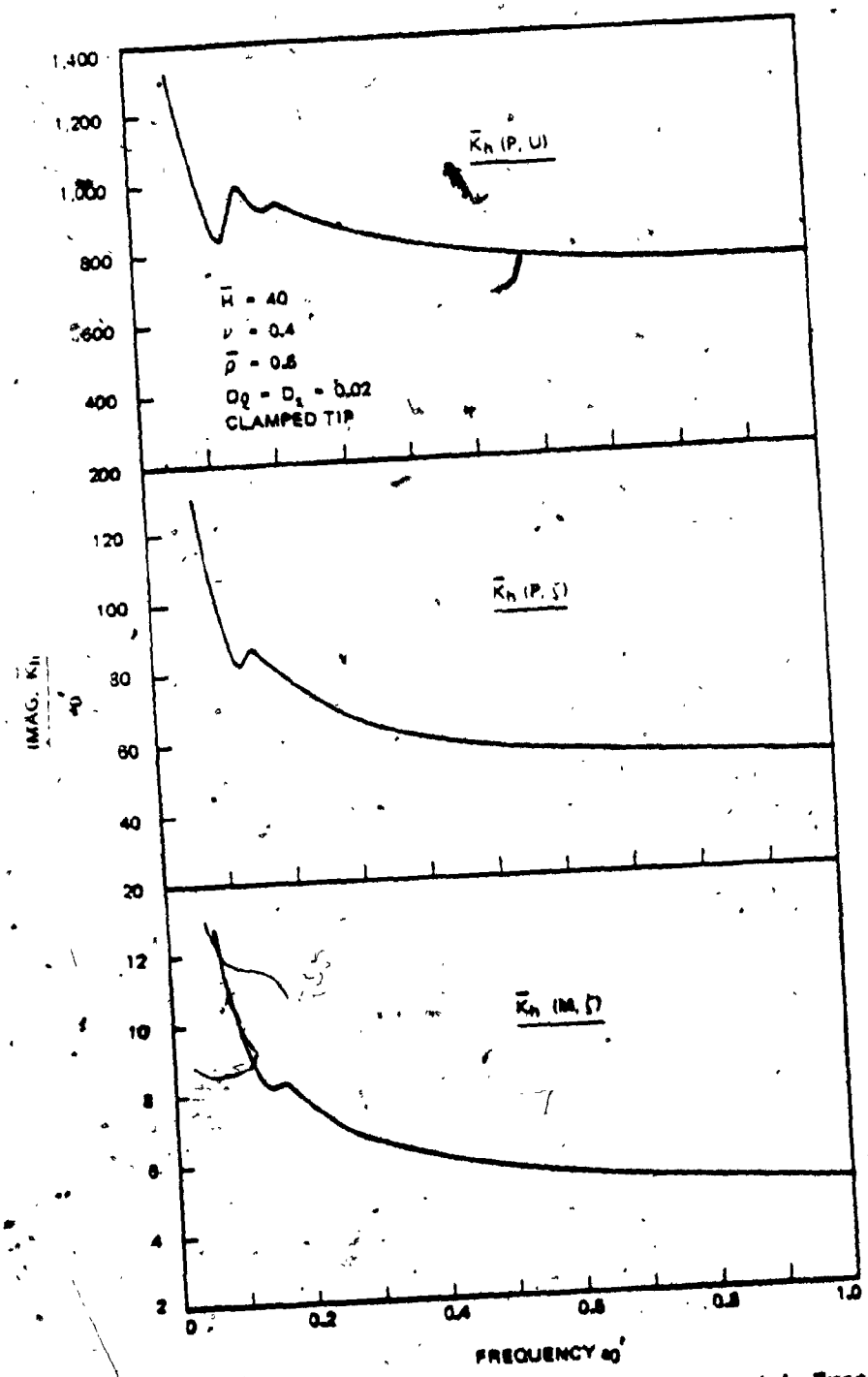

Fig. 3.4-4. Variation of Equivalent Viscous Constant with Frequency a_0' Under Strong Soil Effect in Horizontal Vibration

increase sharply around the frequency where the stiffness becomes zero; this sharp increase is large in $K_h(M,\zeta)$, $K_h(P,\zeta)$, and $K_h(P,U)$ in decreasing order. However, when the effect of soil is strong, the viscous constants seem to be fairly frequency-independent except at relatively low frequencies. As is well known this trend results from the nature of the radiational damping, and was also observed by Novak (1974) for a pile. At relatively low frequencies, a sharp increase of the viscous constant can be seen in the figures under any intensity of soil effect; this sharp increase is larger for the stronger soil effect and more slender pile. Therefore, when the effect of soil is strong and the frequency is well above the first resonant frequency of the stratum, the damping function of the pile foundation can be reasonably replaced by a dashpot with a frequency-independent viscous constant.

CHAPTER 4. DISPLACEMENTS OF AN INSTALLED PILE IN VERTICAL AND HORIZONTAL VIBRATIONS

4.1 Introduction

In the previous chapter, the soil-pile interaction was studied for the stiffness and damping of a soil-pile system at the pile head. As the simplest case to illustrate the found characteristics of the stiffness and damping of a soil-pile system, the structure supported by the pile foundation is eliminated and harmonic excitation forces are applied at the head of an installed pile to obtain the displacements of the pile.

Under harmonic excitation, the complex displacements at the pile head can be obtained by inverting the previously derived complex stiffness of the soil-pile system. The amplitude and its phase shift are, respectively, the absolute value and argument of this complex displacement.

4.2 Displacements of an Installed Pile in Vertical and Horizontal Vibrations

4.2.A Vertical Vibration

The displacement at the pile head subjected to a unit vertical force, D_v, is obtained by inverting the stiffness K_v, and expressed as

$$D_v = K_v^{-1} \tag{4.2-1}$$

The following dimensionless parameters for $\bar{D}_v$ and $\bar{H}\,\bar{D}_v$ are defined for convenience:

$$\bar{D}_v = \frac{E_p S}{H} D_v \qquad (4.2\text{-}2a)$$

$$\bar{H}\,\bar{D}_v = \frac{E_p S}{r_0} D_v \qquad (4.2\text{-}2b)$$

In the above expressions, $\bar{D}_v$ shows fully the variation of pile radius whereas $\bar{H}\,\bar{D}_v$ shows the variation of pile length.

Since $\bar{D}_v$ is a complex number, $\bar{D}_v$ can be rewritten as

$$\bar{D}_v = \bar{A}_v e^{-i\gamma} \qquad (4.2\text{-}3)$$

where

$$\bar{A}_v = |\bar{D}_v| \qquad \text{(amplitude)} \qquad (4.2\text{-}4a)$$

$$\gamma = -\arg \bar{D}_v \qquad \text{(phase shift)} \qquad (4.2\text{-}4b)$$

The amplitude $\bar{A}_v$ and phase shift γ can also be expressed by the complex stiffness as

$$\bar{A}_v = \frac{1}{\text{Real}(\bar{K}_v)} \sqrt{\frac{1}{1 + \tan^2 \gamma}} \qquad (4.2\text{-}5a)$$

$$\tan \gamma = -\frac{\text{Imag.}\ (\bar{K}_v)}{\text{Real}(\bar{K}_v)} \qquad (4.2\text{-}5b)$$

The above expression for $\bar{A}_v$ in Eq. 4.2-5a indicates that the amplitude of the displacement is smaller for a larger phase shift ($\gamma \leq \frac{\pi}{2}$) even if the stiffness in $\bar{K}_v$ is held constant. The expression for γ also indicates that the smaller stiffness and larger damping in $\bar{K}_v$ yield a larger phase shift.

The displacement $\bar{D}_v$ for the static case is shown in Figs. 4.2-1 and 4.2-2. Since no damping appears in this case, the displacement in those figures is simply the inverse of the stiffness shown in Figs. 3.2-2 and 3.2-3.

For the dynamic case, the amplitude and phase shift of the displacement are shown in Figs. 4.2-3 in which the parameters are the same as those used for the complex stiffness shown in Figs. 3.2-5. Two types of peak amplitudes can be seen in this figure. One of them is associated with the resonance of the stratum and the other with the resonance of the soil-pile system. Thus, the first- and second-type peaks appear, respectively, at the resonances of the stratum and the soil-pile system. It is interesting to note that the latter resonance nearly coincides with the natural frequency of the pile. Thus, Fig. 4.2-4 shows approximately the amplifications at the first resonances of the stratum and soil-pile system for various degrees of soil-effect. In this figure, the amplifications of the second-type peak are remarkably high for the weak soil effect and those of the first-type peak are smaller for the more slender pile.

Two types of sharp increases of phase shift can also be seen in Figs. 4.2-3. One is accompanied by the resonance of the stratum and the other by that of the soil-pile system. As the soil effect increases, the second type of sharp increase diminishes and the phase shift grows less with frequency.

The variation of the amplitude and the phase shift with frequency a_0' are shown in Fig. 4.2-5. The important features of this figure are the same as those in Fig. 3.2-8 and were explained in the previous chapter.

3 4

OF/DE

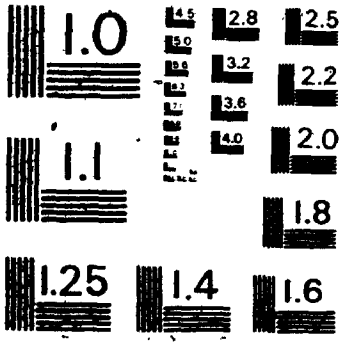

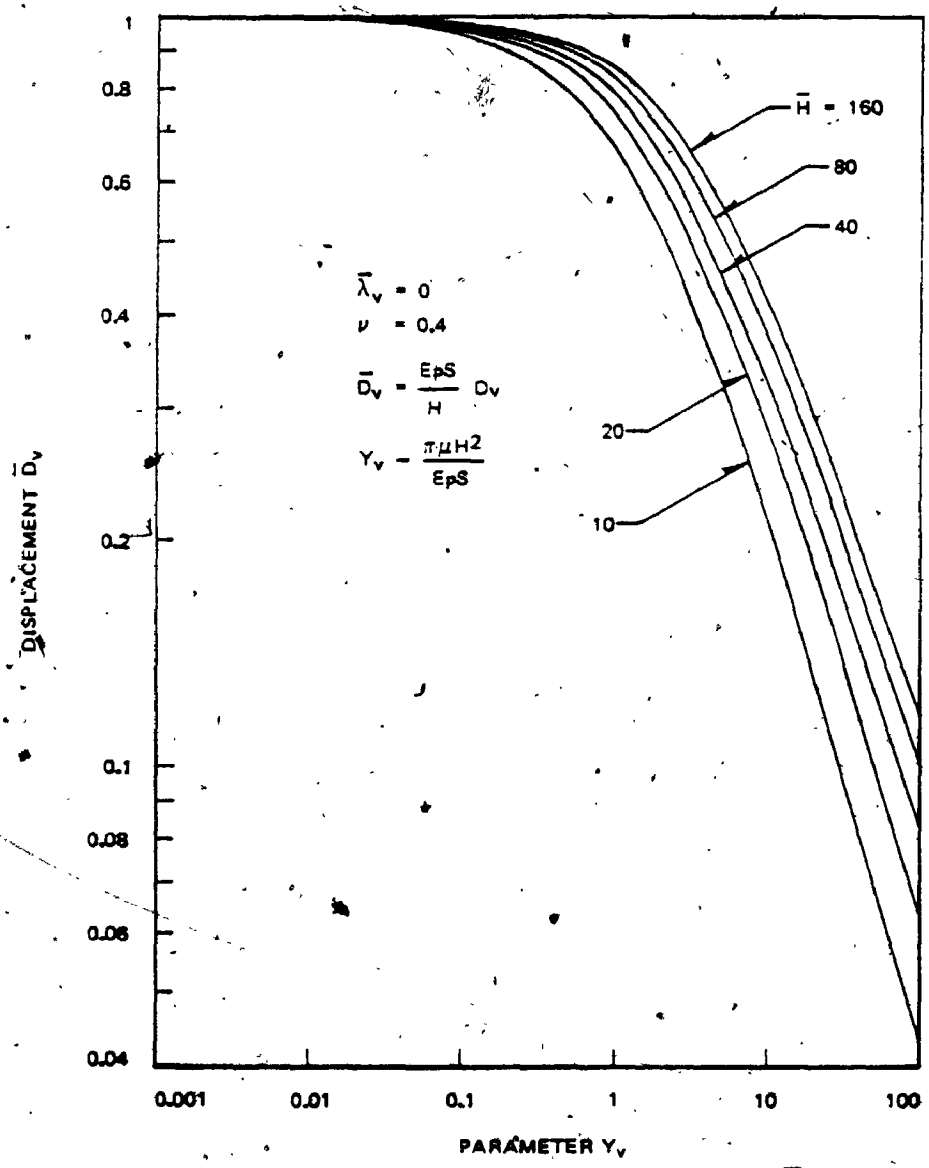

Fig. 4.2-1. Variation of Static Displacement $\bar{D}_v$ with Parameter Y_v

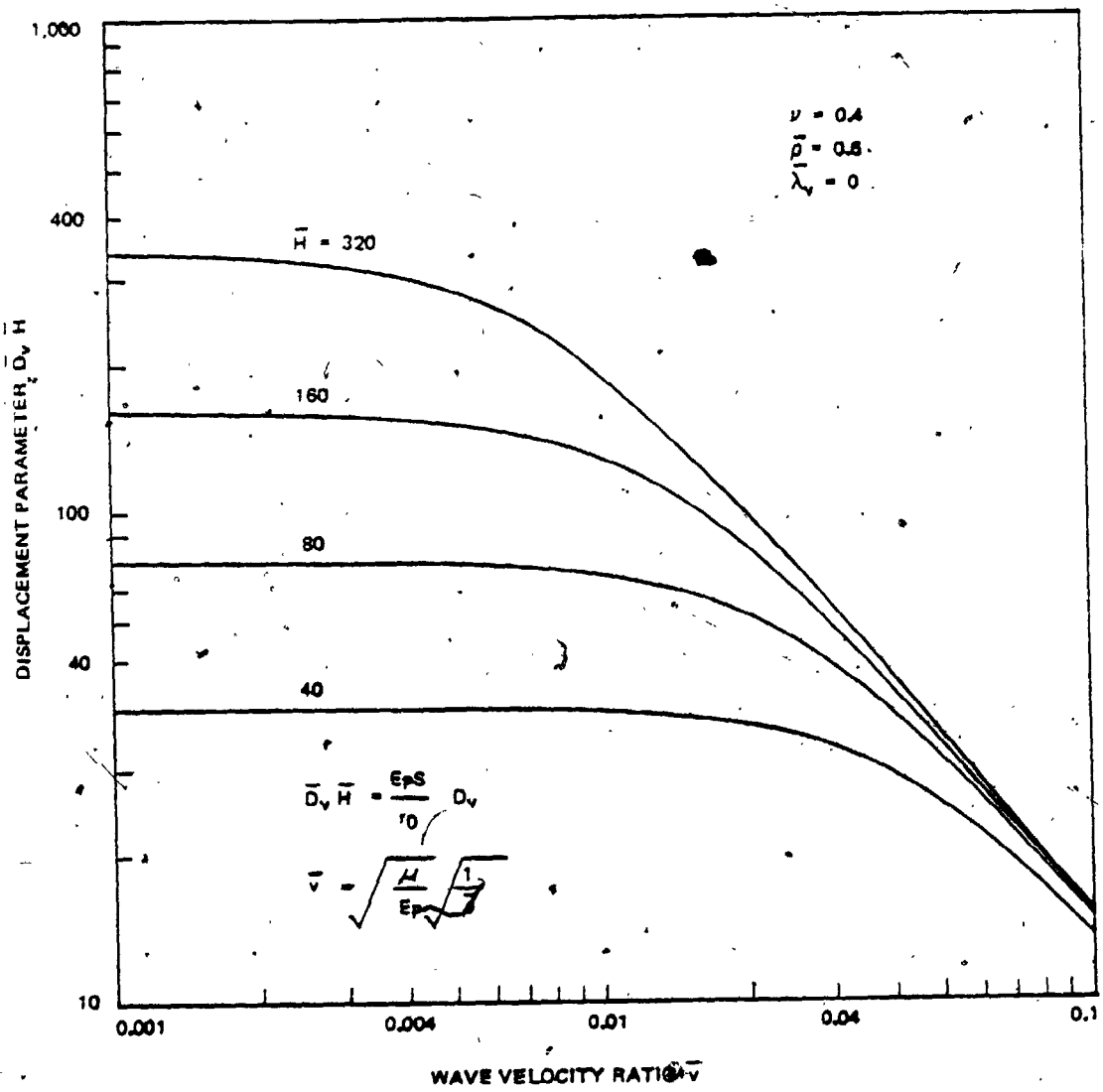

Fig. 4.2-2. Variation of Displacement Parameter $\bar{D}_v \bar{H}$ with Wave Velocity Ratio

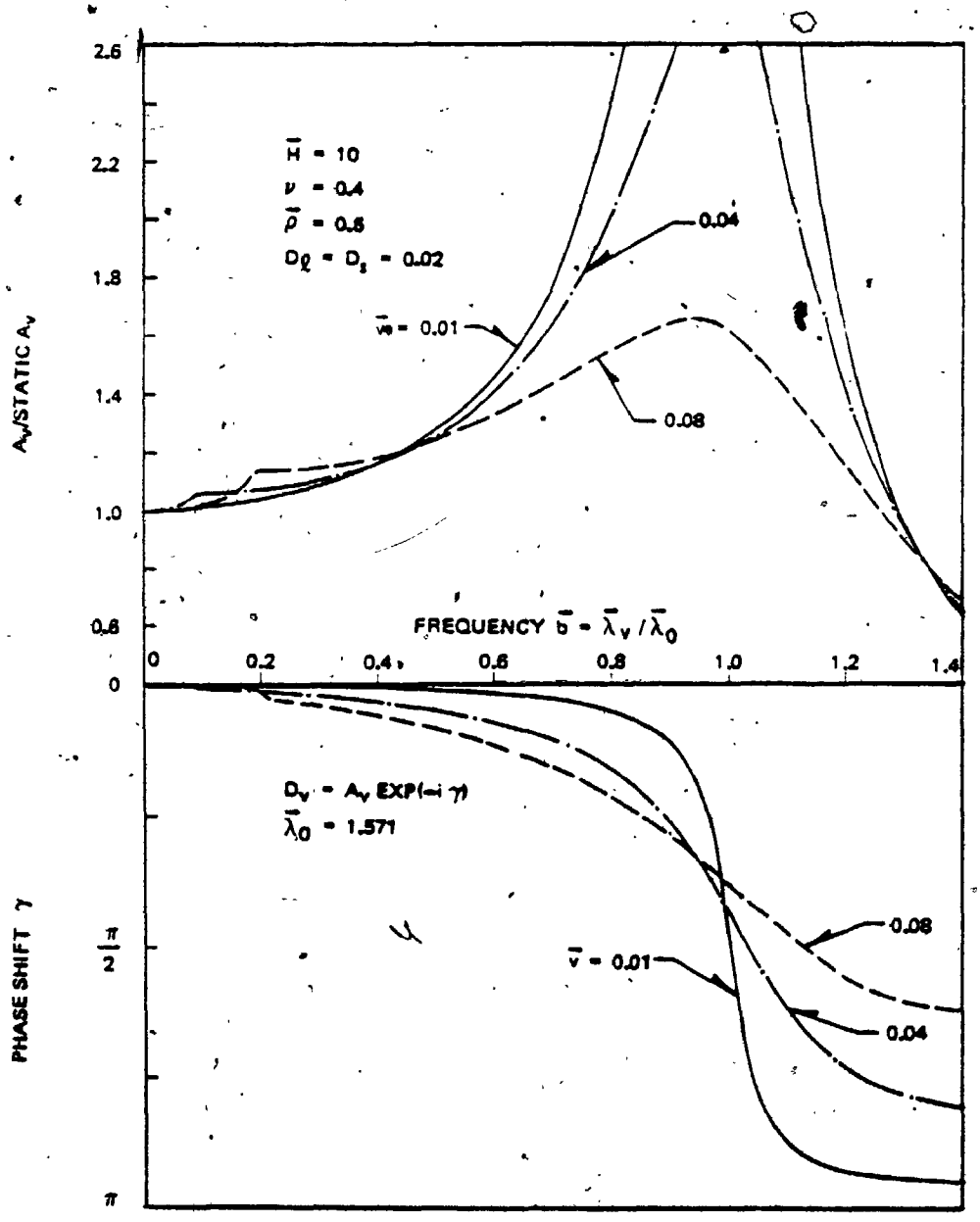

Fig. 4.2-3a. Variation of Displacement D_v with Frequency $\bar{b}$ ($\bar{H}$ = 10)

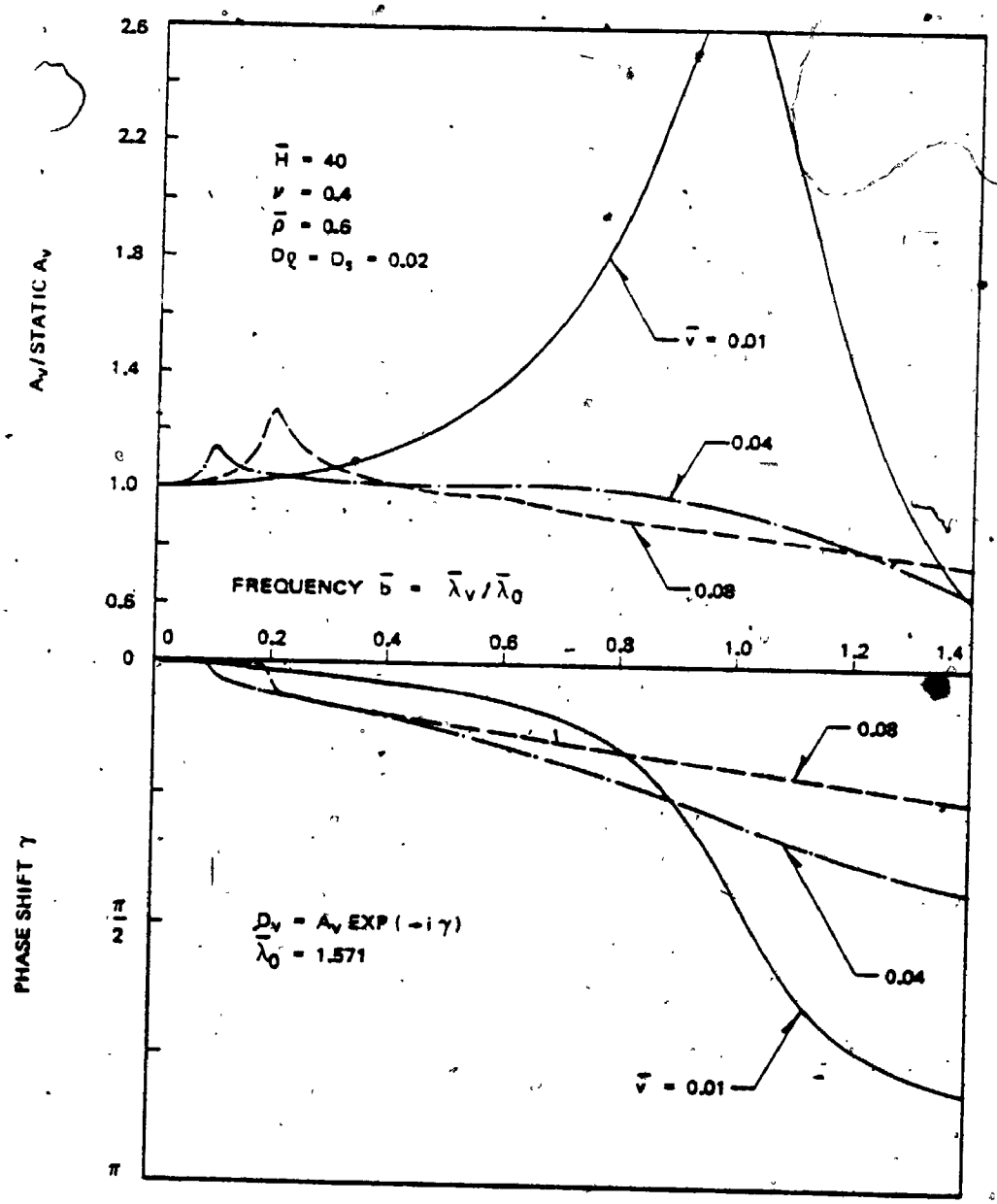

Fig. 4.2-3b. Variation of Displacement D_v with Frequency $\bar{b}$ ($\bar{H}$ = 40)

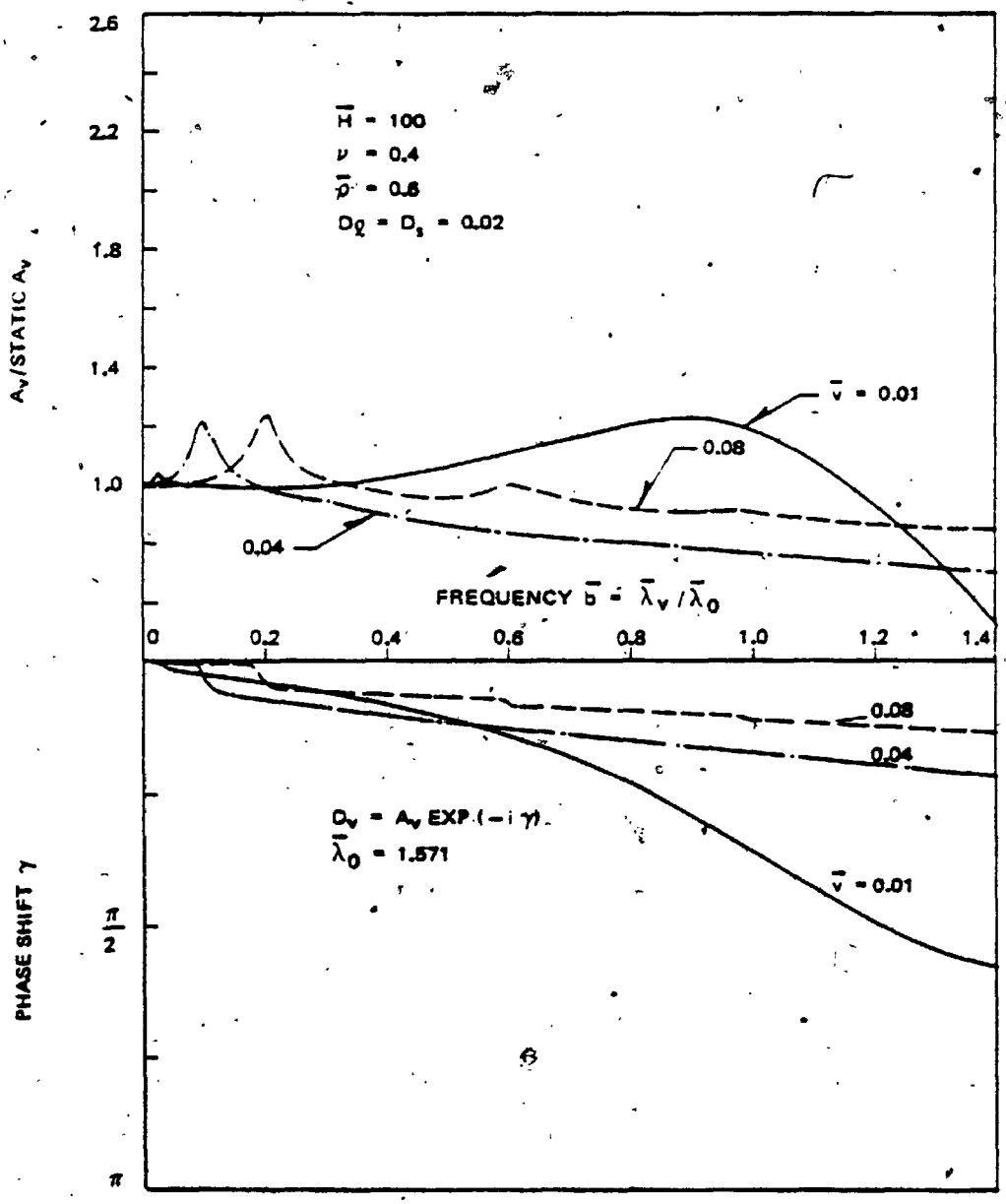

Fig. 4.2-3c Variation of Displacement D_v with Frequency $\bar{b}$ ($\bar{H}$ = 100)

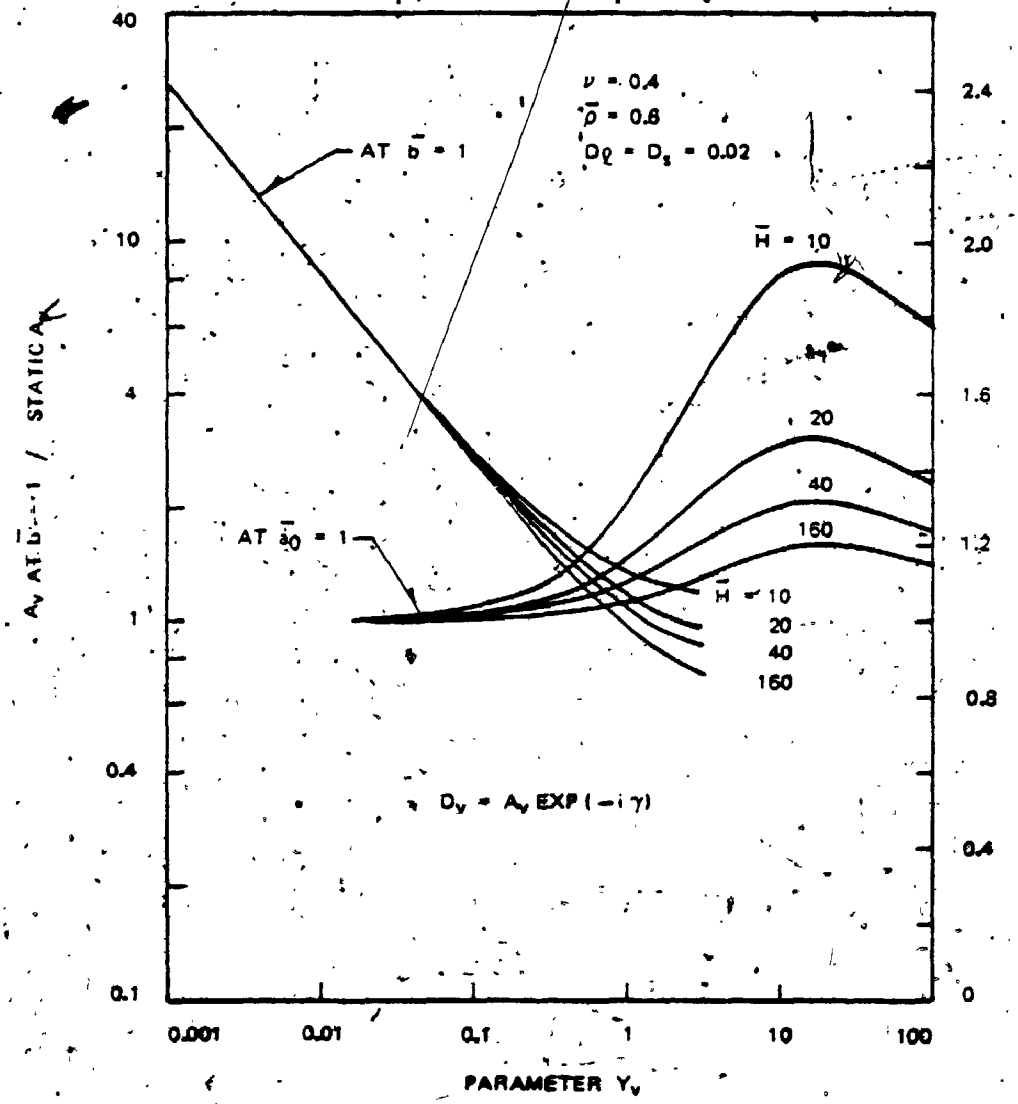

Fig. 4.2-4, Variation of Amplifications at $\bar{a}_0 = 1$ and $\bar{b} = 1$ with Parameter Y_v

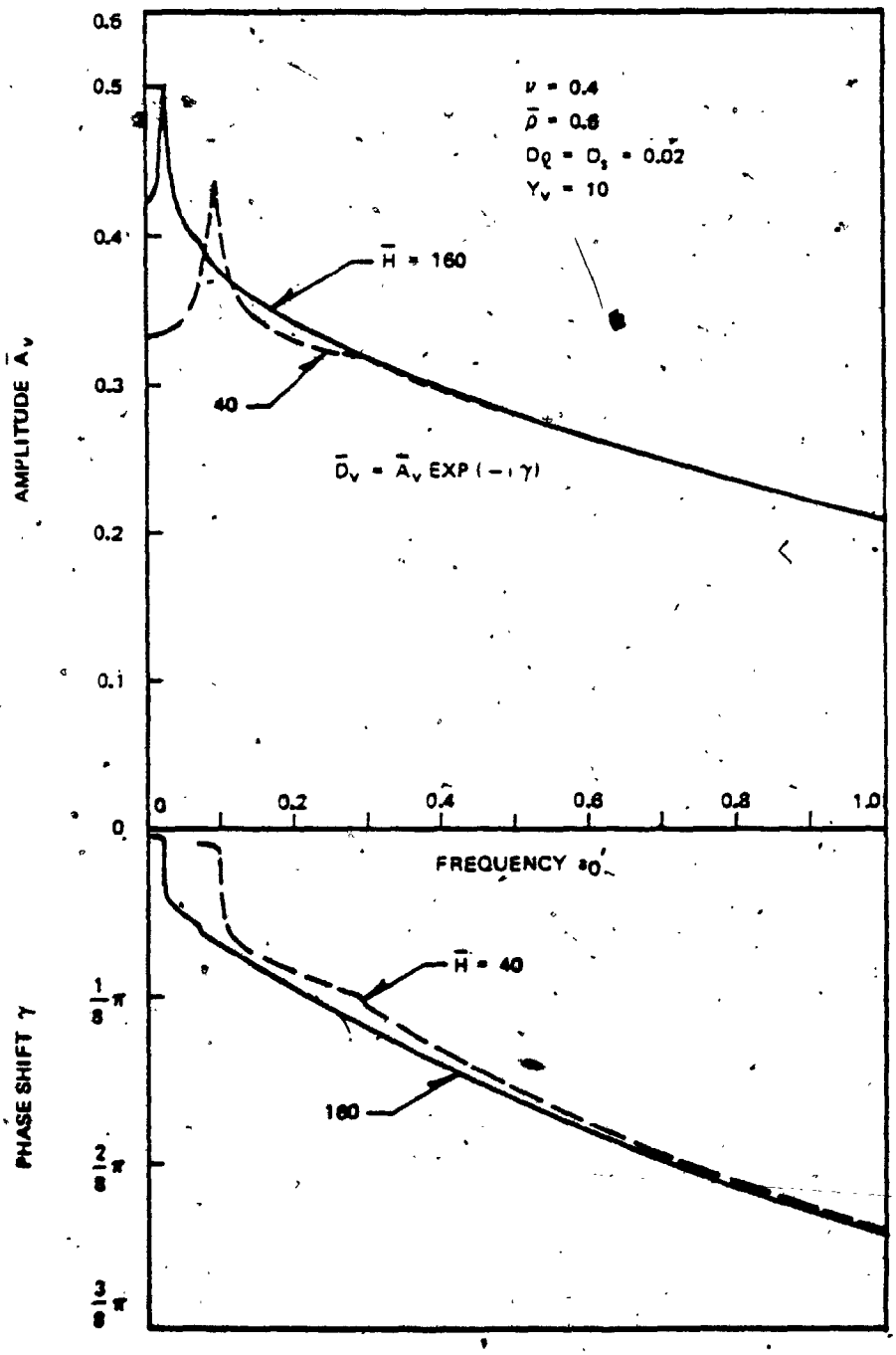

Fig. 4.2-5. Variation of Displacement $\bar{D}_v$ with Frequency a_0' for Various Slenderness Ratios

The variation of Poisson's ratio affects the static displacement $\bar{D}_v$ (Fig. 4.2-6). On the other hand, it affects very little the dynamic displacement $\bar{D}_v$ at the frequencies higher than the first resonant frequency of the stratum as can be seen in Fig. 4.2-7. This trend was observed and explained in the discussion of the complex stiffness.

The variation of the mass ratio affects only the dynamic behavior of the soil-pile system. The amplification around the resonance of the soil-pile system is shown in Fig. 4.2-8 for $\bar{\rho} = 0.3$ and 1.2. This figure indicates that the variation of the mass ratio does not much affect the resonant frequency but does affect the amplification: the lower mass ratio yields higher amplification. Fig. 4.2-9 shows the same trend in the amplification as that observed in Fig 4.2-8. However, under the strong soil effect, the variation of mass ratio does not much affect the amplitude but does affect the phase shift as shown in Fig. 4.2-10 where the lower mass ratio yields a larger phase shift.

4.2.B Horizontal Vibration

The displacements at the pile head subjected to unit forces are obtained by inverting the complex stiffness K_h, and expressed as

$$\begin{bmatrix} D_h(U,P) & D_h(U,M) \\ D_h(\zeta,P) & D_h(\zeta,M) \end{bmatrix} = \begin{bmatrix} K_h(P,U) & -K_h(P,\zeta) \\ -K_h(M,U) & K_h(M,\zeta) \end{bmatrix}^{-1} \qquad (4.2\text{-}6)$$

where $D_h(U,P)$ and $D_h(U,M)$ are the horizontal displacements U due to forces P=1 and M=1, respectively, and $D_h(\zeta,P)$ and $D_h(\zeta,M)$ are rotational displacements ζ due to forces P=1 and M=1, respectively.

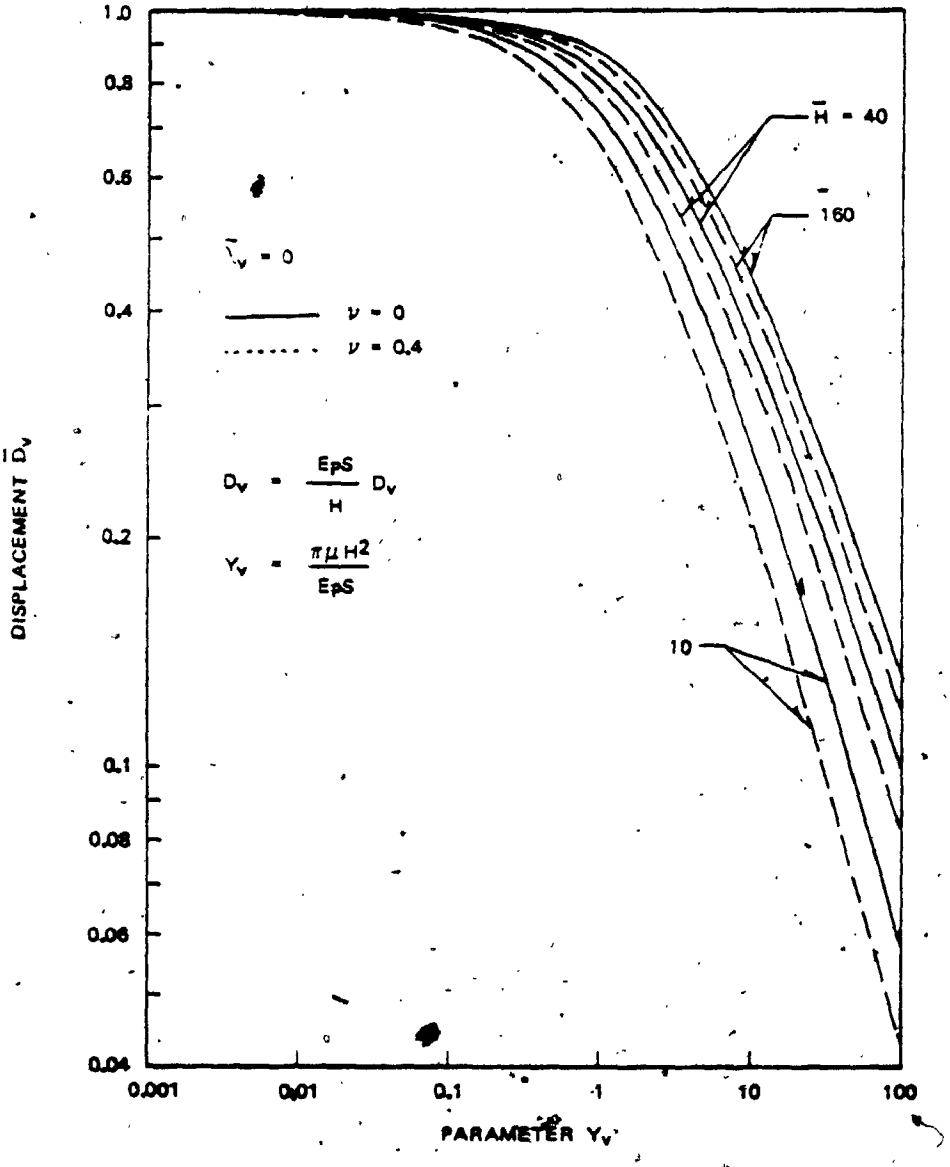

Fig. 4.2-6. Variation of Static Displacement $\bar{D}_v$ with Parameter Y_v for Various Poisson's Ratios

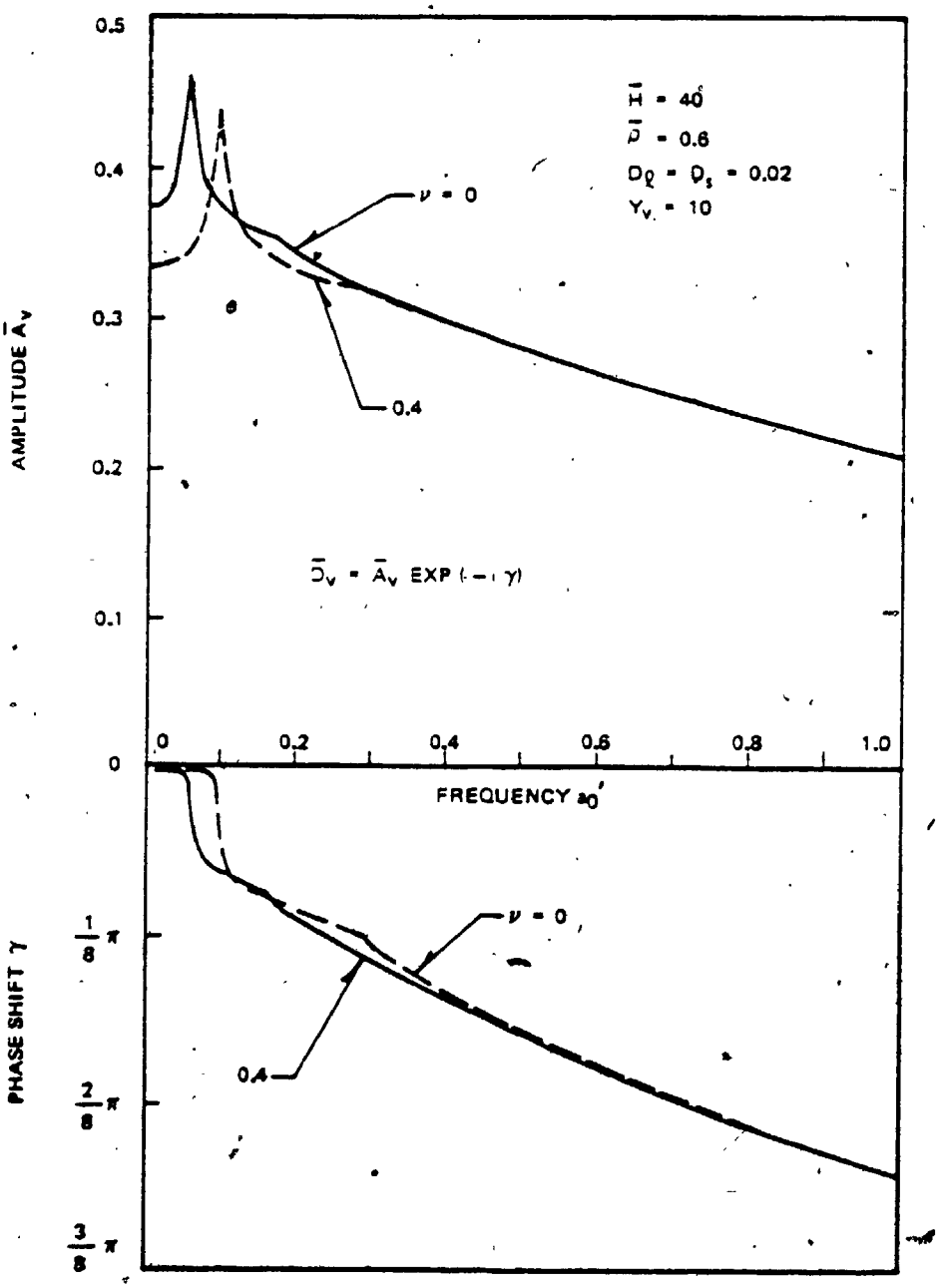

Fig. 4.2-7. Variation of Displacement $\bar{D}_v$ with Frequency a_0' for Various Poisson's Ratios

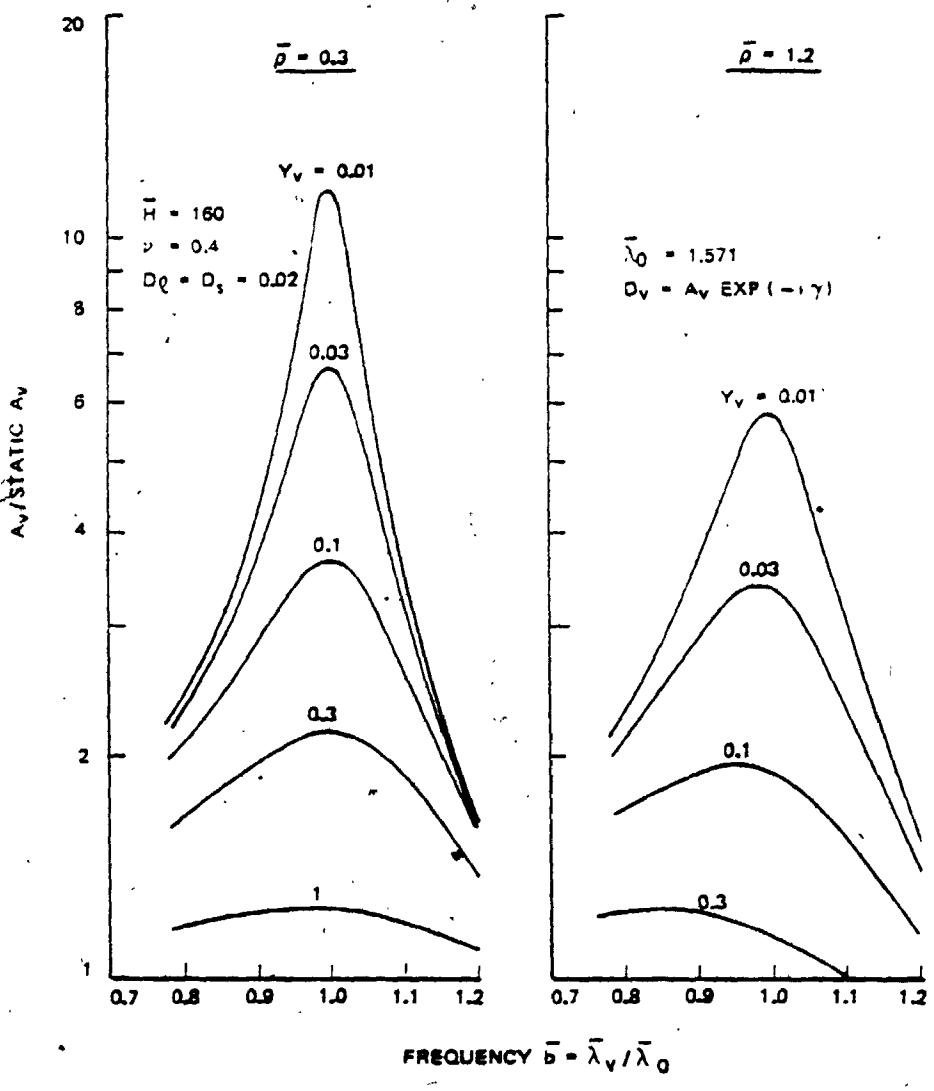

Fig. 4.2-8. Variation of Amplification with Parameter Y_v for Various Mass Ratios

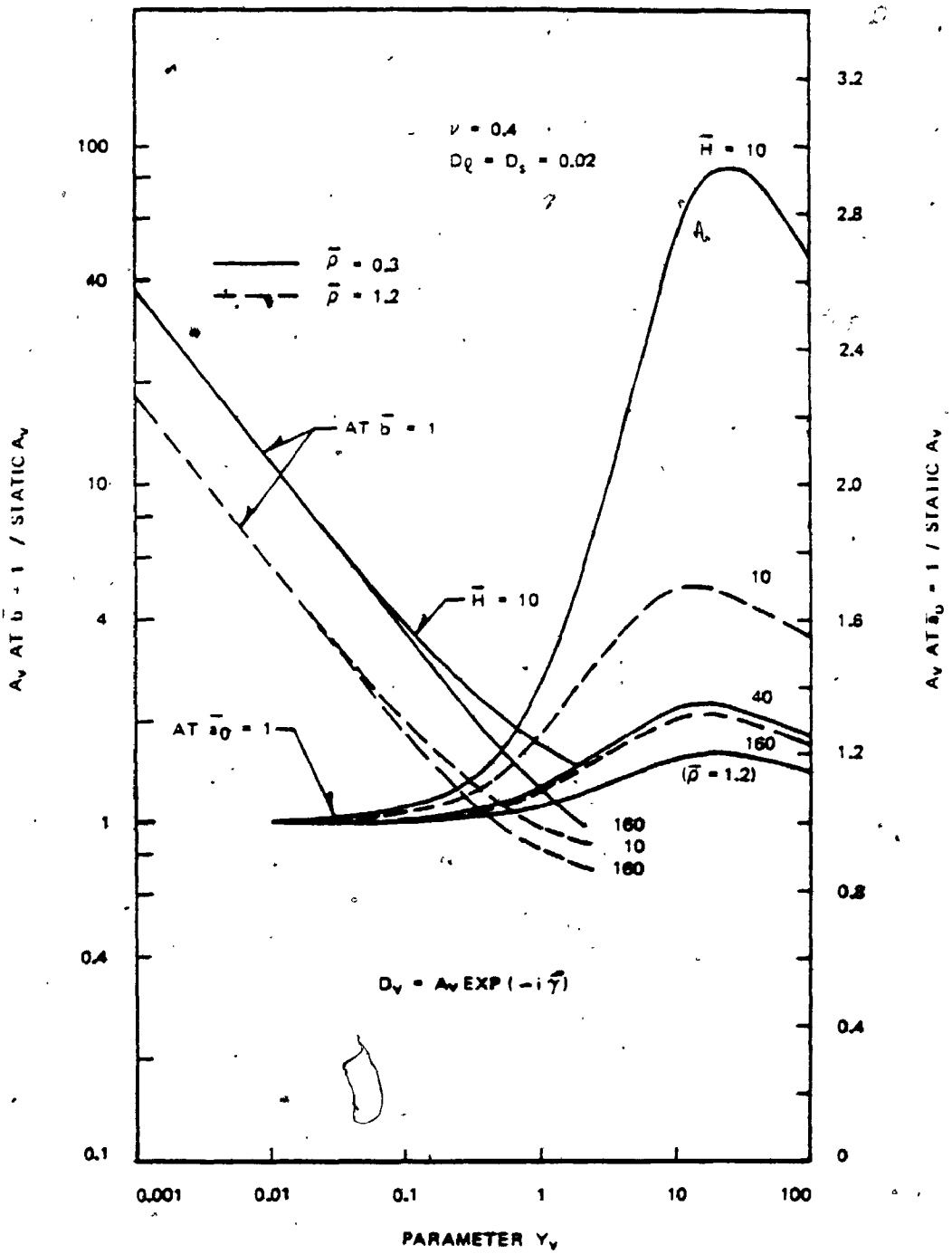

Fig. 4.2-9. Variation of Amplifications at $\bar{a}_0 = 1$ and $\bar{b} = 1$ with Parameter Y_v for Various Mass Ratios

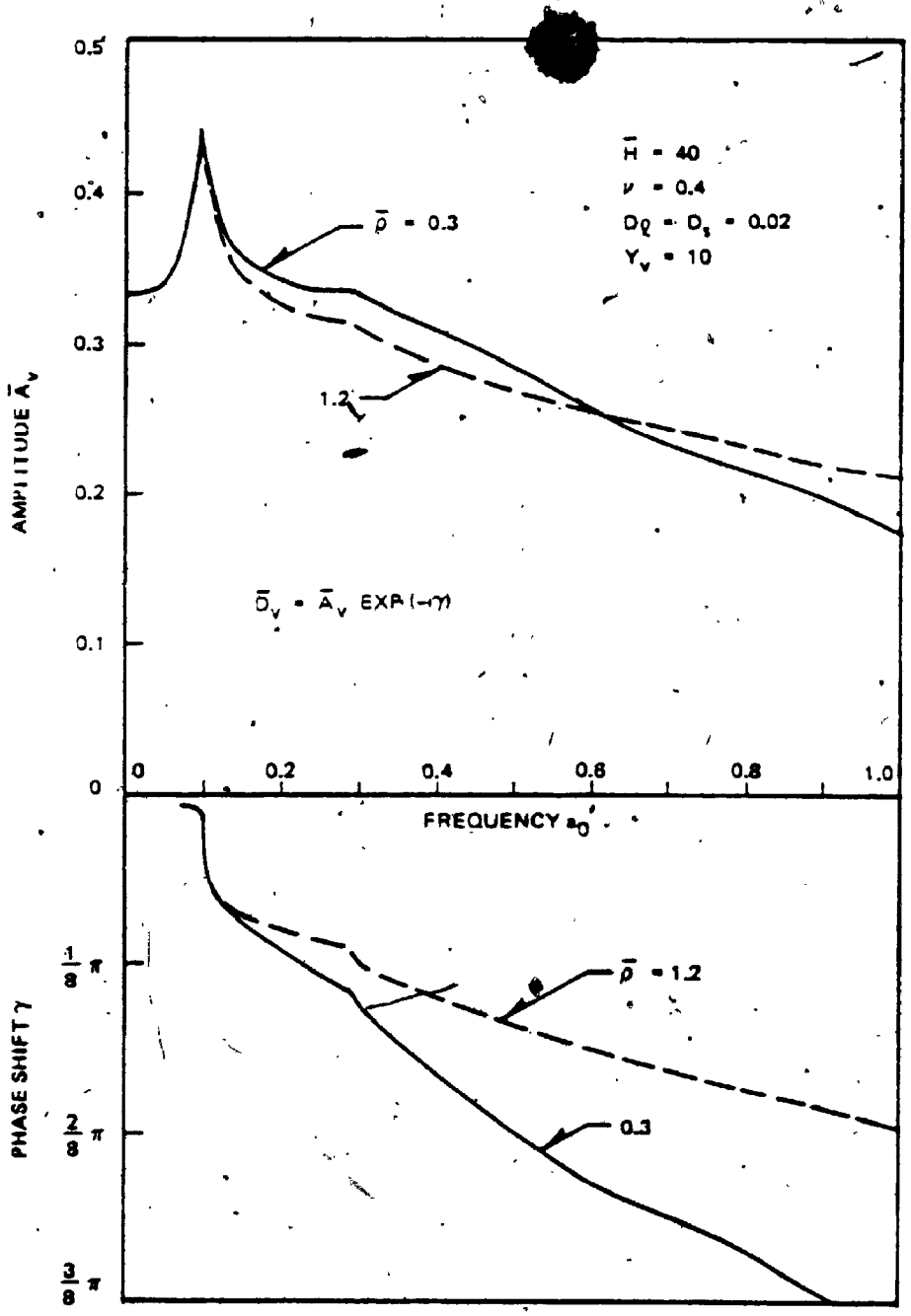

Fig. 4.2-10. Variation of Displacement $\bar{D}_v$ with Frequency a_0' for Various Mass Ratios

The following dimensionless parameters for displacements D_h are defined for convenience.

$$\begin{bmatrix} \bar{D}_h(U,P) & \bar{D}_h(U,M) \\ \bar{D}_h(\zeta,P) & \bar{D}_h(\zeta,M) \end{bmatrix} = E_P I \begin{bmatrix} D_h(U,P)/H^3 & D_h(U,M)/H^2 \\ D_h(\zeta,P)/H^2 & D_h(\zeta,M)/H \end{bmatrix} \tag{4.2-7a}$$

$$\begin{bmatrix} \bar{H}^3\,\bar{D}_h(U,P) & \bar{H}^2\,\bar{D}_h(U,M) \\ \bar{H}^2\,\bar{D}_h(\zeta,P) & \bar{H}\,\bar{D}_h(\zeta,M) \end{bmatrix} = E_P I \begin{bmatrix} D_h(U,P)/r_0^3 & D_h(U,M)/r_0^2 \\ D_h(\zeta,P)/r_0^2 & D_h(\zeta,M)/r_0 \end{bmatrix} \tag{4.2-7b}$$

The dimensionless quantities on the left side of Eq. 4.2-7a fully show the effect of the variation of pile radius. The left side of Eq. 4.2-7b shows the effect of the variation of pile length.

In a manner similar to that used for vertical vibration, the complex displacement $\bar{D}_h$ can be rewritten as

$$\bar{D}_h = \bar{A}_h\, e^{-i\gamma} \tag{4.2-8}$$

where

$$\bar{A}_h = |\bar{D}_h| \tag{4.2-9a}$$

$$\gamma = -\arg \bar{D}_h \tag{4.2-9b}$$

As a special case, the displacement of the pile with the rotationally fixed head is simply the inverse of the complex stiffness $K_h(P,U)$.

The displacements $\bar{D}_h$ for the static case are shown in Figs. 4.2-11 and 4.2-12 for the rotationally fixed head (fixed head) and Figs. 4.2-13 and 4.2-14 for the free head. Since the displacement $D_h(U,P)$ for the rotationally fixed head is related only to $K_h(P,U)$, the soil effect on the displacement of this pile varies with the

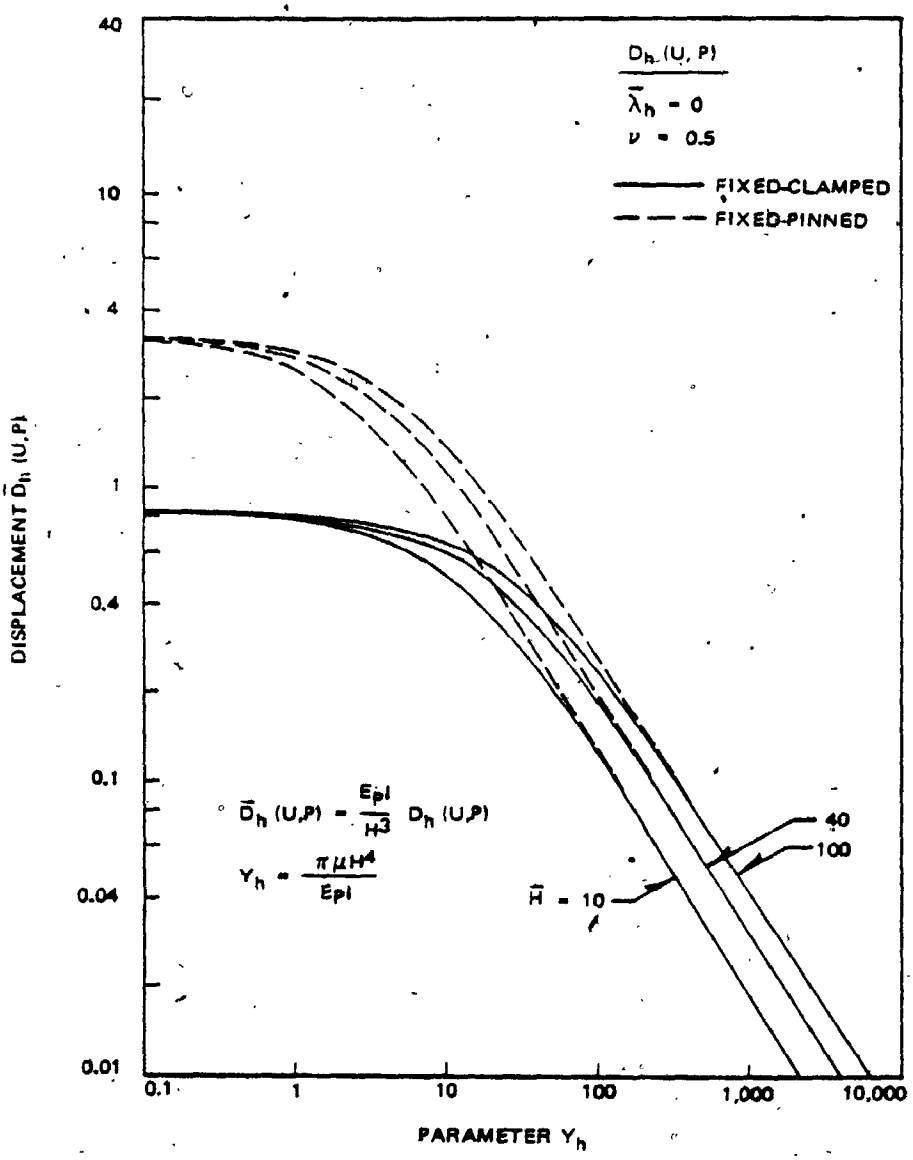

Fig. 4.2-11: Variation of Static Displacement $\bar{D}_h(U,P)$ with Parameter Y_h (Fixed Head)

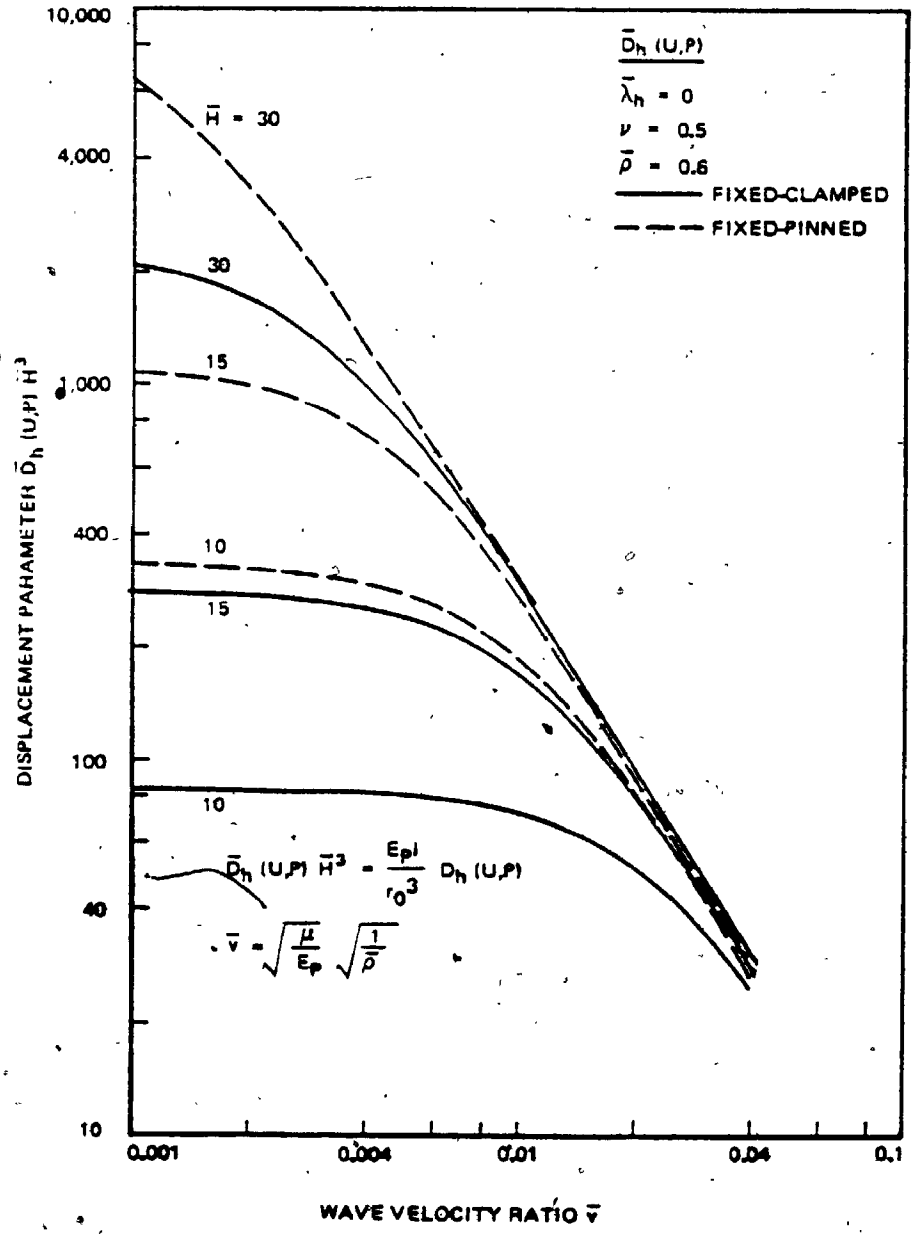

Fig. 4.2-12. Variation of Displacement Parameter $\bar{D}_h(U,P)\bar{H}^3$ with Wave Velocity Ratio (Fixed Head)

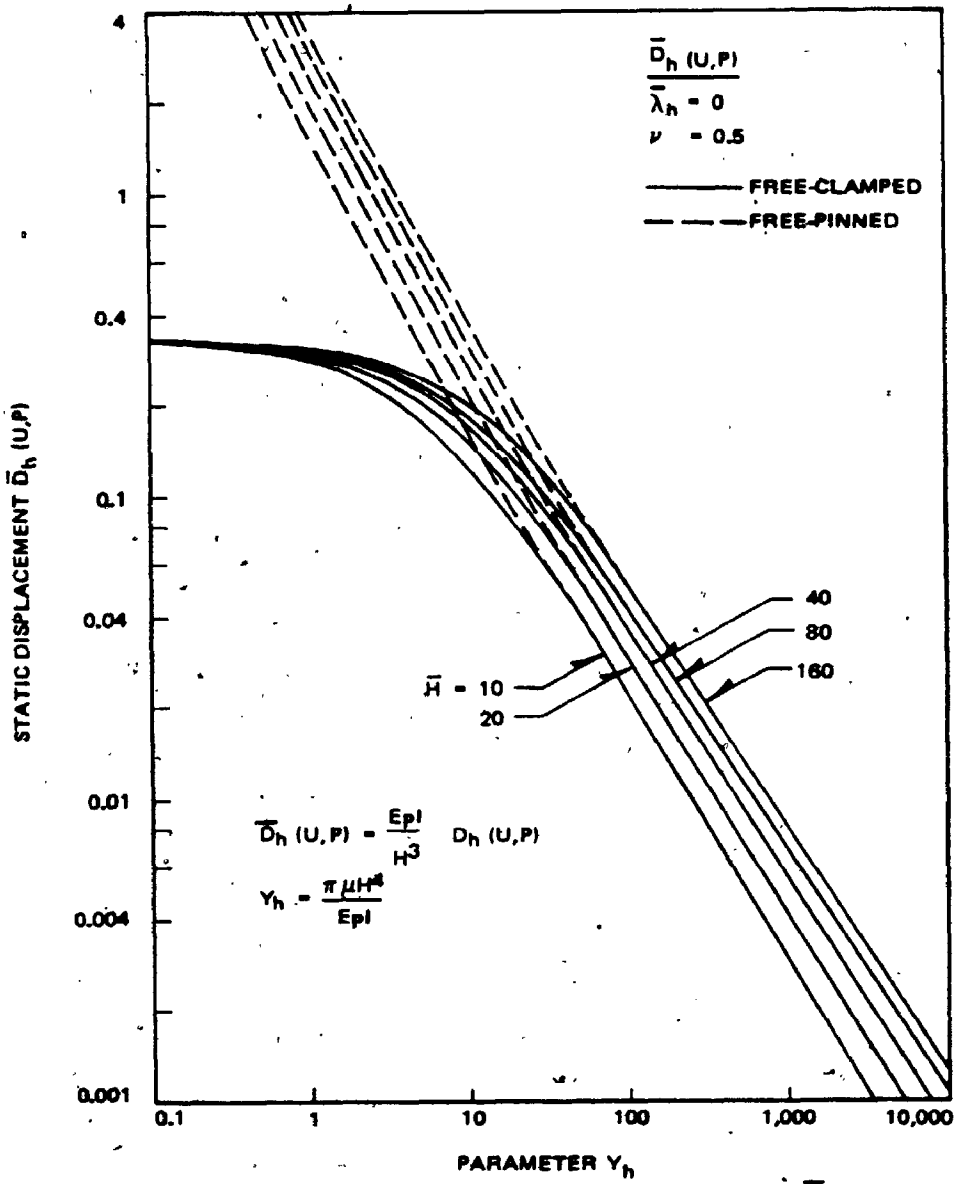

Fig. 4.2-13g. Variation of Static Displacement $\bar{D}_h(U,P)$ with Parameter Y_h (Free Head)

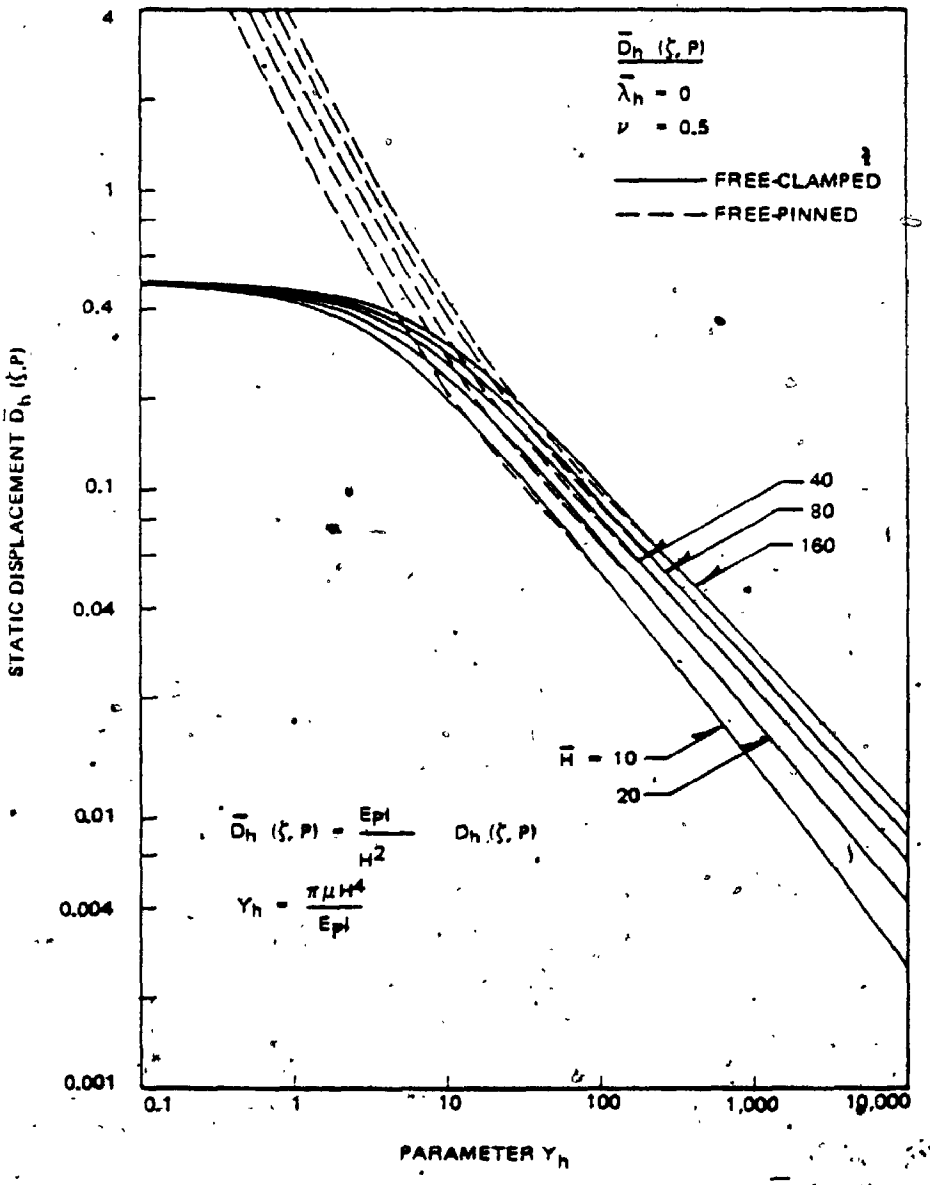

Fig. 4.2-13b. Variation of Static Displacement $\bar{D}_h(\zeta,P)$ with Parameter Y_h (Free Head)

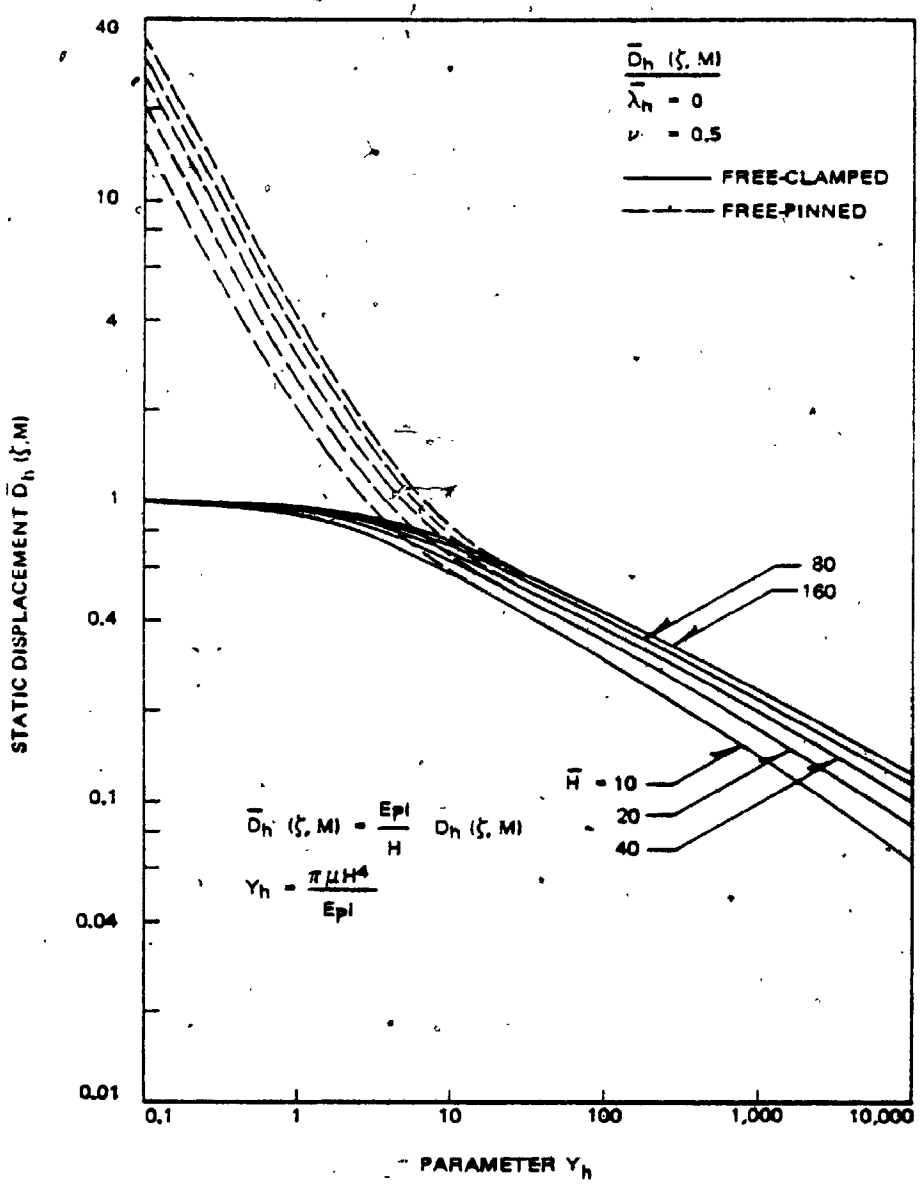

Fig. 4.2-13c. Variation of Static Displacement $\bar{D}_h(\zeta,M)$ with Parameter Y_h (Free Head).

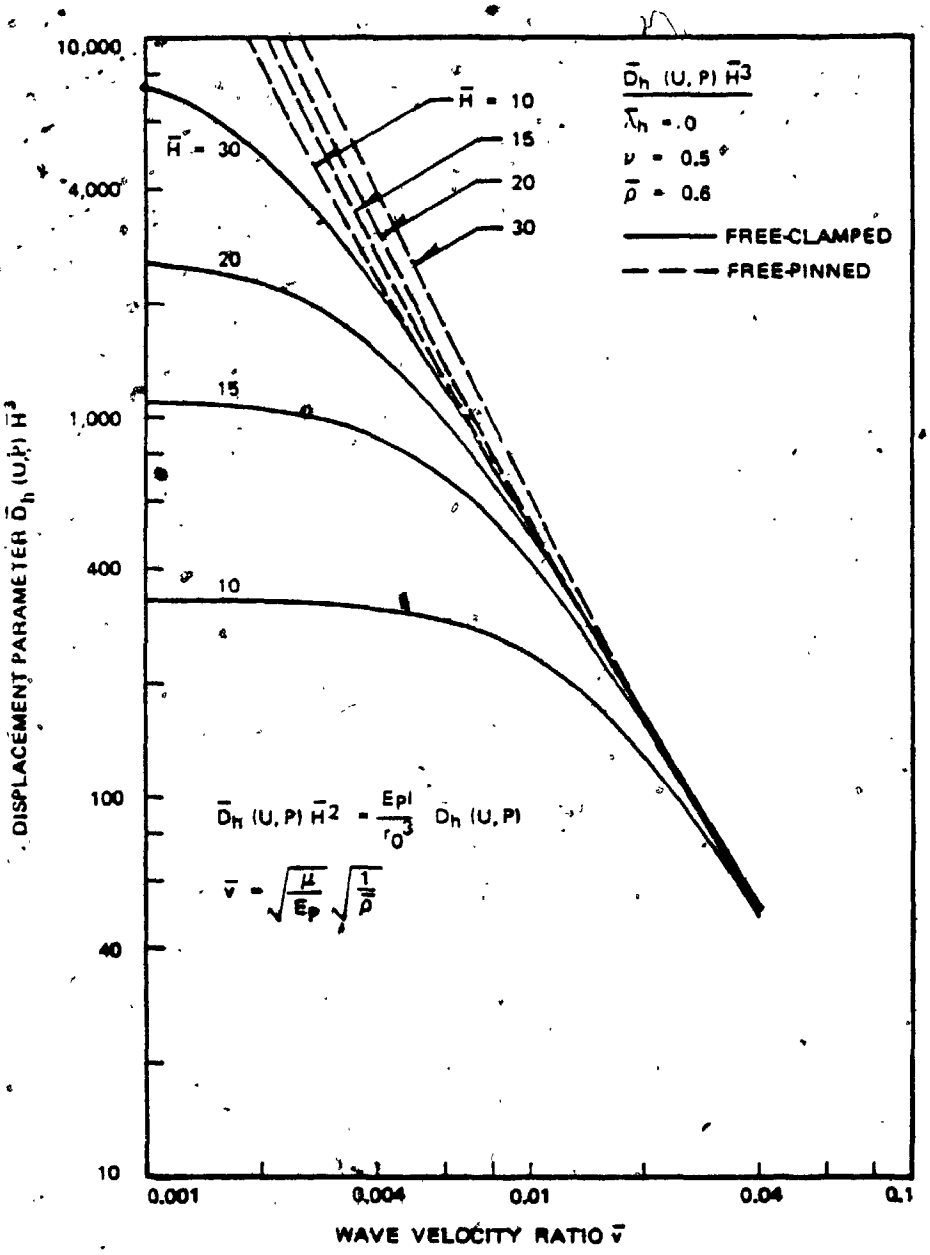

Fig. 4.2-14a. Variation of Displacement Parameter $\bar{D}_h(U,P)\bar{H}^3$ with Wave Velocity Ratio (Free Head)

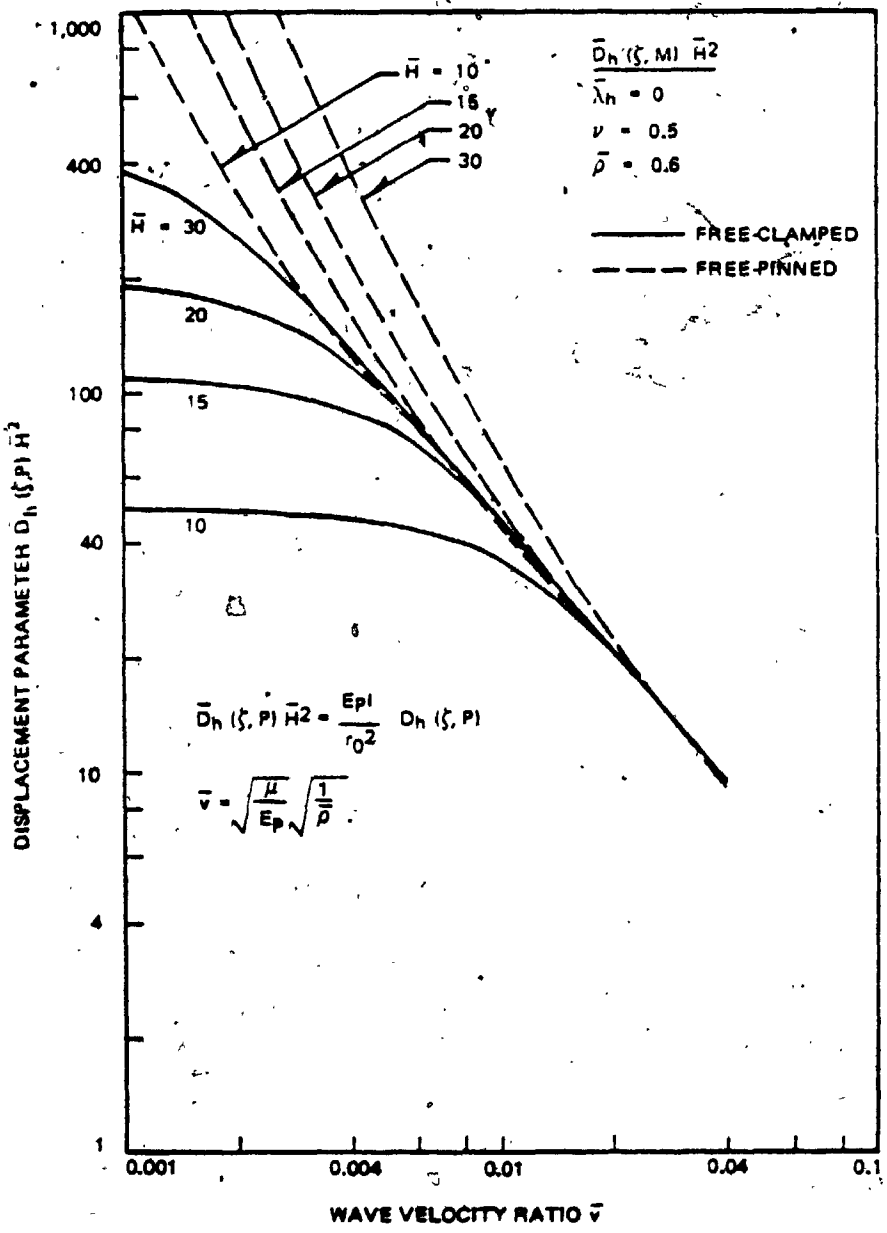

Fig. 4.2-14b. Variation of Displacement Parameter $\bar{D}_h(\zeta,P)\bar{H}^2$ with Wave Velocity Ratio (Free Head)

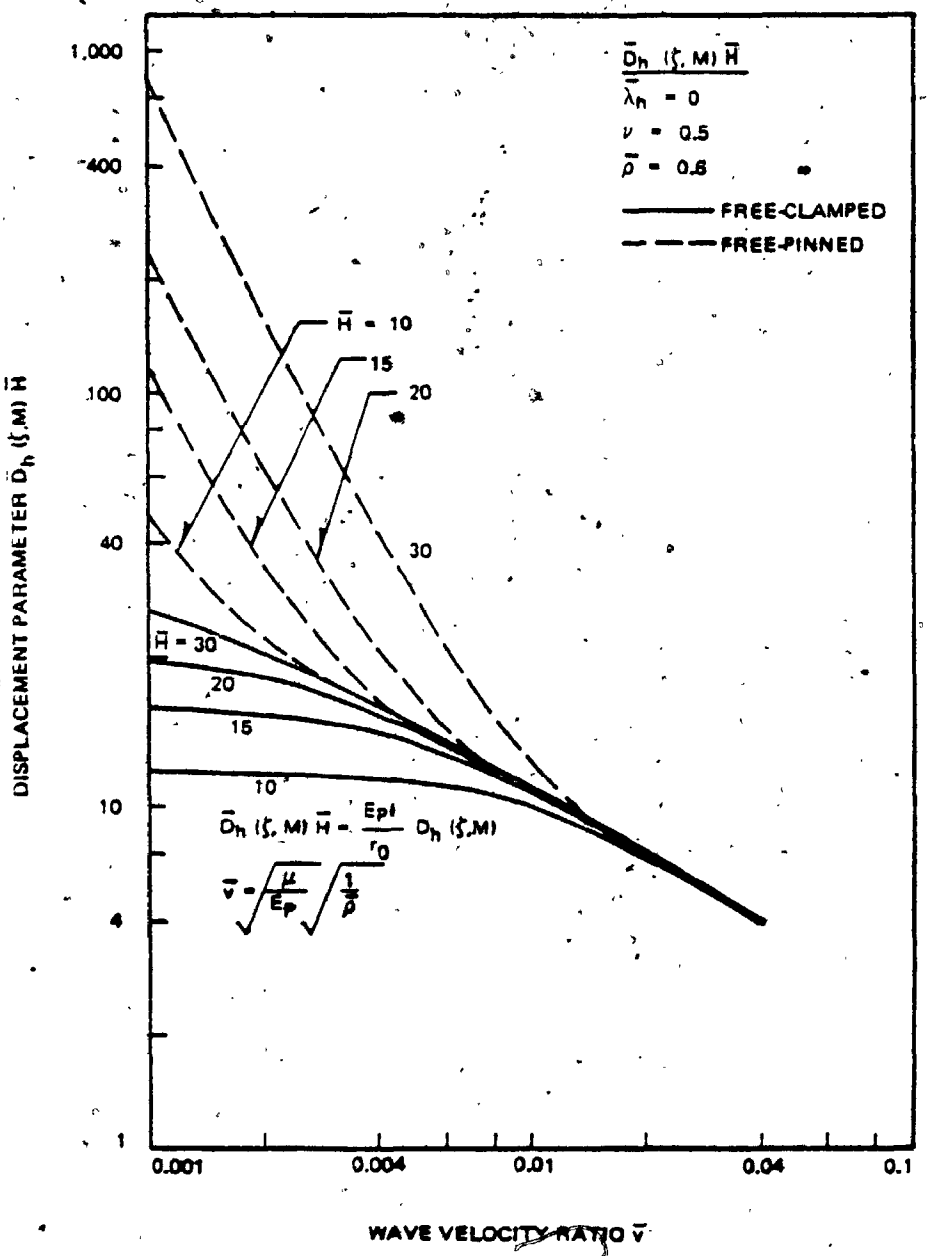

Fig. 4.2-14c. Variation of Displacement Parameter $\bar{D}_h(\zeta,M)\bar{H}$ with Wave Velocity Ratio (Free Head)

parameter Y_h in the same manner as that on the stiffness $K_h(P,U)$ does. On the other hand, the displacements for the free head pile are governed by $K_h(P,U)$, $K_h(P,\zeta)$, and $K_h(M,\zeta)$. Therefore, the soil effect on the displacements for this pile vary with Y_h in a different manner than the soil effect on the stiffnesses does. Since the free head condition provides more flexibility for a pile than the head conditions used in deriving the stiffnesses, the soil effect on the free head pile grows more rapidly with Y_h than those on the stiffnesses do.

For the dynamic case, the displacement D_h is composed of the amplitude and phase shift. They vary with frequency and this variation depends on the effect of soil as shown in Figs. 4.2-15 and 4.2-16. In those figures, the previously mentioned two types of peaks can be clearly seen. Under the small Y_h, the first-type peaks for the free head - pinned tip pile are much more significant than the second-type ones. On the other hand, the first-type peaks for other piles are far less significant than the second ones are. Figs. 4.2-17 also show the different trends in the amplifications at the resonance of the stratum for the free head - pinned tip pile and other piles; the amplification for the free head - pinned tip pile decreases with Y_h, whereas those for other piles increase under the weak soil effect and decrease under the strong soil effect. The variations of the amplifications at the resonance of the soil-pile system with Y_h are shown in Figs. 4.2-18. The trends in this variation are affected very little by the boundary conditions at the ends of the pile.

Figs. 4.2-16 show that even under small Y_h, the phase shift of the free head - pinned tip pile remarkably increases around the resonant frequency of the stratum, and drops thereafter until the next sharp

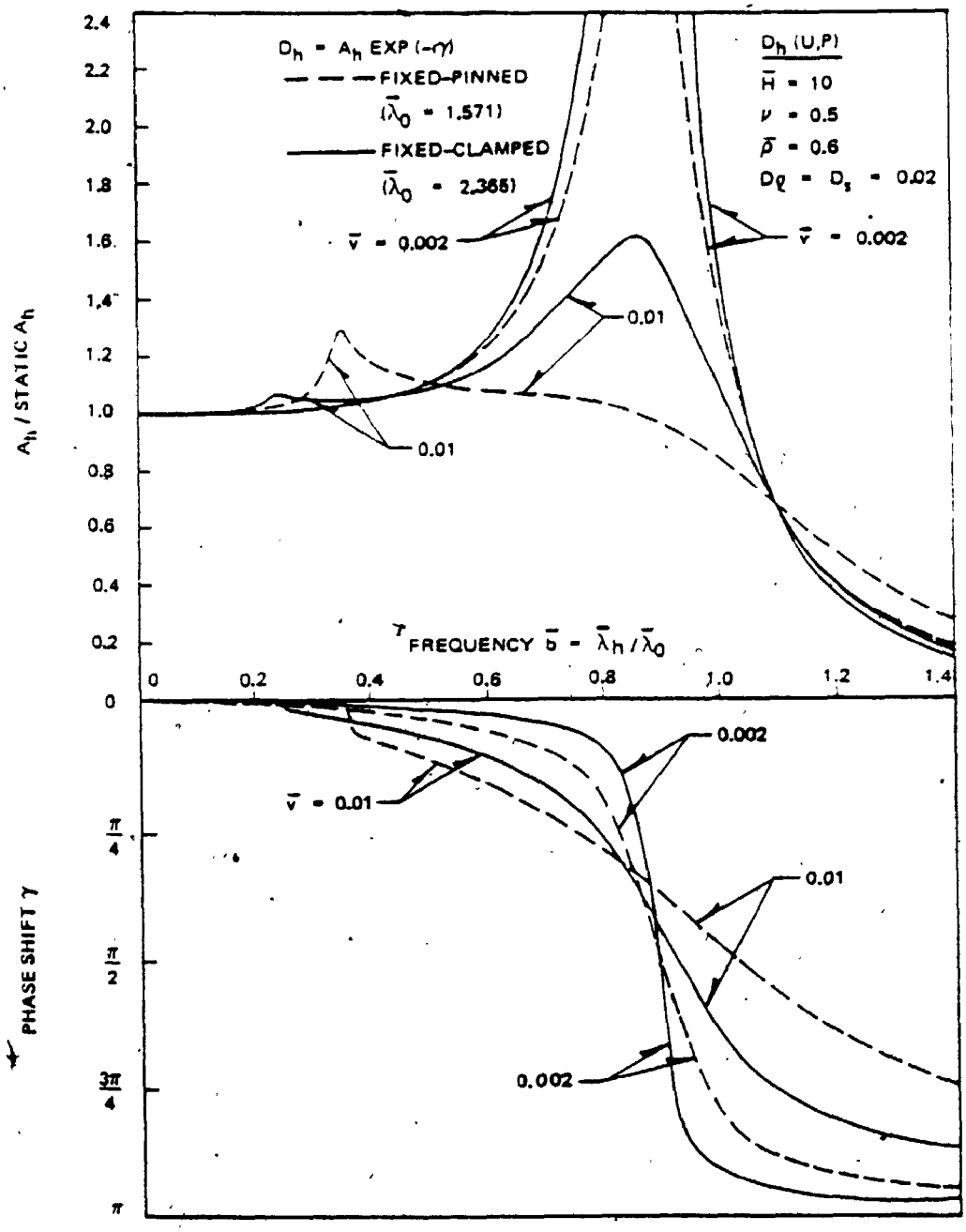

Fig. 4.2-15a. Variation of Displacement D_h (U,P) with Frequency $\bar{b}$ for Various Wave Velocity Ratios ($\bar{H}$ = 10, Fixed Head)

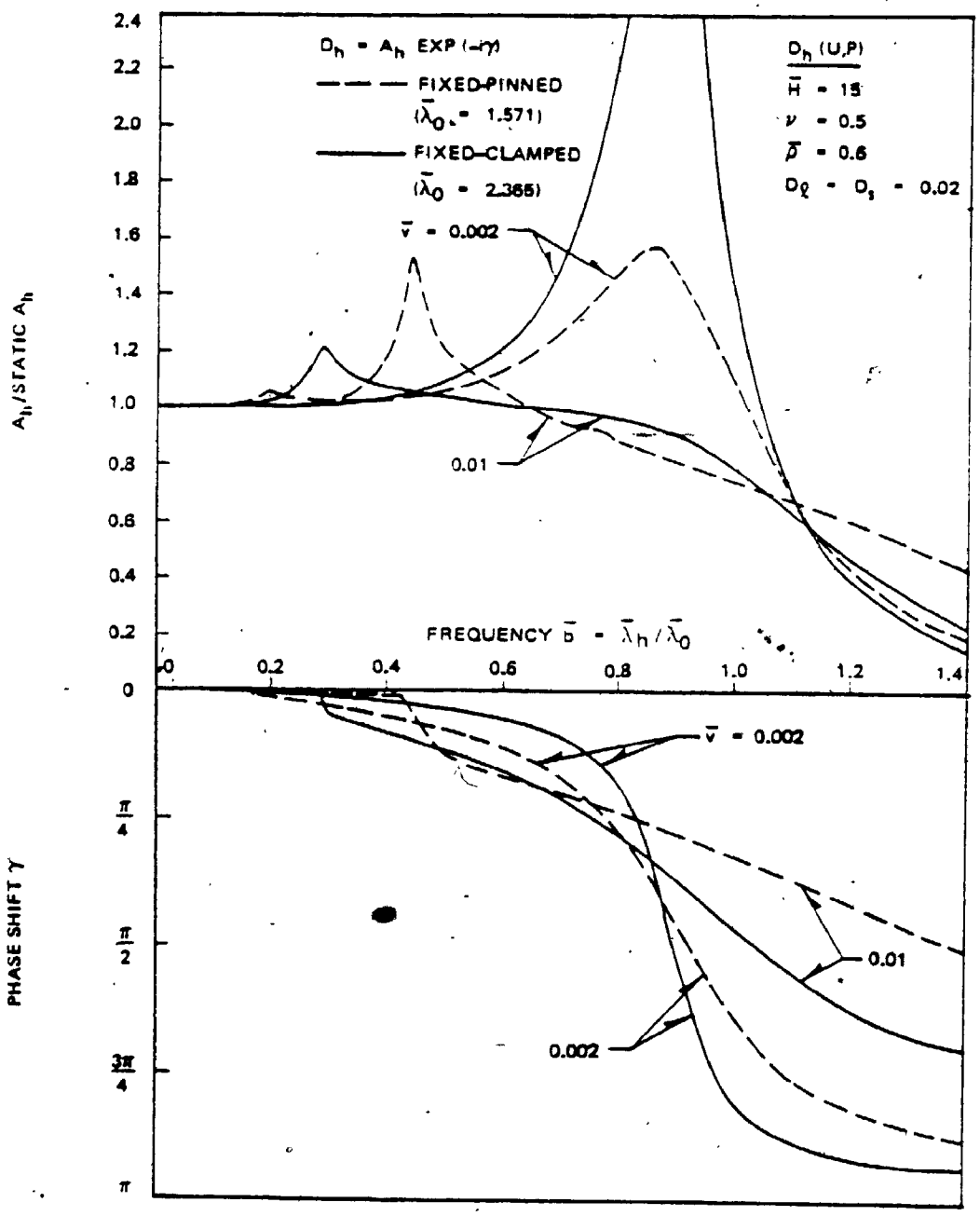

Fig. 4.2-15b. Variation of Displacement D_h(U,P) with Frequency $\bar{b}$ for Various Wave Velocity Ratios ($\bar{H}$ = 15, Fixed Head)

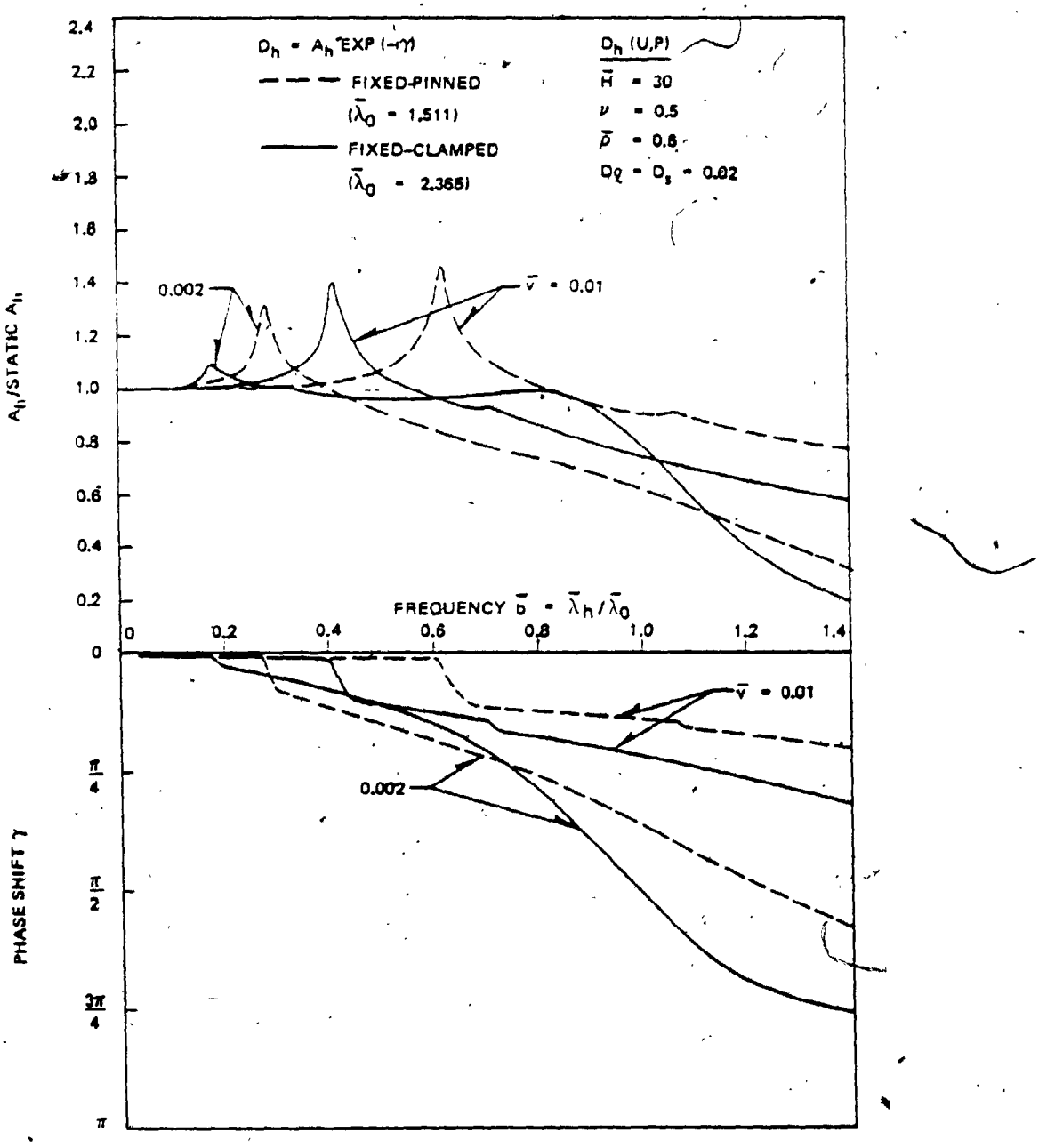

Fig. 4.2-15c. Variation of Displacement D_h(U,P) with Frequency $\bar{b}$ for Various Wave Velocity Ratios ($\bar{H}$ = 30, Fixed Head)

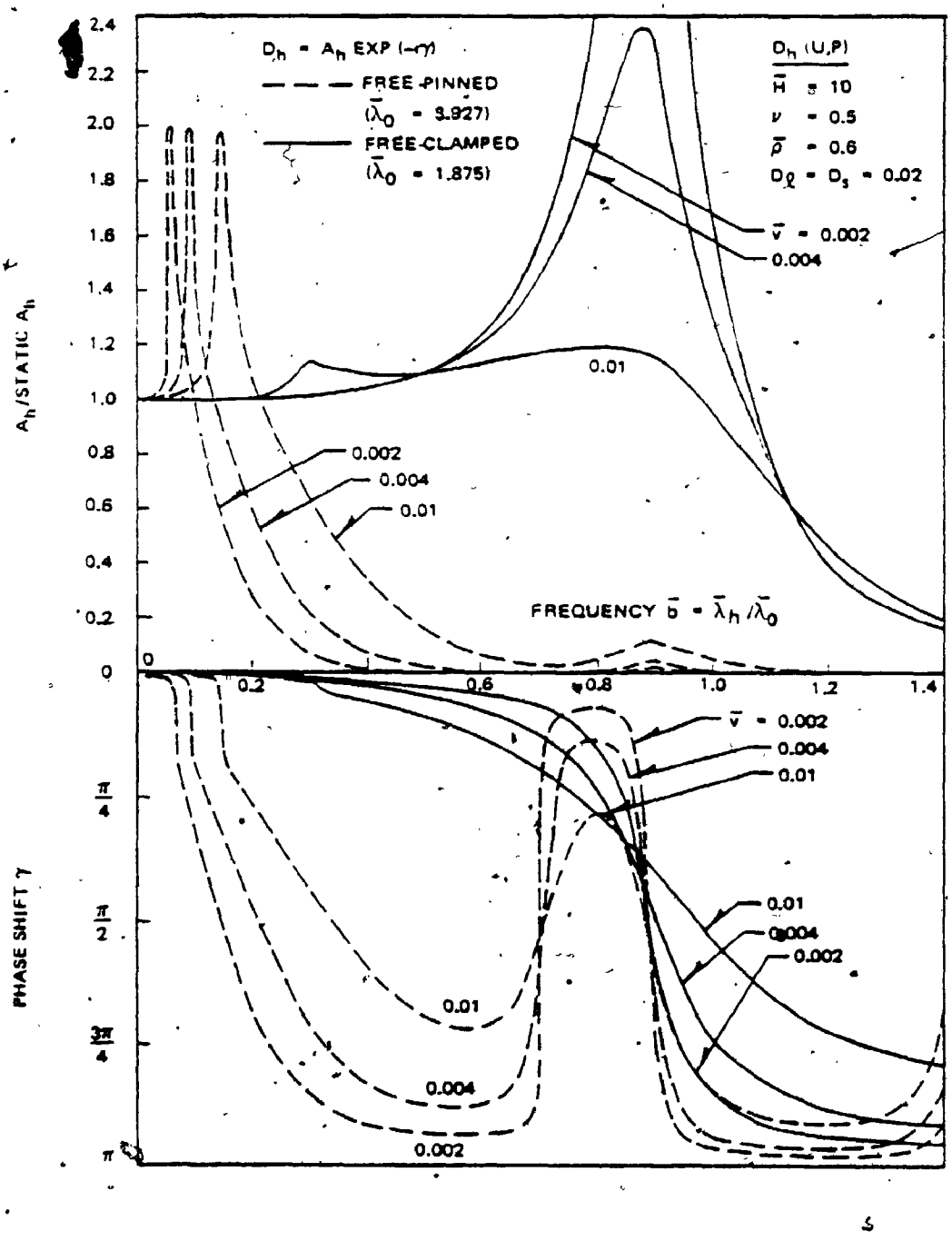

Fig. 4.2-16a. Variation of Displacement $D_h(U,P)$ with Frequency $\bar{b}$ for Various Wave Velocity Ratios ($\bar{H}$ = 10, Free Head)

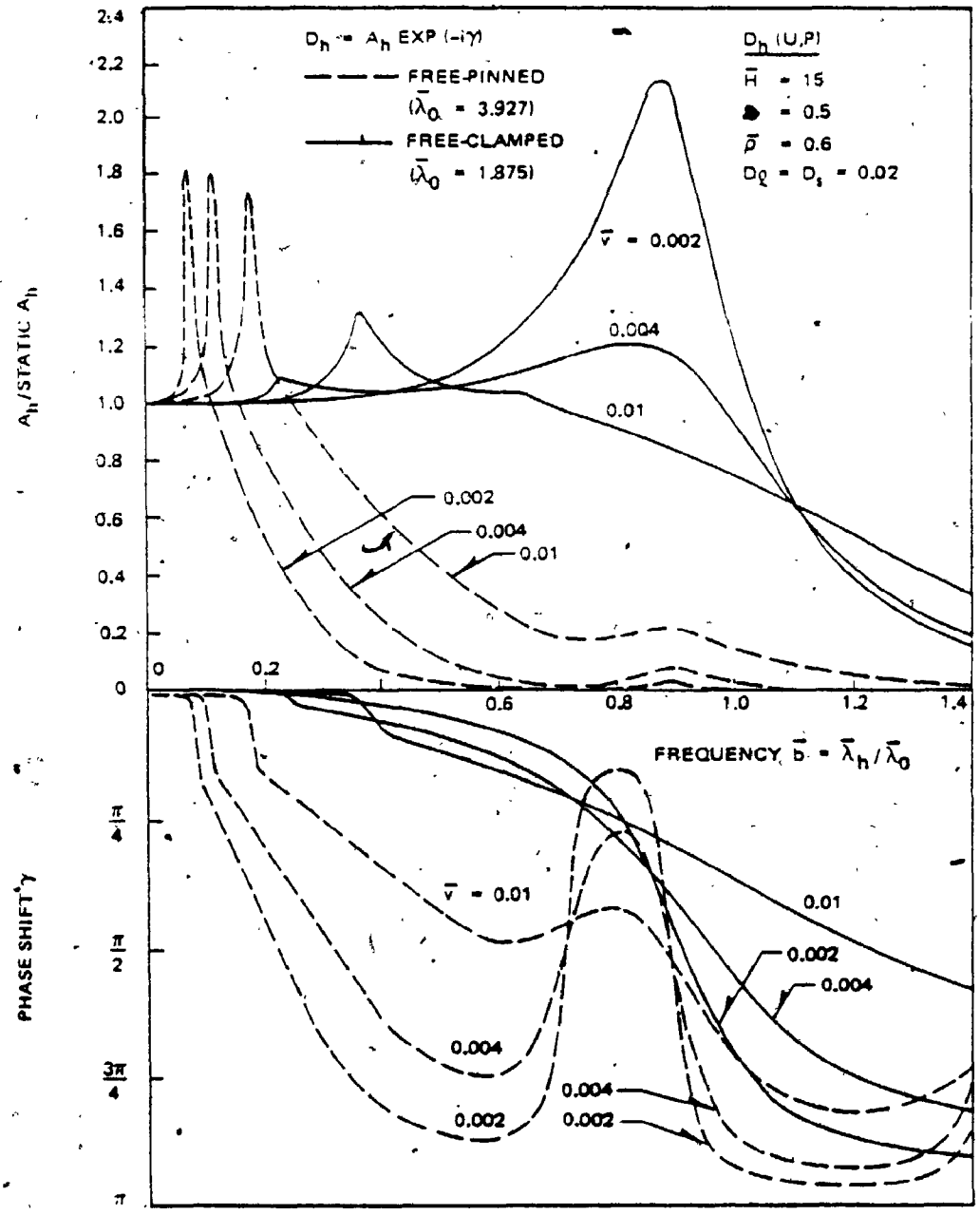

Fig. 4.2-16b. Variation of Displacement $D_h(U,P)$ with Frequency $\bar{b}$ for Various Wave Velocity Ratios ($\bar{H}$ = 15, Free Head)

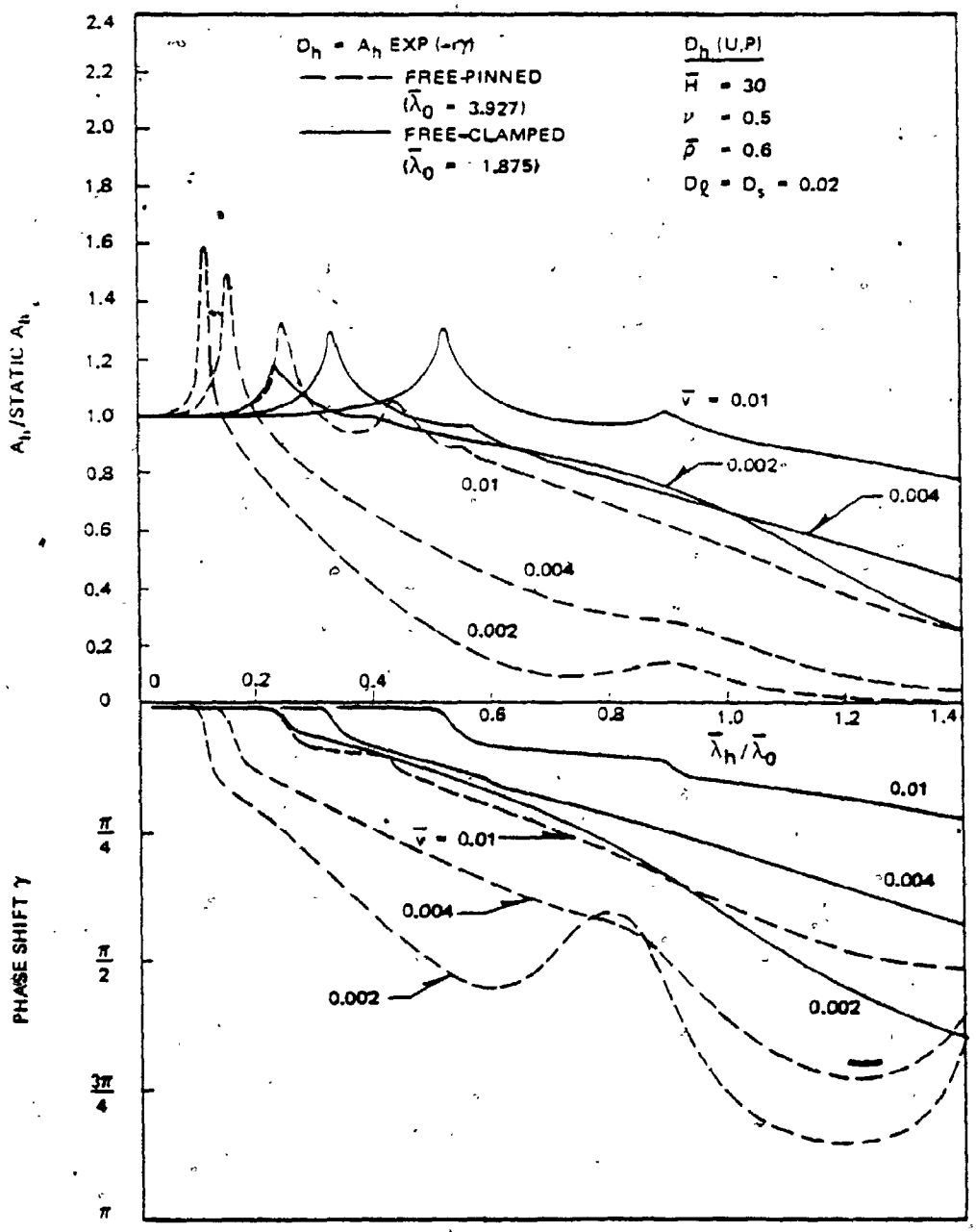

Fig. 4.2-16c. Variation of Displacement D_h (U,P) with Frequency $\bar{b}$ for Various Wave Velocity Ratios ($\bar{H}$ = 30, Free Head)

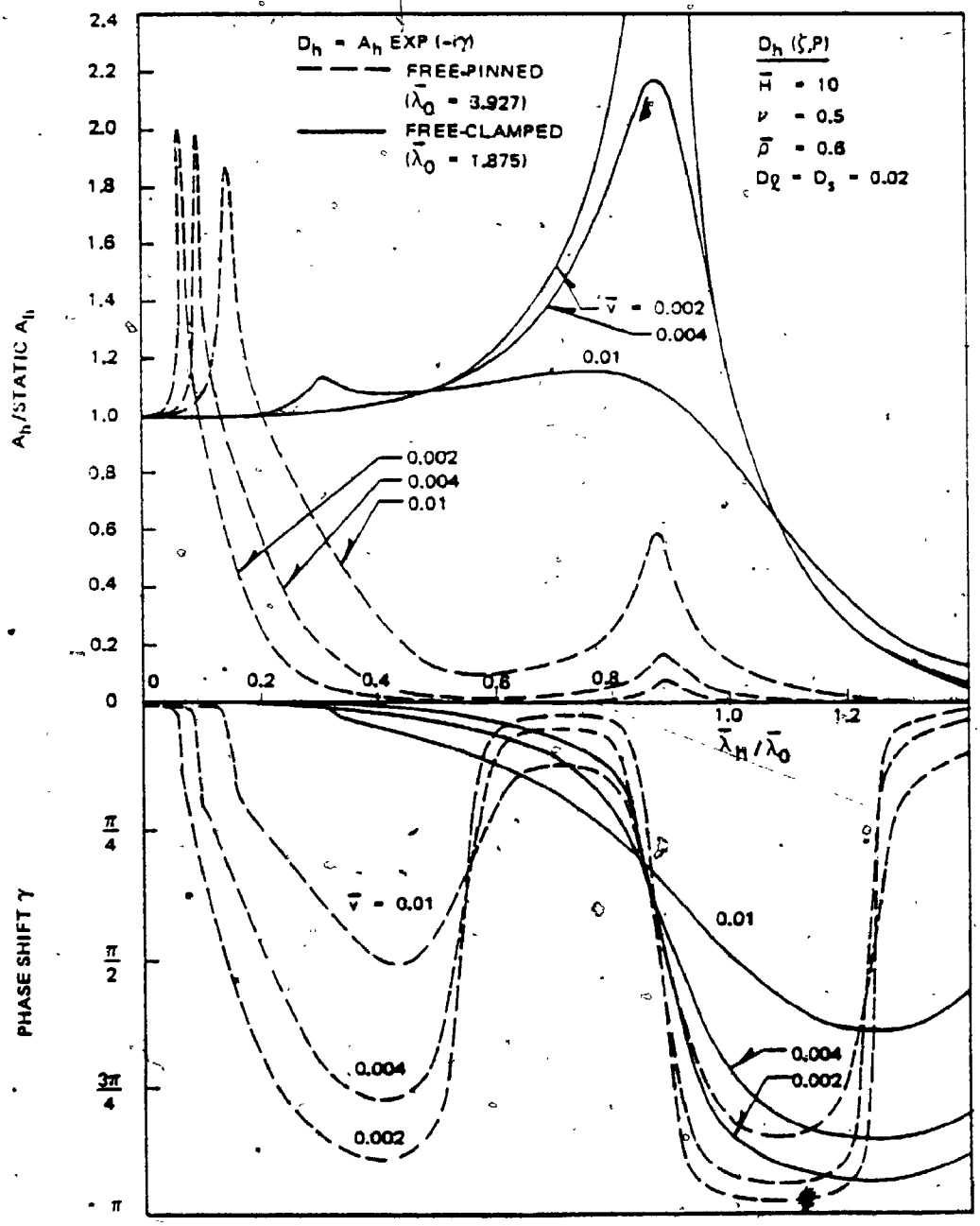

Fig. 4.2-16d. Variation of Displacement $D_h(\zeta,P)$ with Frequency $\bar{b}$ for Various Wave Velocity Ratios ($\bar{H}$ = 10, Free Head)

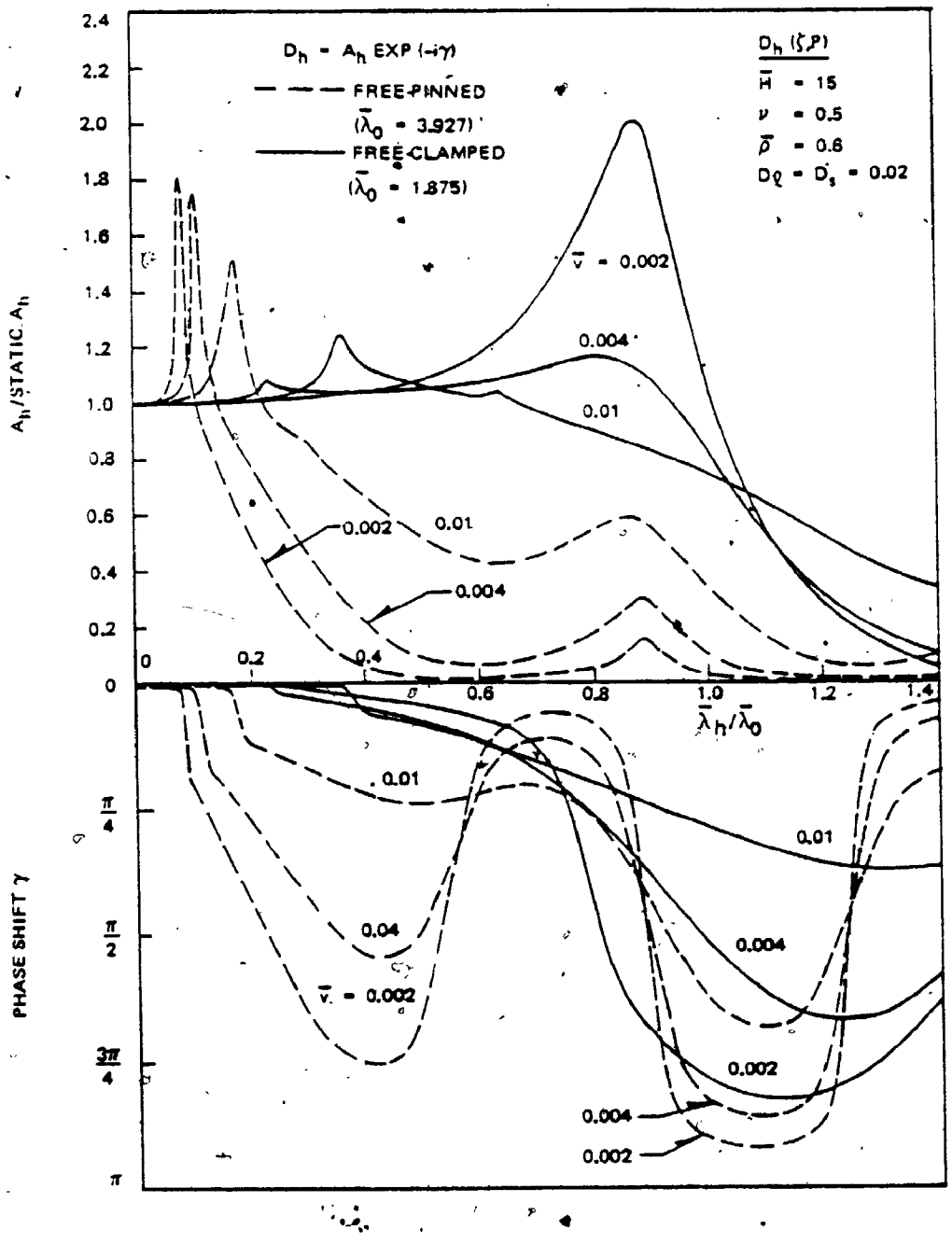

Fig. 4.2-16e. Variation of Displacement $D_h(\zeta,P)$ with Frequency $\bar{b}$ for Various Wave Velocity Ratios ($\bar{H}$ = 15, Free Head)

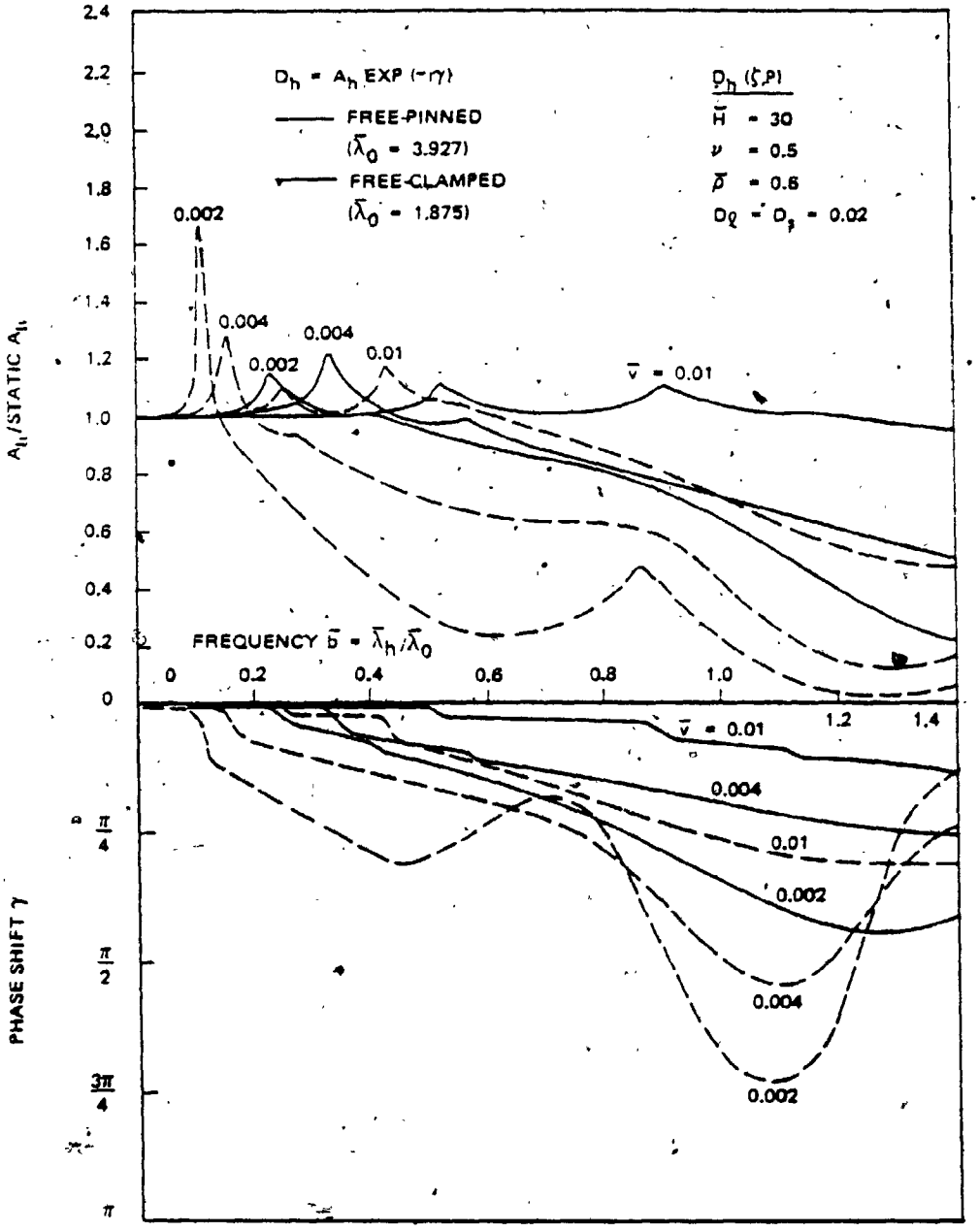

Fig. 4.2-16f. Variation of Displacement $D_h(\zeta,P)$ with Frequency $\bar{b}$ for Various Wave Velocity Ratios ($\bar{H}$ = 30, Free Head)

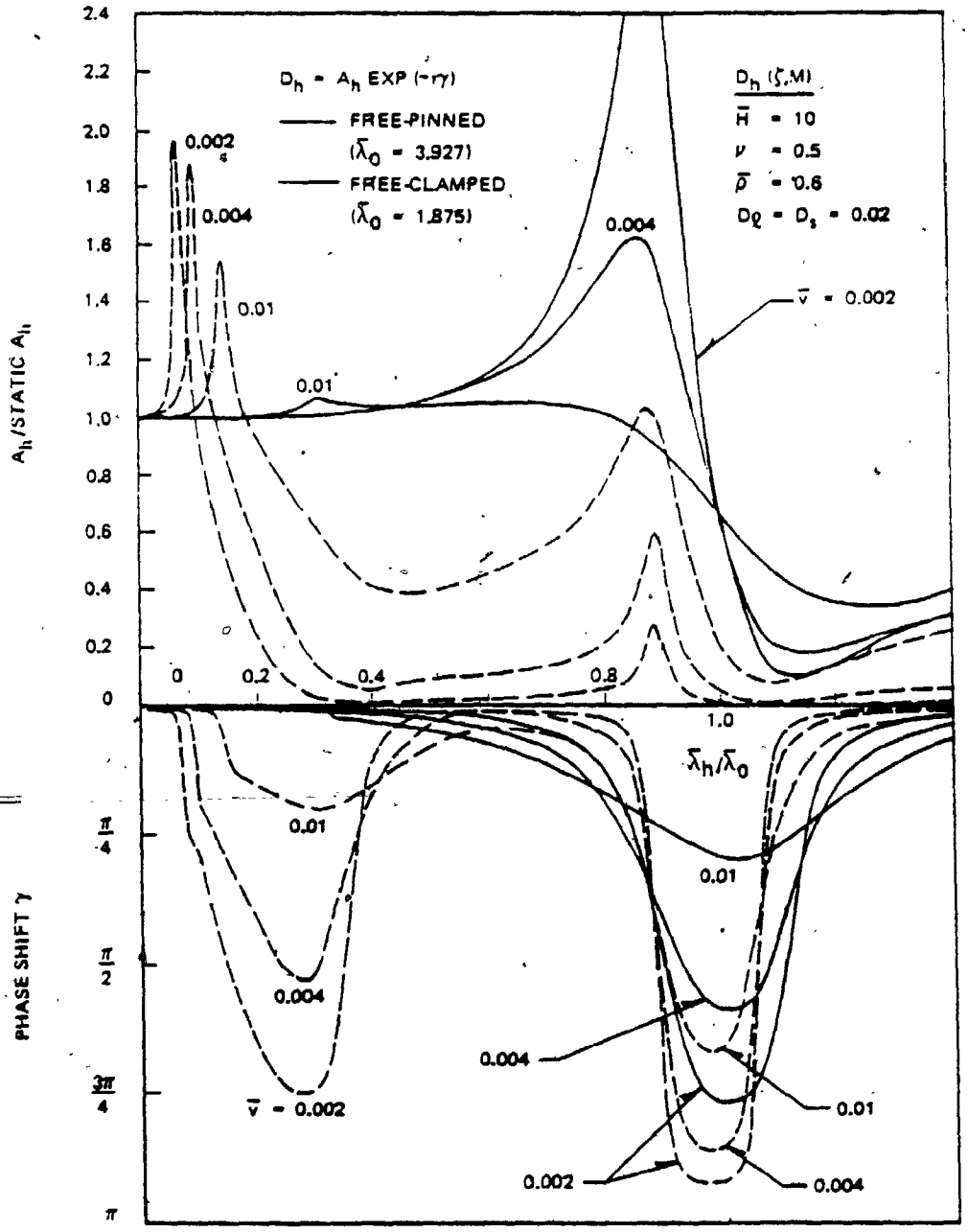

Fig. 4.2-16g. Variation of Displacement $\bar{D}_h(\zeta, M)$ with Frequency $\bar{b}$ for Various Wave Velocity Ratios ($\bar{H}$ = 10, Free Head)

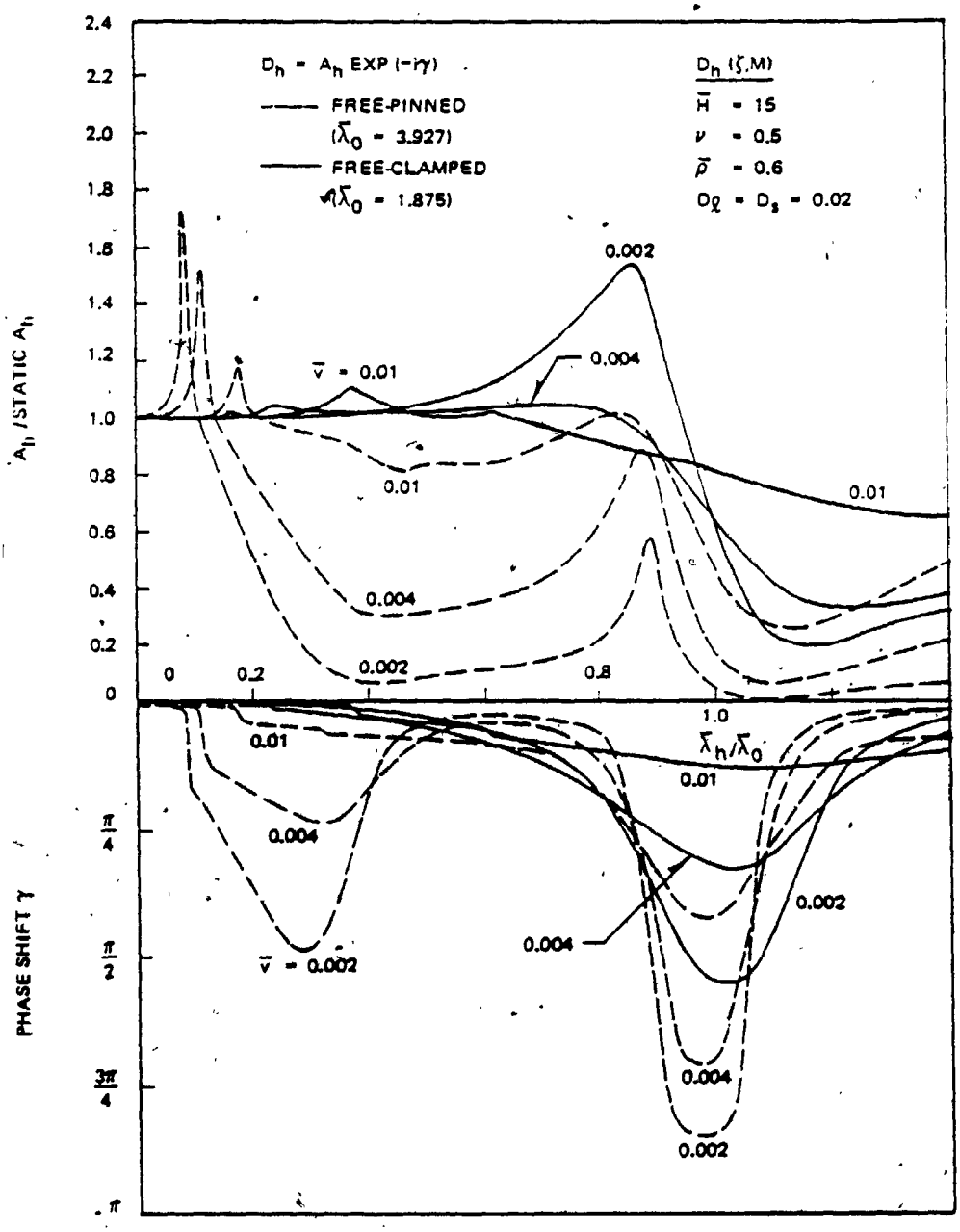

Fig. 4.2-16h. Variation of Displacement $D_h(\zeta,M)$ with Frequency $\bar{b}$ for Various Wave Velocity Ratios ($\bar{H}$ = 15, Free Head)

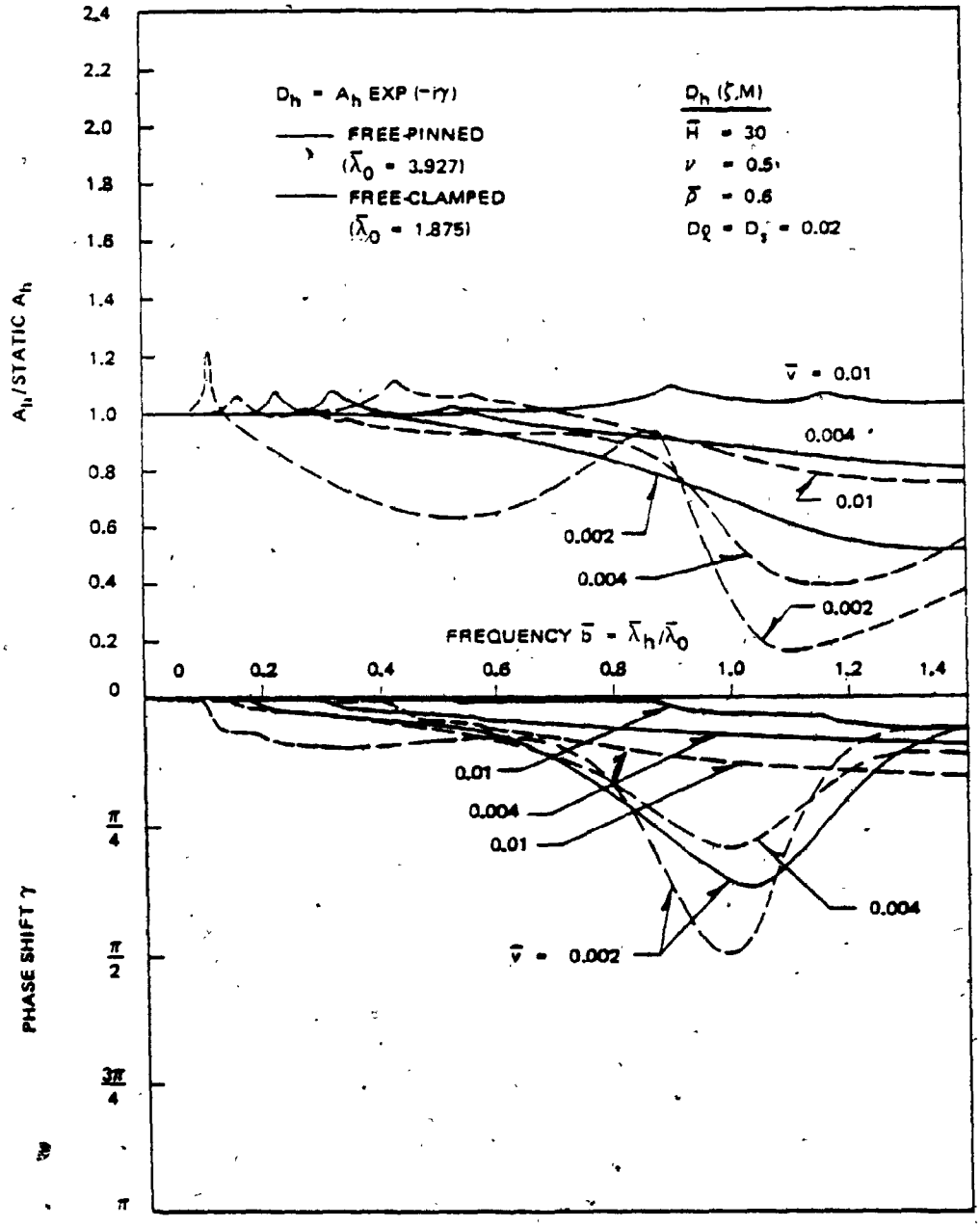

Fig. 4.2-161. Variation of Displacement $D_h(\zeta,M)$ with Frequency $\bar{b}$ for Various Wave Velocity Ratios ($\bar{H}$ = 30, Free Head)

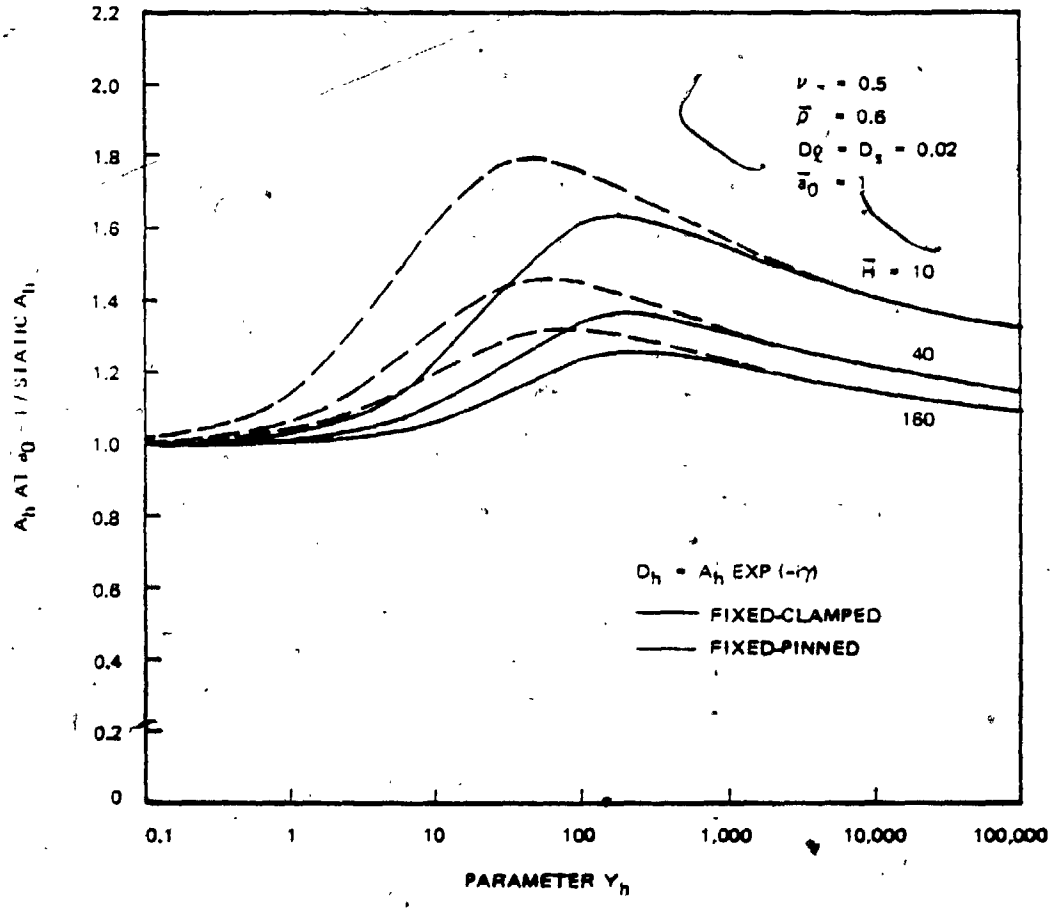

Fig. 4.2-17a. Variation of Amplification at the First Natural Frequency of Stratum with Parameter Y_h (Fixed Head)

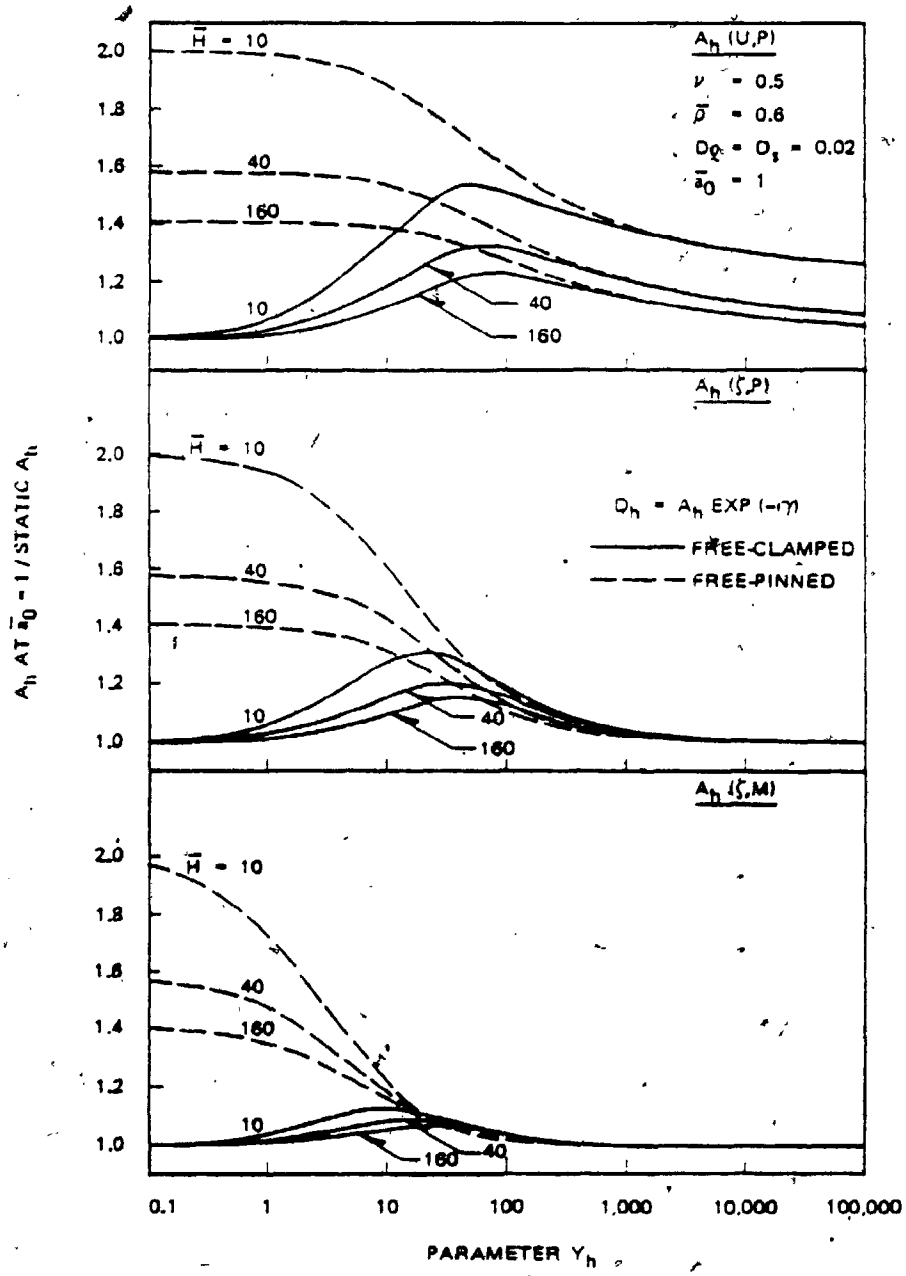

Fig. 4.2-17b. Variation of Amplification at the First Natural Frequency of Stratum with Parameter Y_h (Free Head)

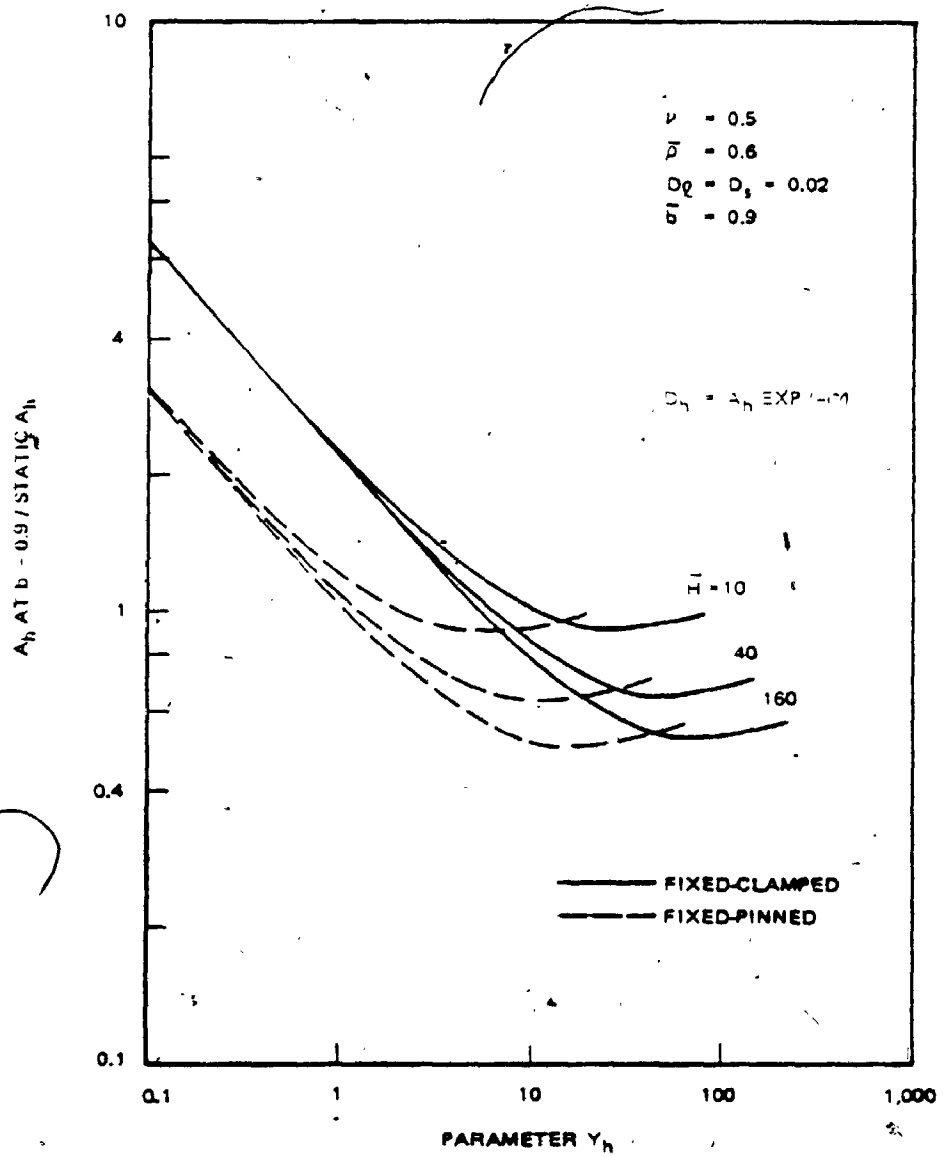

Fig. 4.2-18a. Variation of Amplification at $\bar{b}$ = 0.9 with Parameter Y_h (Fixed Head)

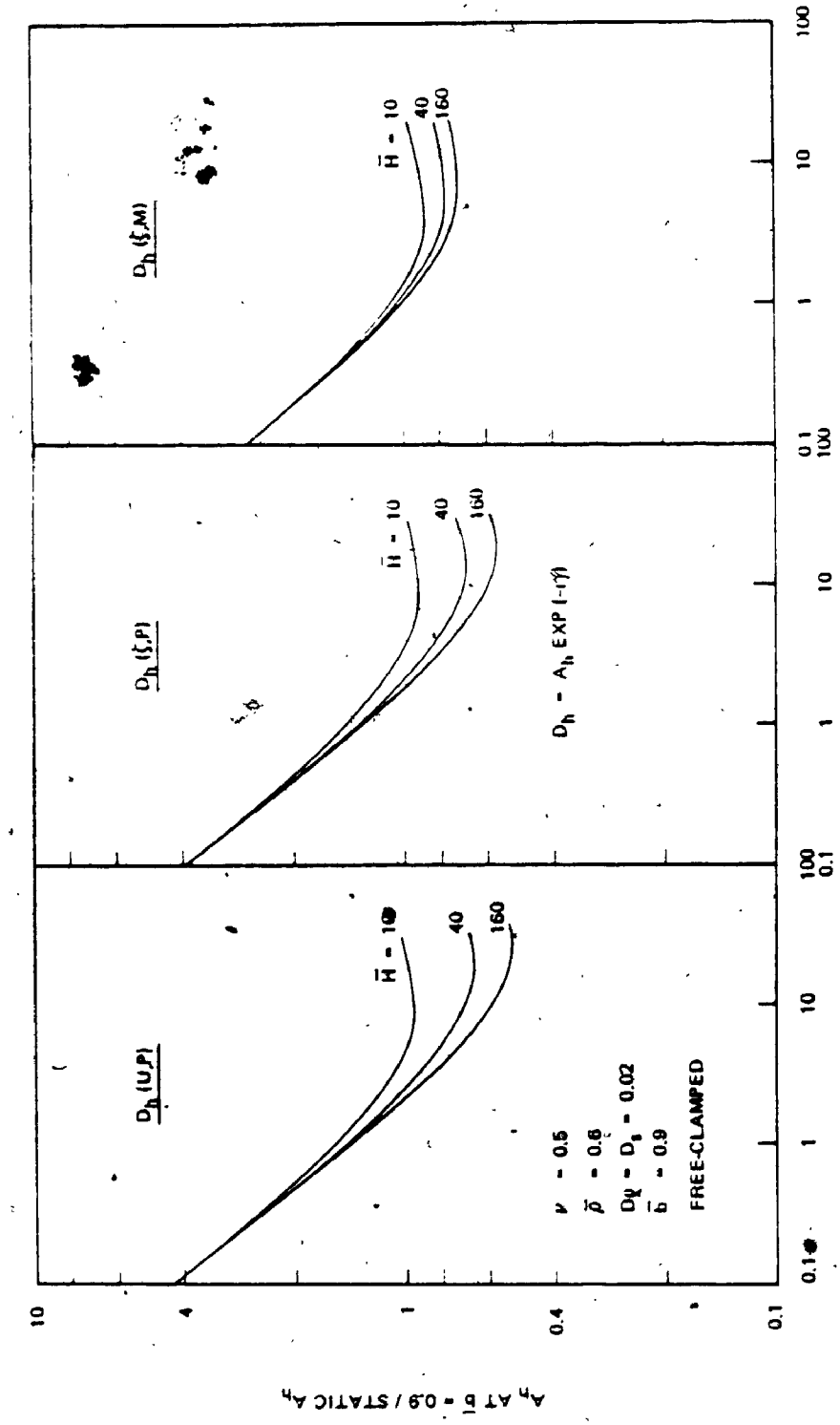

Fig. 4.2-18b. Variation of Amplification at $\bar{b}$ = 0.9 with Parameter Y_h (Free Head)

increase appears. Those trends in phase shift are also quite different from those of other piles observed in Figs. 4.2-15 and 4.2-16.

When the effect of the surrounding soil is very strong, the boundary condition at the pile tip does not affect the behavior of the pile. Therefore, under such condition, the displacements at the head of the clamped-tip pile are very little or no different from those of the pinned-tip pile. The strong soil effect further yields the condition that the relationship between the displacement $\bar{D}_h$ and the frequency a_0' is nearly or completely independent of slenderness of the pile at frequencies higher than the first resonant frequency of the stratum (Figs. 4.2-19).

The variation of Poisson's ratio affects the static displacement $\bar{D}_h$ as shown in Figs. 4.2-20. Trends similar to those in vertical vibration are seen in these figures. When dynamic loadings are applied to a pile under the weak soil effect, the amplitudes for two extreme Poisson's ratios vary with frequency from their statical values as shown in Fig. 4.2-21. In this figure, the peak amplitudes appear at higher frequencies $\bar{b}$ for $\nu = 0$ than for $\nu = 0.5$ ($\bar{b} \approx 1$ for $\nu = 0$ and $\bar{b} \approx 0.9$ for $\nu = 0.5$); the peak amplitude in vertical vibration appears at a nearly constant value of $\bar{b}$ regardless of the value of Poisson's ratio. As can be seen in Figs. 4.2-21 and 4.2-22, the peak amplification under the weak soil effect is higher for $\nu = 0$ than for $\nu = 0.5$. For the strong soil effect, the amplitude varies with frequency a_0' as shown in Figs. 4.2-23. These figures indicate that the phase shift does not depend on Poisson's ratio but the amplitude does; both amplitude and phase shift are nearly independent of Poisson's ratio in vertical vibration. The soil effect in the dynamic case grows with Y_h slightly

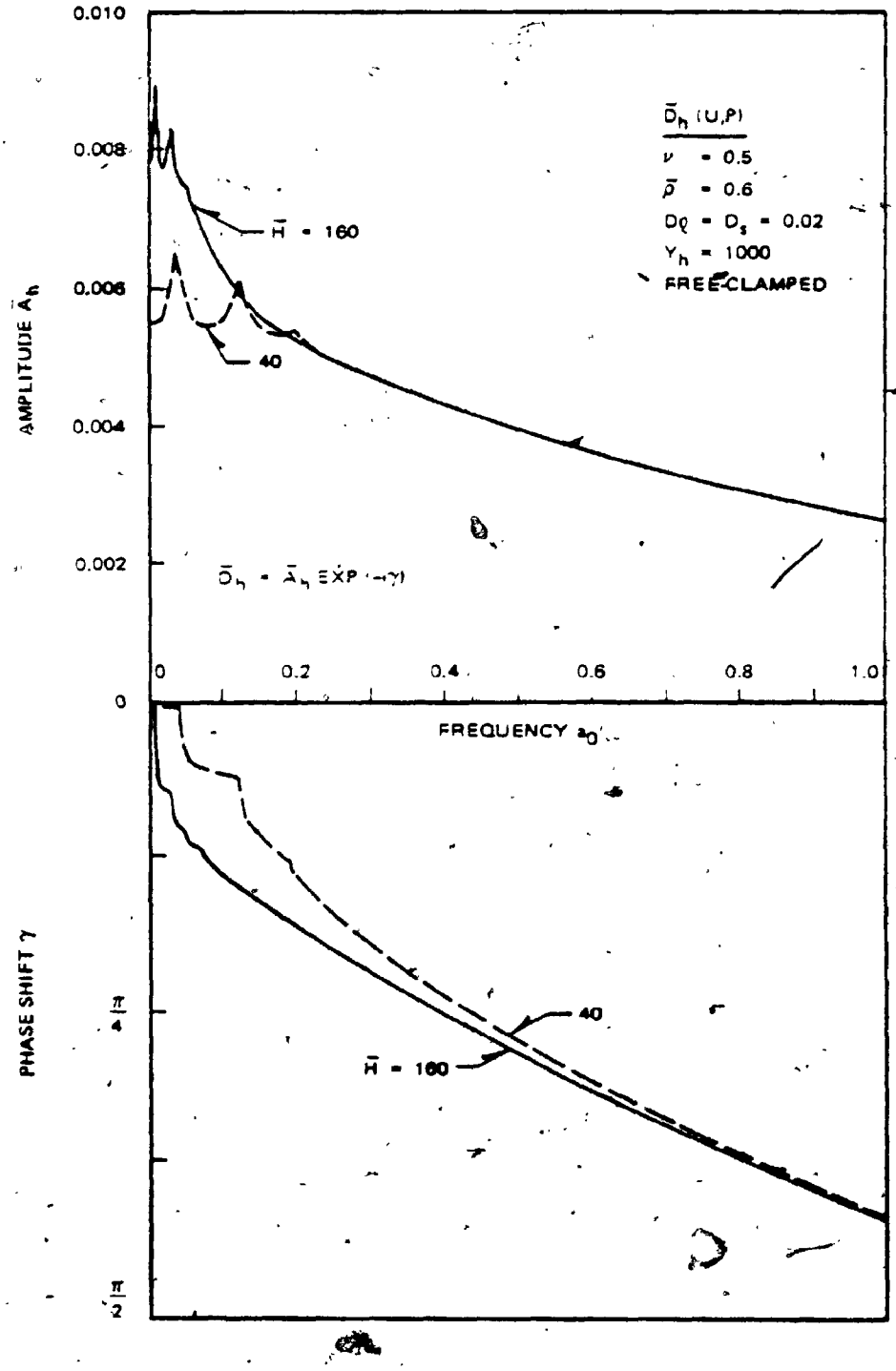

Fig. 4.2-19a. Variation of Displacement $\bar{D}_h(U,P)$ with Frequency a_0'

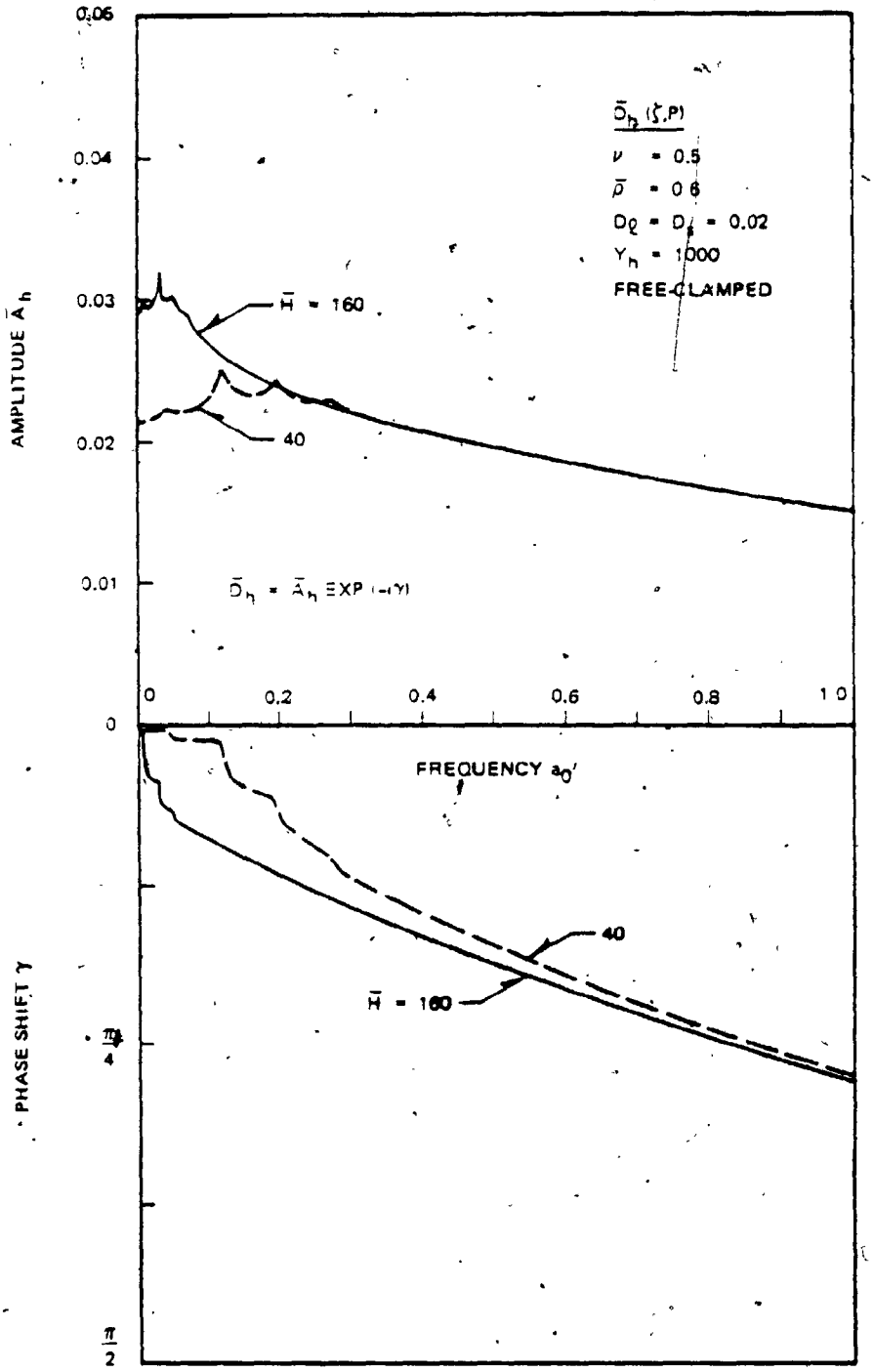

Fig. 4.2-19b. Variation of Displacement $\bar{D}_h(\zeta,P)$ with Frequency a_0'

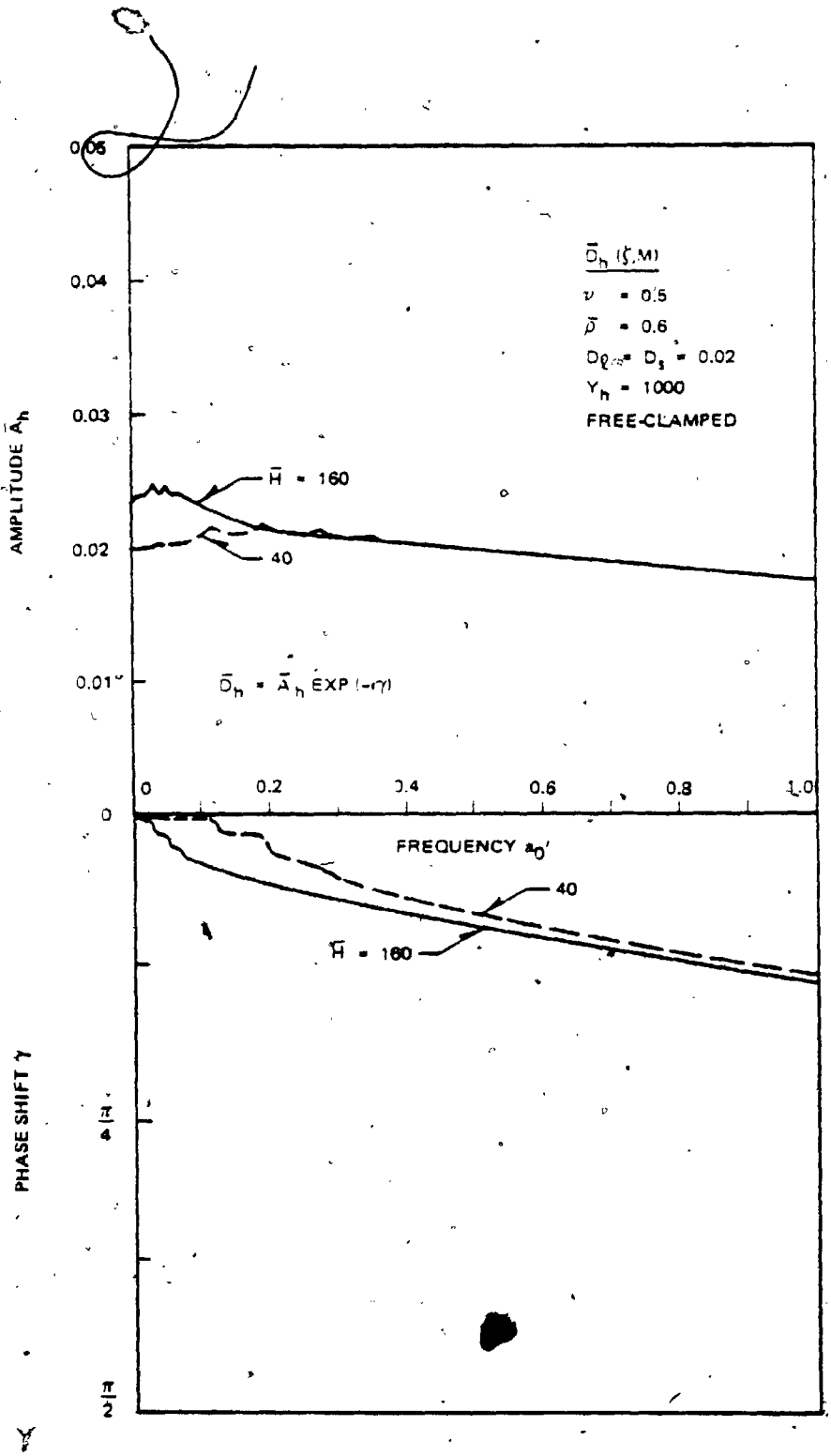

Fig. 4.2-19c. Variation of Displacement $\bar{D}_h(\zeta,M)$ with Frequency a_0'

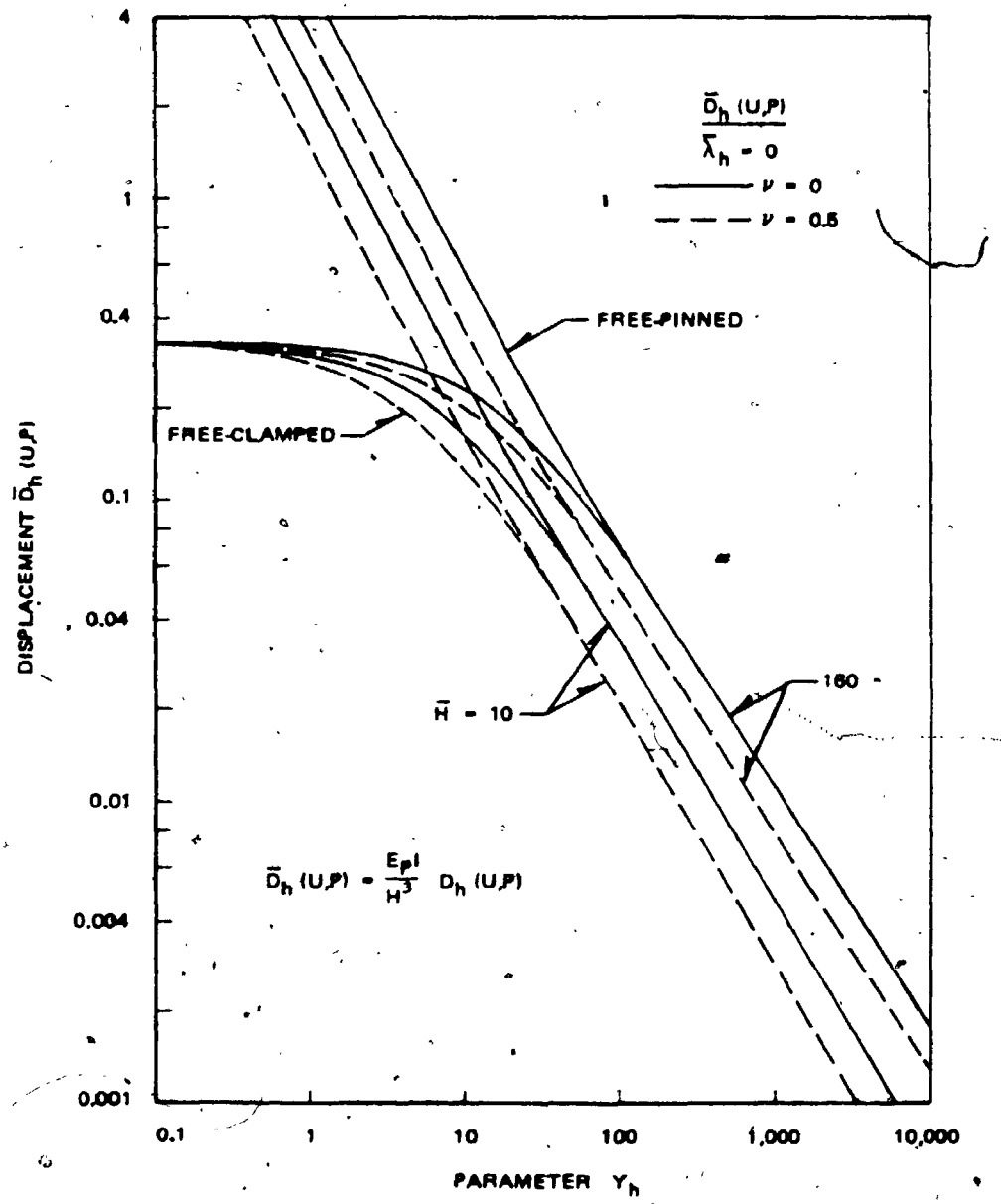

Fig. 4.2-20a. Variation of Static Displacement $\bar{D}_h(U,P)$ with Parameter Y_h for Various Poisson's Ratios

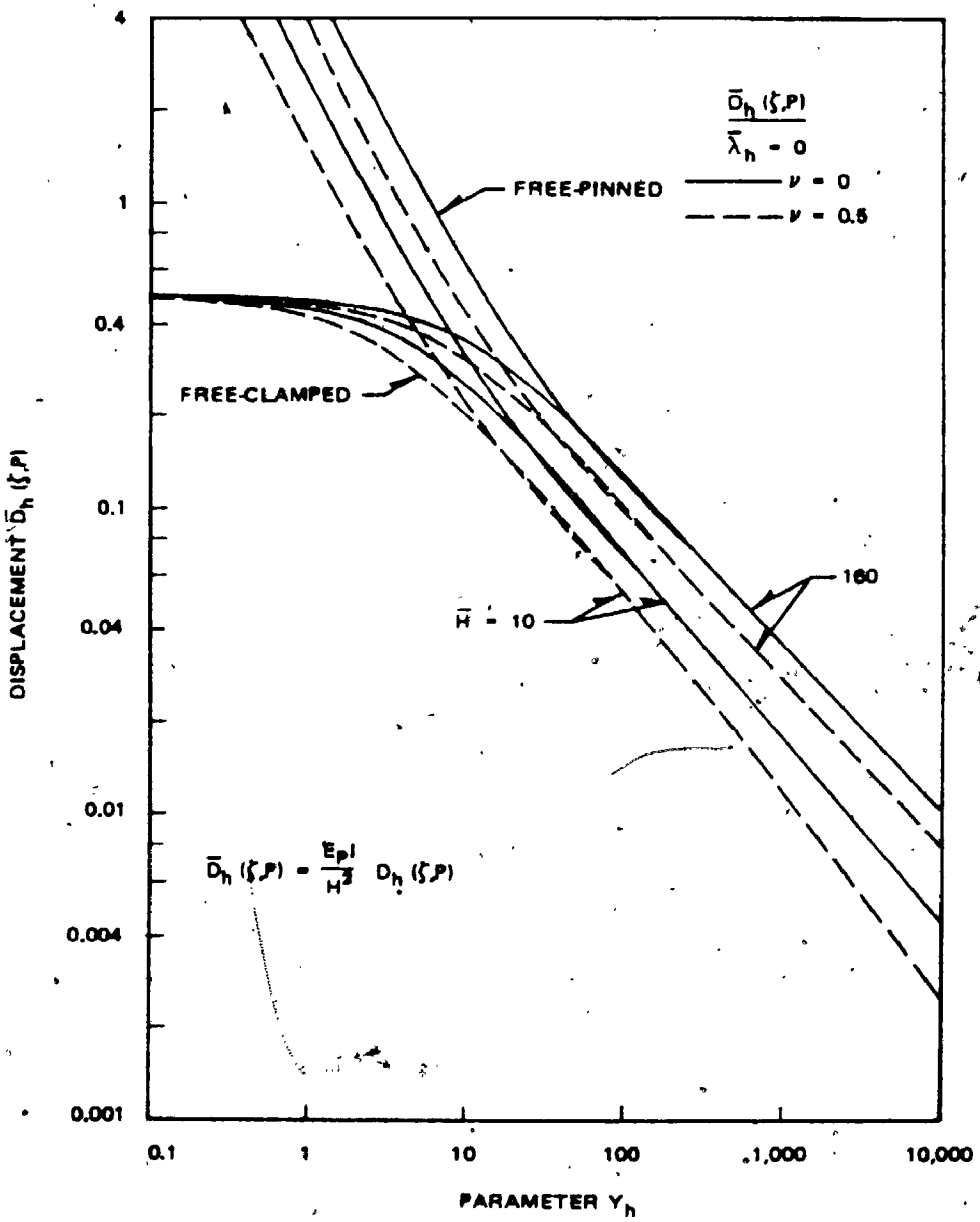

Fig. 4.2-20b. Variation of Static Displacement $\bar{D}_h(\zeta,P)$ with Parameter Y_h for Various Poisson's Ratios

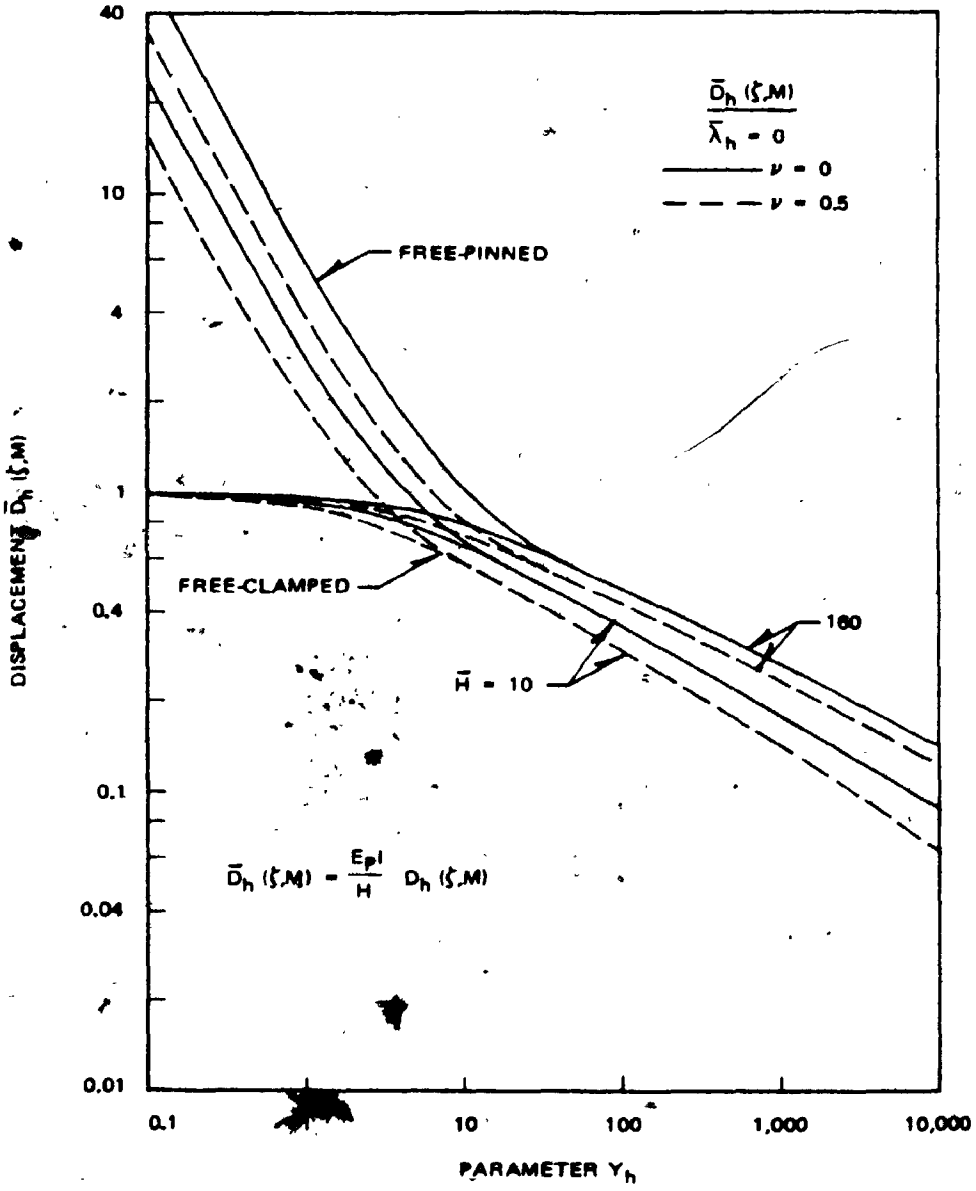

Fig. 4.2-20c. Variation of Static Displacement $\bar{D}_h(\zeta,M)$ with Parameter Y_h for Various Poisson's Ratios

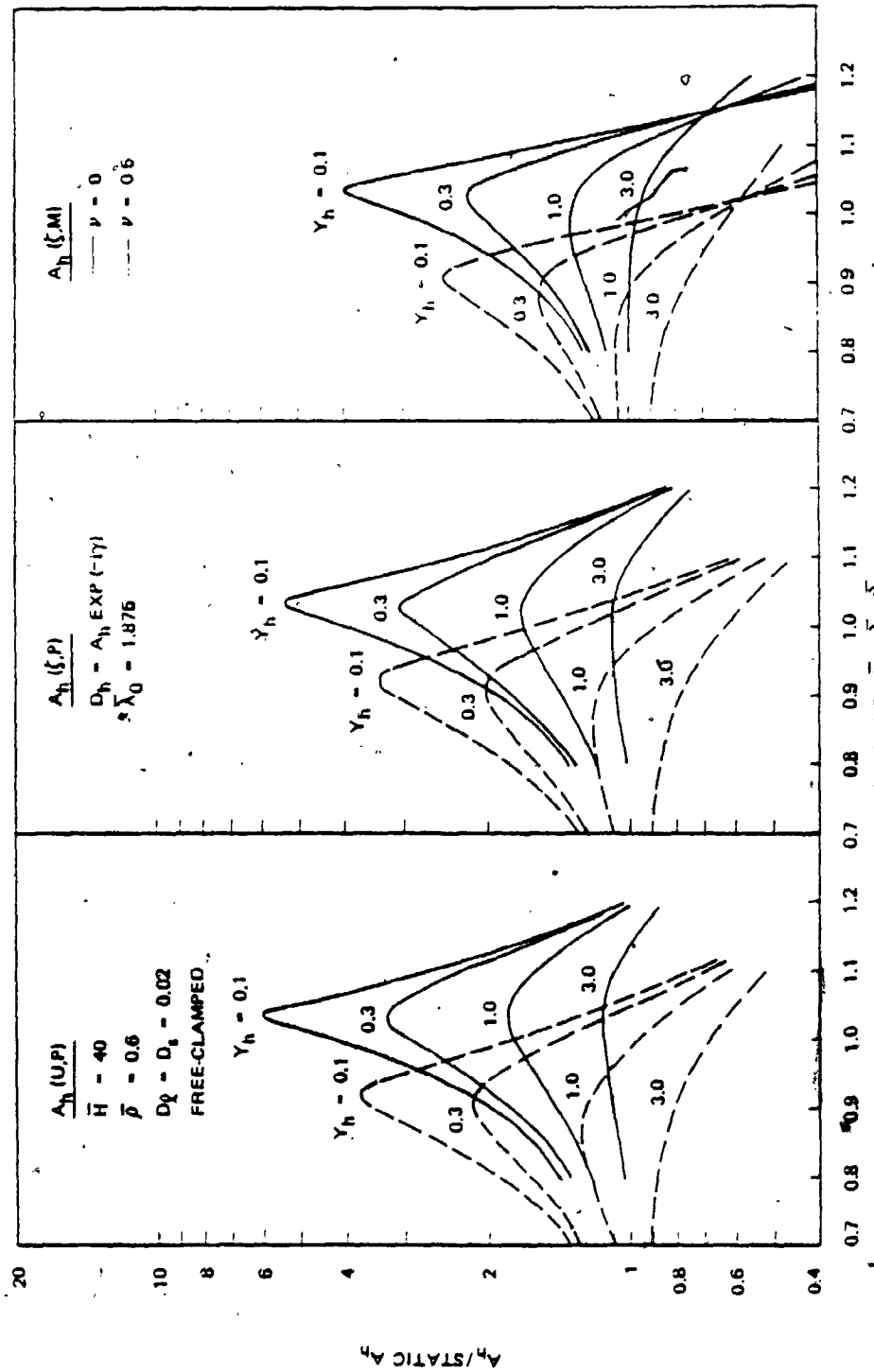

Fig. 4.2-21. Variation of Amplification with Frequency $\bar{b}$ for Various Poisson's Ratios

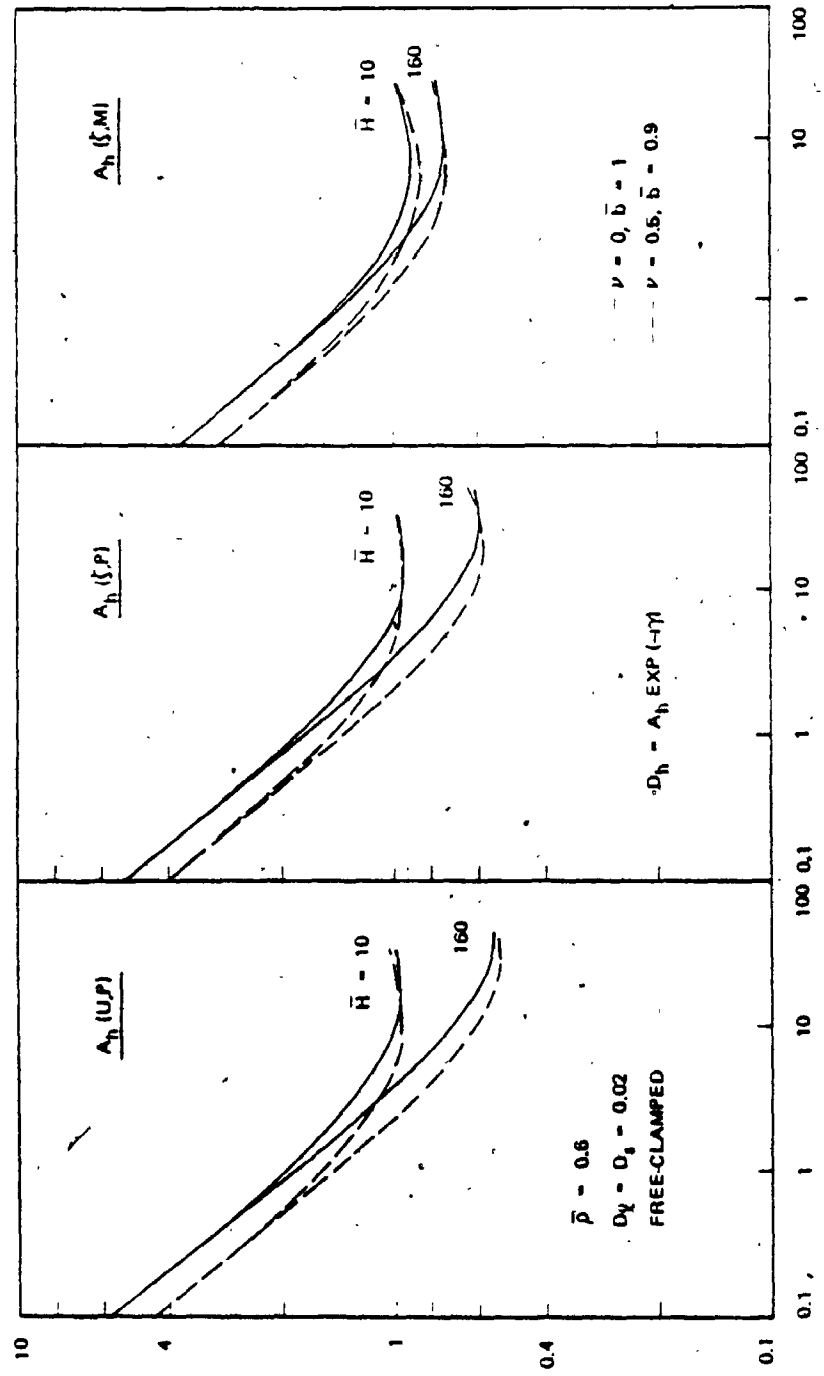

Fig. 4.2-22. Variation of Amplification Around Resonance of the System with Parameter Y_h for Various Poisson's Ratios

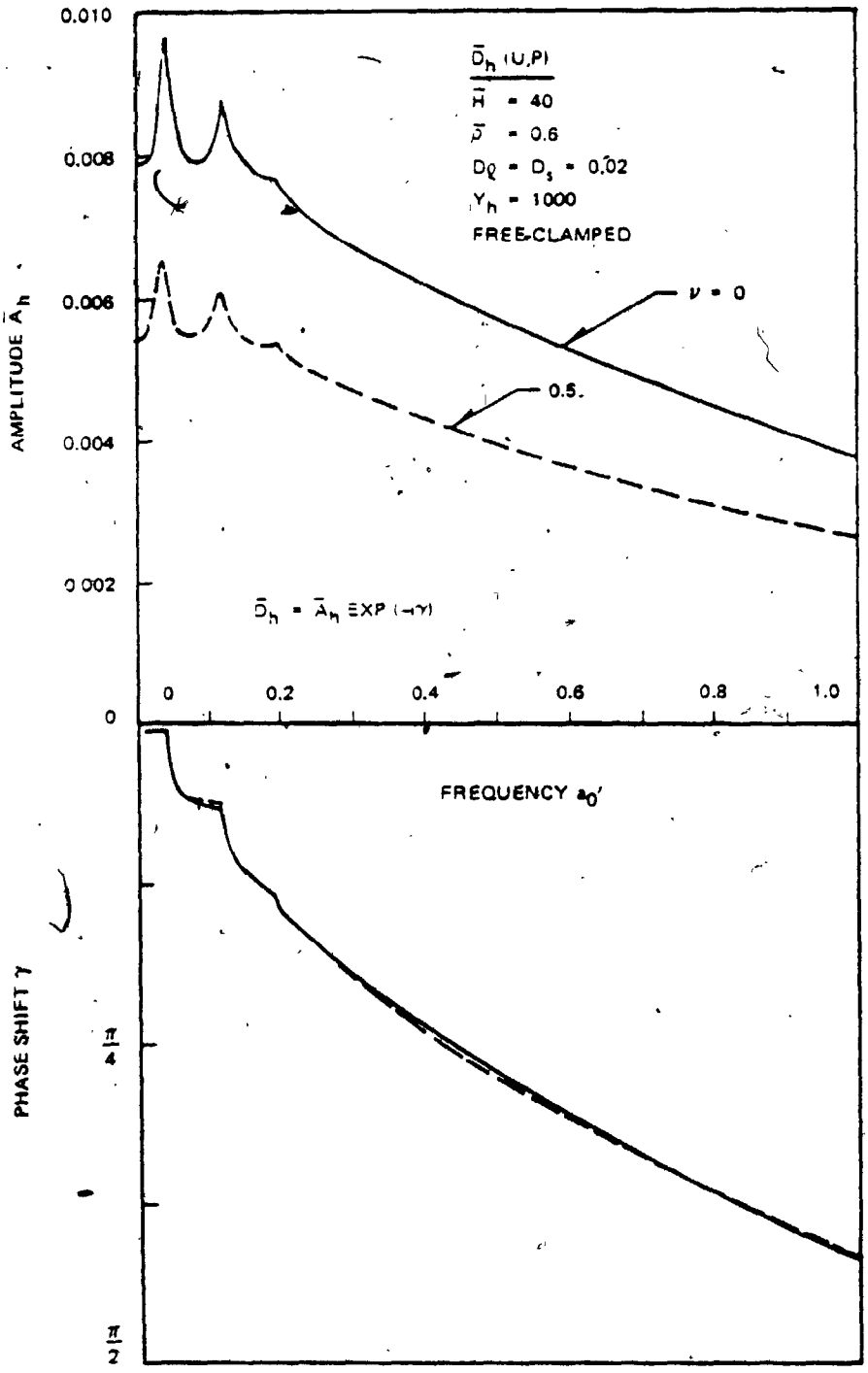

Fig. 4.2-23a. Variation of Displacement $\bar{D}_h(U,P)$ with Frequency a_0' for Various Poisson's Ratios

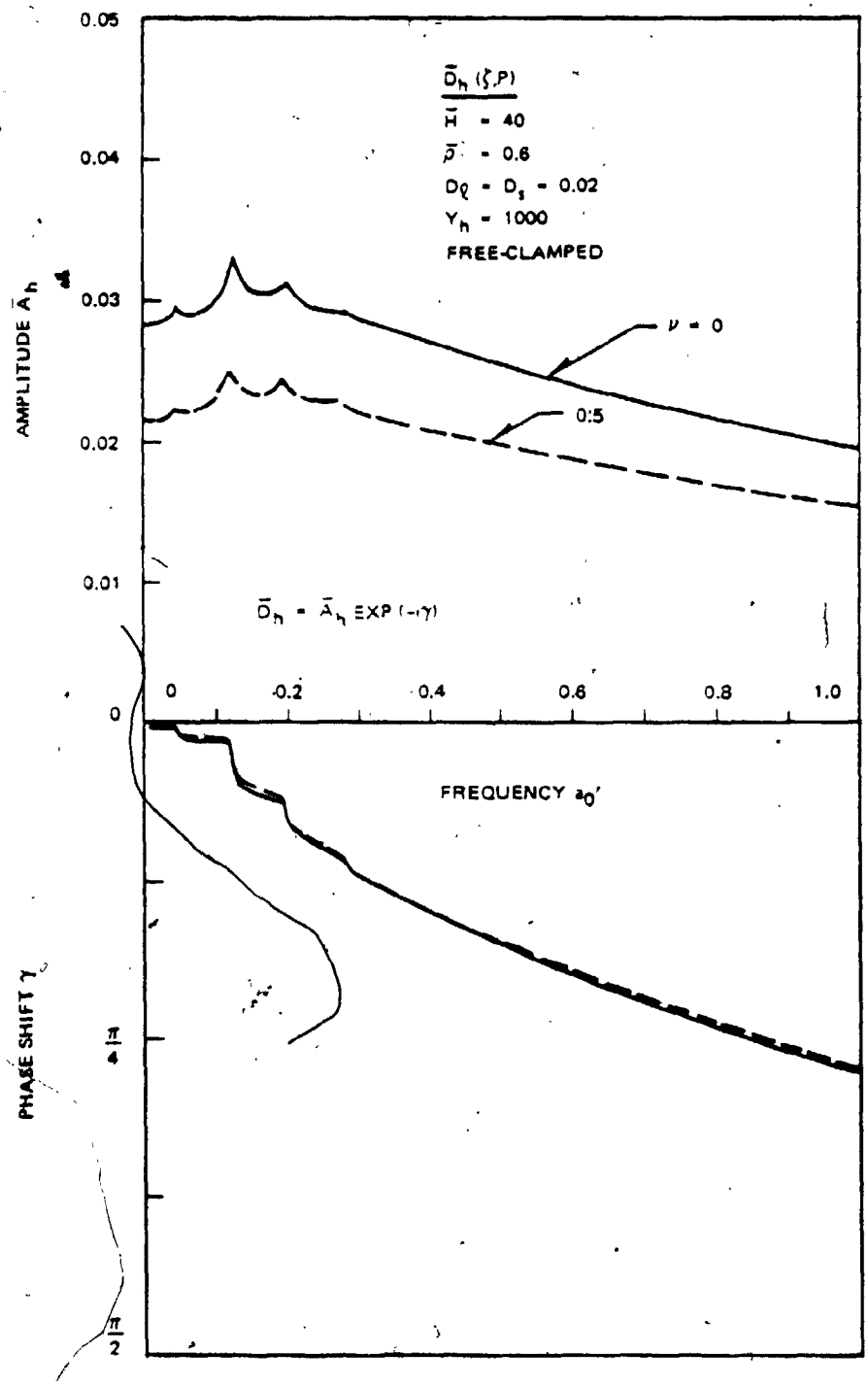

Fig. 4.2-23b. Variation of Displacement $\bar{D}_h(\zeta,P)$ with Frequency a_0' for Various Poisson's Ratios

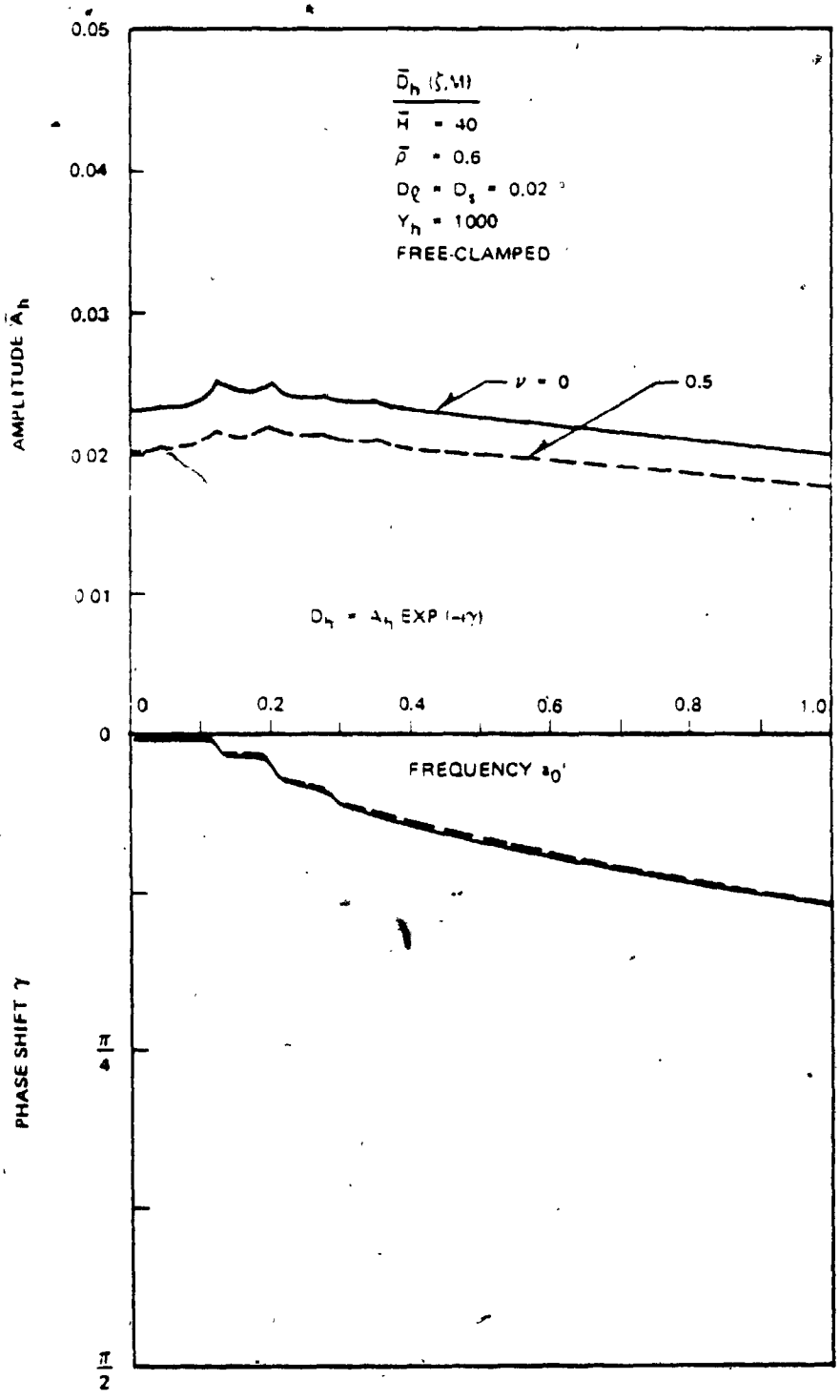

Fig. 4.2-23c. Variation of Displacement $\bar{D}_h(\zeta,M)$ with Frequency a_0' for Various Poisson's Ratios

more rapidly for $\nu = 0.5$ than for $\nu = 0$ as shown in Figs. 4.2-22 and 4.2-24.

The variation of mass ratios affects the displacements of the pile. Under the weak soil effect, the higher mass ratio yields the lower resonant frequency of the soil-pile system (Fig. 4.2-25) and the lower resonant amplifications (Figs. 4.2-25 and 4.2-26). Contrary to the above trend in the resonant frequency, this frequency in vertical vibration is fairly independent of the mass ratio. Under the strong soil effect, the variation of the mass ratio affects the relationship between $\bar{D}_h$ and a_0' as shown in Figs. 4.2-27; the trend follows that in vertical vibration. The variation of the mass ratio ($0.3 \leq \bar{\rho} \leq 1.2$) does not seem to affect very much the relationship between Y_h and the degree of soil effect (Figs. 4.2-26 and 4.2-28).

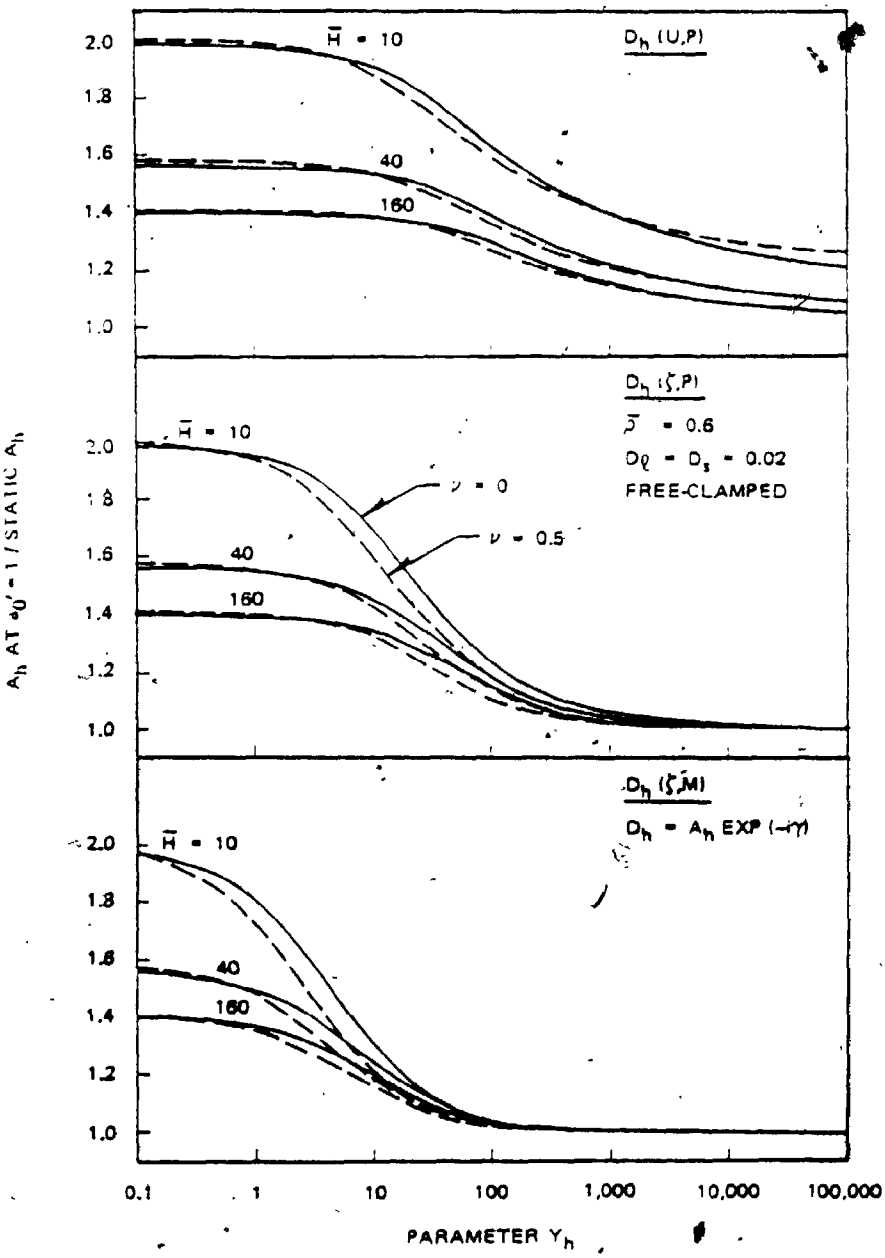

Fig. 4.2-24. Variation of Amplification at the First Natural Frequency of Stratum with Parameter Y_h for Various Poisson's Ratios

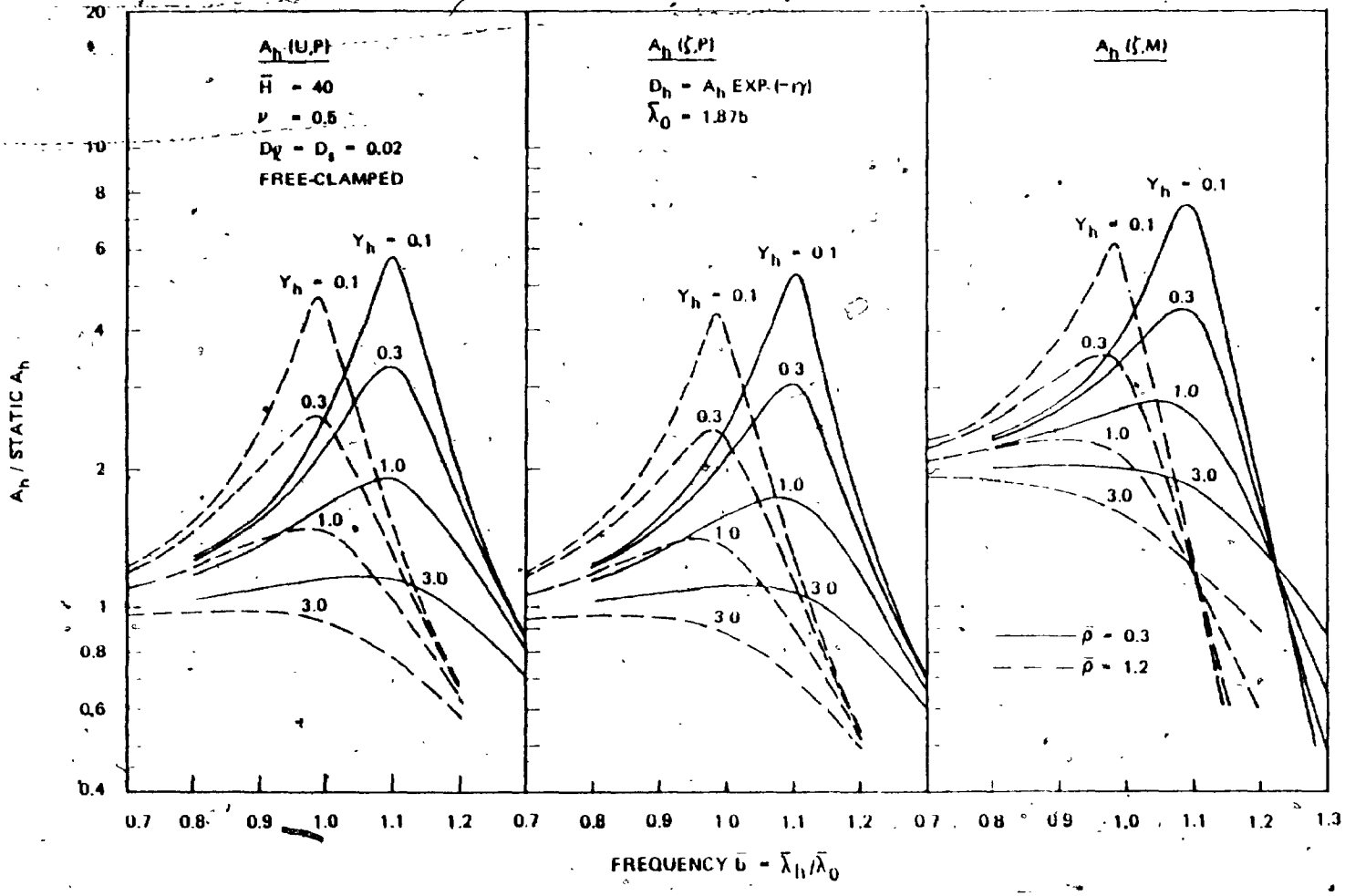

Fig. 4.2-25. Variation of Amplification with Frequency $\bar{b}$ for Various Mass Ratios

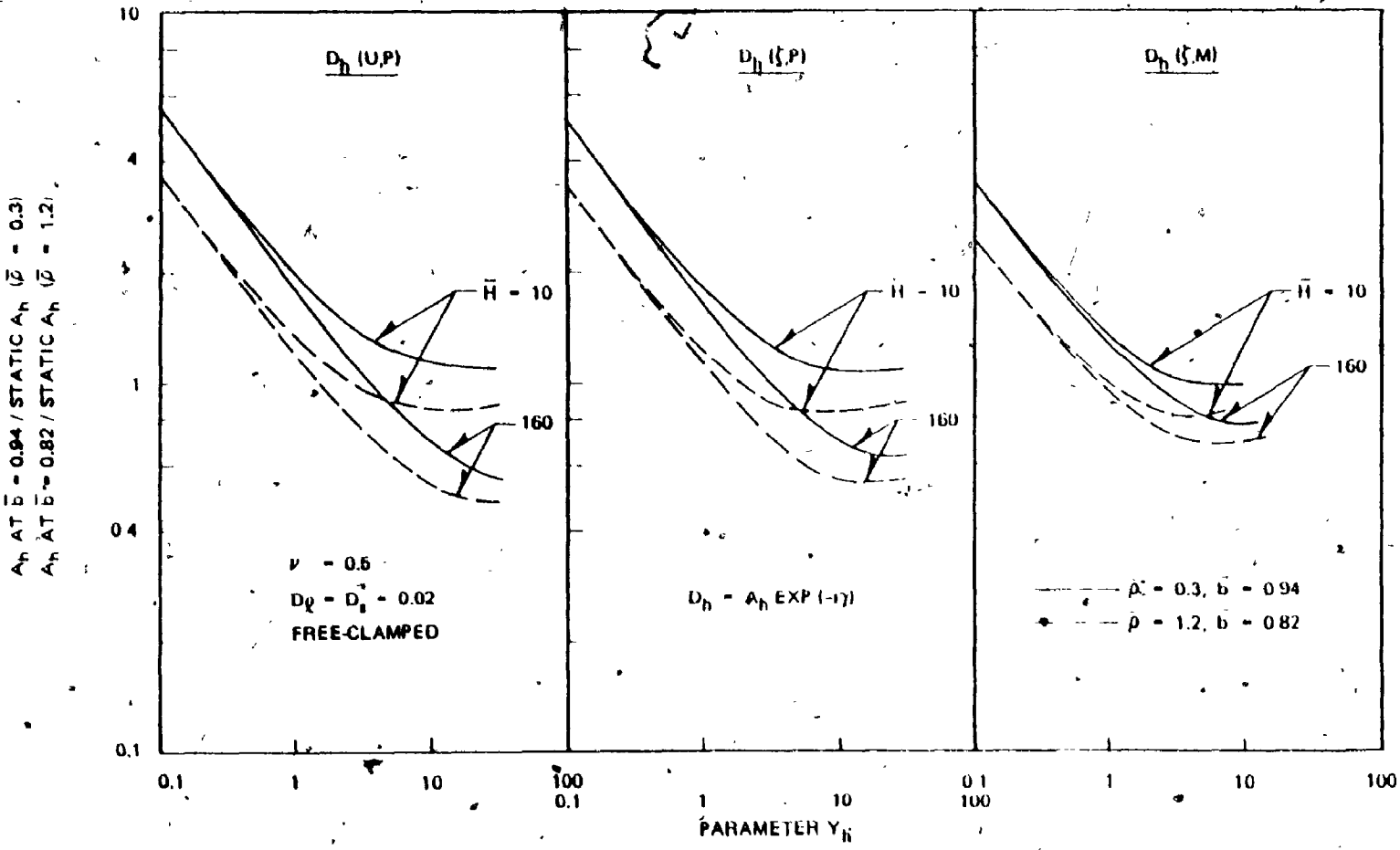

Fig. 4.2-26. Variation of Amplification Around Resonance of the System with Parameter Y_h for Various Mass Ratios

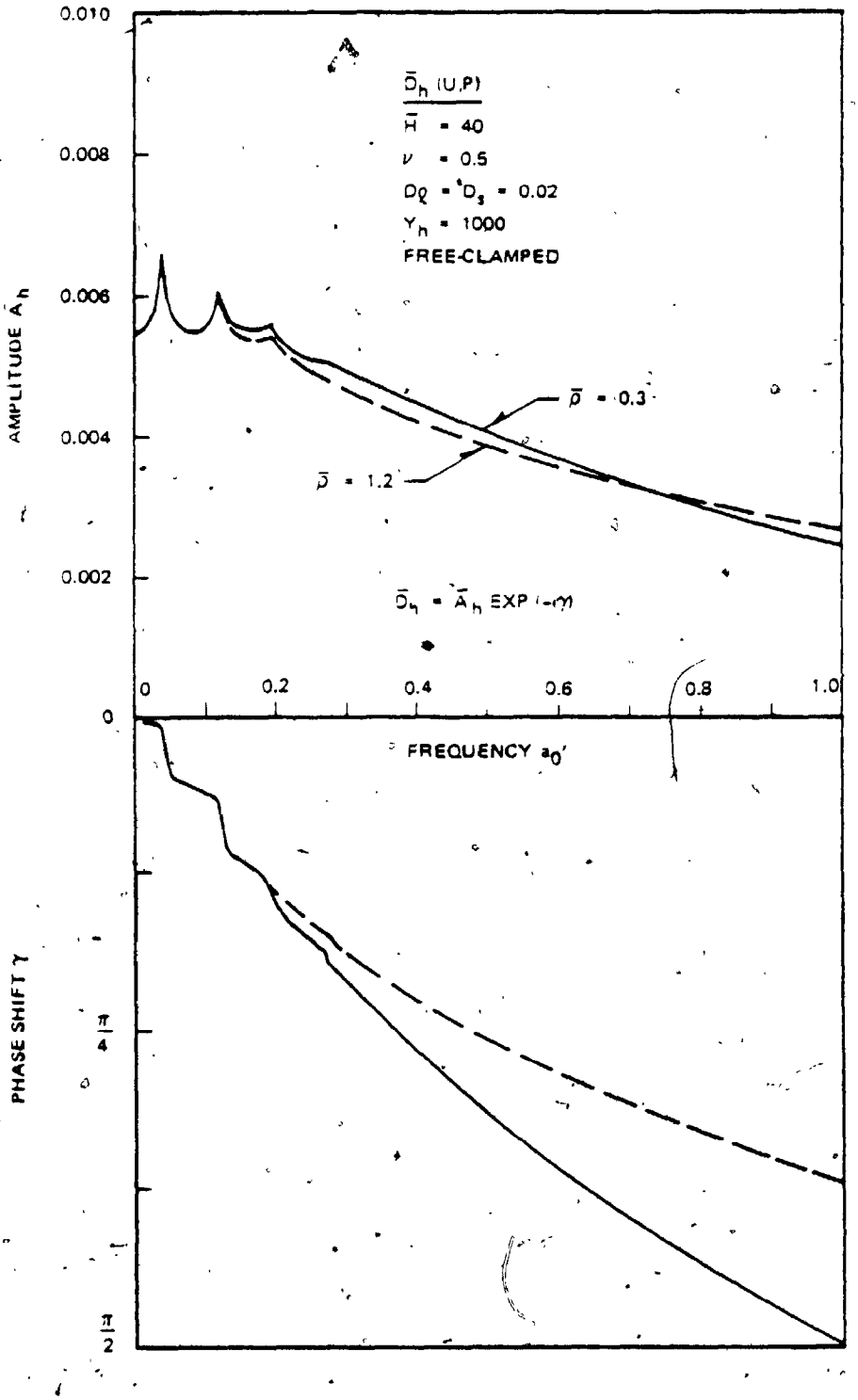

Fig. 4.2-27a. Variation of Displacement $\bar{D}_h(U,P)$ with Frequency a_0' for Various Mass Ratios

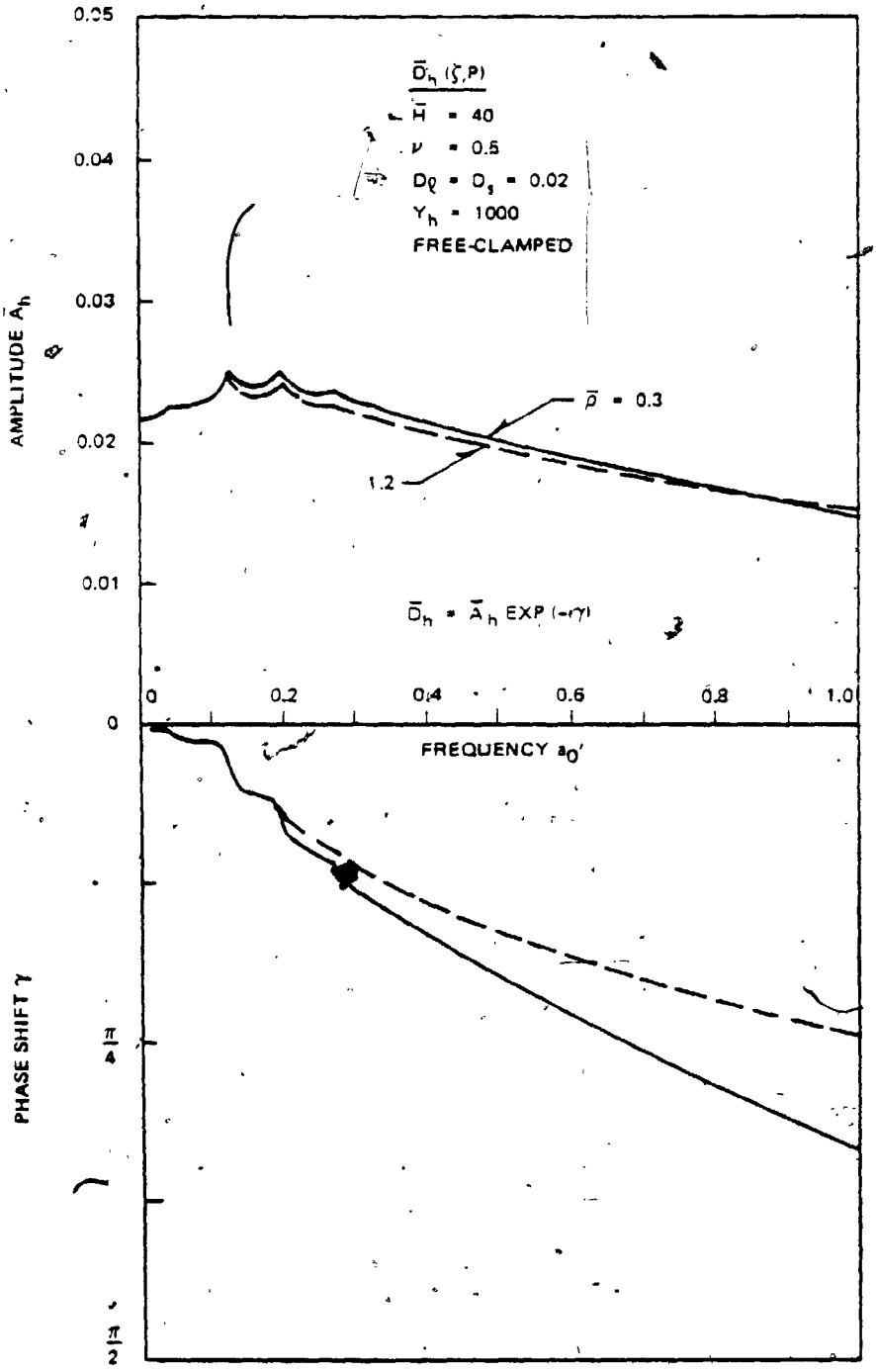

Fig. 4.2-27b. Variation of Displacement $\bar{D}_h(\zeta,P)$ with Frequency a_0' for Various Mass Ratios

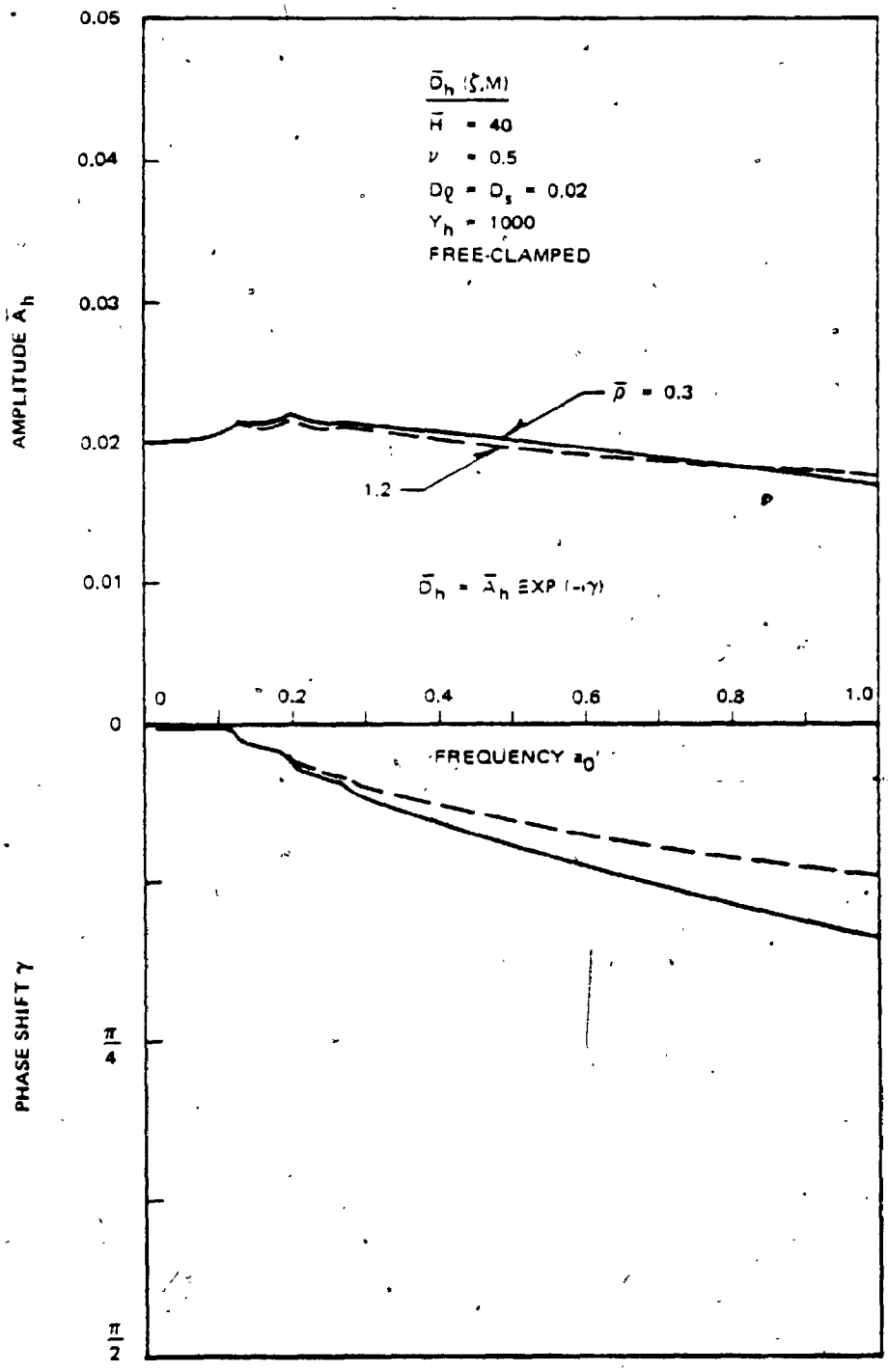

Fig. 4.2-27c. Variation of Displacement $\bar{D}_h(\zeta,M)$ with Frequency a_0' for Various Mass Ratios

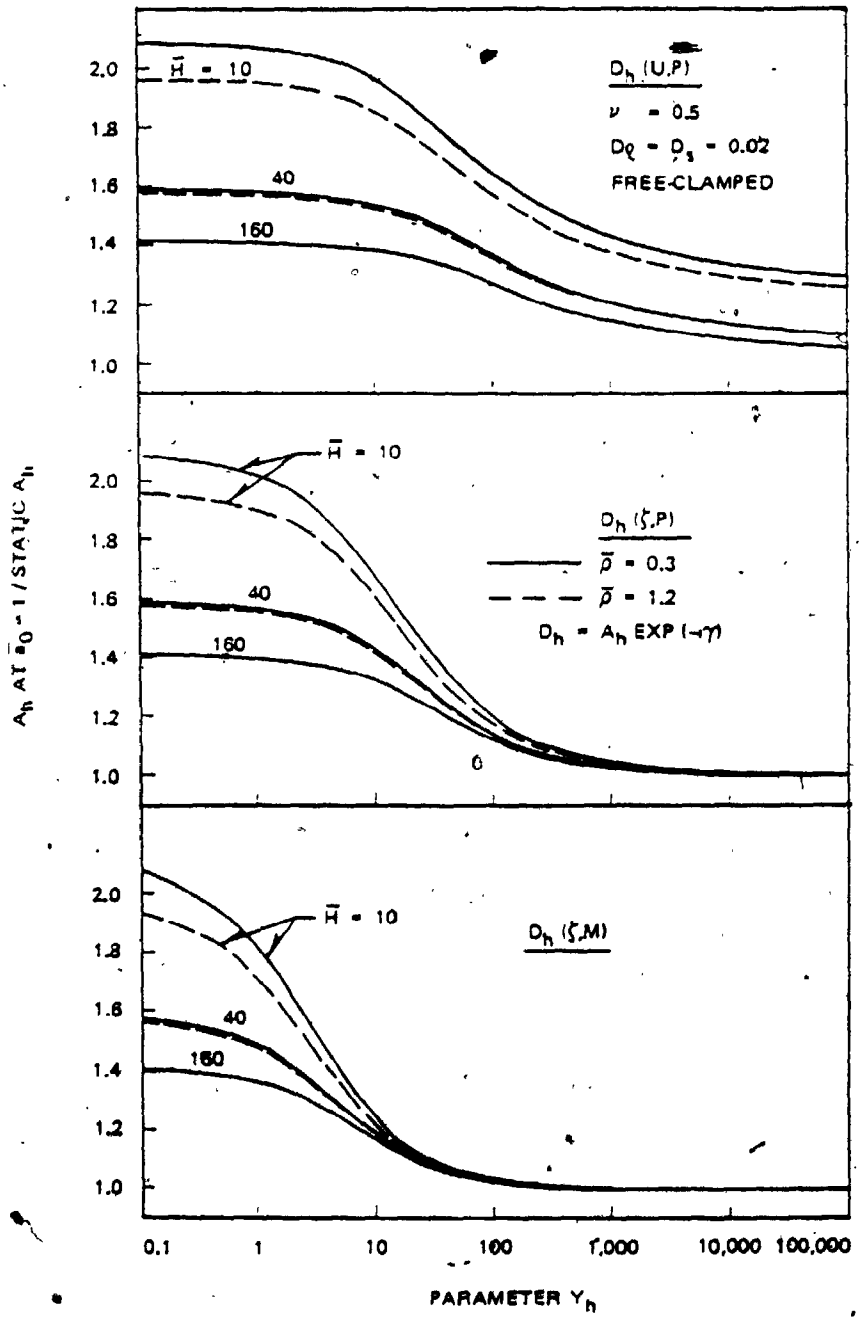

Fig. 4.2-28. Variation of Amplification at the First Natural Frequency of Stratum with Parameter Y_h for Various Mass Ratios

CHAPTER 5. COEFFICIENTS OF SOIL REACTIONS FOR A PILE

5.1 Introduction

In the analysis of pile behavior, the soil resistance to the pile is often assumed to be related to the pile displacement only at the depth where the soil resistance is considered. Adopting such an assumption, many investigators have used the relationship between the pile displacement and soil reaction expressed by

$$p(z) = E_s z^m U^n(z) \qquad (5.1\text{-}1)$$

where $p(z)$ is the soil reaction at depth z, E_s is the constant determined from the elastic character of soil, m and n are the constants governed by the variation of soil properties with depth and the stress-strain relationship of soil, respectively. For example, the following constants m and n were used for the horizontally loaded pile.

n=1, m=0 ... Chan (1937)

n=1, m=1 ... Row (1956), Terzaghi (1955), Reese and Matlock (1960)

n=1, m=arbitrary number ... Palmer and Tomson (1948)

n≠1, m=1 ... Rifaat (1935)

n=0.5, m=1 ... Shinohara and Kubo (1961)

n=0.5, m=0 ... Hayashi and Miyajima (1963)

The relationship expressed in Eq. 5.1-1 leads to the coefficient of soil reaction as

$$k(z) = \frac{p(z)}{U(z)} = E_s z^m U^{n-1}(z) \qquad (5.1\text{-}2)$$

when the soil is a homogeneous and linear elastic medium, the above expression for k(z) is simply expressed as

$$k(z) = E_s \qquad (5.1\text{-}3)$$

Thus, the coefficient of soil reaction is independent of depth for such a case.

In the dynamic case, this coefficient should include the damping and inertia effect of the soil mass. Although many people have conducted research on the coefficient of soil reaction for a pile, the above mentioned important factors in dynamics have not been properly considered in most cases. Baranov (1967) obtained a simple formula to estimate the dynamic coefficient of soil reaction for the embedded foundation in general. This formula is based on a plane strain assumption but includes the previously mentioned important factors in dynamics to a certain extent.

Since the solutions for vibrations of a soil-pile system derived in the previous chapter considered soil as a continuum medium and sufficiently reasonable boundary conditions were assumed, the coefficient can be obtained from those solutions in a rational manner. In this chapter, the coefficients of soil reaction for a pile are derived from the previously obtained solutions for a soil-pile system and the characteristics of those coefficients are investigated. Some of the commonly used methods to estimate the coefficient of soil reaction for a pile and the above mentioned Baranov's formula are also examined.

As a fundamental case, homogeneous and linear elastic soil is considered in this study.

5.2 Derivation of the Coefficients of Soil Reactions

The soil reaction to a pile and the displacement of soil around the circumference of a pile are expressed, respectively, by Eqs. 2.2-13 and 2.2-16 in vertical vibration and by Eqs. 2.2-43 and 2.2-47 in horizontal vibration. They are also expressed with the dimensionless parameters as

$$\begin{Bmatrix} W(\bar{z}) \\ p_v(\bar{z}) \end{Bmatrix} = \sum_{n=1}^{\infty} \begin{Bmatrix} W_n \sin(\bar{h}_n \bar{z}) \\ \pi\mu\, \bar{\alpha}_{vn}\, W_n \sin(\bar{h}_n \bar{z}) \end{Bmatrix} \tag{5.2-1a}$$

$$\begin{Bmatrix} U(\bar{z}) \\ p_h(\bar{z}) \end{Bmatrix} = \sum_{n=1}^{\infty} \begin{Bmatrix} U_n \sin(\bar{h}_n \bar{z}) \\ \pi\mu\, \bar{\alpha}_{hn}\, U_n \sin(\bar{h}_n \bar{z}) \end{Bmatrix} \tag{5.2-1b}$$

According to Eqs. 3.2-9, 3.3-11 and 3.3-22, W_n and U_n are

$$W_n = \frac{HP}{E_p S} \cdot \frac{2(-1)^{n-1}}{\bar{h}_n^{-2} - \bar{\lambda}_v^{-2} + Y_v\, \bar{\alpha}_{vn}} \tag{5.2-2a}$$

$$U_n = \frac{(AF_{1n} + BF_{2n} + CF_{3n} + DF_{4n})(\bar{h}_n^{-4} - \bar{\lambda}^{-4})}{\bar{h}_n^{-4} - \bar{\lambda}_h^{-4} + Y_h\, \bar{\alpha}_{hn}} \tag{5.2-2b}$$

From the definition, the coefficients of soil reaction for vertical and horizontal vibrations at $\bar{z}$ are obtained from the equation,

$$\begin{Bmatrix} k_v(\bar{z}) \\ k_h(\bar{z}) \end{Bmatrix} = \begin{Bmatrix} p_v(\bar{z})/W(\bar{z}) \\ p_h(\bar{z})/U(\bar{z}) \end{Bmatrix} \tag{5.2-3}$$

After substituting Eqs. 5.2-1 into Eq. 5.2-3 and using the expressions for W_n and U_n in Eqs. 5.2-2, the coefficients of soil reaction for a pile can be written as

$$k_{v,h}(\bar{z}) = \mu \bar{k}_{v,h}(\bar{z}) \tag{5.2-4}$$

where

$$\bar{k}_v(\bar{z}) = \frac{\pi \sum_{n=1}^{\infty} \frac{\bar{\alpha}_{vn} \cdot (-1)^{n-1}}{\bar{h}_n^2 - \bar{\lambda}_v^2 + Y_v \bar{\alpha}_{vn}} \sin(\bar{h}_n \bar{z})}{\sum_{n=1}^{\infty} \frac{(-1)^{n-1}}{\bar{h}_n^2 / \bar{\lambda}_v^2 + Y_v \bar{\alpha}_{vn}} \sin(\bar{h}_n \bar{z})} \tag{5.2-5a}$$

$$\bar{k}_h(\bar{z}) = \frac{\pi \sum_{n=1}^{\infty} \frac{\bar{\alpha}_{hn}(AF_{1n}+BF_{2n}+CF_{3n}+DF_{4n})(\bar{h}_n^{-4}-\bar{\lambda}_h^{-4})}{\bar{h}_n^{-4} - \bar{\lambda}_h^{-4} + Y_h \bar{\alpha}_{hn}} \sin(\bar{h}_n \bar{z})}{\sum_{n=1}^{\infty} \frac{(AF_{1n}+BF_{2n}+CF_{3n}+DF_{4n})(\bar{h}_n^{-4}-\bar{\lambda}_h^{-4})}{\bar{h}_n^{-4} - \bar{\lambda}_h^{-4} + Y_h \bar{\alpha}_{hn}} \sin(\bar{h}_n \bar{z})} \tag{5.2-5b}$$

5.3 Characteristics of the Coefficients of Soil Reactions

Fig. 5.3-1 shows the distributions of the static coefficients of soil reactions along the depth for homogeneous and linear elastic soil. The figure indicates that the coefficient is distributed nearly uniformly along the depth for extremely small Y. For increasing values of Y, the coefficients at the shallow depth increase from the above nearly uniform value whereas that at somewhat deeper depth decreases. Thus, even if the soil medium is assumed to be homogeneous and linear elastic, the coefficient is generally not uniform along the depth but tends to decrease with depth. This trend is more significant in a shorter pile. In horizontal vibration, the coefficient can

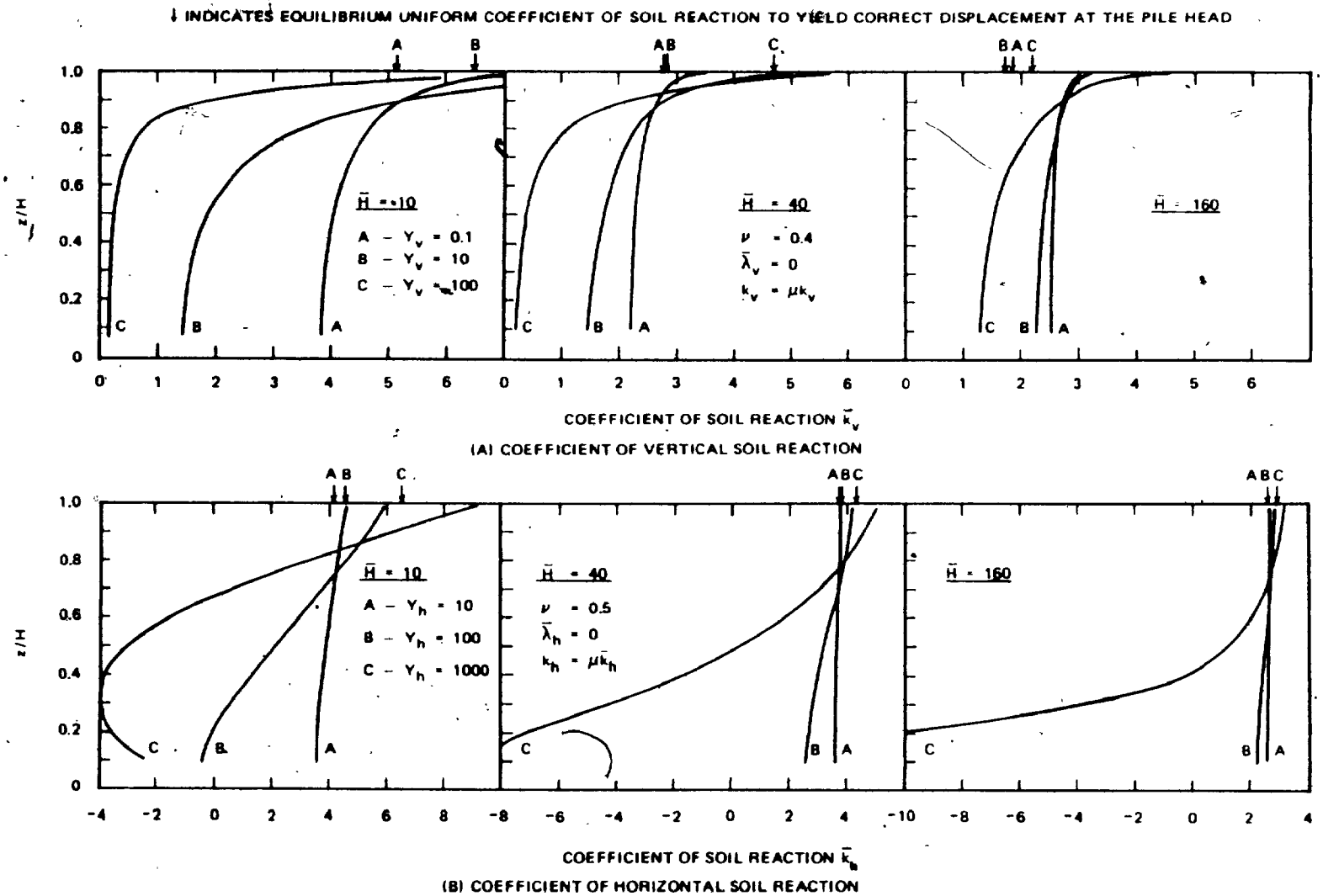

Fig. 5.3-1. Variation of Static Coefficient of Soil Reaction with Depth for Various Slenderness Ratios and Parameter Y_h

be zero and even negative for large Y_h. As can be seen in Fig. 5.3-5, this negative coefficient results from the negative soil reaction under which soil pushes the pile toward the same direction as that of the pile displacement. The above observation for homogeneous soil leads to an idea of the distribution of the coefficient for inhomogeneous soil as shown in Fig. 5.3-2.

Fig. 5.3-3 further shows the distribution of the coefficient obtained from the field test (McClelland and Focht, 1956). In this figure, the coefficient tends to increase with depth until a certain depth and decreases thereafter. Considering an extremely low elastic modulus of soil near the ground surface and strong nonlinear behavior of soil in this region, this trend in the field test agrees with the one drawn from the theoretical analysis. However, the investigators who conducted this test thought that the decrease of the coefficient with depth was unrealistic since the soil strength did not decrease with depth at that test site.

Fig. 5.3-1 implies that the distribution of the coefficient along the depth is mostly governed by the parameter Y and its overall magnitude is governed by slenderness. The variations of overall magnitude of the coefficients with slenderness are shown in fig. 5.3-4 in which extremely small values of Y_v and Y_h are chosen so that the coefficients are nearly uniform along the depth. In this figure, the coefficients decrease with slenderness but nearly linearly increase with r_0/H.

Fig. 5.3-5 shows the distribution of the coefficient along the depth for three different cases. In each case, the shown combinations

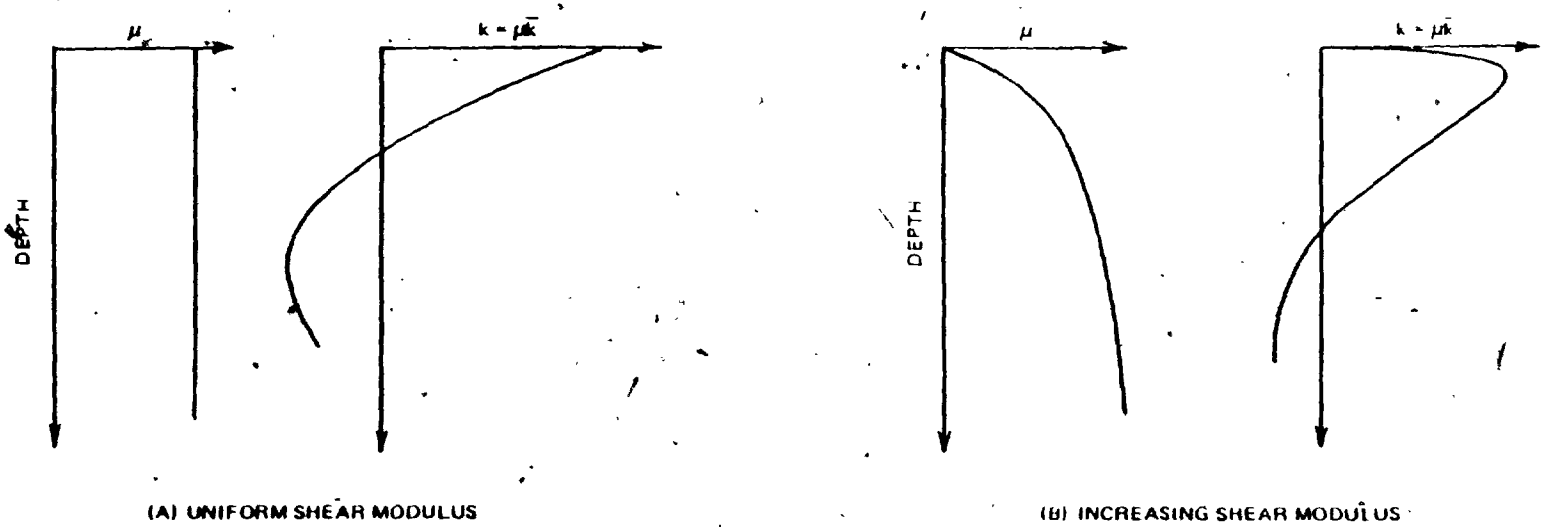

(A) UNIFORM SHEAR MODULUS

(B) INCREASING SHEAR MODULUS

Fig. 5.3-2. Distributions of Static Coefficient of Soil Reaction Along Depth for Uniform and Increasing Shear Modulus with Depth

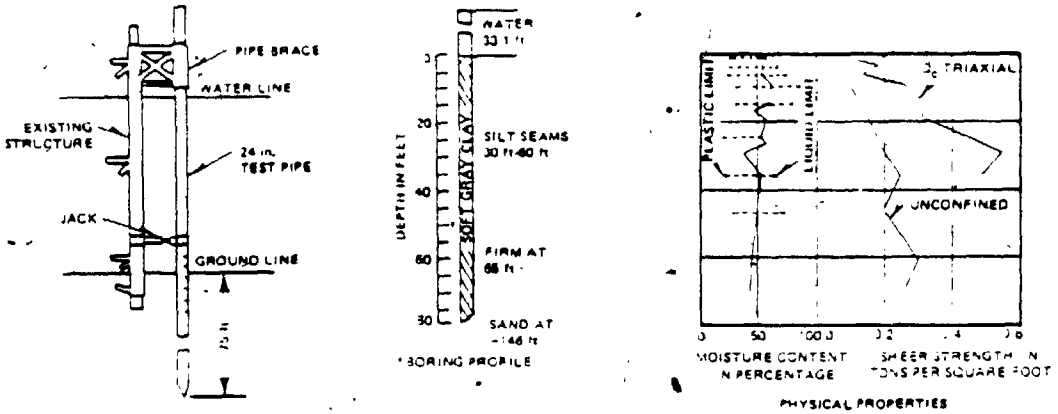

a) TEST LAYOUT

b) SOIL PROPERTIES

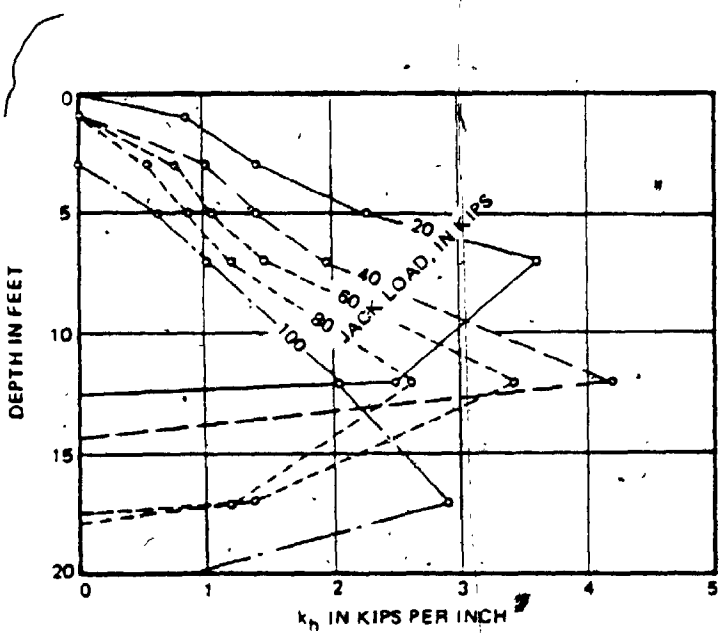

(c) COEFFICIENT OF SOIL REACTION VERSUS DEPTH OBTAINED FROM FIELD TEST

Fig. 5.3-3. Static Coefficient of Soil Reaction k_h Obtained from Field Test (McClelland and Focht, 1956)

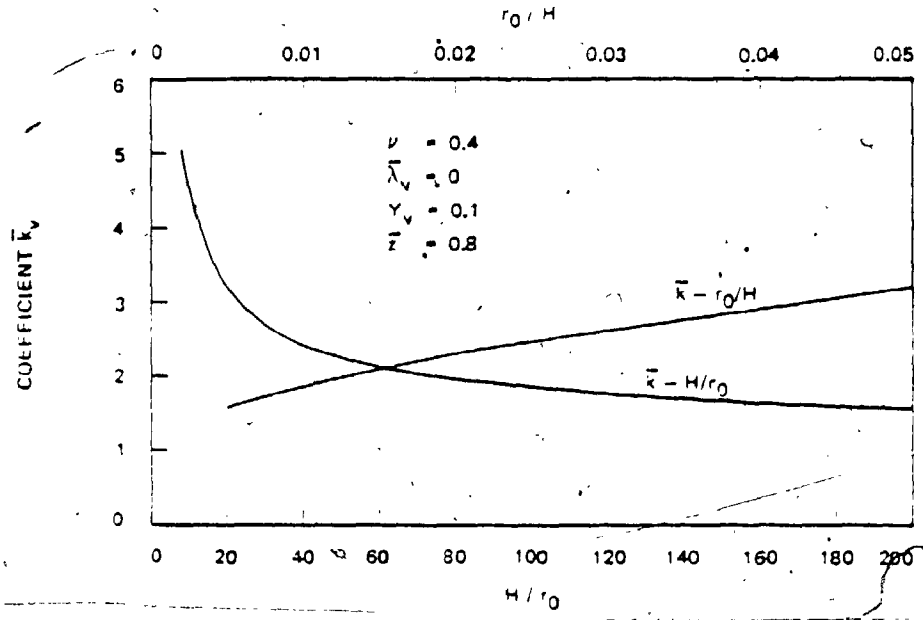

(A) COEFFICIENT OF VERTICAL SOIL REACTION

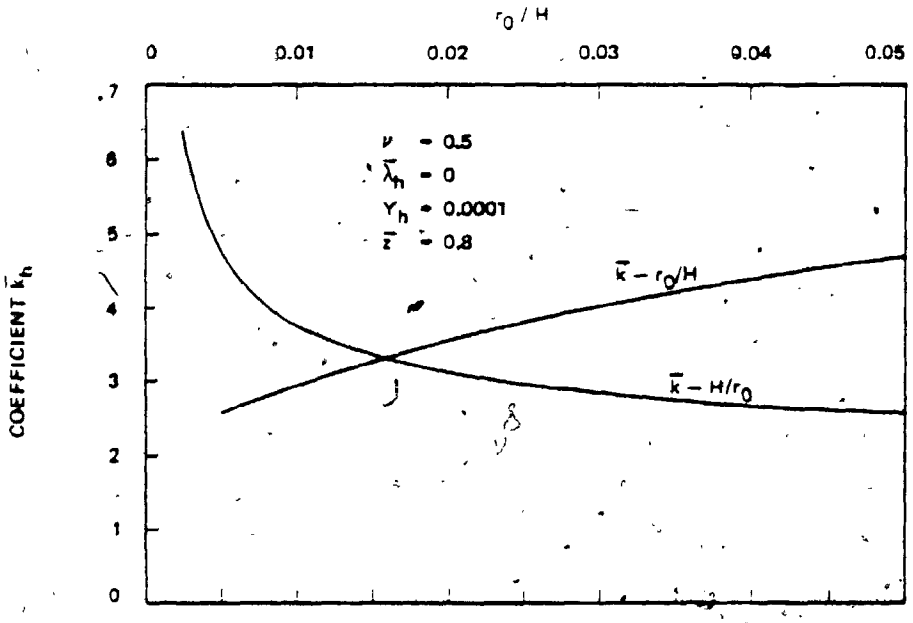

(B) COEFFICIENT OF HORIZONTAL SOIL REACTION

Fig. 5.3-4. Variations of Static Coefficients of Soil Reaction $\bar{k}$ with H/r_0 and r_0/H

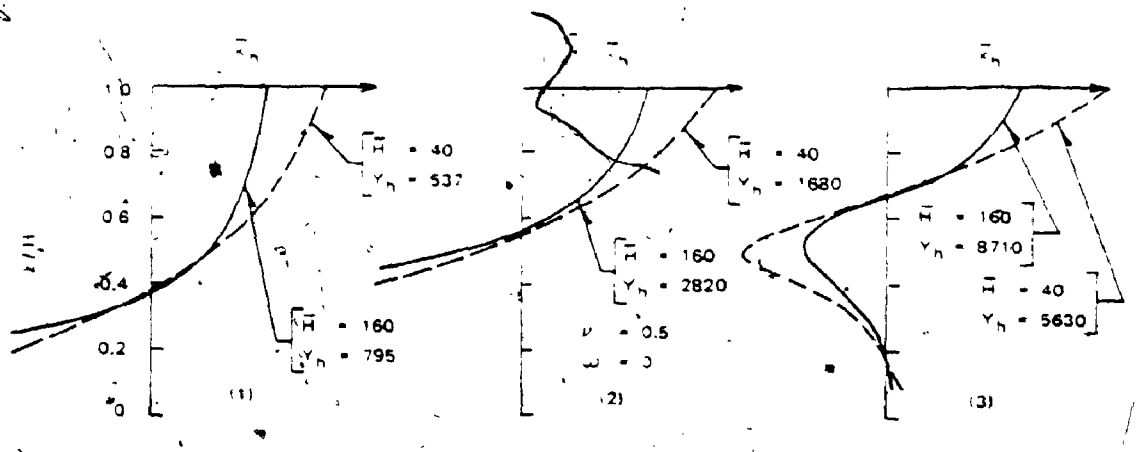

(A) VARIATIONS OF COEFFICIENT $\bar{Y}_h$ WITH z/H UNDER THREE DIFFERENT DISPLACEMENTS $\bar{D}_h$ (U,P)

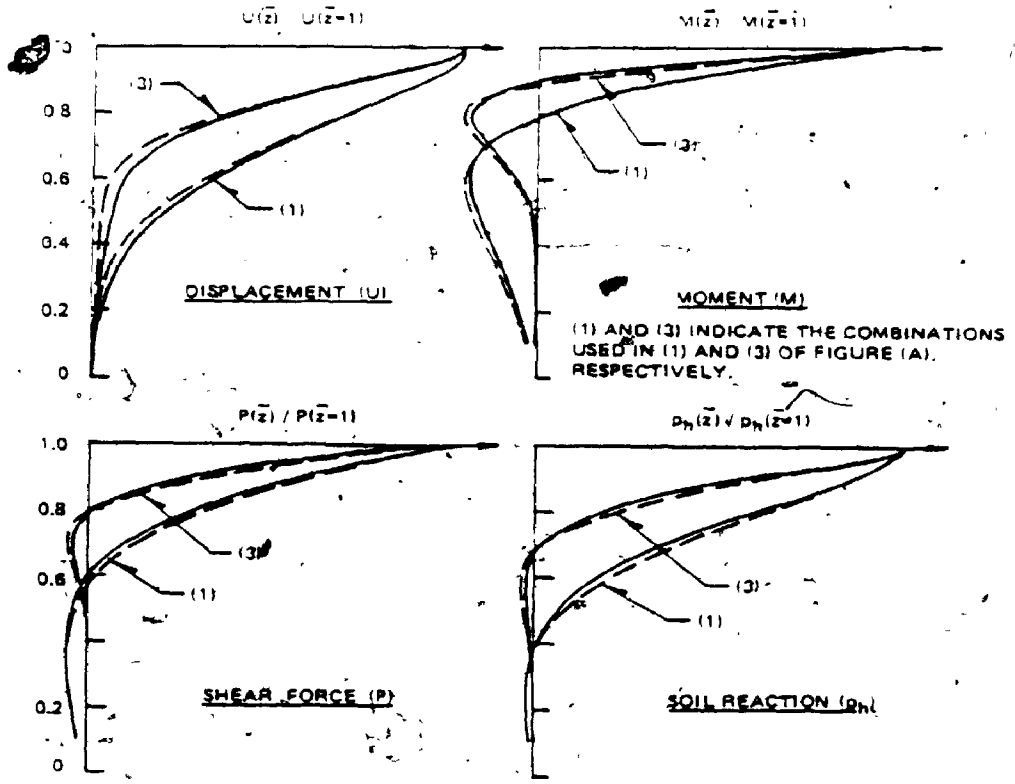

(B) VARIATIONS OF NORMALIZED FORCES AND DISPLACEMENTS OF PILE WITH z/H FOR THE VARIOUS COMBINATIONS OF $\bar{H}$ AND Y_h USED IN FIGURE (A)

Fig. 5.3-5. Nature of the various combinations of $\bar{H}$ and Y_h Under Constant Displacement $\bar{D}_h$ (U,P)

of the parameters $\bar{H}$ and Y_h yield the unique displacement parameter $\bar{D}_h(U,P)$. This figure indicates that, under such combinations of the parameters $\bar{H}$ and Y_h, the distribution pattern of the coefficient along the depth is rather independent of slenderness. Thus, the location of zero stiffness does not vary with slenderness. This is because, as can be seen in the same figure, the variation of the pile displacement with depth is nearly independent of slenderness under such combinations of the parameters so that those of the moment and shear force in the pile and the soil reaction are also independent. Therefore the previously found rather unique relationship between soil effect and Y can be explained from the rather unique relationship between Y and the variation of the pile displacement with the depth, since Y does not vary much with $\bar{H}$ under the constant value of $\bar{D}$ (or $\bar{K}$).

When a pile is subjected to harmonic excitation at the pile head, the distributions of the dynamic coefficients of soil reactions along the depth vary with frequency as shown in Figs. 5.3-6 and 5.3-7. In those figures, it can be seen that the coefficient tends to become more uniform along the depth as frequency increases. The uniform value which the coefficient approaches seems to be the coefficient for the plane strain case. This can be explained from the nature of the wave propagation as explained previously. Since the angle of the ray path in each mode wave and the numbers of progressive waves can be uniquely defined by the frequency parameter a_0, the parameter a_0 or normalized parameter $\bar{a}_0$ is the most useful frequency parameter for indicating how much the coefficient approaches that for the plane strain case at the frequency ω.

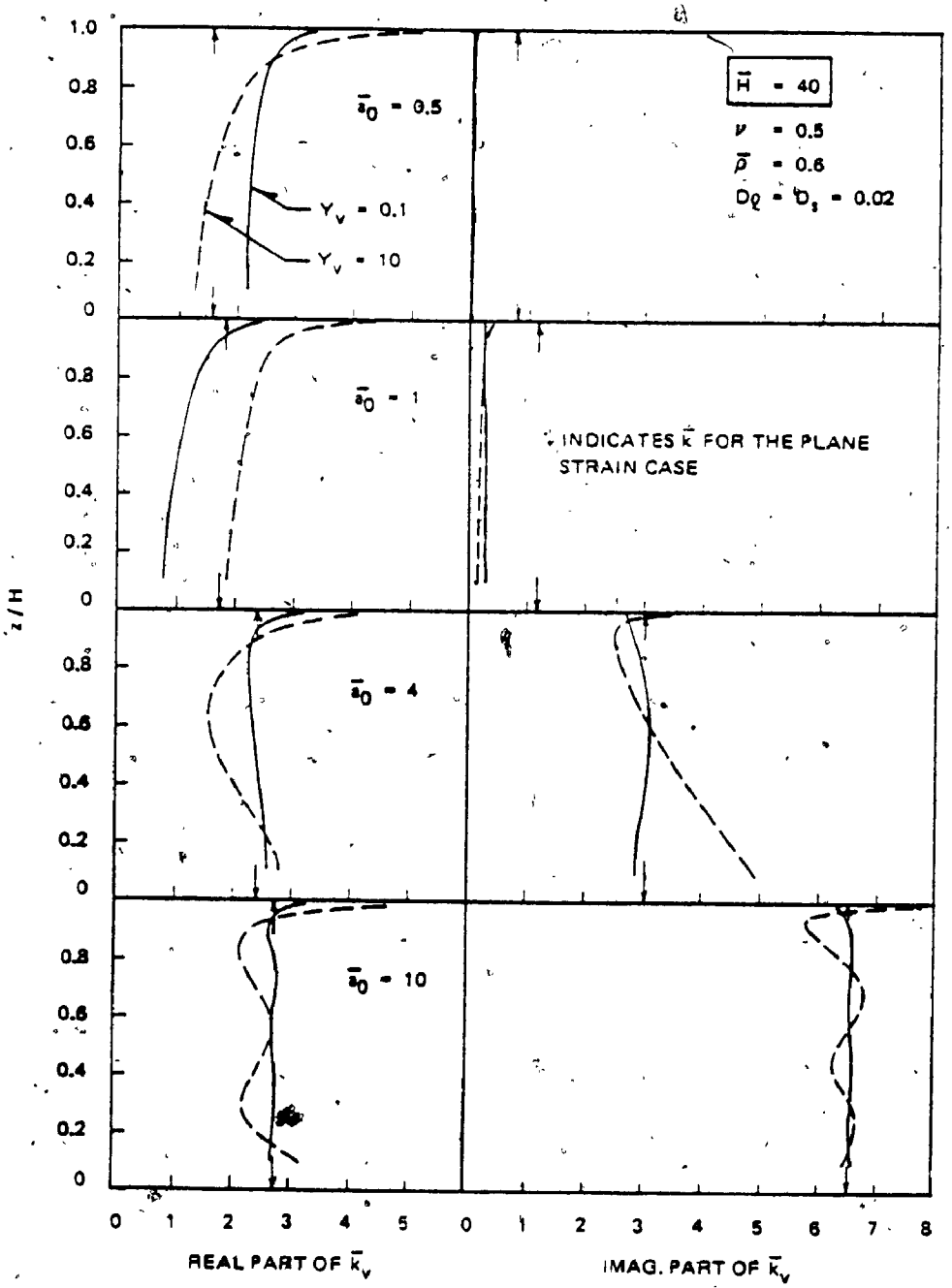

Fig. 5.3-6a. Variation of Coefficient of Soil Reaction $\bar{k}_v$ with Frequency a_0 ($\bar{H}$ = 40)

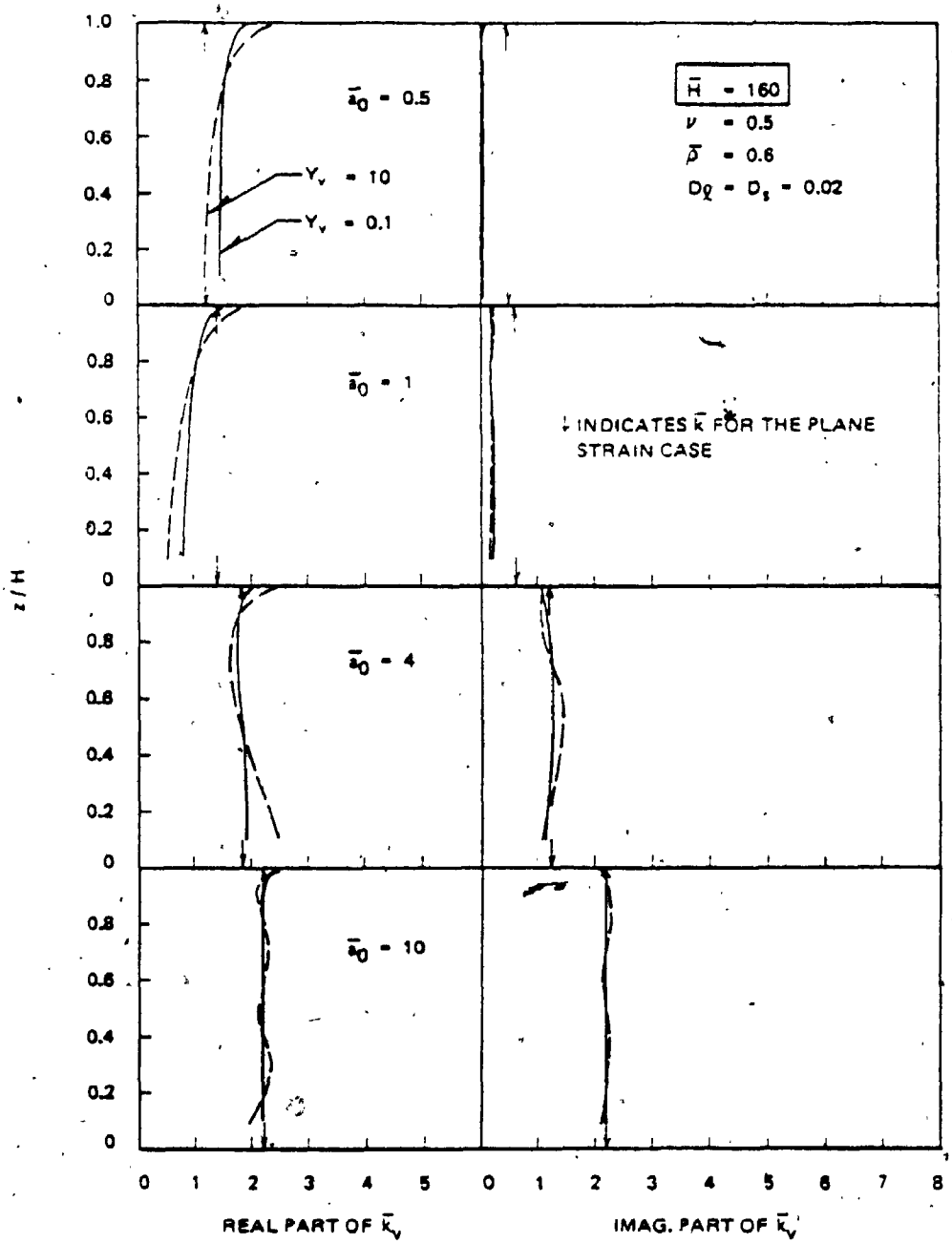

Fig. 5.3-6b. Variation of Coefficient of Soil Reaction $\bar{k}_v$ with Frequency $\bar{a}_0$ ($\bar{H}$ = 160)

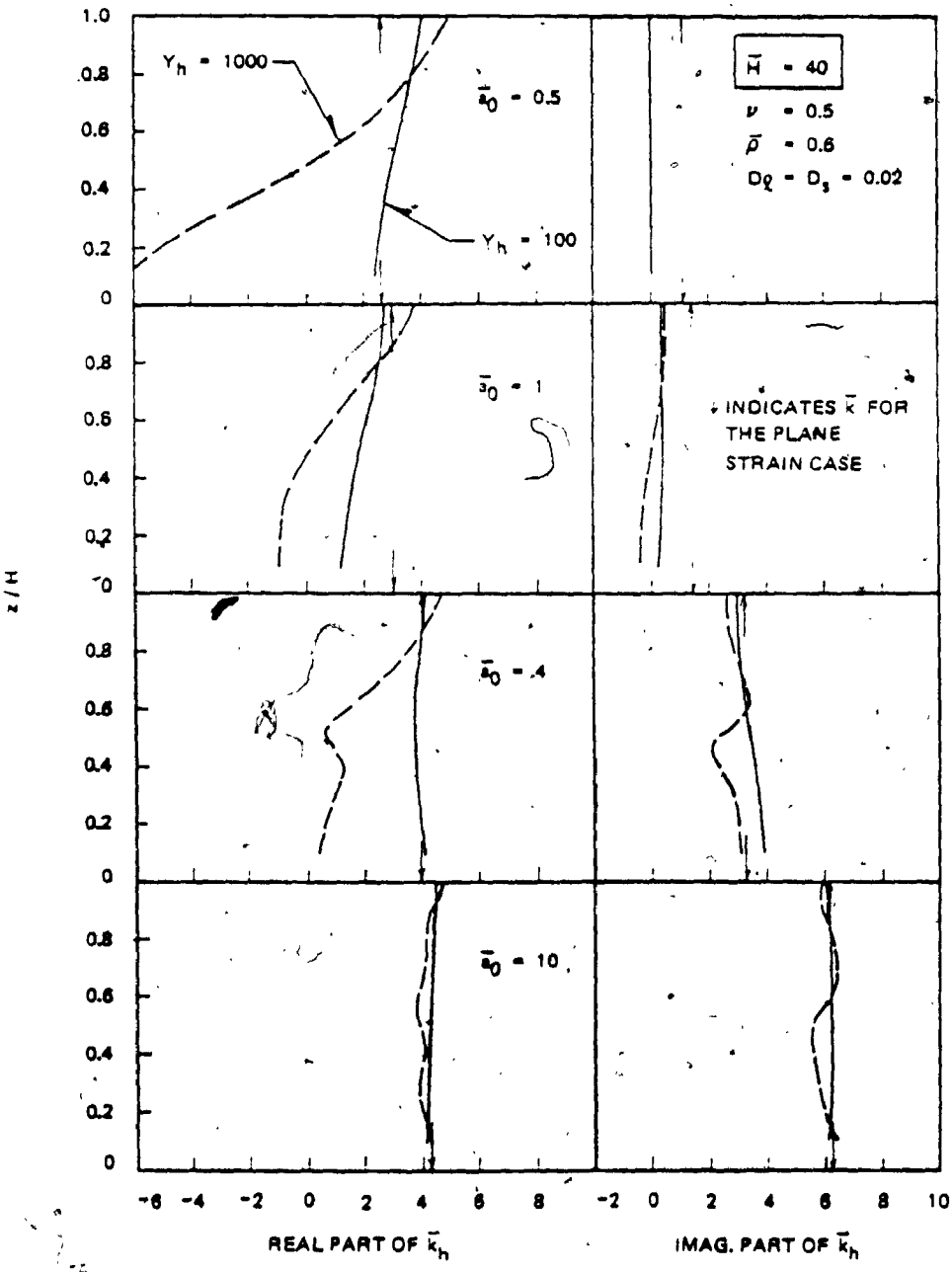

Fig. 5.3-7a. Variation of Coefficient of Soil Reaction $\bar{k}_h$ with Frequency $\bar{a}_0$ ($\bar{H}$ = 40)

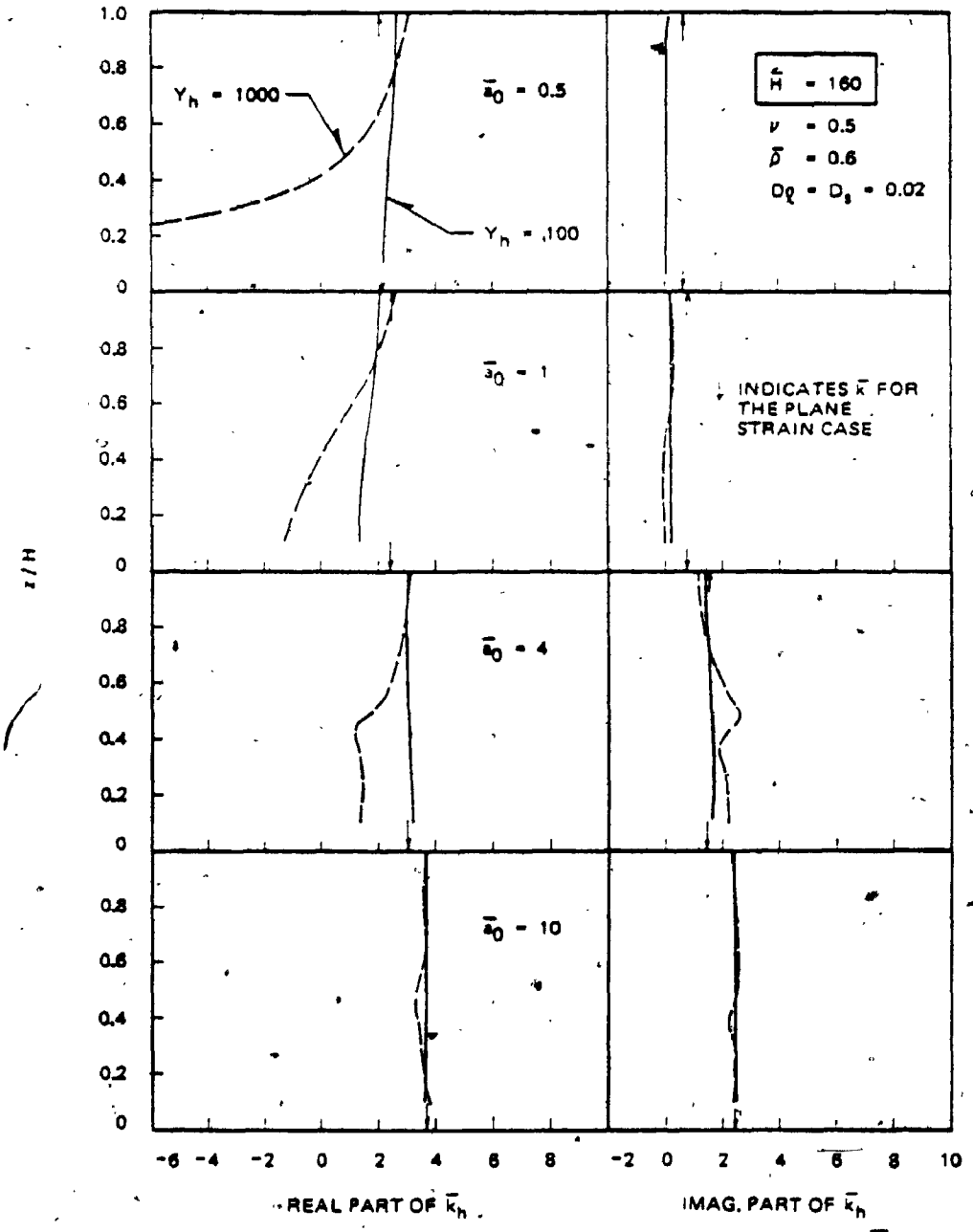

Fig. 5.3-7b. Variation of Coefficient of Soil Reaction $\bar{k}_h$ with Frequency a_0 (H = 160)

Figs. 5.3-8 and 5.3-9 further show how the coefficients at particular depths approach that for the plane strain case as the frequency parameter a_0' increases. Since the frequency parameter a_0 is larger for a more slender pile under a given frequency a_0' or ω, the coefficient for a more slender pile more quickly approaches that for the plane strain case as the frequency a_0' increases.

5.4 Some Considerations on Estimation of the Coefficient of Horizontal Soil Reaction

The coefficient of soil reaction for pile is often estimated from the loading test on the pile, plate loading test, and theoretical formulas for a beam rest on the surface of an elastic medium. Baranov's formula may also be used to estimate the coefficient for a pile for the dynamic case. In the following, the coefficient of horizontal soil reaction estimated by those methods are compared with those obtained from Eq. 5.2-5b.

(i) Coefficient Estimated from Loading Test on a Pile

This test has an advantage since it is conducted under the situation close to the real situation of soil-pile system. However, the problem is how the coefficient is deduced from the test results.

The uniformly distributed equivalent coefficient is often estimated so that this coefficient yields the same displacement at the pile head as that obtained in the test. Obviously, such equivalent uniform coefficient differs from the real one when the soil medium is inhomogeneous. Fig. 5.3-1 shows the estimated equivalent coefficient together with that obtained from Eq. 5.2-5 for a homogeneous and linear

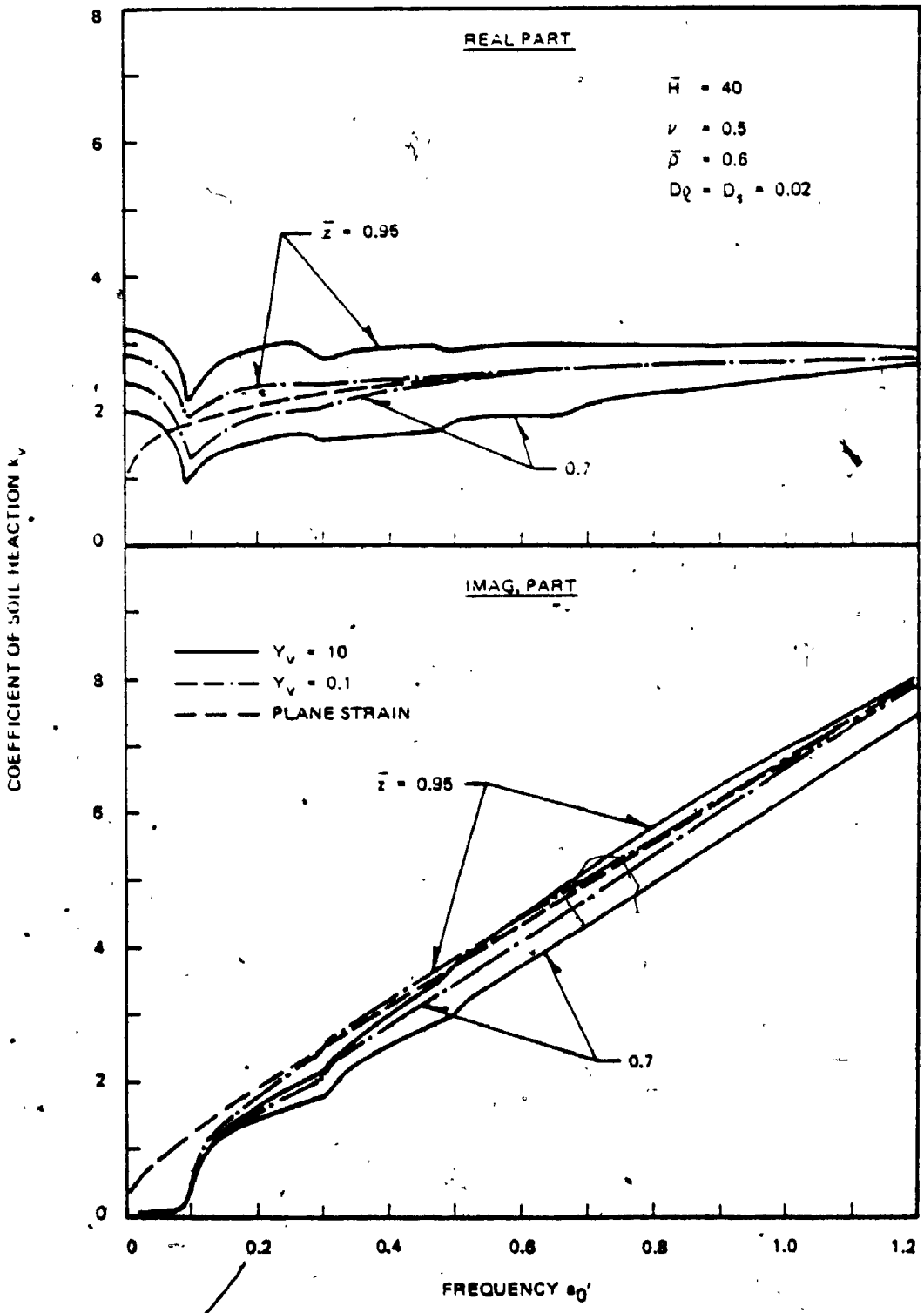

Fig. 5.3-8a. Variation of Coefficient of Soil Reaction $\bar{k}_v$ with Frequency a_0' at Particular Depth ($\bar{H}$ = 40)

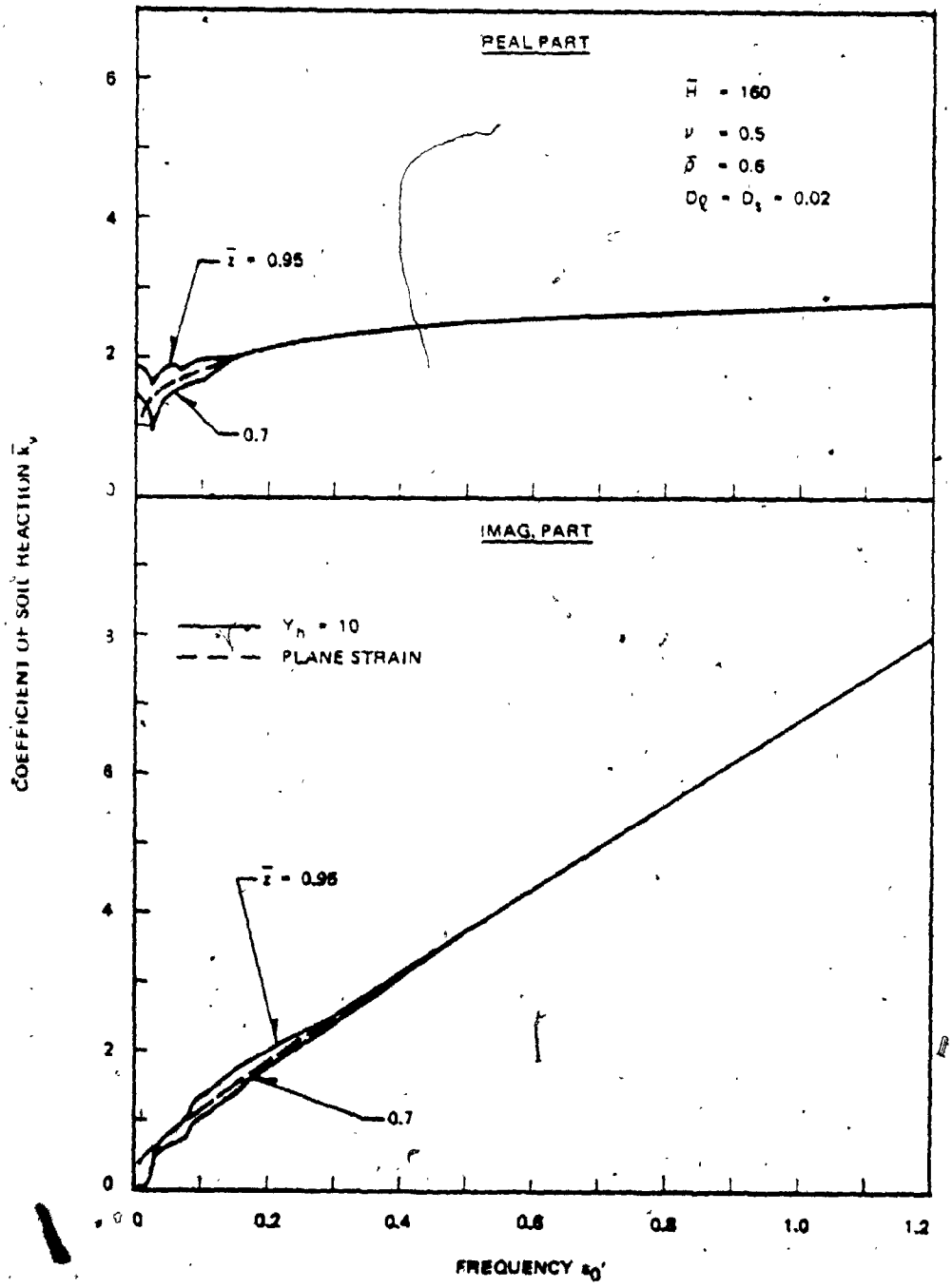

Fig. 5.3-8b. Variation of Coefficient of Soil Reaction $\bar{k}_v$ with Frequency a_0' at Particular Depth ($\bar{H}$ = 160)

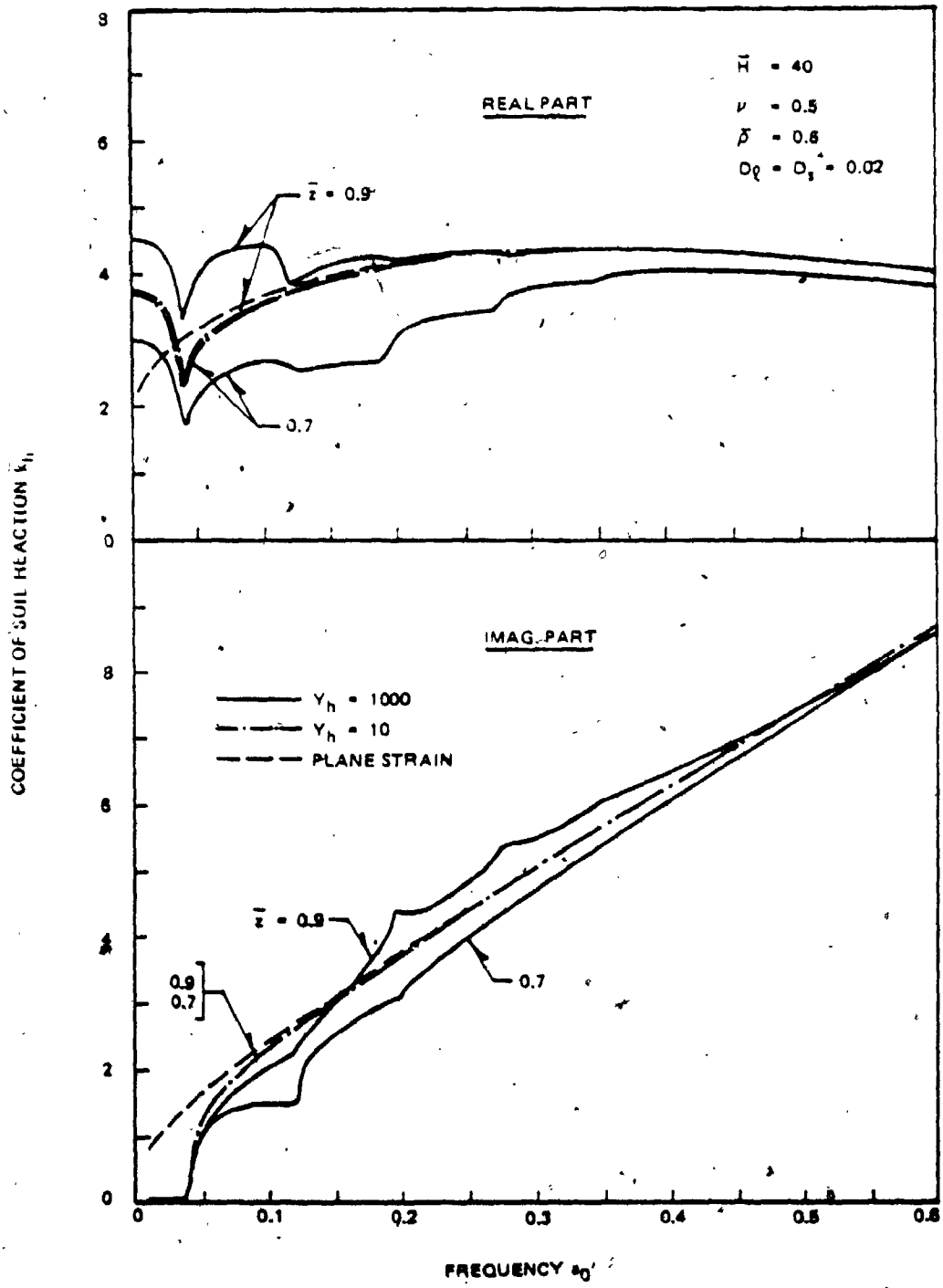

Fig. 5.3-9a. Variation of Dynamic Coefficient of Soil Reaction $\bar{k}_h$ with Frequency a_0 at Particular Depth ($\bar{H}$ = 40)

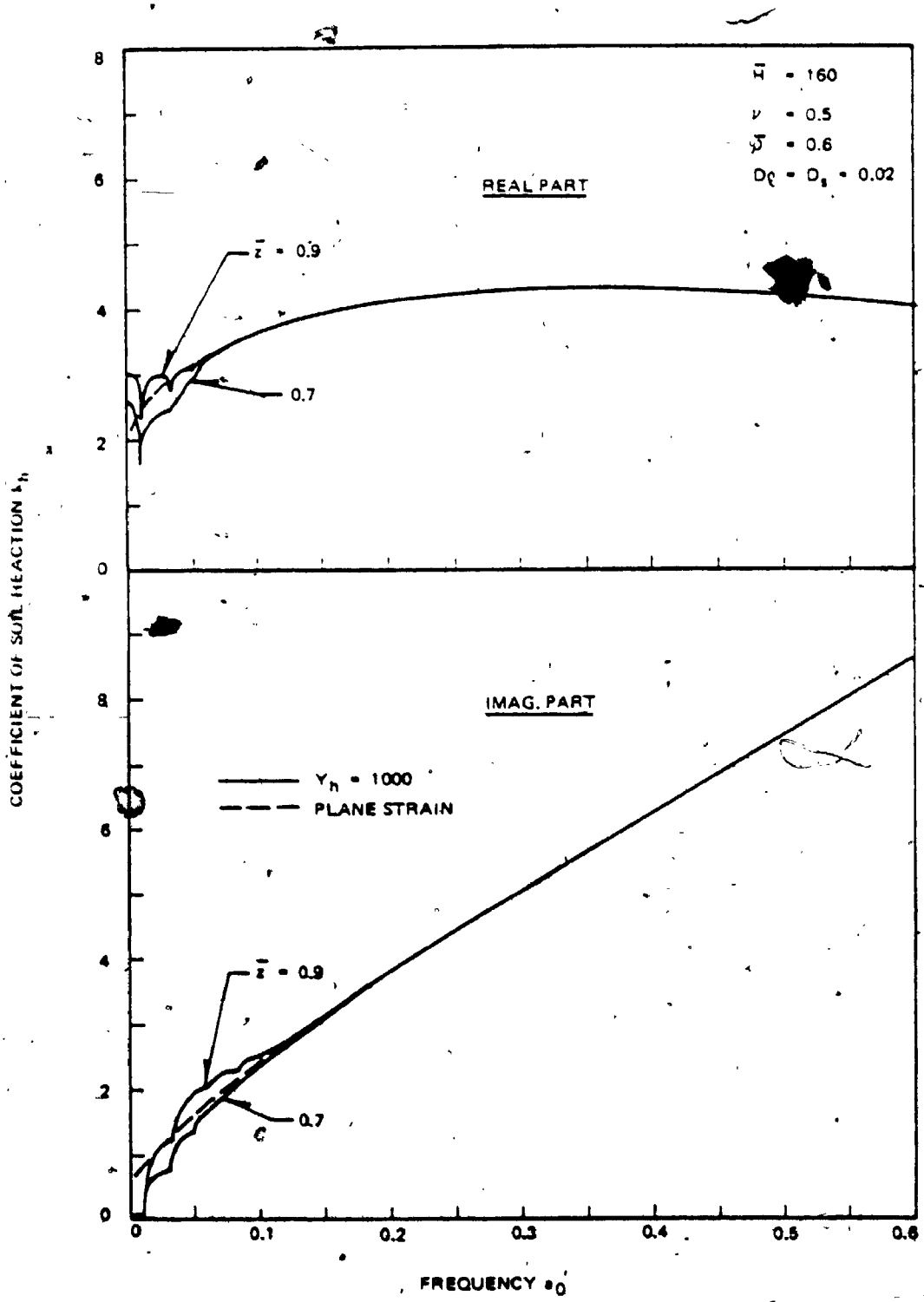

Fig. 5.3-9b. Variation of Coefficient of Soil Reaction $\bar{k}_h$ with Frequency a_0' at Particular Depth ($\bar{H}$ = 160)

elastic soil medium. As can be seen, even if the soil medium is homogeneous and linear elastic, the estimated coefficient generally differs from the one expected in this soil medium. The difference is much more significant for larger Y_h. On the other hand, under small Y_h and slender pile, the estimated one agrees with the expected one.

(ii) Coefficient Estimated from Plate Loading Test

The coefficient of subgrade reaction is often assumed to be related to the coefficient of soil reaction through the relationship

$$k = 2 r_0 k^* \qquad (5.4\text{-}1)$$

where k* is the coefficient of subgrade reaction and is usually obtained from the plate loading test.

When the soil medium is elastic, the theory of elasticity indicates that the coefficient of subgrade reaction is simply inversely proportional to the width of the plate. The coefficient of soil reaction is therefore independent of the width of the plate. According to Terzaghi (1955), this is because the size of the pressure bulb increases proportionally with the width of the plate. He postulated that such a condition existed for the soil-pile system and applied the above mentioned relationship between the coefficient and width of the plate for estimating the coefficient for a pile in clay.

When the soil medium is homogeneous in addition to linear elastic, the coefficient of soil reaction for a pile now may be obtained from that for the circular plate on a homogeneous and linear elastic half space. Thus, the coefficient of soil reaction obtained from the plate loading test is

$$k_h = \mu \bar{k}_h \qquad (5.4\text{-}2a)$$

where

$$\bar{k}_h = \frac{8}{\pi(1-\nu)} \qquad (5.4\text{-}2b)$$

The coefficient obtained from Eq. 5.2-5b has already been shown in Fig. 5.3-4 for homogeneous and linear-elastic soil with $\nu = 0.5$. In this figure, the coefficient decreases with slenderness. On the other hand, the coefficient estimated from the plate loading test for such ideal soil is independent of slenderness as shown in Eqs. 5.4-2 and is $\bar{k}_h = 5.1$. Therefore, the comparison of this value with those in Fig. 5.3-4 reveals that the plate loading test may provide a reasonable estimation for a short pile ($H/r_0 \approx 20$) whereas it may overestimate the coefficients for a slender pile.

(iii) Coefficient Estimated from Theoretical Formulas

There are some theoretical formulas used for estimating the static coefficient of soil reaction. Among them, Vesić's formula is very often used.

Vesić (1963) has proposed a formula for estimating the static coefficient of soil reaction for a uniformly loaded beam on an elastic half-space. Broms (1964), Francis (1964), and Bolows (1968) applied this formula to estimate the coefficient for a pile. However, Francis used the coefficient as large as twice of that obtained by Vesić's formula because a pile is surrounded by soil. After this modification, Vesić's formula for the coefficient of soil reaction is

$$k_h = 1.30 \sqrt[12]{\frac{E\,(2r_0)^4}{E_p I}} \frac{E}{1-\nu^2} \qquad (5.4\text{-}3)$$

where E is Young's modulus of soil. This equation is rewritten by the previously defined dimensionless parameters and is

$$k_h = \mu \bar{k}_h = \mu \frac{2.6}{1-\nu} \sqrt[12]{\frac{Y_h}{\bar{H}^4} \frac{32(1+\mu)}{\pi}} \qquad (5.4\text{-}4)$$

The variation of the coefficient $\bar{k}_h$ with slenderness obtained by Vesić's formula, is shown in Fig. 5.4-1 for various Y_h. It should be noted that the coefficient obtained from Vesić's formula is independent of slenderness; this is because Y_H is expressed by $Y_h = 4\,\bar{v}^2\,\bar{\rho}\,\bar{H}^4$ and therefore $\bar{H}^4$ in Eq. 5.4-4 is cancelled out. Comparison between the coefficient obtained by Vesić's formula and that obtained from Eq. 5.2-5 shows that Vesić's formula gives a reasonable estimation when the parameter Y_h is about equal to 10,000. However, as pointed out before, the variation of the coefficient with depth is large for $Y_h = 10{,}000$.

In the dynamic case, no theoretical work has been done to estimate the coefficient of soil reaction for a pile. However, Baranov's approximate formula for estimating the coefficient of soil reaction for an embedded foundation may be applicable to a pile. The applicability of this formula to a pile may be worthwhile to examine.

Baranov (1967) assumed an elastic medium surrounding an infinitely long, rigid cylinder subjected to harmonic excitation, and derived the formula for the coefficient of soil reaction for this case. This

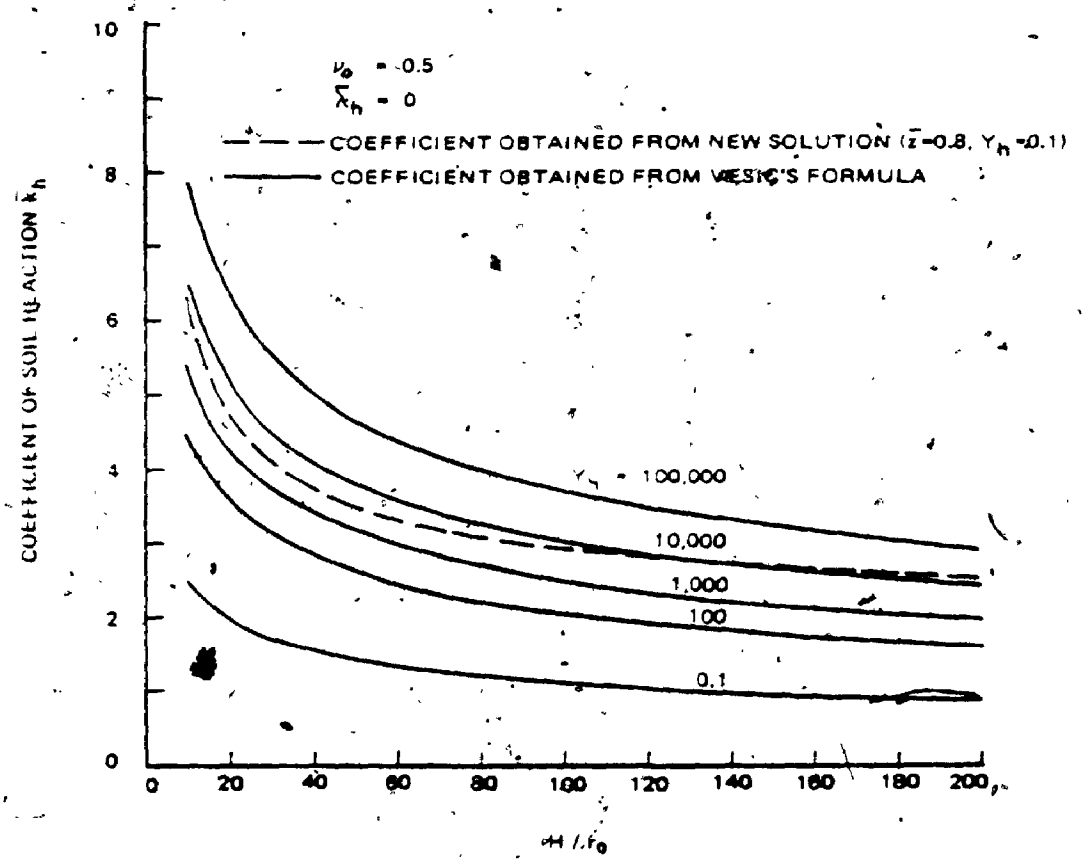

Fig. 5.4-1. Static Coefficient of Soil Reaction $\bar{k}_h$ Obtained from Vesić's Formula

situation does not yield the strain on the plane perpendicular to the axial direction and is viewed as a plane strain case. Since Baranov's formula does not include material damping, his formula is modified in Appendix C so as to include it.

The coefficient estimated by this modified Baranov's formula is shown in Figs. 5.3-7 and 5.8-9 together with the coefficient obtained from Eq. 5.2-5b. In this figure, a significant error in his formula appears in the static case or zero excitation frequency: the real part of this coefficient is zero at zero frequency whereas it is not zero in the real case. This error results from a plane strain assumption.

On the other hand, as is shown in Figs. 5.3-7, the distributed coefficient along the depth approaches that estimated by the modified Baranov's formula as more wave modes accompany the progressive waves. Considering this trend and the trend observed previously in the static coefficient, the plane strain assumption leads to a reasonable estimation of the coefficient for a slender pile with small Y_h and high frequencies. This statement is also applicable to the coefficient for vertical vibration.

Figs. 5.4-2 show the displacements of a pile at the head in horizontal vibration, which are obtained by a rigorous solution derived in this dissertation and an approximate solution. In the approximate solution, the reaction from the soil is calculated from the modified Baranov's formula. Excellent agreement between those amplitudes can be seen at the frequencies above the second resonant frequency of the stratum. However, for the shown frequency range ($\bar{a}_0 \leq 10$), the agreement in the phase shifts are not so good as that in the amplitudes.

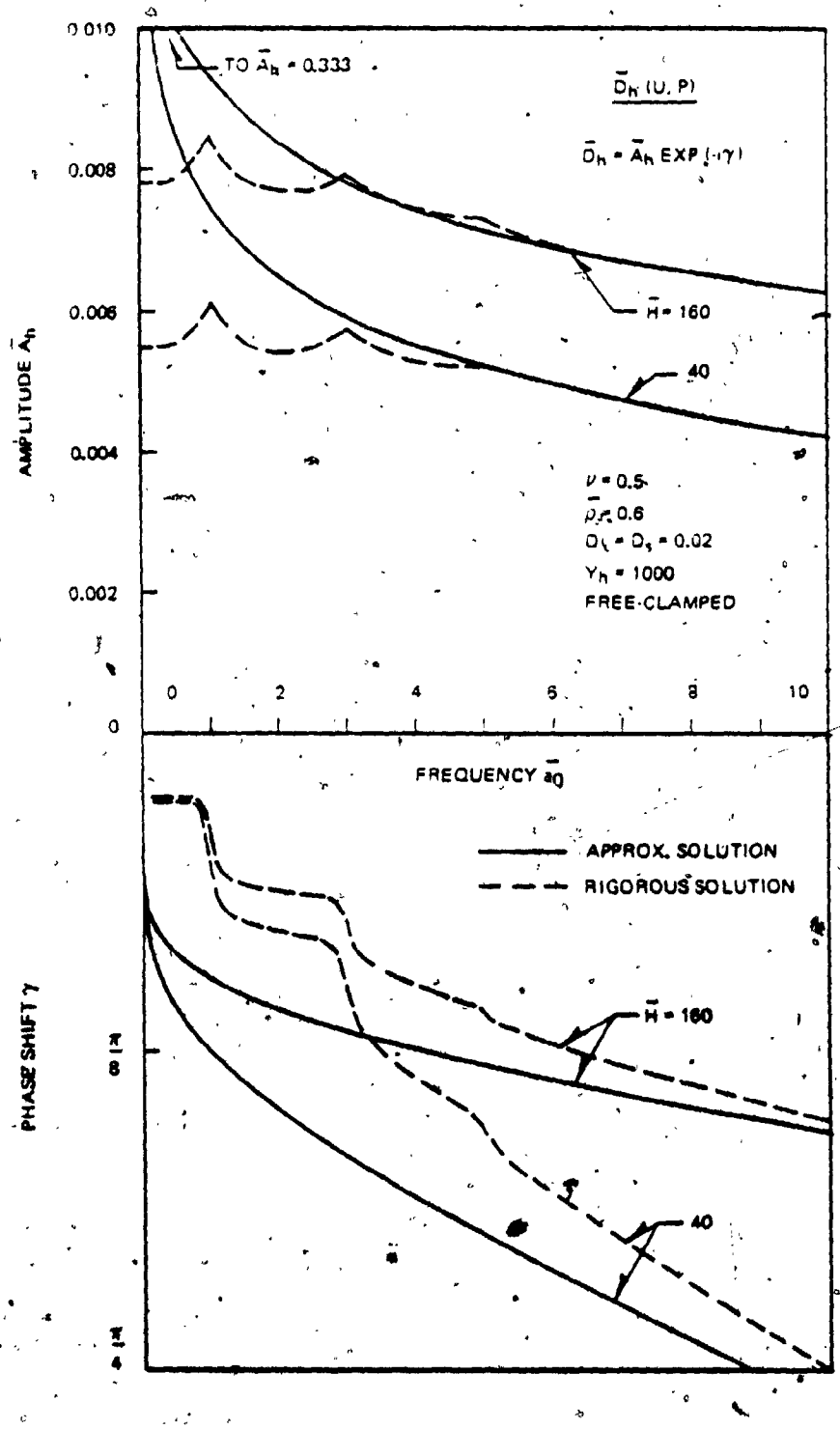

Fig. 5.4-2a. Displacements $\bar{D}_h(U,P)$ Obtained by Approximate and Rigorous Solutions

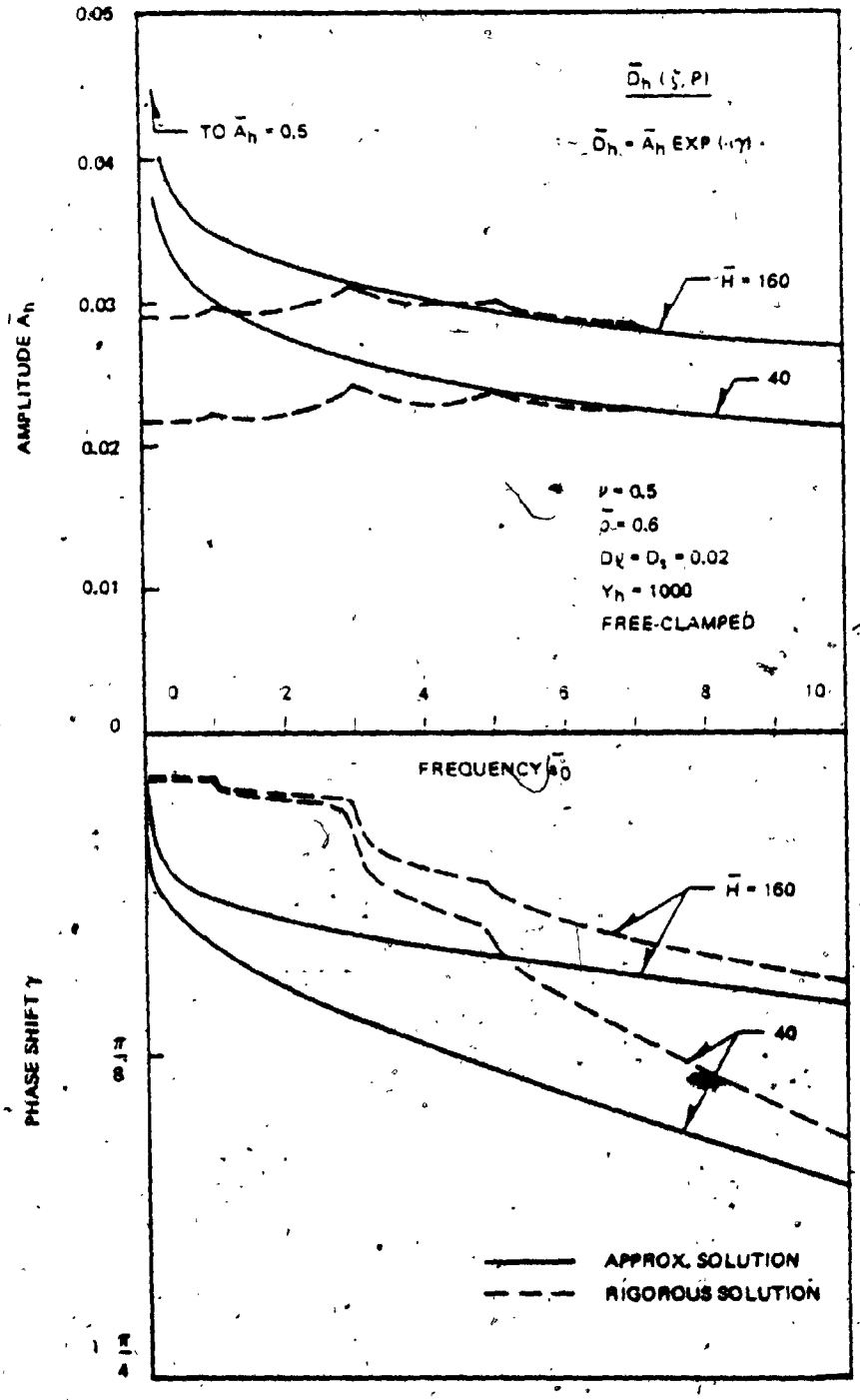

Fig. 5.4-2b. Displacements $\bar{D}_h(\zeta, P)$ Obtained by Approximate and Rigorous Solutions

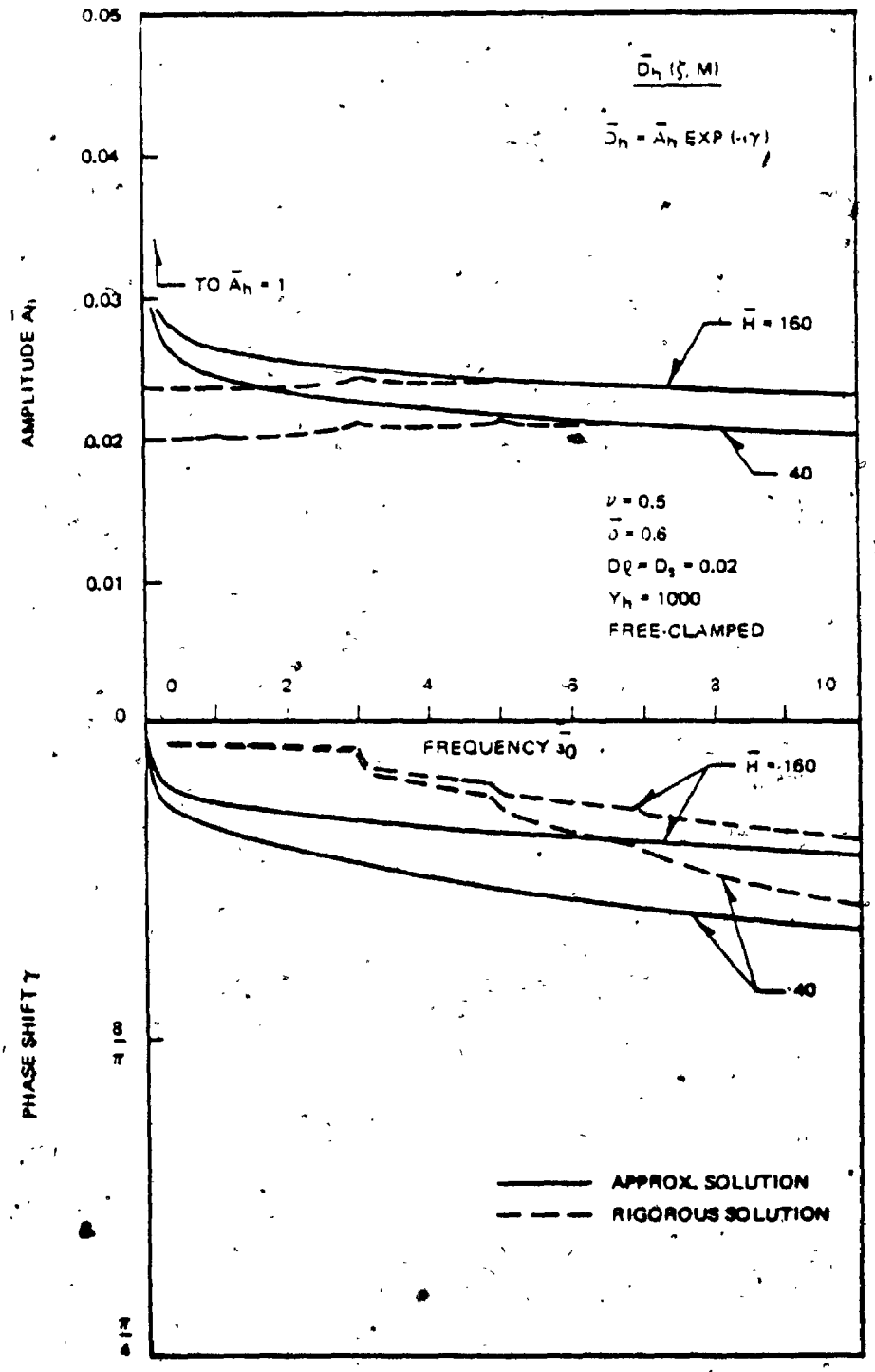

Fig. 5.4-2c. Displacements $\bar{D}_h(\zeta, M)$ Obtained by Approximate and Rigorous Solutions

CHAPTER 6. SUMMARY AND CONCLUSIONS

The dynamic soil-pile interaction and the dynamic coefficients of soil reaction for a pile foundation have been investigated in this dissertation. The main emphasis was placed on obtaining a physical insight of the phenomenon. Thus a rather simple soil-pile system was considered so that important features of the dynamic behavior could be seen clearly.

The behavior of a pile driven into soil is modified by the reaction from the soil, and results in a soil-pile interaction. Infinite modes of waves are generated in the soil medium by the motion of such a pile. The reaction from soil is a net effect of superimposition of those in all waves.

The "soil resistance factor" defined in this dissertation shows quantitatively the functions of the soil medium to a pile in individual wave modes. This factor is a complex number in which the real and imaginary parts represent, respectively, the spring and damping functions of soil medium provided to the pile in individual wave modes. Those functions of the soil medium vary with frequency. The main features of this variation are:

1. Stiffness tends to drop with frequency in the low frequency range and shows its minimum value at the resonance of the stratum.
2. Damping in the low frequency range is nearly independent of frequency when material damping is present.
3. Damping increases sharply around the resonance, and thereafter linearly increases with frequency.

4. As frequency increases above the resonance of the stratum, stiffness and damping become identical with those for the plane strain case.

Those frequency-dependent behaviors of the functions of the soil medium are governed by the dimensionless parameters such as the wave mode number, damping factors (D_l and D_s), Poisson's ratio (ν), and relative thickness of the stratum ($\bar{H}$). They affect the damping and stiffness functions of the stratum ($\bar{H}$). The effect of these parameters on the functions of the soil medium are classified into those in the following three frequency ranges.

in the low frequency range:

1. Stiffness is higher for higher modes and relatively thinner stratum.
2. Damping does not appear for soil without material damping.
3. Damping is larger for larger material damping and higher modes.

around the resonance:

1. The drop of stiffness is smaller for higher material damping and higher modes.

in the high frequency range:

1. Stiffness is reduced by the material damping, and this reduction grows with frequency.
2. Material damping generates the damping, in addition to radiational damping, which is nearly frequency-independent and larger for higher material damping.
3. Stiffness and damping are independent of Poisson's ratio in vertical vibration.

4. In horizontal vibration, the stiffness for higher Poisson's ratio is lower above a certain frequency, whereas the damping for such Poisson's ratio is higher.

5. Stiffness and damping become independent of the relative thickness of the stratum and wave mode as frequency increases.

The above derived resistance factors were used to obtain the stiffness and damping of a soil-pile system at the pile head. The stiffness and damping are expressed, respectively, by the real and imaginary parts of the complex number and were called "complex stiffness." The complex stiffness varies with frequency. The trends of this variation are different for the weak and strong soil effects. The degree of the soil effect on the complex stiffness can be roughly estimated from the parameter Y.

Two types of abrupt changes were observed in the variation of the complex stiffness with frequency: the stiffness drops whereas the damping increases. One is associated with the resonance of the soil medium and the other with the resonance of the soil-pile system. When the soil effect is weak, the first type of abrupt change is not noticeable whereas the second one appears strongly. On the other hand, when the soil effect is strong, only the first type of abrupt change appears.

Other observed main features of the complex stiffness are:

1. Under the strong soil effect, the stiffness $\bar{K}$ quickly becomes independent of slenderness as the frequency a_0' increases above the first resonant frequency of the stratum.

2. The damping $\bar{K}$ is nearly independent of slenderness under any intensity of soil effect, except the above mentioned abrupt change and the damping in the low frequency range.
3. The damping is small and does not vary much when the frequency is lower than the first resonant frequency of the stratum.
4. When the frequency is higher than the first resonant frequency of the stratum, the damping grows nearly linearly with frequency except the above mentioned abrupt change.
5. Under the strong soil effect, the damping relative to the stiffness is high for $K_h(P,U)$, $K_h(P,\zeta)$, and $K_h(M,\zeta)$ in decreasing order, and that for vertical vibration is between those for $K_h(P,\zeta)$ and $K_h(M,\zeta)$.
6. In horizontal vibration, the complex stiffness $K_h(P,U)$ is most sensitive to the variation of the governing parameters but the complex stiffness $K_h(M,\zeta)$ is least.
7. The complex stiffness in vertical vibration varies with frequency nearly independently of Poisson's ratio at frequencies above the first resonant frequency of the stratum.
8. In horizontal vibration, the complex stiffness normalized by the static one varies with frequency nearly independently of Poisson's ratio, although the complex stiffness is higher for higher Poisson's ratio.
9. The effect of the variation of mass ratio increases with frequency.
10. The larger mass ratio leads to the higher stiffness and lower damping.

11. Under the strong soil effect with large mass ratio at high frequencies, the stiffness and damping may be treated as in a standard Voigt model in which the spring and damping constants are frequency independent.

The displacements of a pile subjected to harmonic excitation at its head were calculated. The results showed how the characteristics of the complex stiffnesses affected the displacements of the pile.

The coefficients of the soil reaction to a pile were investigated using the previously derived solutions for a soil-pile system. Major findings for the static coefficients are as follows.

1. Even if the soil medium is uniform, the coefficients are generally not uniform along the depth but tend to decrease with the depth.
2. Smaller Y and a more slender pile yield more uniform coefficients along the depth.
3. The coefficients increase nearly linearly with r_0/H for $20 \leq H/r_0 \leq 200$.
4. Any combination of Y and slenderness which yields the constant $\bar{D}$ leads to nearly unique variation of the coefficients with depth.

The dynamic coefficient of soil reaction is expressed by a complex number, in which the real and imaginary parts represent the local stiffness and damping, respectively. As frequency increases, the coefficients become uniform along the depth and approach those for the plane strain case. The comparison of the coefficients obtained from the derived solution with those for the plane strain case has shown

1. Below the first resonance of the stratum, the real part of the coefficients is higher than that for the plane strain case, whereas the imaginary part is smaller.
2. Around the first resonant frequency of the stratum, the real part of the coefficients is lower than that for the plane strain case.

The coefficient of horizontal soil reactions is usually estimated from the field tests or analytical solutions. Since those estimations rely on certain assumptions, some of the above methods were assessed by comparing the coefficients obtained with them and those obtained from the derived solution for a soil-pile interaction. The main findings are as follows.

1. "Equivalent coefficient" back calculated from field tests on a pile may be underestimated at shallow depths but overestimated at somewhat greater depths.
2. The plate loading test may overestimate the coefficient for a slender pile.
3. Vesić's formula may provide a reasonable overall value of the coefficient for $Y_h \approx 10{,}000$ but overestimate for $Y_h < 10{,}000$.
4. For a slender pile, small Y and high frequency ($\bar{a}_0 \geq 3$), the dynamic coefficient may be reasonably estimated from the plane strain case (modified Baranov's formula).

Some of the above findings have revealed that the spring and damping functions of a soil medium can be replaced by the locally independent spring and damping distributed along the pile length (Winkler's model) in some cases. High frequency, soft soil, and

slender pile produce such favorable cases. The above findings have also shown that the constants for the locally independent spring and damping may be obtained from those for the plane strain case or modified Baranov's formula. When the soil medium is replaced by such a model, the variation of soil properties affects the locally independent spring and damping only through the parameters a_0', D_1 and D_s and the shear modulus, as shown in the formula given in Appendix C. Thus, such modeling of a soil medium will make the dynamic analysis of a pile foundation much simpler.

Suggested Future Study

In this dissertation, the dynamic soil-pile interaction was studied for a single pile. However, pile foundations usually consist of more than one pile and the interaction among piles may not be negligible for such a case. Since the soil medium was treated as a continuum in the derived solution for soil-pile interaction, this solution can easily be extended so that it can account for the pile-to-pile interaction.

The study in this dissertation was aimed to draw the basic characteristics of soil-pile interaction, and thus, extremely ideal conditions for the soil medium and the pile were considered. The obtained results are further affected by many factors neglected in this dissertation, such as inhomogeneity and nonlinear behavior of soil medium and contact conditions between soil and pile. When these effects are considered, it is too complicated to derive the solution treating soil medium as a three dimensional continuum. However, the solution for such a case can be obtained rather easily when Winkler's

model is used for the soil medium. In this model, the spring and damping constants may be obtained from those for the plane strain case as shown in Appendix C. The dynamic case is more favorable for such modeling than the static case.

When the behavior of a pile subjected to seismic loading is analyzed, the driving force from soil medium to pile must be considered in addition to the force from structure to pile. This situation can rather easily be taken into account in the analysis by superimposing the displacements due to those forces.

Therefore, further research on the following is necessary to refine the results obtained in this dissertation, and the analyses for them are feasible.

1. Pile-to-pile interaction.
2. Effects of inhomogeneity and nonlinear behavior of soil and contact condition between soil and pile.
3. Behavior of pile foundation under seismic loading.

Those studies must be carried out experimentally as well as theoretically.

APPENDIX A

DAMPING FACTOR FOR COMPLEX STIFFNESS AND COMPLEX ELASTIC CONSTANTS

The model of a complex spring is shown in Fig. A-1. The force in this model is composed of those in the real and imaginary parts of the complex spring, and expressed as

$$P = p + p' \tag{A-1}$$

where p and p' are the forces in the real and imaginary parts of the spring, respectively. Those forces can be expressed as

$$\begin{aligned} p &= kx \\ p' &= ik'x \end{aligned} \tag{A-2}$$

where x is the deformation of the complex spring; k and k' are the real and imaginary parts of spring constants, respectively.

When the harmonic displacement is given by $x = x_0 \sin \omega t$, the forces p and p' in Eq. A-2 can be rewritten as

$$\begin{aligned} p &= p_0 \sin \omega t \\ p' &= p_0' \cos \omega t \end{aligned} \tag{A-3}$$

where

$$\begin{aligned} p_0 &= kx_0 \\ p_0' &= k'x_0 \end{aligned} \tag{A-4}$$

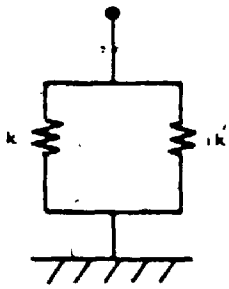

(a) MODEL OF COMPLEX SPRING OR STIFFNESS

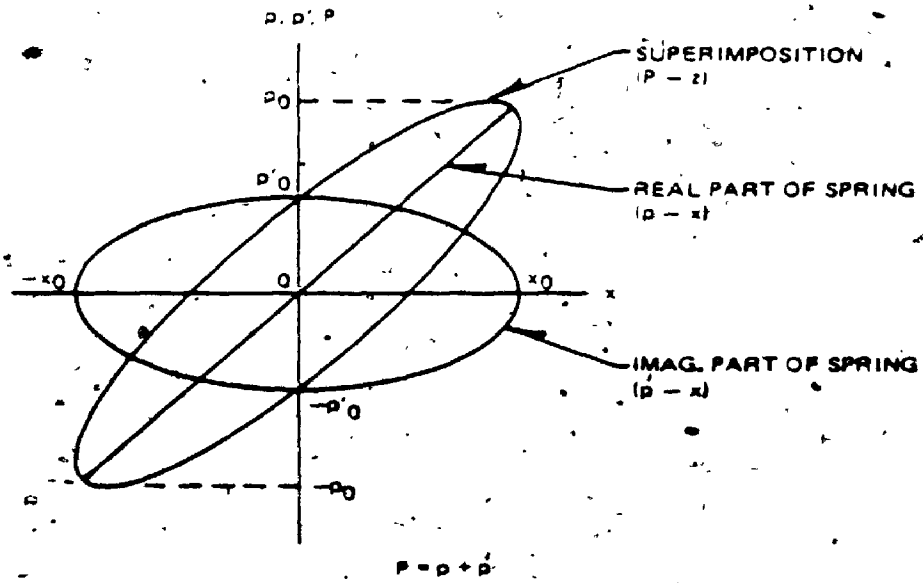

(b) FORCE-DISPLACEMENT RELATIONSHIPS IN REAL AND IMAGINARY PARTS OF COMPLEX SPRING, AND THEIR SUPERIMPOSITION

Fig. A.1, Complex Spring Model and Force–Displacement Relationship in this Model

4 4

OF/DE

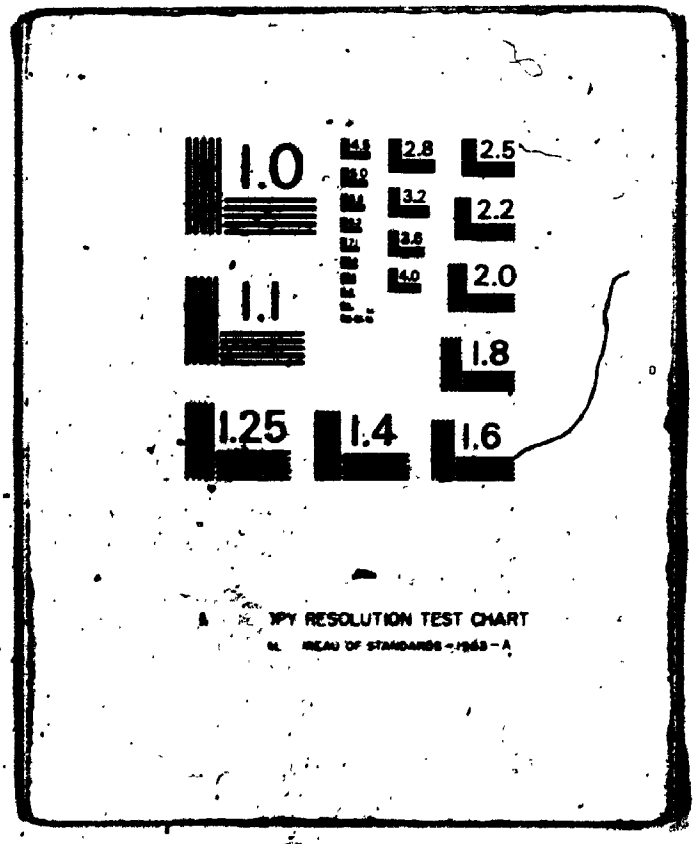
1.0
1.1
1.25
1.4
1.6
1.8
2.0
2.2
2.5
2.8
3.2
3.6
4.0
PY RESOLUTION TEST CHART
BUREAU OF STANDARDS-1963-A

The displacement, x, and force in the imaginary part of the spring, p', lead to the relationship

$$\left(\frac{x}{x_0}\right)^2 + \left(\frac{p'}{p'_0}\right)^2 = 1 \qquad \text{(A-5)}$$

Thus, the force-displacement relationship in the imaginary part of the spring draws a hysteresis loop with an ellipse shape, whereas that in the real part draws a single linear line. Superimposition of those relationships leads to the force-displacement relationship of the complex spring, which is a hysteresis loop as shown in Fig. A-1.

The hysteresis loop in the complex spring indicates that the behavior of the complex spring accompanies an energy loss: the energy loss during one cycle of motion is given by the enclosed area of the loop. Such an energy loss is induced entirely by the imaginary part of the spring as the force-displacement relationships in the real and imaginary parts of the spring indicate. Thus, the energy loss in the complex spring during one cycle of motion, T_d, can be obtained by the area of the hysteresis loop in the imaginary part of the spring. That is

$$T_d = 4 \int_0^{x_0} p' \, dx \qquad \text{(A-6)}$$

With the relationship expressed in Eq. A-5, the integration in Eq. A-6 leads to

$$T_d = \pi p_0' x_0$$
$$= \pi k' x_0^2 \qquad \text{(A-7)}$$

Besides the energy loss, the maximum strain energy stored in the real part of the spring during one cycle of the motion, T_s, is

$$T_s = \frac{1}{2} p_0 x_0$$
$$= \frac{1}{2} k x_0^2 \qquad \text{(A-8)}$$

Using the relationships in Eqs. A-7 and A-8, the ratio between T_d and T_s is given by

$$\frac{T_d}{T_s} = 2\pi \frac{k'}{k}$$
$$= 2\pi D \qquad \text{(A-9)}$$

Therefore, the damping factor D can be calculated from Eq. A-9 after the area of the hysteresis loop, the stiffness of the real part of the complex spring, and the displacement amplitude are obtained from the experiment. The damping factors D_l and D_s used in the dissertation are obtained from the one-dimensional stress-strain relationships under the normal and shear stresses, respectively.

When the imaginary part of the complex spring is replaced with a single standard dashpot, the model becomes a standard Voigt model. The energy loss in this model during one cycle of motion is given by

$$T_d = \pi \omega c x_0^2 \qquad \text{(A-10)}$$

where c is the viscous constant of the dashpot. Then, the ratio between T_d and T_s is

$$\frac{T_d}{T_s} = 2\pi \frac{c\omega}{k} = 2\pi D' \qquad \text{(A-11)}$$

where D' is the damping factor for the standard Voigt model and is

$$D' = \frac{c\omega}{k} \qquad \text{(A-12)*}$$

The expression for D' in Eq. A-12 indicates that the damping factor of a standard Voigt model grows linearly with frequency. On the other hand, the damping factor of the complex spring model is independent of the frequency as shown in Eq. A-9. Since many experiments on soils indicate that the material damping is substantially independent of the frequency of vibration, the complex spring model may be more appropriate model for soils than the standard Voigt model.

*The damping factor D' defined in Eq. A-12 is twice the commonly defined damping factor.

APPENDIX B

COMPARISON OF DISPLACEMENTS OBTAINED FROM NEW SOLUTION WITH THOSE OBTAINED BY POULOS

Poulos (1969, 1972) obtained analytically the static displacements of a pile set in ground, in which soil was treated as a continuum medium. Although the boundary conditions similar to those considered in this dissertation were used, no displacements in the soil medium were neglected. Consequently, the condition of the stress-free surface was satisfied at the top surface of the soil medium.

Figs. B-1 and B-2 show such displacements obtained by Poulos together with those obtained with the new solutions. In Poulos' solution, the pile was divided into small segments and the contact stresses between pile and soil medium were assumed to be distributed uniformly along the length of segment. Utilizing Mindlin's equation for displacements in a semi-infinite medium subjected to an internal point load, the relationship between the pile displacement and the corresponding soil reaction was obtained at the center of each segment. Although Mindlin's equation is for a semi-infinite medium, zero displacements of the stratum at its bottom were approximately satisfied using fictitious "mirror image." For a horizontally loaded pile, the pile was assumed to be a thin strip.

The figures show a fairly good agreement between the displacements obtained by Poulos and the new solution, despite some components of stresses and displacements not being treated rigorously in

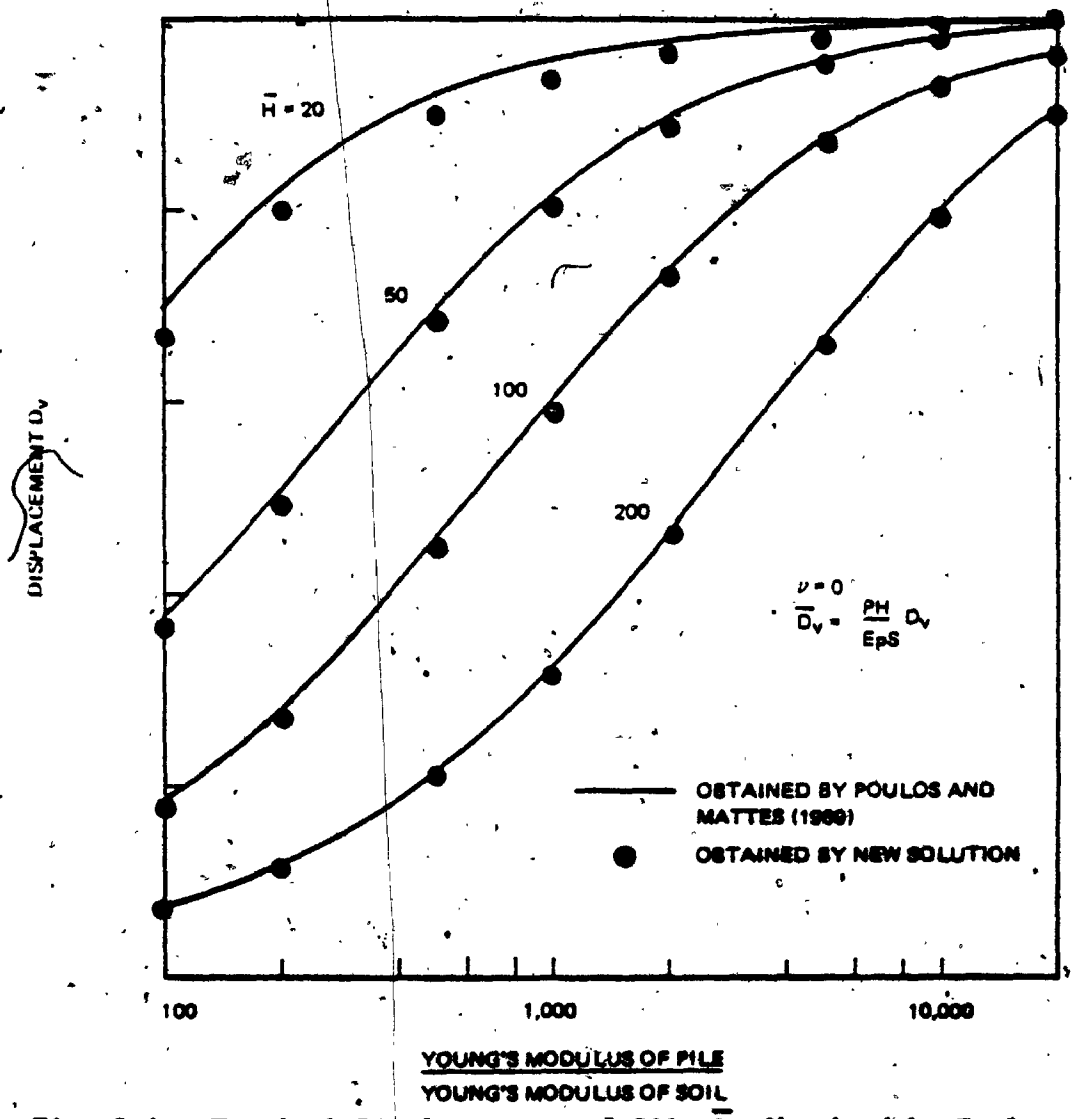

Fig. B.1. Vertical Displacements of Pile $\bar{D}_v$ Obtained by Poulos and Mattes and by New Solution

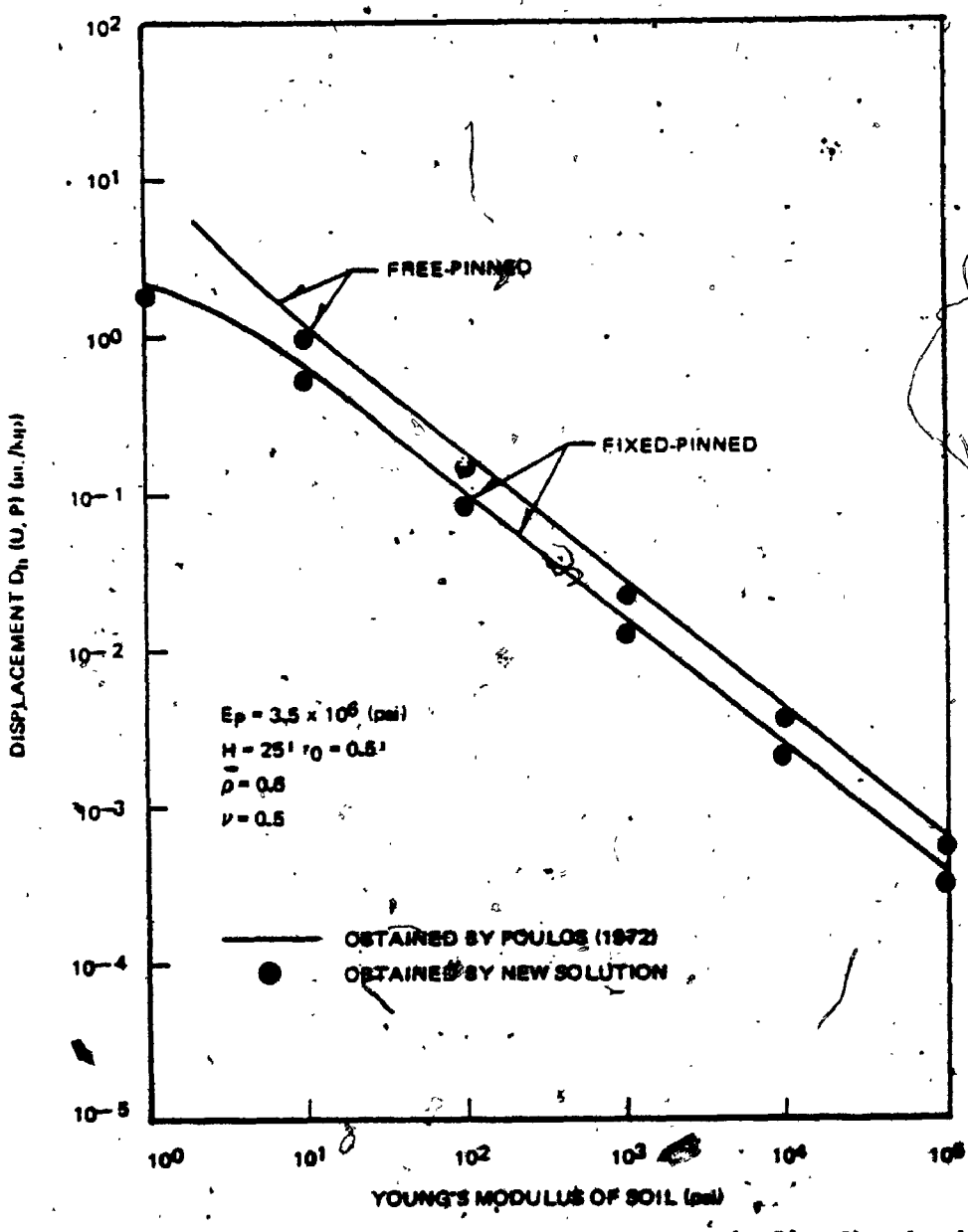

Fig. B.2. Horizontal Displacements of Pile, $D_h(U,P)$, Obtained by Poulos and by New Solution

the new solution. The displacements obtained with the new solution are generally smaller than those obtained by Poulos. This trend, however, tends to diminish as the pile becomes more slender.

APPENDIX C

SOIL REACTIONS FOR THE PLANE STRAIN CASE

When a rigid cylinder extends vertically to infinity in an infinite soil medium and is subjected to lateral and vertical external loads, no strains develop on the plane perpendicular to the axis of the cylinder. Thus, this situation is viewed as a plane strain condition and only a unit thickness of the soil medium is considered for this analysis. Such a slice of soil medium is shown together with a coordinate system in Fig. C-1. The adopted assumptions are

1. Soil medium is infinite, homogeneous, isotropic, and viscoelastic (frequency independent damping).
2. Cylinder is rigid and infinitely long.
3. No separation is allowed between cylinder and soil medium.

The adopted symbols are the same as those used in Chapter 2 unless they are defined.

C.1 Soil Reaction in Vertical Vibration

Under the assumed conditions, the equation of motion of the soil medium can be written as

$$(\mu + i\mu')\left(\frac{1}{r}\frac{\partial}{\partial r} + \frac{\partial^2}{\partial r^2}\right) w(t) = \rho \frac{\partial^2}{\partial t^2} w(t) \qquad \text{(C-1)}$$

Under steady-state motion of frequency ω, the amplitude of the displacement can be separated as

$$w(t) = w\, e^{i\omega t} \qquad \text{(C-2)}$$

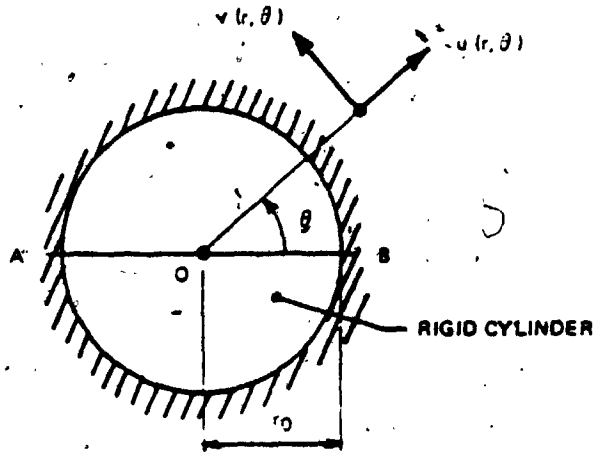

(a) PLANE VIEW

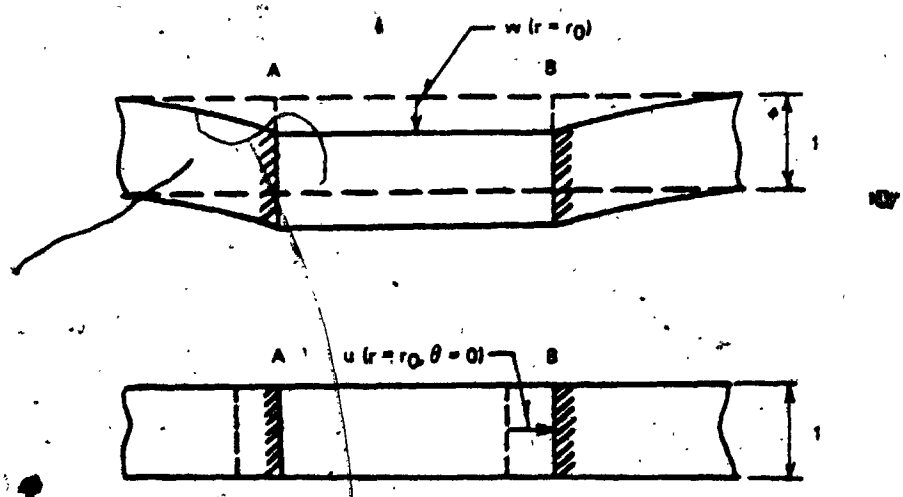

(b) CROSS SECTION VIEW (A - B)

Fig. C.1. Soil-Rigid Cylinder System for Plane Strain Case

After substituting Eq. C-2 into Eq. C-1 and rearranging, the above equation of motion can be rewritten as

$$\frac{d^2w}{dr^2} + \frac{1}{r}\frac{dw}{dr} - (1')^2 w = 0 \qquad \text{(C-3)}$$

where

$$1' = \frac{\left(\frac{\omega}{v_s}\right)i}{\sqrt{1 + iD_s}} \qquad \text{(C-4)}$$

The solution of Eq. C-3 for w is

$$w = A\,K_0(1'r) + B\,I_0(1'r) \qquad \text{(C-5)}$$

Since the stresses and displacements decay with horizontal distance, the constant B must be zero. Thus, the displacement w is

$$w = A\,K_0(1'r) \qquad \text{(C-6)}$$

and the shear stress τ_{rz} is

$$\tau_{rz} = (\mu + i\mu)\frac{\partial w}{\partial r}$$

$$= -\mu(1 + iD_s)\,1'\,K_1(1'r)\,A \qquad \text{(C-7)}$$

Using the above obtained shear stress τ_{rz}, the soil reaction to the cylinder can be derived as follows:

$$P_v = -\int_0^{2\pi} \tau_{rz}(r=r_0) r_0 d\theta$$

$$= 2\pi\mu(1 + iD_s)\, r_0\, 1'\, K_1(1'r_0)\, A \qquad \text{(C-8)}$$

The soil reaction for a unit displacement amplitude of the cylinder can be obtained from Eqs. C-6 and C-8, and hence is

$$k_v = \frac{P_v}{w(r=r_0)}$$

$$= 2\pi\mu r_0(1 + iD_s)\, 1'\, \frac{K_1(1'r_0)}{K_0(1'r_0)} \qquad \text{(C-9)}$$

The above obtained k_v can be rewritten with the dimensionless parameters such that

$$k_v = \mu \bar{k}_v \qquad \text{(C-10)}$$

where

$$\bar{k}_v = 2\pi\bar{1}'(1 + iD_s) \frac{K_1(\bar{1}')}{K_0(\bar{1}')} \qquad \text{(C-11a)}$$

$$\bar{1}' = r_0\, 1' = \frac{a_0'}{\sqrt{1 + iD_s}} \qquad \text{(C-11b)}$$

Then, the soil resistance factor $\bar{\alpha}_v$ for the plane strain case can be obtained from the relationship

$$\bar{\alpha}_v = \frac{\bar{k}_v}{\pi} \qquad \text{(C-12)}$$

C.2 Soil Reaction in Horizontal Vibration

For the assumed conditions, the equations of motions of the soil medium can be written as

$$\left\{(\lambda + 2\mu) + i(\lambda' + 2\mu')\right\} \frac{\partial}{\partial r} \Delta(t) - 2(\mu + i\mu') \frac{1}{r} \frac{\partial}{\partial \theta} \omega_z(t) = \rho \frac{\partial^2}{\partial t^2} u(t) \quad \text{(C-13a)}$$

$$\left\{(\lambda + 2\mu) + i(\lambda' + 2\mu')\right\} \frac{1}{r} \frac{\partial}{\partial \theta} \Delta(t) + 2(\mu + i\mu') \frac{\partial}{\partial r} \omega_z(t) = \rho \frac{\partial^2}{\partial t^2} v(t) \quad \text{(C-13b)}$$

Under steady-state motion of frequency ω, the amplitudes of the displacements can be separated as

$$u(t) = ue^{i\omega t} \quad \text{(C-14a)}$$

$$v(t) = ve^{i\omega t} \quad \text{(C-14b)}$$

After substituting Eqs. C-14 into Eqs. C-13 and rearranging, the above equations of motions can be rewritten as

$$(\lambda + 2\mu)(1 + iD_1) \frac{\partial \Delta}{\partial r} - 2\mu(1 + iD_s) \frac{1}{r} \frac{\partial \omega_z}{\partial \theta} = -\rho\omega^2 u \quad \text{(C-15a)}$$

$$(\lambda + 2\mu)(1 + iD_1) \frac{1}{r} \frac{\partial \Delta}{\partial \theta} + 2\mu(1 + iD_s) \frac{\partial \omega_z}{\partial r} = -\rho\omega^2 v \quad \text{(C-15b)}$$

Using the potential functions ϕ and ψ defined in Eq. 2.2-2b, Eqs. C-15 can be decoupled as

$$\nabla^2\phi + (q')^2\phi = 0 \qquad \text{(C-16a)}$$

$$\nabla^2\psi + (s')^2\psi = 0 \qquad \text{(C-16b)}$$

where

$$q' = \frac{\frac{\omega}{v_1} i}{\sqrt{1 + iD_1}} = \frac{\frac{\omega}{v_s} i}{n\sqrt{1 + iD_1}} \qquad \text{(C-17a)}$$

$$s' = \frac{\frac{\omega}{v_s} i}{\sqrt{1 + iD_s}} \qquad \text{(C-17b)}$$

The solutions of Eqs. C-16 for ϕ and ψ are

$$\phi = \left\{A_1 K_m(q'r) + B_1 I_m(q'r)\right\}\left\{A_2 \sin(m\theta) + B_2 \cos(m\theta)\right\} \qquad \text{(C-18a)}$$

$$\psi = \left\{A_3 K_m(s'r) + B_3 I_m(s'r)\right\}\left\{A_4 \sin(m\theta) + B_4 \cos(m\theta)\right\} \qquad \text{(C-18b)}$$

Since the stresses and displacements decay with horizontal distance r, the constants B_1 and B_3 must be zero. When the horizontal excitation is applied to the cylinder, the induced stresses and displacements conditions in the soil medium require n = 1 and $A_2 = A_4 = 0$. Hence, the potential functions ϕ and ψ are

$$\phi = A K_1(q'r) \cos\theta \qquad \text{(C-19a)}$$

$$\psi = B K_1(s'r) \sin\theta \qquad \text{(C-19b)}$$

With the potential functions derived in Eqs. C-19, the displacements u and v and the stresses σ_r and $\tau_{r\theta}$ can be obtained as

$$u = \frac{\partial \phi}{\partial r} + \frac{1}{r}\frac{\partial \psi}{\partial \theta}$$

$$= \cos\theta \left[- A \left\{ \frac{1}{r} K_1(q'r) + q' K_0(q'r) \right\} + B \frac{1}{r} K_1(s'r) \right] \qquad \text{(C-20a)}$$

$$v = \frac{1}{r}\frac{\partial \phi}{\partial \theta} - \frac{\partial \psi}{\partial r}$$

$$= \sin\theta \left[- A \frac{1}{r} K_1(q'r) + B \left\{ \frac{1}{r} K_1(s'r) + s' K_0(s'r) \right\} \right] \qquad \text{(C-20b)}$$

$$\sigma_r = (\lambda + 2\mu)(1 + iD_1) \nabla^2 \phi - 2\mu(1 + iD_s)\left(\frac{1}{r}\frac{\partial \phi}{\partial r} + \frac{1}{r^2}\frac{\partial^2 \phi}{\partial \theta^2} - \frac{1}{r}\frac{\partial^2 \psi}{\partial \partial \theta} + \frac{1}{r^2}\frac{\partial \psi}{\partial \theta} \right)$$

$$= \cos\theta \left[A(\lambda + 2\mu)(1 + iD_1)(q')^2 K_1(q'r) + 2A\mu(1 + iD_s) \left\{ 2\frac{q'}{r} K_0(q'r) + \frac{1}{r^2} K_1(q'r) \right\} - 2B\mu(1 + iD_s) \right.$$

$$\left. \times \left\{ 2\frac{s'}{r} K_0(s'r) + \frac{1}{r^2} K_1(s'r) \right\} \right] \qquad \text{(C-20c)}$$

$$\tau_{r\theta} = \mu(1 + iD_s)\left(- \frac{1}{r^2}\frac{\partial \phi}{\partial r} + \frac{2}{r}\frac{\partial^2 \phi}{\partial r \partial \phi} + \frac{\partial^2 \psi}{\partial r^2} + \frac{1}{r}\frac{\partial \psi}{\partial r} + \frac{1}{r^2}\frac{\partial^2 \psi}{\partial \theta^2} \right)$$

$$= \sin\theta \left[A\mu(1 + iD_s) \left\{ 4\frac{q'}{r} K_0(q'r) + \frac{2}{r^2} K_1(q'r) \right\} \right.$$

$$\left. + B\mu(1 + iD_s) \left\{ (s')^2 K_1(s'r) + 4\frac{s'}{r} K_0(s'r) + \frac{2}{r^2} K_1(s'r) \right\} \right] \qquad \text{(C-20d)}$$

Furthermore, the horizontal displacement of the circular, rigid cylinder requires that

$$u(r = r_0,\ \theta = 0) = -v\left(r = r_0,\ \theta = \frac{\pi}{2}\right) \qquad \text{(C-21)}$$

Substitution of u and y in Eqs. C-20 into Eq. C-21 lead to

$$B = \frac{2\,K_1(q'r_0) + q'\,r_0\,K_0(q'r_0)}{2\,K_1(s'r_0) + s'\,r_0\,K_0(s'r_0)}\,A \qquad \text{(C-22)}$$

Using the relationship obtained in Eq. C-22, the horizontal displacement of the cylinder can be expressed as

$$u(r=r_0,\theta=0) = \frac{q'K_0(q'r_0)K_1(s'r_0) + s'K_1(q'r_0)K_0(s'r_0) + q's'r_0K_0(q'r_0)K_0(s'r_0)}{2K_1(s'r_0) + s'r_0K_0(s'r_0)}\,A \qquad \text{(C-23)}$$

With the relationship in Eq. C-22 and the stresses σ_r and $\tau_{r\theta}$ in Eqs. C-20, the soil reaction to the cylinder can be derived as follows.

$$p_h = -\int_0^{2\pi} \left\{\sigma_r(r=r_0)\cos\theta - \tau_{r\theta}(r=r_0)\sin\theta\right\} r_0\,d\theta$$

$$= -\pi\mu r_0 \left(\frac{\omega}{v_s}\right)^2 \times \frac{4K_1(q'r_0)K_1(s'r_0) + s'r_0K_1(q'r_0)K_0(s'r_0) + q'r_0K_0(q'r_0)K_1(s'r_0)}{2K_1(s'r_0) + s'r_0K_0(s'r_0)}\,A \qquad \text{(C-24)}$$

The soil reaction for a unit displacement amplitude of the cylinder can be obtained from Eqs. C-23 and C-24, and hence is

$$k_h = \frac{p_h}{u(r=r_0,\ \theta=0)} = \pi\mu r_0 \left(\frac{\omega}{v_s}\right)^2 T' \qquad \text{(C-25)}$$

where

$$T' = -\frac{4K_1(q'r_0)K_1(s'r_0) + s'r_0K_1(q'r_0)K_0(s'r_0) + q'r_0K_0(q'r_0)K_1(s'r_0)}{q'K_0(q'r_0)K_1(s'r_0) + s'K_1(q'r_0)K_0(s'r_0) + q's'r_0K_0(q'r_0)K_0(s'r_0)} \qquad \text{(C-26)}$$

The above obtained k_h can be rewritten with the dimensionless parameters such that

$$k_h = \mu \bar{k}_h \qquad \text{(C-27)}$$

where

$$\bar{k}_h = \pi (a_0')^2 \bar{T}' \qquad \text{(C-28a)}$$

$$\bar{T}' = -\frac{4\,K_1(\bar{q}')\,K_1(\bar{s}') + \bar{s}'\,K_1(\bar{q}')\,K_0(\bar{s}') + \bar{q}'\,K_0(\bar{q}')\,K_1(\bar{s}')}{\bar{q}'\,K_0(\bar{q}')\,K_1(\bar{s}') + \bar{s}'\,K_1(\bar{q}')\,K_0(\bar{s}') + \bar{q}'\bar{s}'\,K_0(\bar{q}')\,K_0(\bar{s}')} \qquad \text{(C-28b)}$$

$$\bar{q}' = q'\,r_0 = \frac{a_0'}{\eta\sqrt{1 + iD_1}}\,i \qquad \text{(C-28c)}$$

$$\bar{s}' = s'\,r_0 = \frac{a_0'}{\sqrt{1 + iD_s}}\,i \qquad \text{(C-28d)}$$

Then, the soil resistance factor $\bar{\alpha}_h$ for the plane strain case can be obtained from the relationship

$$\bar{\alpha}_h = \frac{\bar{k}_h}{\pi} \qquad \text{(C-29)}$$

The parameters a_0', $\bar{l}'$, $\bar{q}'$ and $\bar{s}'$ can be also expressed as

$$\begin{Bmatrix} \bar{l}' \\ \bar{q}' \\ \bar{s}' \end{Bmatrix} = \frac{1}{\bar{H}} \begin{Bmatrix} \bar{l}_n \\ \bar{q}_n \\ \bar{s}_n \end{Bmatrix} \quad \text{with } \bar{h}_n = 0 \qquad \text{(C-30a)}$$

$$a_0' = \frac{1}{\bar{H}} a_0 \qquad \text{(C-30b)}$$

The relationships in Eqs. C-30 indicate that $\bar{\alpha}_h$ and $\bar{\alpha}_v$ for the plane strain case are identical to $\bar{\alpha}_{hn}$ and $\bar{\alpha}_{vn}$, respectively, when $\bar{h}_n$ is equal to zero.

APPENDIX D

ANALYTICAL SOLUTION FOR THE BEHAVIOR OF SOIL-PILE SYSTEM IN HORIZONTAL VIBRATION BY USING MODAL ANALYSIS

The assumptions adopted in this solution are exactly the same as those adopted in the direct solution for horizontal vibration in Chapter 3. Forces applied to a pile, soil reaction, and the coordinate system are shown in Fig. 3.3-1. When the soil reaction $p_h(z)\, e^{i\omega t}$ is treated as an external force to the pile, the equation of free vibration of the pile can be written from Eq. 3.3-1 as

$$E_p I \frac{\partial^4}{\partial z^4}\left(U(z)\, e^{i\omega t}\right) + m \frac{\partial^2}{\partial t^2}\left(U(z)\, e^{i\omega t}\right) = 0 \qquad \text{(D-1)}$$

The solution of Eq. D-1 for U(z) can be expressed by

$$U(z) = A \sin(\lambda_h z) + B \cos(\lambda_h z) + C\, sh(\lambda_h z) + D\, ch(\lambda_h z) \qquad \text{(D-2)}$$

Using the horizontal displacement U(z) in Eq. D-2, the boundary conditions for free vibration of pile lead to four simultaneous, homogeneous, linear equations with unknowns A, B, C, and D. An infinite number of mode shapes and natural frequencies can be obtained from those equations. With those mode shapes and natural frequencies, the horizontal and rotational displacements of the pile can be expressed, respectively, by

$$U(t,z) = \sum_{n=1}^{\infty} \xi_n(z)\, \eta_n \qquad \text{(D-3a)}$$

$$\zeta(t,z) = \sum_{n=1}^{\infty} \xi_n'(z)\, \eta_n \qquad \text{(D-3b)}$$

where

$U(t,z) = U(z)e^{i\omega t}$

$\zeta(t,z) = \zeta(z)e^{i\omega t}$

$\xi_n(z)$ = n-th mode shape of pile free from soil effect

$\eta_n(t)$ = n-th generalized coordinate

$\xi_n'(z) = \dfrac{\partial\, \xi_n(z)}{\partial z} = \zeta(z)$

Lagrange's equation for a pile subjected to external forces in the j-th generalized coordinate, is

$$\frac{d}{dt}\left(\frac{\partial T_k}{\partial \dot{\eta}_j}\right) - \frac{\partial T_k}{\partial \eta_j} + \frac{\partial T_s}{\partial \eta_j} = N_j \qquad \text{(D-4)}$$

where T_k, T_s, and N_j are the kinetic and strain energies and the generalized force in the j-th generalized coordinate, respectively, and

$$\dot{\eta}_j = \frac{\partial \eta_j}{\partial t} \qquad \text{(D-5)}$$

The kinetic and strain energies can be written as

$$T_k = \frac{1}{2}\int_H m\, \dot{U}(t,z)\, dz$$
$$T_s = \frac{1}{2}\int_H E_p I\, U''(t,z)\, dz \qquad \text{(D-6)}$$

where

$$\dot{U}(t,z) = \frac{\partial U(t,z)}{\partial t} \qquad \text{(D-7a)}$$

$$U''(t,z) = \frac{\partial^2 U(t,z)}{\partial z^2} \qquad \text{(D-7b)}$$

Substitution of T_k and T_s in Eqs. D-6 into Eq. D-4 leads to

$$\frac{d^2\eta_j}{dt^2}\int_H m\,\xi_j^2(z)\,dz + \lambda_{hj}^4\,\eta_j\int_H E_P I\,\xi_j^2(z)\,dz = N_j \qquad \text{(D-8)}$$

where λ_{hj} is the j-th natural frequency (in terms of λ_h) of the pile. Since harmonic excitations with frequency ω are applied, η_j can be expressed as

$$\eta_j = c_j\,e^{i\omega t} \qquad \text{(D-9)}$$

Using the expression for η_j in Eq. D-9, Eq. D-8 can be rewritten as

$$c_j\left(\lambda_{hj}^4 - \lambda_h^4\right)E_P I\int_H \xi_j^2(z)\,dz\,e^{i\omega t} = N_j \qquad \text{(D-10)}$$

The external forces on the pile, $Pe^{i\omega t}$, $Me^{i\omega t}$ and $p_h(z)e^{i\omega t}$, are shown in Fig. 3.3-1. The virtual work done by those forces on the virtual displacements, $\delta U(t,z)$ and $\delta\zeta(t,z)$, is given by

$$\delta w = P\,e^{i\omega t}\cdot\delta U(t,z=H) + M\,e^{i\omega t}\cdot\delta\zeta(t,z=H) - \int_H p_h(z)\,e^{i\omega t}\cdot\delta U(z)\,dz \qquad \text{(D-11)}$$

Substituting the expressions of U and ζ in Eqs. D-3 into Eq. D-11, the above virtual work done can be rewritten as

$$\delta w = \sum_{n=1}^{\infty} \left\{ P\, e^{i\omega t}\, \xi_n(H) + M\, e^{i\omega t}\, \xi_n'(H) - \int_H p_h(z)\, e^{i\omega t}\, \xi_n(z)\, dz \right\} \delta\eta_n \qquad \text{(D-12)}$$

On the other hand, the work done by the generalized forces (N_1, N_2, N_3, ...) on the virtual displacements ($\delta\eta_1$, $\delta\eta_2$, $\delta\eta_3$, ...) is

$$\delta w = \sum_{n=1}^{\infty} N_n \cdot \delta\eta_n \qquad \text{(D-13)}$$

Comparison of the expression of δw in Eq. D-12 with that in Eq. D-13 leads to the j-th generalized force such that

$$N_j = e^{i\omega t} \left\{ P\, \xi_j(H) + M\, \xi_j'(H) - \int_H p_h(z)\, \xi_j(z)\, dz \right\} \qquad \text{(D-14)}$$

After substituting the generalized force N_j in Eq. D-14 into Eq. D-10, Lagrange's equation can be rewritten as

$$C_j \left(\lambda_{hj}^4 - \lambda_h^4 \right) E_p I \int_H \xi_j^2(z)\, dz = P\, \xi_j(H) + M\, \xi_n'(H) - \int_H p_h(z)\, \xi_j(z)\, dz \qquad \text{(D-15)}$$

After substituting η_j in Eq. D-9 into Eqs. D-3 for j=1, 2, 3, ..., the displacement amplitudes of the pile can be described by

$$U(z) = \sum_{n=1}^{\infty} C_n \xi_n(z) \tag{D-16a}$$

$$\zeta(z) = \sum_{n=1}^{\infty} C_n \xi_n'(z) \tag{D-16b}$$

Since a perfect connection between the pile and the soil is assumed, the horizontal displacement of the pile in Eq. D-16a must be equal to that of the surrounding soil in Eq. 2.2-43. This condition leads to

$$\sum_{n=1}^{\infty} U_n \sin(h_n z) = \sum_{n=1}^{\infty} C_n \xi_n(z) \tag{D-17}$$

Expanding $\xi_n(z)$ with a sine Fourier series with an argument of $h_n z$, Eq. D-17 can be rewritten as

$$\sum_{n=1}^{\infty} U_n \sin(h_n z) = \sum_{n=1}^{\infty}\sum_{l=1}^{\infty} C_l D_{nl} \sin(h_n z) \tag{D-18}$$

where

$$D_{nl} = \frac{2}{H}\int_H \xi_l(z) \sin(h_n z)\, dz \tag{D-19}$$

Therefore, U_n can be expressed as

$$U_n = \sum_{l=1}^{\infty} C_l D_{nl} \qquad \text{(D-20)}$$

With the expression for U_n in Eq. D-20, the soil reaction $p_h(z)$ in Eq. 2.2-47 can be rewritten as

$$p_h(z) = \sum_{n=1}^{\infty} \alpha_{hn} \sin(h_n z) \sum_{l=1}^{\infty} C_l D_{nl} \qquad \text{(D-21)}$$

After substitution of $p_h(z)$ in Eq. D-21 into Eq. D-15, Eq. D-15 is expressed by

$$C_j \left(\lambda_{hj}^4 - \lambda_h^4\right) E_p I \int_H \xi_j^2(z)\, dz = P\, \xi_j(H) + M\, \xi_j'(H) - \frac{H}{2} \sum_{n=1}^{\infty} \alpha_{hn} D_{nj} \sum_{l=1}^{\infty} C_l D_{nl} \qquad \text{(D-22)}$$

where

$$D_{nj} = \frac{2}{H} \int_H \xi_j(z) \sin(h_n z) \qquad \text{(D-23)}$$

Lagrange's equation for all other generalized coordinates leads to equations similar to Eq. D-22. Thus, simultaneous linear equations for C_n (n=1, 2, 3, ...) are established. Such equations, considering up to the r-th mode of the pile, can be expressed in a matrix form

$$P\begin{Bmatrix} \xi_1(H) \\ \xi_2(H) \\ \vdots \\ \xi_n(H) \\ \vdots \\ \xi_r(H) \end{Bmatrix} + M\begin{Bmatrix} \xi_1'(H) \\ \xi_2'(H) \\ \vdots \\ \xi_n'(H) \\ \vdots \\ \xi_r'(H) \end{Bmatrix} = \begin{bmatrix} a_{11}+b_1 & a_{12} & \cdots & a_{1n} & \cdots & a_{1r} \\ a_{21} & a_{22}+b_2 & \cdots & a_{3n} & \cdots & a_{2r} \\ \vdots & \vdots & & \vdots & & \vdots \\ a_{n1} & a_{n2} & \cdots & a_{nn}+b_n & \cdots & a_{nr} \\ \vdots & \vdots & & \vdots & & \vdots \\ a_{r1} & a_{r2} & \cdots & a_{rn} & \cdots & a_{rr}+b_r \end{bmatrix} \begin{Bmatrix} C_1 \\ C_2 \\ \vdots \\ C_n \\ \vdots \\ C_r \end{Bmatrix} \qquad \text{(D-24)}$$

where

$$a_{jl} = \frac{1}{E_p I} \frac{H}{2} \sum_{n=1}^{\infty} \alpha_{hn} D_{nj} D_{nl} \qquad \text{(D-25a)}$$

$$b_j = \left(\lambda_{hj}^4 - \lambda_h^4\right) \int_H \xi_j(z)\, dz \qquad \text{(D-25b)}$$

Using the dimensionless parameters, Eq. D-24 can be rewritten as

$$\frac{PH^4}{E_p I}\begin{Bmatrix} \xi_1(1) \\ \xi_2(1) \\ \vdots \\ \xi_n(1) \\ \vdots \\ \xi_r(1) \end{Bmatrix} + \frac{MH^3}{E_p I}\begin{Bmatrix} \xi_1'(1) \\ \xi_2'(1) \\ \vdots \\ \xi_n'(1) \\ \vdots \\ \xi_r'(1) \end{Bmatrix} = \begin{bmatrix} \bar{a}_{11}+\bar{b}_1 & \bar{a}_{12} & \cdots & \bar{a}_{1n} & \cdots & \bar{a}_{1r} \\ \bar{a}_{21} & \bar{a}_{22}+\bar{b}_2 & \cdots & \bar{a}_{2n} & \cdots & \bar{a}_{2r} \\ \vdots & \vdots & & \vdots & & \vdots \\ \bar{a}_{n1} & \bar{a}_{n2} & \cdots & \bar{a}_{nn}+\bar{b}_n & \cdots & \bar{a}_{nr} \\ \vdots & \vdots & & \vdots & & \vdots \\ \bar{a}_{41} & \bar{a}_{r2} & \cdots & \bar{a}_{rn} & \cdots & \bar{a}_{rr}+\bar{b}_r \end{bmatrix} \begin{Bmatrix} C_1 \\ C_2 \\ \vdots \\ C_n \\ \vdots \\ C_r \end{Bmatrix} \qquad \text{(D-26)}$$

where

$$\bar{a}_{jl} = H^3 a_{jl} = \frac{Y_h}{2} \sum_{n=1}^{\infty} \bar{\alpha}_{hn} D_{nj} D_{nl} \qquad \text{(D-27a)}$$

$$\bar{b}_j = H^3 b_j = \left(\bar{\lambda}_{hj}^4 - \bar{\lambda}_h^4\right) \int_0^1 \xi_j(\bar{z})\, d\bar{z} \qquad \text{(D-27b)}$$

$$D_{nj} = 2 \int_0^1 \xi_j(\bar{z}) \sin(\bar{h}_n \bar{z})\, d\bar{z} \qquad \text{(D-27c)}$$

$$D_{nl} = 2 \int_0^1 \xi_l(\bar{z}) \sin(\bar{h}_n \bar{z})\, d\bar{z} \qquad \text{(D-27d)}$$

Since the mode shapes of the pile free from soil are used to express the displacement of the pile, many mode shapes are required to describe the displacements of the pile strongly affected by the soil. This situation leads to a large number of simultaneous linear equations.

As a special case, the mode shapes of a pile with a rotationally fixed head and pinned tip (fixed-pinned pile) are

$$\xi_n(\bar{z}) = \sin(\bar{\lambda}_{hn} \bar{z}) \quad n = 1, 2, 3, \ldots \qquad \text{(D-28)}$$

where

$$\bar{\lambda}_{hn} = \frac{\pi}{2}(2n-1) \qquad \text{(D-29)}$$

Those mode shapes of a pile indicate that $\bar{D}_{nj}$ and $\bar{D}_{nl}$ are zero when j and l are not equal to n, respectively. Therefore, for such a special case, Eq. D-26 can be reduced to

$$\frac{PH^4}{E_pI}\begin{Bmatrix}\xi_1(1)\\ \xi_2(1)\\ \vdots\\ \xi_n(1)\\ \vdots\\ \xi_r(1)\end{Bmatrix}+\frac{MH^3}{E_pI}\begin{Bmatrix}\xi_1'(1)\\ \xi_2'(1)\\ \vdots\\ \xi_n'(1)\\ \vdots\\ \xi_r'(1)\end{Bmatrix}=\begin{bmatrix}\bar{a}_{11}+\bar{b}_1 & 0 & \cdots & 0 & \cdots & 0\\ 0 & \bar{a}_{22}+\bar{b}_2 & \cdots & 0 & \cdots & 0\\ \vdots & \vdots & & \vdots & & \vdots\\ 0 & 0 & \cdots & \bar{a}_{nn}+\bar{b}_n & \cdots & 0\\ \vdots & \vdots & & \vdots & & \vdots\\ 0 & 0 & \cdots & 0 & \cdots & \bar{a}_{rr}+\bar{b}_r\end{bmatrix}\begin{Bmatrix}C_1\\ C_2\\ \vdots\\ C_n\\ \vdots\\ C_r\end{Bmatrix} \qquad \text{(D-30)}$$

which are not simultaneous but independent equations.

With those obtained constants, the displacements of the pile can be obtained from Eqs. D-3 along with Eq. D-9.

REFERENCES

Arnold, R. N., Bycroft, G. N. and Warburton, G. B. (1955), "Forced Vibrations of a Body on an Infinite Elastic Solid," J. App. Mech., Trans. ASME 77.

Awojobi, A. O. (1972), "Vertical Vibration of a Rigid Circular Foundation on Gibson Soil," Geotechnique 22, No. 2.

Awojobi, A. O. and Groatenhuis, P. (1965), "Vibration of Rigid Bodies on Semi-Infinite Elastic Media," Philosophical Trans. Royal Soc. of London A287.

Balows, J. E. (1968), "Foundation Analysis and Design," McGraw-Hill, 503-507.

Baranov, V. A. (1967), "On the Calculation of Excited Vibrations of an Embedded Foundation," Voprosy Dynamiki Prochnoti, No. 14, Polytech. Inst. Riga, 195-209 (in Russian).

Bolows, J. E. (1968), "Foundation Analysis and Design," McGraw-Hill, 503-507.

Broms, B. B. (1964), "Lateral Resistance of Piles in Cohesive Soils," Proc. ASCE 90, SM2, 27-63.

Bycroft, G. N. (1956), "Forced Vibrations of a Rigid Circular Plate on a Semi-Infinite Elastic Space and on an Elastic Stratum," Philosophical Trans. Royal Society of London A248.

Chan, Y. L. (1937), Discussion on "Lateral Pile-Loading Tests" by Feagin, Trans. ASCE 102, 272-278.

Dobry, R. (1970), "Damping in Soils: Its Hysteretic Nature and the Linear Approximation," Research Report R70-14, M.I.T., Department of Civil Engineering.

Elorduy, J., Nieto, J. A. and Szekely, E. M. (1967), "Dynamic Response of Base of Arbitrary Shape Subjected to Periodic Vertical Loading," Proc. Inst. Symp. on Wave Propagation and Dynamic Properties of Earth Materials, University of New Mexico Press, Albuquerque.

Francis, A. J. (1964), "Analysis of Pile Groups with Flexual Resistance," Proc. ASCE 90, SM3, 20-23.

Hardin, B. O. and Drnevich, V. P. (1972), "Shear Modulus and Damping in Soils: Measurement and Parameter Effects," Proc. ASCE 98, SM6, 603-624.

Hayashi, S. and Miyajima, N. (1963), "Study on the Horizontal Resistance of H-Piles," Port and Habour Res. Inst. and Yawata Steel Ltd. (in Japanese).

Kobori, T., Minai, R., Suzuki, T. and Kusakabe (1967), "Dynamic Ground Compliance of Reotangular Foundation on a Semi-Infinite Elastic Medium," Bull. Disas. Prev: Inst. 10A, Kyoto University.

Kobori, T., Minai, R. and Suzuki, T. (1968), "Dynamic Ground Compliance of Rectangular Foundation on an Elastic Stratum Overlying Rigid Base," Bull. Disas. Prev. Inst. 11A, Kyoto University.

Kobori, T., Minai, R. and Suzuki, T. (1971), "The Dynamic Ground Compliance of a Rectangular Foundation on a Viscoelastic Stratum," Bull. Disas. Prev. Inst. 20, Part 4, No. 183, 289-329, Kyoto University.

Krizek, R. J. and Franklin, A. G. (1967), "Energy Dissipation in Soft Clay," Proc. Int. Symp. on Wave Propagation and Dynamic Properties of Earth Materials, 797-807, University of New Mexico Press, Albuquerque.

Luco, J. E. and Westman, R. A. (1971), "Dynamic Response of Circular Footings," Proc. ASCE 97, EM5, 1381-1395.

Luco, J. E. and Westman, R. A. (1972), "Dynamic Response of a Rigid Footing Bonded to an Elastic Half-Space," J. App. Mech., Trans. ASME 94.

Luco, J. E. (1976), "Vibrations of a Rigid Disc on a Layered Viscoelastic Medium," Nuclear Engineering and Design 36, 325-340.

McClelland, B. and Focht, J. Jr. (1958), "Soil Modulus for Laterally Loaded Piles," Trans. ASCE 123, 1049-1086.

Novak, M. and Beredugo, Y. (1971), "The Effect of Embedment on Footing Vibrations," Proc. the First Canadian Conf. on Earthquake Engineering Research, University of British Columbia.

Novak, M. (1974), "Dynamic Stiffness and Damping of Piles," Canadian Geotechnical J. 11, No. 4, 574-598.

Penzien, J. (1970), "Soil-Pile Interaction," Earthquake Engineering by R. L. Wiegel et al., Chapter 14, Prentice-Hall, 349-381.

Poulos, H. G. and Mattes, N. S. (1969), "The Behavior of Axially Loaded End-Bearing Piles," Geotechnique 19, No. 2, 301-306.

Poulos, H. G. (1972), "Behavior of Laterally Loaded Piles," Proc. ASCE 98, SM4, 341-360.

Richart, F. E. Jr., Hall, J. R. and Woods, R. D. (1970), Vibrations of Soils and Foundation, Ch 6 and 7, Prentice-Hall.

Rifaat, I. (1935), Die Spundwand als Erdbruck Problem, A. G. Gebr. Leeman and Zurich Co.

Reissner, E. (1936), "Statienäre, Axialsymmetrishee durch eine Schüttelnde Masse eregte Schwingungen eines Homogenen Elastischen Halbraumes," Ingenieur-Archiv 7, Part 6.

Row, P. W. (1956), "The Single Pile Subjected to Horizontal Force," Geotechnique, June.

Seed, H. B. and Idriss, I. M. (1970), "Soil Moduli and Damping Factors for Dynamic Response Analysis," Report EERC 70-10, University of California, Berkeley.

Shinohara, T. and Kubo, K. (1961), "Experimental Study on the Lateral Resistance of Piles (Part 1)," Monthly Report of Transportation Technical Research Inst., Vol. 11, No. 6.

Tajimi, H. (1969), "Dynamic Analysis of a Structure Embedded in an Elastic Stratum," Proc. 4th WCEE.

Terzaghi, K. (1955), "Evaluation of Coefficient of Subgrade Reaction," Geotechnique 5, No. 4, 1970-326.